Public University of Navarre
Department of Electrical and Electronic Engineering

Contribution to the advancement of Brillouin optical time-domain analysis sensors

This dissertation is submitted for the degree of Doctor of Philosophy

HARITZ IRIBAS PARDO

Advisor: Alayn Loayssa Lara
Professor

Iruñea, May 2018

Esker-emateak/Acknowledgements

Lehenik eta behin, eskerrik beroenak etxekoei, guraso eta anaiari. Urte luze hauetan emandako laguntza eta sostengu guztiari esker izan ez balitz, nekez iritsi izango bainintzen tesia bukatzera.

Ezin ahaztu Mikel, nire tesi zuzendaria zena. Zurekin hasi nuen bide zoro hau, zurekin pasa nituen lehenengo urteak, lehenengo sufrikarioak, baina baita momentu gozo asko ere. Zure gomendioei eta ereduari esker karrera garaietatik ikasi dudan guztiak ez du ordainik. Penaz bidea elkarrekin bukatzerik ez dugula izan, baina ziur naiz etorkizunean berriro zerbaitetan egingo dugula topo.

A los compañeros de fatiga, Javi, Jon y Juanjo. Por toda la innumerable ayuda para poder llevar a buen puerto esos BOTDA que siempre parecían fallar. Por todo ello, pero también por todos los buenos ratos que hemos pasado, en el lab, pero sobre todo fuera. En esos viajes exóticos por Brasil y Corea, dando vueltas con la bici, con los míticos 29 segundos de ventaja en Larrau incluidos, y en las cenas y comidas que hemos hecho. Juanjo moltes gràcies pel teu interès en aprendre euskera. Asko eskertzen da saiakera, animo, lortuko duzula!

Je tiens à remercier vivement mes amis de Saint-Imier, à savoir Sébastien, Miguel, Valentin, Maxime et Yves. Pour votre accueil chaleureux, l'ouverture de vos maisons, toute l'aide apportée, les matchs de foot, les excursions à vélo, les soirées... Enfin, pour tout ce que nous avons vécu pendant trois mois. Vous m'avez fait sentir comme chez-moi. Finalement, un grand merci pour tout ce que j'ai appris dans votre groupe de recherche.

Eskerrak eman nahi dizkiet baita ere tesi hau posible egin duten instituzio guztiei: Nafarroako Unibertsitate Publikoari, ikertzaileak prestatzeko dirulaguntza, atzerriko egonaldia zein bestelako laguntza moten bidez; Espainiako Ekonomia eta Lehiakortasun Ministerioari, TEC2013-47264-C2-2-R eta TEC2016-76021-C2-1-R proiektuen bidez; Europako Eskualde Garapenerako Funtsari (FEDER funds). I would also like to thank the University of Applied Sciences, Western Switzerland in Saint-Imier (Haute École ARC Ingénierie, HE-ARC), for the research stay, which was really helpful for the development of this thesis.

Y finalmente, al director de esta tesis, Alayn, por su orientación, asesoramiento, enseñanzas y dedicación durante todos estos años, gracias a lo cual he conseguido convertir todo este largo camino de investigación en esta tesis. Muchas gracias.

Iruñea, 2018ko maiatzean

Haritz Iribas Pardo

Abstract

Distributed fiber optic sensors (DFOS) are becoming an increasingly used technology to monitor the integrity of structures. This is due to the fact that this technology can be embedded within the structure and provide distributed information of several relevant parameters for the structure, such as stress, temperature or strain. In DFOS the fiber itself is the transducer, and the measurement of a given parameter is provided continuously along the fiber at a particular spatial resolution, without blind spots. This is the main advantage of DFOS compared to other sensing technologies, the fact that DFOS provide information of a given parameter over thousands or hundreds of thousands of positions along the optical fiber. Conversely, other sensing technologies only give information over the specific points where they are installed, that is to say, they are point sensors. This characteristic of distributed fiber sensors makes them enormously interesting when many points of a structure need to be monitored. In this case, a single distributed fiber sensor can replace many point sensors, which considerably reduces the cost per sensing point when monitoring large structures. In addition, due to the properties of the optical fiber, these sensors have a better performance compared to other kind of sensors. Among other important features, DFOS present a low signal loss, electromagnetic interference immunity, remote sensing and multiplexing capabilities, light weight, and are chemically passive, which make them a very attractive technology for field measurements. Therefore, DFOS have the added advantage of being electrically, magnetically, and chemically passive, so that can be placed in harsh environments, such as nuclear plants or areas with gas concentration, where, due to the possibility of a short circuit, electronic sensors cannot be placed. Al these characteristics make this technology unique.

Among the different types of DFOS, those based on stimulated Brillouin scattering, and more specifically, those that build upon the Brillouin optical time-domain analysis (BOTDA) technique, are one of the most promising. The main characteristic that makes BOTDA sensors as promising, is the ability to perform distributed strain and temperature measurements over long distances at high spatial resolution. For the functioning of the sensor, the general interaction that takes place in the BOTDA technique involves two optical waves: a continuous wave probe and a counter-propagating pump pulse. The performance of the sensor response is limited, among others, by the maximum optical power of both waves that can be injected into the fiber. In this way, the main research line in BOTDA sensors is focused on the study of the physical limitations of the technique as well as the development of solutions to these constraints. Another important line relies on the simplification of the sensor setup so as to reduce the complexity and the cost of the sensor. This thesis dissertation contributes to the development of BOTDA sensors by means of different contributions in these two research lines.

Several theoretical and experimental studies have been conducted to accurately determine the main limits to the sensor performance in terms of the maximum optical power of the pump and probe waves that can be used. One of the most important limitation in BOTDA sensors is the onset of non-local effects, which limits the maximum pump and probe waves power that can be injected in the fiber, and hence, the signal-to-noise ra-

tio (SNR) at the receiver is worsen. The so-called non-local effects generate measurement errors, because the Brillouin spectra measured at distant locations depend on the interaction at previous positions in the fiber. In this research line, we have examined the effects caused by the limited extinction ratio (ER) of the pump pulse, finding that, among other impairments, it leads to the onset of a new non-local effect originated in the depletion of the pedestal of the pump wave. In addition, it has been found that the pedestal deformation caused by the transient response of erbium-doped fiber amplifiers, which are typically deployed to amplify the pump pulse, also constrains the performance of the sensor. Another contribution is the study of the techniques presented in the literature to mitigate the impairments caused by second-order non-local effects, which cause a frequency-dependent spectral deformation of the pulse. The findings of this study show that these techniques are only applicable when the Brillouin frequency shift (BFS) of the fiber is uniform, which is hard to find in real applications. Lastly, another subject of study is the limitations of the pump and probe optical power in coded-pump wave BOTDA configurations. We have observed that, in addition to some known limitations, there are two important restrictions that have to be taken into account: the onset of non-local effects and the non-linear amplification of the probe wave, both generated by the successive gain induced by the multiple pulses of the coded-pump wave.

As a consequence of the findings of these studies, BOTDA configurations intended to solve these limitations have also been proposed during the thesis work. A technique to mitigate the constraints induced by the limited ER of the pump pulse has been presented. This method is based on adding a dithering to the optical source used to generate the two waves involved in the BOTDA sensor, so that the optical wavelength of both signals is modulated. In this way, the Brillouin interaction between the pedestal and the probe wavefronts become uncorrelated, and hence, the influence of the pedestal is greatly reduced. Another contribution is a technique focused on completely overcome the onset of second-order non-local effects. This method is based on continuously tracking the BFS distribution of the fiber, which combined with the probe-dithering method, has allowed, to the best of our knowledge, to inject the highest demonstrated probe wave power in a BOTDA sensor to date. In addition, in order to improve the SNR of the sensor, a novel BOTDA sensor has been proposed. This analyzer combines mono-color cyclic coding and probe-dithering techniques, so that the impairments caused by a coded pump wave are reduced, and hence, it is possible to increase the optical power and consequently enhance the sensing distance range.

Finally, a novel simplified BOTDA sensor has been presented, which relies on passive optical filtering of the spectral components generated in a single optical source. In this way, the sensor setup is simplified reducing the number of optical devices, and therefore, the cost of the sensor is also reduced. This BOTDA configuration has been shown to have a performance comparable to more complex setups.

Contents

List of Figures

List of Tables

Contents

Motivation

The development of optical fiber communications has revolutionized the telecommunications industry, making distance no longer a barrier to broadband communication. The use of optical fiber cables has allowed the optical communications to achieve telecommunication links over much larger distances due to a significant reduction of the attenuation of the signal level in the transmission medium, and, probably the more important, it has enabled the use of higher data rates due to the large bandwidth of the fiber. This, in turn, has led to an important deployment of optical fiber cables around the world.

Throughout the last decades, the development of fiber optic sensors (FOS) has benefited from the deployment of optical fiber cables and the growth of fiber optic communications. Among other applications, FOS have been used to monitor parameters such as temperature, pressure, vibration, gas concentration or fluid levels. Compared to other sensing technologies, as for instance electric sensors, FOS offer some advantages, such as a small size, a very wide operating range or immunity to electromagnetic and radio-frequency interference. In addition, FOS can be placed in passive networks, so that they do not need external power supplies, opening the field to remote sensing. Due to all these reasons, FOS are an attractive and competitive solution for different applications in which other technologies could not be placed.

There are different FOS technologies available at the market, which can be grouped into two types of sensors: the point sensors, like for instance fiber Bragg grating sensors or interferometric sensors, and the so-called distributed sensors. The main difference between both types of sensors lies in the way they monitor the structure. The point sensors only analyze the particular point where they are placed, whereas the distributed sensors uses the optical fiber as the sensing element, i.e., the optical fiber is the transducer, and hence, distributed sensor allow measuring every few meters over all along the conventional optical fiber. In this way, with distributed sensors there are not blind spots that cannot be sensed, unlike using point sensors that can only measure in the specific locations where the sensors have been placed. This is the main advantage of distributed sensors when compared to point sensors.

This characteristic of distributed fiber sensors makes them enormously interesting when many points of a structure need to be monitored. In this case, a single distributed fiber sensor can replace many point sensors, which considerably reduces the cost per sensing point when monitoring large structures. This is the reason for the success of distributed

fiber sensors. In addition, a further reduction in costs comes from the fact that standard telecommunication optical fibers without any modification can be deployed as transducers. For all these reasons, distributed fiber sensors have become an important technology in the field of structural health monitoring. Therefore, these kind of sensors are increasingly being used. As a consequence of the proliferation of distributed FOS, their global market size was valued at USD 708.6 million in 2016, and is expected to reach USD 2.39 billion by 2025, according to a new report by Grand View Research, Inc [1].

Distributed fiber sensors are based on different kinds of scattering phenomena such as Raman, Rayleigh or Brillouin scattering. Among the different scattering phenomena used in distributed fiber sensors, the ones based on stimulated Brillouin scattering are of great interest. This is due to the ability to monitor strain and temperature changes in long distances with high spatial resolution. With this technology, resolutions in the millimeter range can be achieved in short fibers. However, it is in long range measurements where Brillouin sensors stand out, since measurements over more than 100 km have been achieved with 1-m spatial resolution.

When the fiber is embedded within materials and structures, distributed Brillouin sensors provide information of changes that the structure is suffering in the form of strain, cracks, temperature variations, and others like for instance nuclear radiation. Due to the capability to measure these changes, Brillouin based sensors can be deployed in many practical fields, such as in civil and structural engineering to monitor bridges, tunnels, dams, in nuclear power plants, assessment of high voltage cables, railway inspection, or monitoring of oil and gas pipelines, among many other structural health monitoring applications. In addition to the long range applications, distributed Brillouin sensors also provide the ability to dynamically assess the state of short structures, such as the monitoring of wind turbine blades. The numerous applications described above and the interest of other industries make Brillouin distributed sensors a very interesting tool. However, there are still some impairments that constrain the performance of these sensors. Therefore, especial effort must be made in order to improve the performance of Brillouin distributed sensors and also to increase the applications in which these kind of sensors can be used.

Objectives of the thesis

The main objective of this thesis dissertation is to contribute to improve the performance of Brillouin optical time-domain analysis (BOTDA) sensors, which is one of the most studied and developed type of Brillouin distributed sensor. In order to achieve this general goal, we have focused our research work into two different lines. On the one hand, the thesis introduces the study of some limitations of BOTDA sensors that constrain its performance. As will be presented in this thesis, one of the major constraints faced by BOTDA sensors is the maximum optical power of the two optical waves involved in the technique, the continuous probe wave and the pulsed pump wave, that can be injected into the fiber before the onset of several detrimental effects. On the other hand, solutions to these and other impairments and limitations of BOTDA sensors are presented and analyzed. The following lines represent the different research field addressed during this

thesis:

- Study of the impairments caused by non-local effects in BOTDA sensors, which are amongst the main obstacles on the performance of BOTDA sensors. First-order and second-order non-local effects, which are due to the depletion and the spectral deformation of the pump pulse, respectively, introduce measurement errors, because the Brillouin spectra measured at distant locations depend on the interaction at previous positions in the fiber. In addition, we have analyzed the limitations imposed by the low extinction ratio (ER) of the pump pulses in a BOTDA sensor, studying the negative impact that the low ER has on non-local effects.

- Study and analyze the multiple advantages of the probe-dithering technique. This technique, which was devised in our research group, is based on adding a frequency modulation to the probe wave, so that the wavelength of both the pump and probe waves is uncorrelated. This leads to a significant reduction of several limitations of BOTDA sensors.

- The signal-to-noise ratio (SNR) is the parameter that ultimately defines the performance of the sensor. Therefore, it is of paramount importance the enhancement of the SNR. In this way, we investigated techniques to improve the SNR of the sensor.

- One of the main limitations of BOTDA sensors is their cost, which makes them out of reach from industries where the final cost is a major restriction. This is due to the fact that most BOTDA setups, in order to generate the optical waves involved in the technique, use expensive components. Therefore, we investigate methods that are focused on simplifying the existing BOTDA setups, so as to reduce the final cost of the sensor.

Structure of the thesis

The content of this thesis dissertation is divided in seven chapters.

The first chapter is an introduction to BOTDA sensors. To that end, first of all it is essential to understand the physical underpinnings of the Brillouin scattering phenomena. Then, the different types of Brillouin distributed optical fiber sensors are introduced, with particular emphasis describing BOTDA sensors, considering that these kind of sensors are the ones studied in this thesis. After that, the different factors that limit the performance of BOTDA sensors are discussed together with the proposed solutions at the current state of the art.

In chapter 2, the origins of non-local effects in BOTDA sensors are introduced, as well as their detrimental consequences. Specifically, first-order and second-order non-local effects are presented, together with the main proposals made to overcome, or at least mitigate, the constraints that these effects bring on.

In chapter 3 the effects caused by the limited ER of the pump pulse are studied. First, the increment of first-order non-local effects is analyzed, and then two previously unknown

non-local effects are described. To do this, we conduct a theoretical investigation together with experimental measurements, which clarify and properly explain the details of these effects.

In chapter 4, we theoretically and experimentally proved how all the techniques presented to date to reduce second-order non-local effects are only valid if the fiber has a uniform Brillouin frequency shift (BFS). In addition, a new technique to completely overcome second-order non-local effects is presented, which is based on continuously tracking the BFS of the fiber. Finally, we show how the technique based on dithering of the optical source used to generate the pump and probe waves mitigate the constraints induced by the limited ER of the pump pulses.

In chapter 5, the different coding techniques used to enhance the SNR in BOTDA sensors are presented, focusing on the mono-color cyclic coding technique. Next, two important limitations in a coded pump pulse BOTDA sensor are introduced. These limitations are due to the onset of first-order non-local effects and because of the non-linear amplification of the probe that the successive pulses of the coded pump wave involves. Afterward, a new BOTDA sensor based on combining mono-color cyclic coding and probe-dithering techniques is presented, which improves the SNR of the sensor.

In chapter 6, another research line is introduced: the simplification of the setup in order to reduce the cost of the sensor. The chapter begins by providing details of some of the most important contributions to simplify the configuration of BOTDA sensor presented to date, and then, a novel approach to simplify the sensor setup is introduced.

Finally, chapter 7 summarizes the conclusions obtained from the work carried out during this thesis, and also presents the open lines of this thesis.

Chapter 1: Introduction to distributed optical fiber sensors based on Brillouin scattering

Contents

1.1 Introduction

In recent years, fiber-optics communication has been used as one of the main information channels, by sending pulses of light through the optical fiber. That is why there is currently a large deployment of fiber optics around the world, which will increase in the coming years. However, apart from communication purposes, fibers optics can be used to detect, to monitor, and even to measure external perturbations.

Traditionally, the different sensing methods have been relied on measuring at predetermined points, nevertheless, in recent years the demand for distributed measurements has been grown. This, in turn, has led to a proliferation of distributed fiber sensors. This technology uses the optical fiber as the sensing element, without any additional transducers in the optical path. Distributed fiber sensing is a technology that enables continuous, real-time measurements along the entire length of a fiber optic cable. In this manner, distributed optical fiber sensing is the only physical-contact sensor technology capable of accurately estimating physical fields with spatial continuity along the fiber. In addition,

as the fiber is the sensor, it is also a cost-effective method. Therefore, distributed optical fiber sensors can play an essential role in many monitoring applications [2, 3].

Distribute fiber sensors are based on scattering phenomena, employing either Rayleigh, Raman, or Brillouin scattering (see Fig. 1.1). The components of the scattered light can be down-shifted in frequency (Stokes component), or shifted to higher frequencies (anti-Stokes components). In particular, the principle of operation of Rayleigh and Brillouin scattering based sensors relies on the scattering phenomena induced by fluctuations in the optical properties of the fiber, which may be associated with local or temporary changes of the refractive index. Depending on the scattering process, the sensor allows to measure different physical quantities. The contributions of this thesis dissertation are focused on improving distributed measurements of temperature and strain using the Brillouin scattering effect. Accordingly, this chapter will describe the working principles of Brillouin based distributed fiber sensors, so as to gain a better understanding of this technique.

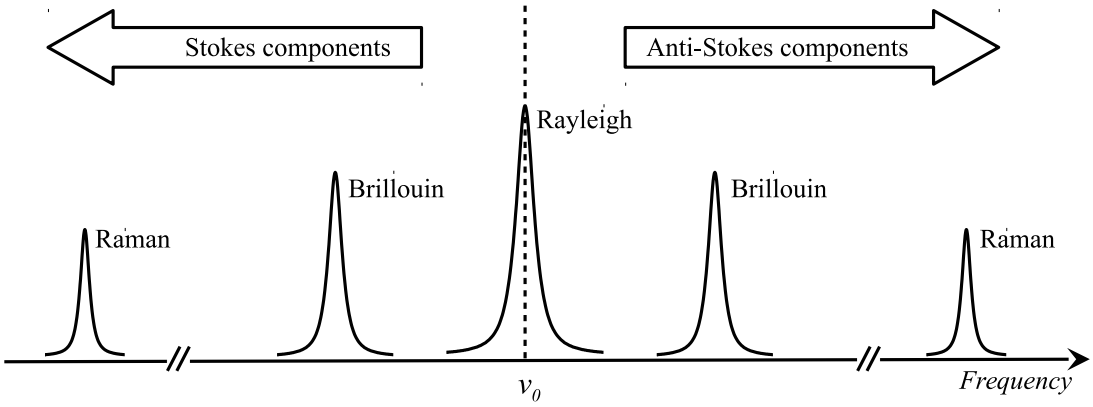

Figure 1.1: *Schematic spectrum of scattered light resulting from three scattering processes in inhomogeneous medium.*

The chapter begins with a detailed explanation of the spontaneous and stimulated Brillouin scattering effects in optical fibers. Afterward, different types of Brillouin based distributed sensors are described, before focusing on the Brillouin optical time-domain analysis (BOTDA) sensors, which is the primary aim of the research developed in this thesis dissertation. Hence, a detailed study of BOTDA sensors is performed, by developing the classical theoretical model for the Brillouin interaction of the optical waves involved in the technique and, also, by discussing the factors that limit such sensors. Finally, the current state of the art is reviewed, which is defined to a great extent by the several limiting factors of the BOTDA technique.

1.2 Brillouin scattering

Brillouin scattering is an effect caused by the non-linearity of a medium, specifically by that part of the non-linearity which is related to acoustic phonons [4]. In other words, is an effect caused by acoustic vibrations in the medium, as for instance an optical fiber, when a laser light travels through it. Depending on the intensity of the incident light beam, one can distinguish between spontaneous and stimulated scattering effects. When

the intensity of the injected light into the medium is low, the effect occurs spontaneously, and hence, the fluctuations that cause the light scattering are excited by thermal or by quantum-mechanical zero-point effects [5]. On the other hand, once the intensity of the incident light exceeds a certain threshold, the scattering effect becomes stimulated, since the fluctuations are induced by the presence of the light beam itself [5]. In the following, both scattering processes will be described in detail.

1.2.1 Spontaneous Brillouin scattering in optical fibers

Spontaneous Brillouin scattering (SpBS) can be described by the analysis of the pressure waves that induce fluctuations in the dielectric permittivity. In order to describe the SpBS effect, the equation of motion for a pressure wave (Δp) should be used. Which is a well-known equation from the field of acoustics and is given by [5]:

$$\frac{\partial^2 \Delta p}{\partial t^2} - \Gamma \nabla^2 \frac{\partial \Delta p}{\partial t} - v_a \nabla^2 \Delta p = 0 \tag{1.1}$$

where Γ is a damping parameter and v_a is the velocity of the acoustic wave in the medium, which can be expressed in terms of thermodynamic variables as [5]:

$$v_a = \sqrt{\frac{K_s}{\rho}} = \sqrt{\frac{1}{C_s \rho}} \tag{1.2}$$

where K_s is the bulk modulus, ρ is the density of the medium and C_s is the constant entropy of the compressibility. For instance, in fused silica the acoustic velocity is $v_a = 5.97x10^3$ m/s.

As an illustration of the nature of the acoustic wave equation (Eq. (1.1)), the propagation wave can be considered as follows [5]:

$$\Delta p = \Delta p_0 \exp\left[i\left(\mathbf{q}\cdot\mathbf{r} - \Omega t\right)\right] + \text{c. c.} \tag{1.3}$$

where Ω is the frequency of the acoustic wave and satisfies the dispersion relation $\Omega = v_a|\mathbf{q}|$, and $\mathbf{q}$ is its wave vector. In order to study the interaction between the incident beam light and the acoustic wave, the incident optical field is given by [5]:

$$\mathbf{E} = E_0 \exp\left[i\left(\mathbf{k}\cdot\mathbf{r} - \omega t\right)\right] + \text{c. c.} \tag{1.4}$$

where ω is the optical frequency of the incident field and $\mathbf{k}$ is the wave vector. The scattered field obeys the driven wave equation [5]:

$$\nabla^2 \mathbf{E} - \frac{n^2}{c^2}\frac{\partial^2 \mathbf{E}}{\partial t^2} = \frac{1}{\epsilon_0 c^2}\frac{\partial^2 \mathbf{P}}{\partial t^2} \tag{1.5}$$

where n is the refractive index of the medium, c is the speed of light in vacuum, $\mathbf{E}$ is the electric field of the wave, ϵ_0 is the permittivity of free space, and $\mathbf{P}$ is the polarization field induced by electric dipoles.

Let's us consider the case in which the scattering of the light occurs as the result of fluctuations in the dielectric constant and in which these fluctuations are themselves the

result of fluctuations in thermodynamic variables. In this case, the polarization depends linearly on the electric field as follows [5]:

$$\mathbf{P} = \Delta\chi\mathbf{E} = \Delta\epsilon\mathbf{E} \tag{1.6}$$

where $\Delta\chi$ is the fluctuation of the dielectric susceptibility and $\Delta\epsilon$ is the fluctuation of the dielectric constant averaged over the scattering volume. Assuming the dynamical behavior of the density fluctuations that give rise to light scattering, Eq. (1.6) leads to [5]:

$$\mathbf{P} = \epsilon_0 \left(\frac{\partial\epsilon}{\partial\rho}\right)\left(\frac{\partial\rho}{\partial p}\right)\Delta p\,\mathbf{E} = \epsilon_0\gamma_e C_s \Delta p\,\mathbf{E} \tag{1.7}$$

where γ_e is the electrostrictive constant given by [5]:

$$\gamma_e = \left(\rho\frac{\partial\epsilon}{\partial\rho}\right)_{\rho=\rho_0} \tag{1.8}$$

Finally, by combining Eq. (1.5) through Eq. (1.3), it is found that the scattered field must obey the following wave equation [5]:

$$\begin{aligned}\nabla^2\mathbf{E} - \frac{n^2}{c^2}\frac{\partial^2\mathbf{E}}{\partial t^2} = -\frac{\gamma_e C_s}{c^2}\Big[&(\omega-\Omega)^2 E_0\Delta p_0^* \exp\left[i\left(\mathbf{k}-\mathbf{q}\right)\cdot\mathbf{r} - i\left(\omega-\Omega\right)t\right] \\ &+ (\omega+\Omega)^2 E_0\Delta p_0 \exp\left[i\left(\mathbf{k}+\mathbf{q}\right)\cdot\mathbf{r} - i\left(\omega+\Omega\right)t\right] + \text{c. c.}\Big]\end{aligned} \tag{1.9}$$

Note that the first term in this expression leads to the Brillouin Stokes scattering component with frequency $\omega' = \omega - \Omega$ and wave vector $\mathbf{k}' = \mathbf{k} - \mathbf{q}$ [5]. Whereas the second term results in the Brillouin anti-Stokes scattering component with frequency $\omega' = \omega + \Omega$ and wave vector $\mathbf{k}' = \mathbf{k} + \mathbf{q}$ [5]. In both cases, the frequency and the wave vector of the incident optical field are related according to [5]:

$$\omega = |\mathbf{k}|\frac{c}{n} \tag{1.10}$$

In addition, the frequency (Ω) and the wave vector of the acoustic wave ($\mathbf{q}$) satisfy the following relationship [5]:

$$\Omega = |\mathbf{q}|\upsilon_a \tag{1.11}$$

This component of the polarization can efficiently couple energy to the scattered Brillouin optical wave only if ω' and $\mathbf{k}'$ are related by the dispersion relation for optical waves, namely [5]:

$$\omega' = |\mathbf{k}'|\frac{c}{n} \tag{1.12}$$

In order to satisfy the requirements of Eqs. (1.10) through (1.12) simultaneously, the sound-wave frequency and wave vector must each have a particular value for any scattering direction [5]. Figure 1.2 and 1.3 show the relation that acoustic, incident and scattered

waves must satisfy in the case of Stokes and anti-Stokes for the case of scattering at the angle θ, respectively.

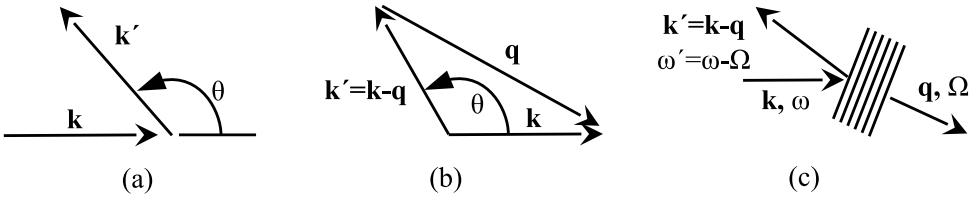

Figure 1.2: *Illustration of Stokes Brillouin scattering.*

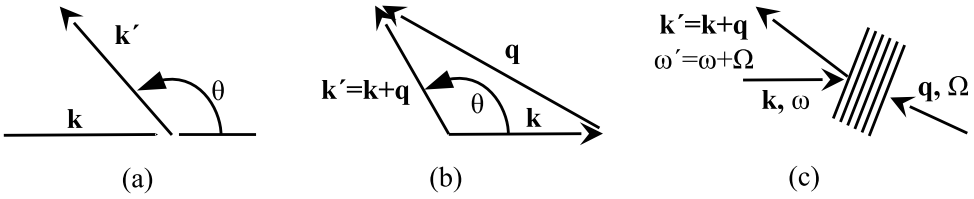

Figure 1.3: *Illustration of anti-Stokes Brillouin scattering.*

Part (a) of Figs. 1.2 and 1.3 shows the relative orientations of the wave vectors of the incident and scattered fields. Figure 1.2(b) and 1.3(b) depicts how the wave vector of the acoustic disturbance is related to those of the incident and scattered optical radiation for both Brillouin components, Stokes and anti-Stokes, respectively. Finally, as shown in Fig. 1.2(c), Stokes scattering can be visualized as the scattering of light from a retreating acoustic wave propagating in the same direction of the incident light, whereas as illustrated in Fig. 1.3(c), the anti-Stokes component can be considered as scattering resulting from an oncoming acoustic wave with respect to the direction of the incident light.

Conservation of momentum and energy

The momentum of the acoustic phonons of Brillouin scattering grows proportionally to the phonon frequency, by a proportional factor given by the acoustic velocity of the medium. Any scattering process must accomplish the conservation of both momentum and energy [6]. Therefore, the energy and the momentum must be conserved during the interaction, and hence, by applying this energy and momentum conservation to the 3 interacting waves in the Stokes case, defined in Table 1.1, the following relation is obtained [7]:

$$\text{Energy conservation:} \qquad \frac{h}{2\pi}\omega = \frac{h}{2\pi}\left(\omega' + \Omega\right) \tag{1.13}$$

$$\text{Momentum conservation:} \qquad h\,\mathbf{k} = h\left(\mathbf{k}' + \mathbf{q}\right) \tag{1.14}$$

where h is the Planck constant. As Ω is much smaller than the optical frequencies, it can be assumed that $\mathbf{k}$ has a close value to $\mathbf{k}'$, which is valid for both Stokes and anti-Stokes components. Therefore, the wave vector of the acoustic wave can be expressed as [5]:

$$|\mathbf{q}| = 2|\mathbf{k}|sin\left(\frac{\theta}{2}\right) \tag{1.15}$$

Now, considering that the acoustic velocity is much smaller than the light velocity, the dispersion relation given by Eq. (1.11) shows that the acoustic frequency is [5]:

$$\Omega = \frac{2n\omega v_a}{c} \sin\left(\frac{\theta}{2}\right) \tag{1.16}$$

From this expression it follows that the acoustic frequency depends on the angle of the scattered light. In this way, Ω is equal to zero for forward scattering ($\theta = 0$), and maximum for backward scattering ($\theta = \pi$). Hence, the maximum frequency shift, known as the Brillouin frequency shift (BFS), occurs for backward scattering and is given by [8, 5]:

$$\Omega_B = \frac{2n\omega v_a}{c} = \frac{2n\omega}{c}\sqrt{\frac{(1-\Theta)E_1}{(1-2\Theta)(1+\Theta)\rho}} \tag{1.17}$$

where Θ is Poisson's ratio and E_1 is the Young's modulus.

Note that in a single-mode fiber (SMF), the scattered light can only propagate in two possible directions, forward or backward. Therefore, Brillouin scattering signal is a backscattered light, which for the 3-th optical transmission window (~ 1550 nm) exhibits its maximum frequency shift ($\nu_B = \Omega_B/2\pi$) close to 10.8 GHz.

	Frequency	Wave vector	Relation
Incident wave	ω	$\mathbf{k}$	$\omega = \lvert\mathbf{k}\rvert\,(c/n)$
Scattered Stokes wave	$\omega' = \omega - \Omega$	$\mathbf{k}' = \mathbf{k} - \mathbf{q}$	$\omega' = \lvert\mathbf{k}'\rvert\,(c/n)$
Acoustic wave	Ω	$\mathbf{q}$	$\Omega = \lvert\mathbf{q}\rvert v_a$

Table 1.1: *Frequencies and wave vectors of the 3 waves involved in Brillouin scattering process and the relation between the frequency and the wave vector.*

Brillouin spectrum and linewidth

So far, the attenuation of the acoustic wave has been ignored in the analysis. However, the Brillouin scattered light of a monochromatic incident light has a certain linewidth due to the attenuation of the acoustic wave presented in Eq. (1.3). Substituting the acoustic wave propagation introduced in Eq. (1.3) into the acoustic wave equation, Eq. (1.1), it follows that q and Ω must be related by the following dispersion relation [5]:

$$\Omega^2 = q^2\left(v_a^2 - i\Omega\Gamma\right) \tag{1.18}$$

This expression can be rewritten as follows [5]:

$$q^2 = \frac{\Omega^2}{v_a - i\Omega\Gamma} = \frac{\Omega^2/v_a^2}{1 - i\Omega\Gamma/v_a^2} \simeq \frac{\Omega^2}{v_a^2}\left(1 + \frac{i\Omega\Gamma}{v_a^2}\right) \tag{1.19}$$

From this equation it is found that [5]:

$$q \simeq \frac{\Omega}{v_a} + \frac{i\Gamma_B}{2v_a} \tag{1.20}$$

where $\Gamma_B = \Gamma q^2$ is the phonon decay rate (also called acoustic damping coefficient). Substituting the latter expression into Eq. (1.3), it is observed that the acoustic wave intensity varies spatially as [5]:

$$|\Delta p\,(z)\,|^2 = |\Delta p_0|^2 \exp\left(-\alpha_{snd} z\right) \tag{1.21}$$

where α_{snd} is the acoustic absorption coefficient given by [5]:

$$\alpha_{snd} = \frac{\Gamma_B}{\upsilon_a} \tag{1.22}$$

so that the average lifetime of the acoustic phonon in the medium can be defined as [5]:

$$\tau_p = \frac{1}{\Gamma_B} \tag{1.23}$$

As a consequence of the acoustic-wave absorption presented in Eq. (1.21), it emerges that, in the frequency domain, the Brillouin components are not monochromatic and exhibit a Lorentzian spectral profile given by [5]:

$$g_B\,(\nu) = g_0 \frac{\left(\Delta\nu_B/2\right)^2}{\left(\nu - \nu_B\right)^2 + \left(\Delta\nu_B/2\right)^2} \tag{1.24}$$

where $\Delta\nu_B = \Gamma_B/2\pi$ is the full-width at half-maximum Brillouin linewidth and g_0 is the peak value of the Brillouin gain coefficient occurring at resonance $\nu = \nu_B$.

1.2.2 Stimulated Brillouin scattering in optical fibers

As mentioned above, SpBS is an effect that can be observed under low intensity conditions, whereas stimulated Brillouin scattering (SBS) occurs when higher intensities are injected in the medium. This high optical intensity alters the optical properties of the medium and, hence, the scattering turns into a stimulated process, which is typically more efficient than the previously presented spontaneous scattering effect. In this section the details of the stimulated process are introduced.

As a result of the high intensities used to stimulate the process, the total polarization, $\mathbf{P}$, induced by the electric dipoles is a non-linear function of the electric field, $\mathbf{E}$, given by [9]:

$$\mathbf{P} = \epsilon_0 \left(\chi^{(1)}\mathbf{E} + \chi^{(2)}\mathbf{E} + \chi^{(3)}\mathbf{E} + \dots\right) \tag{1.25}$$

where $\chi^{(j)}$ $(j = 1, 2, 3, \dots)$ is the j-th order susceptibility. $\chi^{(1)}$ is the linear susceptibility and, under normal conditions, optical fibers do not exhibit second-order non-linear effects. Actually, non-linear effects in optical fibers are mainly dominated and originated from the $\chi^{(3)}$, leading to phenomenas such as the Kerr effect and stimulated scattering. Thus, the polarization field induced by the electric dipoles is now a non-linear function of the electrical field given by [9]:

$$\mathbf{P^{NL}} = \epsilon_0 \chi^{(3)} \vdots \mathbf{EEE} \tag{1.26}$$

Taking into account the attenuation coefficient of the medium, α, and the non-linear induced polarization field, $\mathbf{P^{NL}}$, the perturbed wave equation shown in Eq. (1.5) can be defined as [10]:

$$\nabla^2\mathbf{E} - \frac{n^2}{c^2}\frac{\partial^2\mathbf{E}}{\partial t^2} - \frac{\alpha n}{c}\frac{\partial\mathbf{E}}{\partial t} = \mu_0\frac{\partial^2\mathbf{P^{NL}}}{\partial t^2} \tag{1.27}$$

where μ_0 is the magnetic permittivity in vacuum. SBS is a non-linear process generated due to the interaction between a laser beam, a Stokes wave and an acoustic wave [9]. Specifically, the beating of the laser and the acoustic wave tends to boost the Stokes wave, while the interference of the laser wave and Stokes waves tends to reinforce the acoustic wave. Under appropriate conditions, the positive feedback created by both interactions entails an exponential growth of the amplitude of the Stokes wave. There are two different physical mechanisms by which the interference of the laser wave and the Stokes wave can drive the acoustic wave: electrostriction and optical absorption [5]. Absorptive SBS can occur only in lossy optical media, so that is less commonly used than electrostrictive SBS [5]. For this reason, only the electrostrictive case will be studied in this chapter.

Electrostriction

Electrostriction is a property of all electrical non-conductors, or dielectrics, that causes a compression of the material under the application of an electric field [5]. The great interest in the electrostriction effect is due to two reasons: because it is a mechanism that leads to a third-order non-linear optical response and, also, as a coupling mechanism that leads to SBS [5].

In this sense, SBS process is a consequence of an electrostriction effect that occurs in an optical fiber due to the interference generated between two counter-propagated signals: a pump wave and a probe wave. When the frequency detuning between both waves is around the BFS of the fiber, an acoustic wave is generated through electrostriction. The generated acoustic wave modulates the refractive index of the fiber and, hence, generates a moving Bragg grating that scatters the pump wave.

Due to the Doppler effect [11], when the acoustic wave propagates in the same direction than the pump wave the scattered light is down-shifted in frequency, whereas it is up-shifted otherwise. In the first case, the Stokes wave is added constructively to the probe wave, reinforcing the acoustic wave. And, in the second case, the anti-Stokes wave is depleted due to the energy transferred to the pump wave.

From a global point of view, the origin of the electrostrictive force can be understood as a consequence of the maximization of stored energy [5]. Therefore, the potential energy per unit volume of a material located in an electric field of field strength, E, can be obtained by [5]:

$$u = \frac{1}{2}\epsilon\epsilon_0 E^2 \tag{1.28}$$

where ϵ is the relative dielectric constant. Consequently, the total amount of energy of the system, $\int u\ dV$, is maximized by allowing the slab to move into a region with a

strongest field.

On the other hand, from a microscopic point of view, this effect can be considered as an acting force on each individual molecule placed in the electric field, developing a dipole moment [5]. Molecules are extracted from the surrounding medium into the region between the capacitor plates, increasing the density in this region. As a consequence of the increase in density, the dielectric constant changes from ϵ to the value $\epsilon + \Delta\epsilon$, where $\Delta\epsilon$ is defined as follows [5]:

$$\Delta\epsilon = \left(\frac{\partial\epsilon}{\partial\rho}\right)\Delta\rho \tag{1.29}$$

As a result, the field energy density changes following the expression [5]:

$$\Delta u = \frac{1}{2}\epsilon_0 E^2 \Delta\epsilon = \frac{1}{2}\epsilon_0 E^2 \left(\frac{\partial\epsilon}{\partial\rho}\right)\Delta\rho \tag{1.30}$$

Nevertheless, in accordance with the first law of thermodynamics, this change in energy, Δu, must be equal to the work made in compressing the material; where the work done per unit volume is given by [5]:

$$\Delta w = p_{st}\frac{\Delta V}{V} = -p_{st}\frac{\Delta\rho}{\rho} \tag{1.31}$$

where p_{st} is the strictive pressure, defined as the contribution to the pressure of the material that is due to the presence of the electric field. Now, considering that $\Delta u = \Delta w$, the strictive pressure is obtained by [5]:

$$p_{st} = -\frac{1}{2}\epsilon_0\rho\left(\frac{\partial\epsilon}{\partial\rho}\right)E^2 = -\frac{1}{2}\epsilon_0\gamma_e E^2 \tag{1.32}$$

Note that since p_{st} is negative, the total pressure is reduced in regions of high field strength. In addition, the fluid tends to be drawn into these regions and the density increases. This change in density can be written considering Eq. (1.32) as [5]:

$$\Delta\rho = -\rho\left(\frac{1}{\rho}\frac{\partial\rho}{\partial p}\right)p_{st} = -\rho C p_{st} \tag{1.33}$$

where $C = \rho^{-1}\left(\partial\rho/\partial p\right)$ is the compressibility of the medium. By combining Eq. (1.32) with Eq. (1.33), the change in density can be obtained by [5]:

$$\Delta\rho = \frac{1}{2}\epsilon_0\rho C\gamma_e\langle\mathbf{E}\cdot\mathbf{E}\rangle \tag{1.34}$$

where the angular brackets denote a time average over an optical period. The changes in the susceptibility in the presence of an optical field are represented as $\Delta\chi = \Delta\epsilon$, where $\Delta\epsilon$ is calculated as $\left(\partial\epsilon/\partial\rho\right)\Delta\rho$, and $\Delta\rho$ is given by Eq. (1.34). In addition, if two monochromatic waves that differ by approximately the BFS of the fiber are assumed, so that $\langle\mathbf{E}\cdot\mathbf{E}\rangle = 2\mathbf{E}\cdot\mathbf{E}^*$, then it leads to [5]:

$$\Delta\chi = \epsilon_0 C_T\gamma_e^2\mathbf{E}\cdot\mathbf{E}^* \tag{1.35}$$

Consequently, the complex amplitude of the non-linear polarization fields can be represented as [5]:

$$\mathbf{P^{NL}} = \epsilon_0 C_T \gamma_e^2 |\mathbf{E}|^2 \mathbf{E} \tag{1.36}$$

By combining this equation with the perturbed wave equation presented in Eq. (1.27) for the two optical waves involved in the SBS effect, and considering the acoustic wave, the coupled-wave equations for SBS can be calculated, which are introduced below.

Theoretical model of SBS (steady-state solution)

The complete interaction process described above between the probe wave, the pump signal and the acoustic wave, generates SBS in optical fibers. This process can be modeled (in time and space, under the assumption of plane-wave interaction) by the following system of three coupled equations [5]:

$$\left[\frac{\partial}{\partial z} + \frac{n}{c}\frac{\partial}{\partial t} + \alpha_P\right] E_P(z,t) = \frac{i\omega_P \gamma_e}{2nc\rho_0} Q E_S(z,t) \tag{1.37a}$$

$$\left[-\frac{\partial}{\partial z} + \frac{n}{c}\frac{\partial}{\partial t} + \alpha_S\right] E_S(z,t) = \frac{i\omega_S \gamma_e}{2nc\rho_0} Q^* E_P(z,t) \tag{1.37b}$$

$$\left[-2iqv_a^2\frac{\partial}{\partial z} - 2i\Omega\frac{\partial}{\partial t} + \left(\Omega_B^2 - \Omega - i\Omega\Gamma_B\right)\right] Q(z,t) = \epsilon_0 \gamma_e q^2 E_P(z,t) E_S^*(z,t) \tag{1.37c}$$

where $E_S(z,t)$, $E_P(z,t)$ and $Q(z,t)$ are the slowly-varying envelopes of the pump, Stokes and acoustic waves, respectively; ω_P and ω_S are the pump and Stokes frequencies, respectively; α_P and α_P are the attenuation coefficients for the pump and the Stokes wave, respectively; and ρ_0 is the density of silica fiber.

Unfortunately, this system of equations does not have an analytical solution. So, in order to obtain a solution, the previous system of equations can be solved either directly, through numerical integration, or analytically but with some preliminary simplifications. In this sense, the three wave equations system can be solved using the steady-state approach, provided that the interaction of the waves is longer than the acoustic lifetime (τ_p). In such a situation, all time derivatives can be neglected [7]. Moreover, the acoustic velocity is much smaller than the light velocity, so that the acoustic wave can be considered as static and, in addition, it vanishes after propagation over a few optical wavelengths (distance over which any change of the optical field is negligible [7]). Consequently, the spatial derivative of Eq. (1.37c) is set equal to zero. After considering all these approximations, Eq. (1.37c) can be simplified, and the amplitude of the acoustic wave can be directly solved following [7]:

$$Q(z) = \epsilon_0 \gamma_e q^2 \frac{E_P(z) E_S^*(z)}{\Omega_B^2 - \Omega^2 - i\Omega\Gamma_B} \tag{1.38}$$

Considering that the frequencies of pump and probe waves are close in the optical range ($\omega = \omega_S \approx \omega_P$), the attenuation experienced by both optical waves can be considered approximately equal ($\alpha = \alpha_S \approx \alpha_P$). Using this assumption and substituting Eq. (1.38)

into Eqs. (1.37a) and (1.37b), the coupled-wave equations of pump and Stokes fields are found to be [5]:

$$\frac{d}{dz}E_P(z) = \frac{i\epsilon_0\omega\gamma_e^2 q^2}{2nc\rho_0}\frac{|E_S(z)|^2 E_P(z)}{\Omega_B^2 - \Omega^2 - i\Omega\Gamma_B} - \alpha E_P(z) \tag{1.39a}$$

$$\frac{d}{dz}E_S(z) = -\frac{i\epsilon_0\omega\gamma_e^2 q^2}{2nc\rho_0}\frac{|E_P(z)|^2 E_S(z)}{\Omega_B^2 - \Omega^2 + i\Omega\Gamma_B} + \alpha E_S(z) \tag{1.39b}$$

From Eq. (1.39b) it follows that SBS is a pure gain process, whose gain depends on the optical intensity. Defining the intensity as $I(z) = 2n\epsilon_0 c|E(z)|^2$, the coupled intensity equations can be found as [5, 9]:

$$\frac{d}{dz}I_P(z) = -g_B(\nu)\, I_P(z)\, I_S(z) - \alpha I_P(z) \tag{1.40a}$$

$$\frac{d}{dz}I_S(z) = -g_B(\nu)\, I_P(z)\, I_S(z) + \alpha I_S(z) \tag{1.40b}$$

where I_P and I_S are the intensities of pump and Stokes waves, respectively, and g_B is the Brillouin gain transfer defined by Eq. (1.24), where the peak value of the Brillouin gain coefficient is given by [5]:

$$g_0 = \frac{\gamma_e^2\omega^2}{nv_a c^3\rho_0\Gamma_B} \tag{1.41}$$

In order to solve the system of equations in (1.40), the depletion of the pump wave must be neglected, so that the pump intensity exponentially decays along the fiber due to the attenuation of the fiber ($I_P(z) = I_P(0)\exp(-\alpha z)$, where $I_P(0)$ is the pump intensity at the input of the fiber in $z = 0$). On this basis, using Eq. 1.40a and integrating it over the fiber length, L, the following analytical solution for the Stokes wave is found [9]:

$$\begin{aligned} I_S(z) = I_S(L)\exp\left[-\alpha(L-z)\right]\cdot \\ \cdot\exp\left[g_B(\nu)\, I_P(0)\exp(-\alpha z)\,\frac{1-\exp\left[-\alpha(L-z)\right]}{\alpha}\right] \end{aligned} \tag{1.42}$$

where $I_S(L)$ is the injected optical intensity of the Stokes wave at $z = L$, i.e., in the opposite extreme of the fiber from where the pump wave is introduced. Note that the expression in brackets of the second exponential term represents the whole interaction length of I_S from $z = L$ to $z = 0$. From this expression the well-known parameter of the effective length of the fiber can be obtained, which is conventionally defined from $z = 0$, obtaining [9]:

$$L_{eff} \equiv \frac{1-\exp(-\alpha L)}{\alpha} \tag{1.43}$$

Eq. (1.42) shows that the Stokes wave intensity grows exponentially due to SBS along its propagation through the fiber and, at the same time, the intensity is attenuated due to the attenuation coefficient of the optical fiber.

SBS threshold

As shown in Eq. (1.42), the injected Brillouin Stokes intensity grows exponentially as it propagates through the fiber due to Brillouin amplification occurring as a result of SBS [9]. However, in absence of this initially injected signal, the Stokes wave grows from noise or SpBS that is initiated by phonons resulting from thermal agitation in the fiber when a high pump power is used. The pump power at which the Stokes component at $z = 0$ is equal to the pump power at the fiber output, $z = L$, is defined as the Brillouin threshold. The critical pump power defined as the SBS threshold can be obtained following [9]:

$$P_{th}^{SBS} \approx 21 \frac{A_{eff}}{g_0 L_{eff}} \tag{1.44}$$

where A_{eff} is the effective area. Using the typical parameters for SMFs in the 3-th window of optical communication systems (1550 nm), i.e., A_{eff} =80 μm^2, $L_{eff} \approx 22$ km ($\alpha = 0.2$ dB/km) and g_0 =1.5·10^{-11} m/W, the critical power is approximately 5.6 mW, which makes SBS a dominant non-linear process in optical fibers.

1.3 Distributed fiber sensors based on Brillouin scattering

The SBS effect can be used to detect temperature or strain changes of the optical fiber in a distributed manner. This is because there is a linear dependence of the BFS with the refractive index and the acoustic velocity of the optical fiber, as it can be deduced from Eq. (1.17). In addition, note that, from this expression, it follows that the acoustic velocity depends on the density and Young's modulus of the fiber. Therefore, as the BFS depends on the effective refractive index and the acoustic velocity of the fiber, and these, in turn, vary whenever the local environmental temperature and strain conditions change, the BFS value is modified. In this way, by monitoring changes in the BFS along the fiber length, it is possible to map out the distribution of temperature or strain over long distances [9]. Furthermore, it has been proved that BFS variations show an excellent linearity for both physical phenomenons, temperature and strain, over a wide range [8, 12]. This relationship can be described with the following expression [13]:

$$\nu_B\left(T, \delta\epsilon\right) - \nu_{B0} = A \cdot \delta\epsilon + B \cdot \left(T - T_0\right) \tag{1.45}$$

where ν_{B0} is the BFS measured at reference temperature, T_0, and in loose state of the fiber, $\delta\epsilon$ is the strain difference, T is the temperature, A is the strain coefficient in units of MHz/$\delta\epsilon$ and B is the temperature coefficient in units of MHz/°C. The strain and temperature normalized coefficients, A' and B', are given by [13]:

$$A' = \frac{A}{\nu_{B0}} = \frac{\partial n}{n\partial\epsilon} - \frac{\partial\rho}{2\rho\partial\epsilon} + \frac{\partial E_1}{2E_1\partial\epsilon} \tag{1.46a}$$

$$B' = \frac{B}{\nu_{B0}} = \frac{\partial n}{n\partial T} - \frac{\partial\rho}{2\rho\partial T} + \frac{\partial E_1}{2E_1\partial T} \tag{1.46b}$$

where E_1 is the second-order non-linear coefficient of Young's modulus of the fiber. In

addition to the dependence of the BFS, there exist another reliance between the Brillouin gain and linewidth with the temperature or strain [14]. However, the BFS is the parameter measured with highest resolution and, hence, the most interesting for distributed Brillouin fiber sensors. On the other hand, Brillouin gain and linewidth measurements are usually neglected since they are more sensible to noise.

There exist different types of Brillouin distributed sensors, and they are classified depending on the principle used to scan the Brillouin spectrum along the fiber:

- The techniques that measure in the correlation domain, denominated Brillouin optical correlation-domain analysis (BOCDA) sensors.
- The techniques that measure in the frequency domain, denominated Brillouin optical frequency-domain analysis (BOFDA) sensors.
- The techniques that measure in the time domain, depending if they are based on spontaneous or stimulated Brillouin scattering, are called Brillouin optical time-domain reflectometry (BOTDR) sensors or Brillouin optical time-domain analysis (BOTDA) sensors, respectively.

During the following subsections, the BOCDA, BOFDA and BOTDR techniques will be described, to finally focus in the most interesting among them, the BOTDA sensor. The latter will be explored in detail, since the aim of this thesis is to contribute to the development of this particular type of Brillouin distributed sensor.

1.3.1 Brillouin optical correlation-domain analysis sensors

The method based on the correlation domain, the BOCDA technique, was proposed for the first time in 2000 [15]. The BOCDA system is a very attractive solution to achieve high spatial resolution measurements, in the millimeter range, over short distances [15]. From its beginnings, this technique has been enhanced substantially [16]. Among other important achievements, we could highlight the detection of variations of temperature or strain with a length of a few millimeters [17], or the reduction of the measurement time [18].

The BOCDA technique is based on the counter-propagation of two frequency modulated signals with a frequency difference near the BFS of the fiber: a continuous wave (CW) pump and a probe wave. In addition, both waves are identically frequency-modulated by a sinusoidal function. Thus, when both waves counter-propagate through the fiber, their frequency difference is kept constant for some points of the fiber (called correlation peaks), whereas the frequency difference continuously varies in the rest of the fiber. Considering that both waves are frequency-shifted by the BFS of the fiber, the maximum energy exchange due to SBS occurs at these correlation peak positions. On the contrary, in the rest of the fiber, as the frequency difference is further away from the BFS, the Brillouin transfer is significantly smaller.

By sweeping the frequency difference between pump and probe, the whole Brillouin spectrum is scanned. In order to scan different sections of the fiber, the correlation peak must appear in different positions of the fiber. This can be easily performed by simply

varying the modulation frequency applied to the signals and repeating again the frequency swept, so that the whole length of the fiber is scanned. It must be remarked that the frequency of the sinusoidal function and the delay induced by one of the branches must be carefully selected to have just one correlation peak in the fiber, and hence, scan only one point of the fiber.

The spatial resolution is defined by the modulation depth and the Brillouin intrinsic linewidth, and consequently, it can reach high spatial resolution measurements. However, there are three main drawbacks of this technique. The first one is that the length of the fiber that can be monitored is related to the spatial resolution, considering that both depends on the modulation frequency, in such a way that by increasing the fiber length, the spatial resolution worsens. The second is the complexity of the setup. Finally, the third one is that the measurement time increases with the resolution, since each point of the sensing fiber must be individually scanned before continuing with the next point.

1.3.2 Brillouin optical frequency-domain analysis sensors

BOFDA sensors are based on the frequency domain and were firstly presented in 1996 [19]. As with the BOCDA technique, BOFDA sensors deploy two counter-propagating signals: a probe wave and a CW pump. The technique is based on the measurement of the distributed transfer function of the fiber given by the relation between the amplitudes of the pump and probe waves. For that purpose, the probe wave is frequency-shifted by the BFS and its amplitude is modulated by a sine function. After SBS interaction with the counter-propagating pump signal, the probe is detected and demodulated using the same frequency varying signal by two separate photoreceivers that fed a network analyzer. The procedure is repeated by changing the frequency modulation of the sinusoidal function. Afterward, the network analyzer provides the transfer function of the fiber by performing the Inverse Fourier Transform of the acquired data, so that the Brillouin response for each section of the fiber is retrieved.

This technique can provide measurements with high spatial resolution, which depends on the modulating frequency variation range. However, in contrast to the previously presented BOCDA technique, the spatial resolution is limited by the lifetime of the acoustic phonons and, consequently, by the Brillouin gain spectrum (BGS) linewidth. This makes the interaction for high spatial resolution to become very weak, leading to a low signal-to-noise ratio (SNR). Therefore, the performance of this sensor is worse than other Brillouin distributed fiber sensors. Nevertheless, recently, its ability to carry out high performance measurements has been demonstrated, by use of a post-processing method that allows to monitor 5.5 km with 3 cm of spatial resolution, proving this kind of sensor as a valid solution for distributed sensing [20].

1.3.3 Brillouin optical time-domain reflectometry sensors

BOTDR sensors are based in SpBS in the fiber, and were firstly presented in 1995 [21]. This technique is named after OTDR techniques, because the measuring technique and setup, although more complicated, is really similar to that of an OTDR. In this method

there is not an externally injected Stokes wave, so, just a pulsed pump wave is launched into the fiber. Therefore, as the pulsed pump wave propagates through the fiber and interacts with thermally excited phonons, a Stokes wave is generated in the opposite direction. Finally, the Stokes wave is monitored at the start of the fiber.

The signal arriving at the photoreceiver at each moment has been generated at a particular position of the fiber by the pulsed pump wave, so that its frequency difference with the pump wave gives the BFS, and consequently, the characteristics of the fiber at that point. Note that the only difference with OTDR sensors is that the monitored signal is the Stokes wave instead of the Rayleigh backscattered signal. For this reason, a filtering process is required to avoid any crosstalk between the two signals. In BOTDR sensors, the spatial resolution is given by the length of the pump pulse, and hence, there is a limit in spatial resolution due to the phonon lifetime, which is near 1-m.

BOTDR sensors have some advantages compared to other Brillouin distributed sensors. Firstly, the sensor configuration needed to perform such measurements is simpler compared to the other Brillouin distributed sensing setups. In addition, only access at one end of the fiber is needed, which is a characteristic that is well suited for some applications. However, since the Stokes wave is generated from the interaction with noise, the generated signal is weak and noisy. Therefore, the performance of the sensor is worse than other types of distributed Brillouin sensors. In any case, recent enhancements of the setup have led to long range measurements [22, 23], or measurements with a spatial resolutions below 1-m [24, 25].

1.3.4 Brillouin optical time-domain analysis sensors

The most widely used Brillouin distributed sensors are based on the BOTDA technique, and were first demonstrated in 1990 for temperature and strain monitoring [26, 27]. From then on, BOTDA technology has been extensively researched due to its potential applicability in numerous fields [2, 28, 29]. The operating principle of the technique is depicted in Fig. 1.4. As shown in Fig. 1.4(a), the sensor relies on the Brillouin interaction between two counter-propagating signals in the fiber: a pulsed pump wave and a CW probe. Therefore, the principles of BOTDA sensors are very similar to those of the BOTDR technique, but in this case the measurements are based on SBS.

During the propagation of the two waves along the fiber, an acoustic wave is locally generated at each position where the pulse and the probe wave meet, whose characteristics depend on the fiber section where both signals are located. In this way, an exchange of energy between both optical waves is generated. Depending on the relative optical frequency of the probe and pump waves, the probe wave experiences amplification or depletion at each location of the fiber. Specifically, if the probe wave frequency (ν_S) is smaller than the pump wave frequency (ν_P) and the frequency difference is close to the BFS, the probe wave is amplified, otherwise the probe wave is depleted. Therefore, two different measurement configurations for BOTDA sensors can be implemented: the so-called Brillouin gain ($\nu_P - \nu_S \approx \nu_B$) and Brillouin loss ($\nu_S - \nu_P \approx \nu_B$) configurations [30], which are highlighted in Figs. 1.4(b) and 1.4(c), respectively. It should be pointed out that

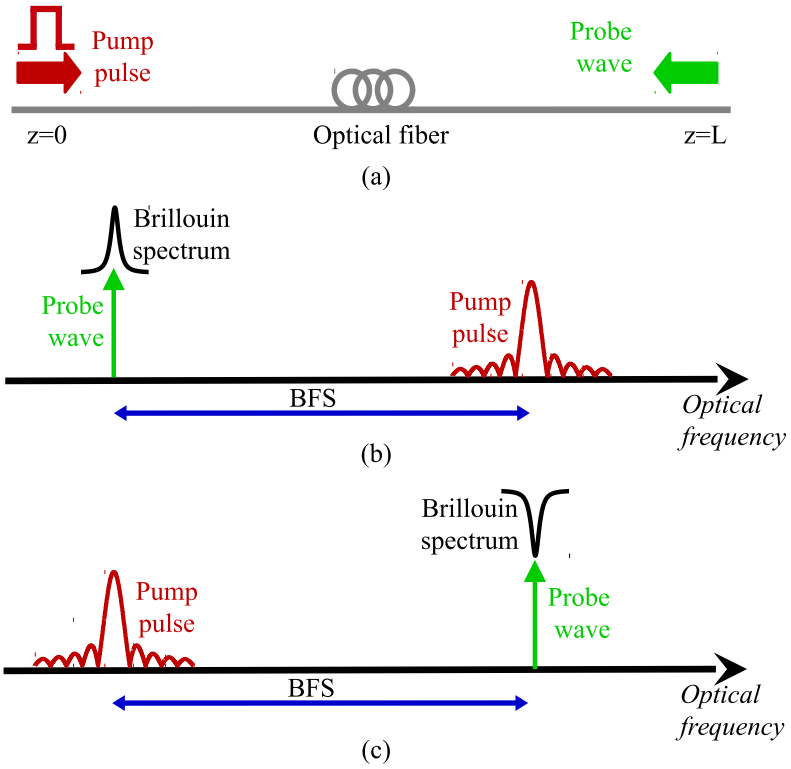

Figure 1.4: *Operation principle of BOTDA: (a) pulsed pump wave and a CW signal counter-propagates through an optical fiber. (b) Energy transfer from pump to probe signal in a Brillouin gain configuration. (b) Energy transfer from pump to probe signal in a Brillouin loss configuration.*

in normal conditions both configurations are equivalent in terms of performance [31].

By monitoring the probe wave at the output of the fiber, the gain/loss generated for a certain frequency shift between pump and probe is measured. That is, the time-dependent information of the probe wave serves as reference to measure the Brillouin gain/loss for a given frequency detuning. Figure 1.5 depicts the detected probe wave power as a function of time or distance in a gain configuration at the output of the fiber (BOTDA trace). As it can be observed, the probe wave arriving at each moment to the end of the fiber has been amplified at a given localization in the fiber by the pump pulse. This temporal evolution of the probe wave can be directly translated to a position-dependent information using the following round-trip time relation:

$$z = \frac{c}{2n} t \tag{1.47}$$

where t is the time since the pump pulse signal enters the fiber and z the particular location where the pulse and the probe wave meet.

In addition, the amplitude of the detected probe wave at each moment depends on the frequency shift between pump and probe waves and the BFS of the given fiber section. Therefore, in order to measure the BFS of the fiber, it is necessary to determine the frequency difference at which the gain/loss is maximum for each location of the fiber. For that purpose, a frequency sweep of the frequency difference between pump and probe waves

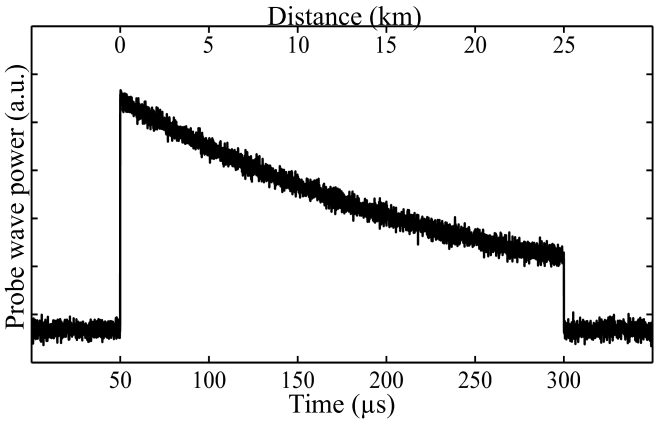

Figure 1.5: *Evolution of the probe wave power in BOTDA sensors along the fiber for a given frequency difference between probe and pump waves.*

must be performed, and store each time-domain BOTDA trace that has been obtained. Ordering the measured traces, the Brillouin gain/loss spectrum for each point of the fiber is reconstructed, which can be seen in Fig. 1.6 for a gain configuration. Finally, the accurate BFS of the fiber is obtained by fitting the measured spectra to the theoretical model for the Brillouin gain presented in Eq. (1.24).

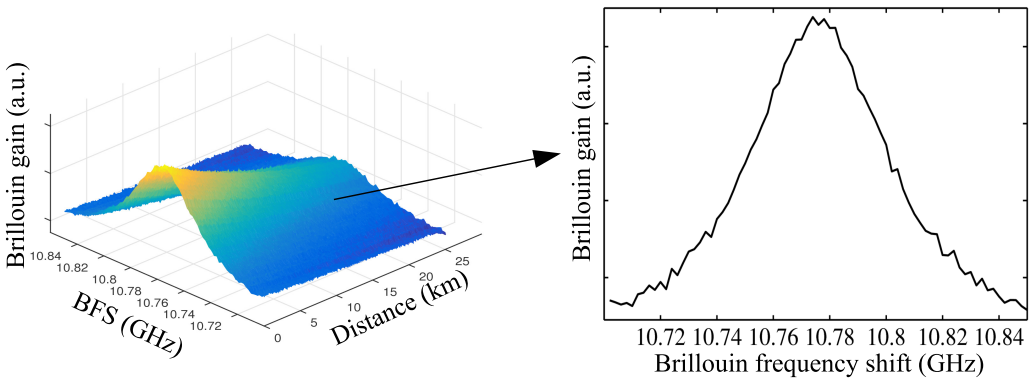

Figure 1.6: *Reconstructed Brillouin gain distribution spectra along the fiber.*

1.4 Theoretical modeling of BOTDA sensors

As previously mentioned, BOTDA sensors can operate in gain or loss configuration. In this section a Brillouin gain configuration ($\nu_S < \nu_P$) will be assume for theoretical explanation. However, this model can be directly extrapolated to a loss configuration by simply changing the sign for the Brillouin interaction term in the equations.

With this in mind, it is worth remembering that, in a gain configuration, as the pulsed signal propagates along the fiber, it transfers energy to the probe wave. If we consider optical pulses longer than the phonon lifetime ($\sim$ 10 ns), the steady-state equation system introduced in (1.39) can be used to model the SBS pump-probe interaction. In order to facilitate the understanding of the explanation, the system of equations is repeated here and is also simplified by the use of Eq. 1.41, giving rise to:

$$\frac{d}{dz}E_P(z) = \left[-\frac{g_0}{2}\frac{i\Delta\nu_B}{i\Delta\nu_B + 2\Delta\nu}|E_S|^2 - \frac{\alpha}{2}\right]E_P \tag{1.48a}$$

$$\frac{d}{dz}E_S(z) = \left[-\frac{g_0}{2}\frac{i\Delta\nu_B}{i\Delta\nu_B - 2\Delta\nu}|E_P|^2 + \frac{\alpha}{2}\right]E_S \tag{1.48b}$$

where E_P and E_S are the optical field of pump and probe waves, respectively, and $\Delta\nu = \nu_S - \nu_P + \nu_B$ is the detuning of the probe wave frequency from the Brillouin peak frequency. Note that the pump pulse is injected from $z = 0$ location of the fiber, whereas the probe wave is introduced from $z = L$. Assuming that the pulsed signal is only affected by the fiber attenuation through its propagation, i.e., the Brillouin interaction is negligible, then Eq. (1.48a) can be directly solved, obtaining:

$$E_P(z) = E_{Pi}\exp\left[-\frac{\alpha}{2}z\right] \tag{1.49}$$

where E_{Pi} is the pump wave optical field at the input of the fiber. Then, the probe optical field can be calculated substituting the latest equation into Eq. (1.48b), so that the Brillouin interaction experienced by the probe wave at a particular location, z, is calculated as:

$$E_S(z - \Delta z) = E_S(z)\exp\left[\frac{g_0}{2}\frac{(\Delta\nu_B/2)^2 - i(\Delta\nu\Delta\nu_B/2)}{(\Delta\nu_B/2)^2 + \Delta\nu^2}|E_P(z)|^2\Delta z\right] \tag{1.50}$$

where $\Delta z = T_P \cdot c/(2n)$ is the spatial resolution of the system and T_P is the temporal pulse duration. Note that in Eq. (1.50), due to the short interaction length between both optical waves, a constant pump pulse power has been considered during the Brillouin interaction, i.e., the pulse attenuation has been ignored. In addition, from Eq. (1.50) it can be deduced that the probe field changes in amplitude and phase due to the SBS process just at the particular z location where it meets the pulse. However, at all other locations along the fiber, the probe wavefronts are only attenuated, so that at the receiver the optical field can be calculated as:

$$E_S(z)\Big|_{rx} = E_{Si}\exp\left(-\frac{\alpha}{2}L\right)\exp\left(\frac{g_0}{2}\frac{(\Delta\nu_B/2)^2 - i(\Delta\nu\Delta\nu_B/2)}{(\Delta\nu_B/2)^2 + \Delta\nu^2}|E_P(z)|^2\Delta z\right) \tag{1.51}$$

where E_{Si} is the input probe optical field at the beginning of the fiber in $z = L$. By replacing Eq. (1.49) into Eq. (1.51) and calculating the detected optical power, the following expression is obtained:

$$P_S(z)\Big|_{rx} = P_{Si}\exp(-\alpha L)\exp\left(\frac{g_0}{A_{eff}}\frac{(\Delta\nu_B/2)^2}{(\Delta\nu_B/2)^2 + \Delta\nu^2}P_{Pi}\exp(-\alpha z)\Delta z\right) \tag{1.52}$$

where P_{Pi} and P_{Si} are the injected optical powers of the pump and probe waves, respectively. Assuming that the Brillouin gain is very small, and hence, considering that

BOTDA sensors operate in a small signal regime, Eq. (1.52) can be further simplified, giving rise to:

$$P_S(z)\Big|_{rx} \approx P_{Si}\exp(-\alpha L)\left[1+\frac{g_0}{A_{eff}}\frac{(\Delta\nu_B/2)^2}{(\Delta\nu_B/2)^2+\Delta\nu^2}P_{Pi}\exp(-\alpha z)\,\Delta z\right] \tag{1.53}$$

where the second term in the bracket represents the Brillouin gain. Note that the Brillouin gain is proportional to the gain coefficient, the local pump power and the pulse duration [32]. In addition, the Brillouin gain at a distant L must propagate back to the receiver and, therefore, the fiber attenuation turns to be doubled ($\exp(-2\alpha L)$). This fact is essential to understand how the sensing distance affects on the detected signal of BOTDA traces at the far end of the fiber [32]. Therefore, under standard BOTDA conditions, the worst-case sensor precision is at the far end of the fiber, where the detected optical power of the probe wave is given by [32]:

$$P_S(L)\Big|_{rx} \approx P_{Si}\exp(-\alpha L)+\frac{g_0}{A_{eff}}\frac{(\Delta\nu_B/2)^2}{(\Delta\nu_B/2)^2+\Delta\nu^2}P_{Pi}P_{Si}\exp(-2\alpha L)\,\Delta z \tag{1.54}$$

1.5 State of the art and main limitations in BOTDA sensors

The research of BOTDA sensors is mainly focused on analyzing the fundamental factors that determine their ultimate performance, which are defined by the needs of the potential application fields of this sensing technology. In addition, great efforts are made to enhance the performance of the sensor by overcoming the constraints of the technique.

The objective of BOTDA sensors is to characterize the temperature and strain profile of the fiber by obtaining the BFS of the latter, with the highest precision and as many sensing points along the fiber as possible. Note that the precision of the measurements is related to the uncertainty of BOTDA sensors when calculating the BFS, which can be defined by the standard deviation of the BFS. In a recent work, the relation between the standard deviation of the BFS and the parameters of the measured Brillouin spectrum has been established [32]. This is done by calculating the propagation of errors on the parameters obtained from a least-square parabolic fit, giving rise to the propagated error on the estimated resonance central frequency, expressed as [32]:

$$\sigma_{BFS}(z)=\frac{1}{SNR(z)}\sqrt{\frac{3\cdot\delta\cdot\Delta\nu_B}{8\sqrt{2}(1-\zeta)^{3/2}}} \tag{1.55}$$

where δ is the frequency sampling step and ζ is the fraction of the peak level over which the quadratic least-square fitting is carried out. Note that the SNR compares the power level of the BOTDA signal to the power level of the background noise (total noise power of the system).

As observed in Eq. (1.55), the accuracy of the sensor depends on the SNR parameter, the Brillouin linewidth and the data used for the parabolic fit. Thus, the standard deviation

of the BFS can be enhanced by increasing the probe power, increasing the pump power or by enlarging the number of points scanned within the Brillouin spectrum. Nevertheless, all these improvement mechanisms are limited by different phenomenons. In addition, it is worth mentioning that Eq. (1.55) does not take into consideration the complexity and cost of the sensor, which are of paramount importance in many application fields.

During the following subsections, the main limitations on BOTDA sensors will be explained, as well as the principal proposed solutions to solve or alleviate them.

1.5.1 Non-local effects and spontaneous Brillouin scattering

As it has been explained, the accuracy of the sensor can be improved by increasing the probe wave power, because this results in an enhancement of the SNR. However, the maximum probe power that can be injected in the fiber is firstly limited by the onset of the so-called non-local effects [31, 33], and secondly by the onset of intense amplified SpBS [34].

In a BOTDA sensor, as mentioned above, two counter-propagating optical waves interact exchanging energy via SBS process: a CW probe and a pump pulse [35]. Due to this interaction, the pump pulse wave is exposed to frequency dependent distortions, which, in turn, lead to measurement errors [31, 33]. This results in the need to reduce the probe wave power at the beginning of the fiber, which directly implies a worsening of the SNR. To date, two non-local effects have been studied, the so-called first-order non-local effects, which are due to the depletion of the pump pulse [35, 31], and second-order non-local effects, that are related to the onset of linear distortion of the pump pulse spectrum [33]. The study of non-local effects is an important contribution of this thesis dissertation, and hence, the physical origins of these effects will be fully explained in chapter 2. In addition, in chapters 3, 4 and 5 we introduce important contributions in relation to non-local effects that have been studied throughout this thesis dissertation.

On the other hand, another important limitation comes from the injection of high power components into the optical fiber, which can lead to SBS amplification of thermally-induced SpBS waves. This effect limits the maximum probe wave power that can be injected in the fiber by the so-called Brillouin threshold of the fiber [36]. This threshold establishes the maximum probe wave power that can be injected in a fiber before a significant power begins to reflect back and, consequently, the launched signal is depleted. Moreover, it has been found that when injecting a probe wave power above the Brillouin threshold, there is an important noise addition to the detected probe wave [36, 34]. The theoretical limit imposed by the Brillouin threshold of the fiber is around 6 dBm for a typical SMF [34].

1.5.2 Modulation instability, self-phase modulation and spontaneous Raman scattering

Another alternative to enhance the performance of BOTDA sensors is to increase the pump pulse power. However, the maximum pump pulse power is limited by the onset of non-linear effects such as modulation instability (MI) or self-phase modulation(SPM).

MI appears in optical fibers when the optical power of the pump pulses is very large. This effect is the consequence of the interplay between anomalous dispersion and the

Kerr effect in the fiber [37]. The onset of this effect causes depletion on the pump pulse power [38, 39] and it can also distorts the sensor performance [40]. As a consequence, two symmetric sidebands are generated around the frequency of the pump pulse [37], and during the propagation of the pump wave through the fiber, there is a power exchange between these sidebands and the pump pulse. This leads to power fluctuations of the pump pulse, which are directly translated into the BOTDA trace. Consequently, some sections of the fiber are not correctly monitored due to the low SNR. Moreover, in some sections of the fiber, the pump pulse spectrum suffers such a broadening that can completely suppress the Brillouin gain.

In addition, in BOTDA sensors the pump pulse wave is typically amplified by an erbium-doped fiber amplifier (EDFA), increasing the amplified spontaneous emission (ASE). It has been observed that this background noise increases the effects of MI [37]. In order to reduce this impairment a filter can be used before launching the pump pulse into the fiber, so that the ASE is reduced [41]. The power limitation of the pump pulse power imposed by MI is around 20 dBm (for lengths longer than 22 km) [37]. Recently, a technique to mitigate the constraints of MI in Brillouin distributed fiber sensors has been presented [42]. This technique relies on the use of orthogonal polarization pulses to decrease the pump depletion due to MI.

The power limitation imposed by MI can also be mitigated by using dispersion shifted fibers (DSF) with normal dispersion [43]. This is due to the fact that DSFs have a normal dispersion at 1550 nm and, hence, the MI effect is eliminated. However, this kind of fiber presents a reduced effective area and a lower dispersion, so that favors the apparition of other non-linear effect, such as Raman scattering [39]. In this case, when Raman scattering occurs, a rapid pump depletion is observed, which severely limits the sensing distance range. In any case, the threshold limit is higher than for other non-linear effects, inasmuch as, for very long fibers, the maximum value of the pump pulse before the onset of spontaneous Raman scattering is around 30 dBm [39].

Another limitation related, in this case, to the power and the temporal shape of the pump pulse, is the onset of SPM. In long sensing fibers, when the temporal shape of the pulse is not completely rectangular, i.e., the rising and falling times of the pulse are not negligible, SPM can appear [44]. As a consequence, the pump pulses suffer a spectral broadening that can have significant effects on the measured Brillouin spectrum, and hence, cause a reduction of the measurement precision. However, this effect can be easily avoided by using perfectly shaped rectangular pump pulses with sharp rising and falling edges.

1.5.3 Extinction ratio of the pump pulse induce impairments

In the theoretical explanation of BOTDA sensors given in section 1.4, a pump pulse with an infinite extinction ratio (ER) has been assumed. Nevertheless, any practical device that is used to generate the pump pulses has a limited ER. Therefore, as highlighted in Fig. 3.1, there are various interactions that take place in the sensing fiber between the pump pulse wave with limited ER and the probe wave. On the one hand, there is the interaction between the pump pedestal with the probe wave, and on the other hand, the

previously studied interaction between the pulse and the probe wave. The net effect of the presence of the pulse pedestal is that the probe wave experiences more gain than just that due to the pulse itself [45].

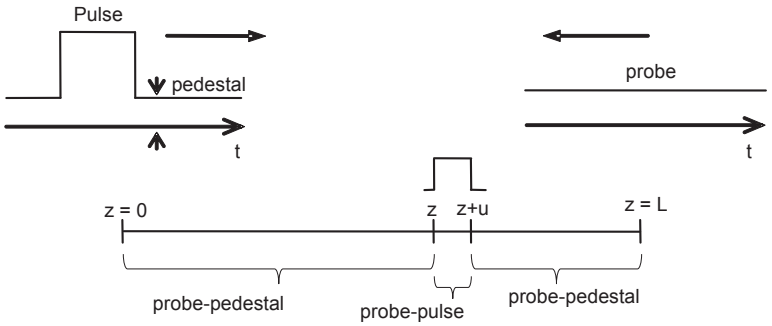

Figure 1.7: *Schematic depiction of probe and pump pulse wave interaction along the fiber.*

This extra gain experienced by the probe wave is not useful for sensing, quite the contrary, it leads to detrimental effects. The study of the constraints imposed by a limited ER pump pulse wave in a BOTDA sensor is one of the main contributions of this thesis dissertation, and will be explained in detail in chapter 3.

1.5.4 Signal-to-noise ratio of BOTDA sensors

During the last years, a great effort has been made to increase the sensing range of BOTDA sensors. This effort to enlarge the measurement range is mainly driven by applications where there is a need to monitor large structures, such as gas and oil pipelines, railways or power lines. In recent years, sensing distances up to 120 km in a normal configuration or 200 km in a fiber loop configuration have been achieved [46, 47].

As explained in section 1.4, specifically in Eq. (1.54), the attenuation of the probe and pump waves when crossing the fiber affects twice the measured Brillouin response at the far end of the fiber. Hence, the Brillouin signal is usually very weak, and consequently the detected SNR at the end of the fiber is reduced, leading to a poor performance of the sensor, as shown in Eq (1.55). The larger the fiber, the greater the signal attenuation and, therefore, the SNR worsens. Accordingly, the sensing range of BOTDA sensors is limited by the maximum pump and probe powers that can be injected in the fiber. A simple solution to enhance the SNR is to increase the number of averages, however, this solution also increases the measurement time.

As it has been discussed in previous subsections, the pump and probe power signals in BOTDA sensors need to be kept below the thresholds given by MI, Raman Scattering, SPM, non-local effects and noise induced by SpBS. An initial approach to improve the SNR consists in exceeding the different power threshold limits. This has been accomplished by different techniques, such as the frequency modulation of the probe waves [48, 49] or the use of orthogonal polarization pulses [42], which enable to increase the probe and pump pulse power, respectively.

Another alternative to enhance the SNR is to amplify the probe and/or the pump pulse waves. This has been demonstrated by the use of in-line EDFAs as pump pulse wave

repeaters along the sensing fiber [50]. However, this technique needs a power supply for the in-line EDFAs, which is inconvenient for its real applicability. Another solution is to use first-order or second-order distributed Raman amplification by injecting a Raman pump in the sensing fiber, so as to amplify the probe and/or pump powers along the fiber [51, 52, 53]. Nevertheless, this requires the use of a very high optical power in the fiber, so that the relative intensity noise (RIN) of the Raman pump laser can be translated to the detected probe wave, degrading the measurement performance [53]. The use of distributed Brillouin pump amplification to increase the pulse power is another effective solution to improve the SNR of the sensor [54, 55, 56].

In addition, it has been extensively studied the self-heterodyne detection technique for SNR improvement [57]. Another alternative to enhance the SNR of BOTDA sensors is the use of different coding techniques, such as Simplex coding [58], cyclic coding [59], bipolar coding [60] and color coding [61, 47], which have proved to be useful for long sensing range analyzers. In this thesis dissertation, we have contributed to the analysis of coding techniques in BOTDA sensors. In chapter 5, the different contributions made will be described, which consist in the analysis of several constraints in coded BOTDA sensors, as well as a novel technique that combines mono-color cyclic coding and probe-dithering techniques. In addition, in chapter 5, in order to have a better understanding of the contributions, a detailed analysis of coding techniques will be made. On the other hand, in recent years, a solution focused on intensifying the response of distributed optical fiber sensors using 2D and 3D image restoration methods has been presented [62, 63].

Finally, another point of view to improve the SNR is to reduce the noise level of the system [64]. In this way, some numerical solutions suggest that the performance of BOTDA sensors is limited by RIN, so that reducing this noise the sensing distance could be considerably increased [65]. Recently, it has been identified that Raman-assisted BOTDA sensors are limited by RIN transfer of the Raman laser [66]. Two different solutions have been proposed to reduce this noise [67, 68].

1.5.5 Number of resolved points: the spatial resolution

The spatial resolution (Δz) of the sensor is determined by the temporal pulse duration (T_P), which are related by:

$$\Delta z = T_P \cdot c/\left(2n\right) \tag{1.56}$$

The previous expression shows that the shorter the pulse duration, the better the spatial resolution of the sensor. For instance, for a given pulse duration of 10 ns, the spatial resolution of the analyzer is around 1-m. However, the use of short pulses introduces two important limitations. The first one is that as the Brillouin interaction is shorter, the obtained Brillouin gain is reduced (see Eq. (1.53)) and, hence, the SNR is worsen. On the other hand, when the duration of the pulse is shorter than the phonon lifetime (∼10 ns), the linewidth of the Brillouin spectrum considerably broadens from 30 MHz to more than 100 MHz, so that the accuracy of the sensor is worsen [69, 70]. Therefore, the spatial resolution of conventional BOTDA sensors is typically limited to 1-m.

During the last years, the improvement of the spatial resolution has been an area of intensive research that has concentrated great efforts. This is due to the fact that many potential applications of Brillouin distributed sensors require the highest possible spatial resolution. The vast majority of proposed techniques are based on a pre-excitation of the acoustic wave, so that it is possible to reach an steady-state response and a reduced linewidth of the Brillouin spectrum.

The first of the methods taking advantage of the pre-excitation of the acoustic wave is the so-called bright pulse technique, which uses pulses with a significant level of leakage [71]. That is, this technique is based on counter-propagating a CW probe with a pulse combined with a small CW component, so that the latter excites the acoustic wave before the pulse enters the fiber. Based on the previous technique, we can found the so-called Pulse Pre-pumping of BOTDA method [72]. However, instead of using a CW, it uses a pulse of low intensity to pre-activate the acoustic wave. Another way to pre-excite the acoustic wave, is by taking advantage of the so-called dark-pulse BOTDA technique [73]. This technique relies on the immediate interruption of the Brillouin scattering when one of the waves, either the probe or the pump wave, is switched off. In this way, the temporal suppression, or the length of the dark pulse, gives the spatial resolution of the sensor.

More recently, an enhanced physical explanation for the acoustic wave pre-excitation has been developed, leading to an optimized setup based on using optical phase-shift instead of optical intensity pulses [74]. The operating principle is similar to the one of dark-pulses technique, but the main advantage is that the response is twice larger for an identical pump power. Finally, for the application of high resolution measurements the so-called differential pulse-width pair technique was presented [70]. This technique relies on the subtraction of two different Brillouin measurements, which are made using pulses with a slightly different time duration, both larger than the phonon lifetime.

1.5.6 Measurement time and dynamic sensing

As explained in section 1.3.4, in BOTDA sensors the process to measure the Brillouin spectra distribution is carried out by sweeping the frequency difference between probe and pump waves. As a result of this frequency sweep, the measurement takes several seconds and even minutes. Therefore, due to this time consuming procedure, the use of BOTDA sensors is typically restricted to static measurements, since the detection of real time or dynamic events is not possible. However, in recent years, due to the growing interest of some applications to monitor vibrations in different structures, a new research trend consisting in reducing the BOTDA measuring time has been thoroughly studied.

The so-called slope-assisted (SA) BOTDA uses just one pump pulse and one probe wave at a fixed frequency shift, so that the probe wave lies in the slope of the BGS. Any strain/temperature change causes a variation in the frequency shift, and hence, it translates to amplitude variations of the BOTDA interaction, which are interpreted as a change of the BFS [75]. The relation between both parameters is given by the shape of the Brillouin gain spectrum. However, since the frequency of the probe and pump waves is fixed, initially this technique is valid just when the BFS of the fiber is uniform. This is because for a

fiber section with a BFS out of the measurement frequency range, given by the Brillouin spectrum, the section will not be monitored. To solve this and other constraints, over the years this technique has undergone different improvements and modifications, such as the use of SA BOTDA with tailored probe wave [76], the double SA BOTDA [77] or the multi-SA BOTDA sensor technique [78].

Another approach to reduce the measurement time and provide dynamic measurements is the so-called Sweep-free BOTDA [79, 80]. This method is based on counter-propagating a comb of probe and pump waves. That is, multiple probe waves simultaneously propagate in the fiber against an equal number of sequentially-launched short pump pulses of matching frequencies. In this way, each pair of probe and pump waves scan a different point of the Brillouin spectrum, and hence, the acquisition of the Brillouin spectrum is solely limited by the round-trip time of the measurement.

The so-called Fast BOTDA sensor is another dynamic analyzer [81]. The technique relies on the fast switching of the optical frequency that provides an electronic arbitrary waveform generator. Thus, the frequency difference between probe and pump is rapidly achieved, so that each frequency of the probe wave is launched one after the other with a period given by the round-trip time. Consequently, the speed of the sensor is basically limited by the fiber length and the number of required averages.

Finally, another solution has also been presented in recent years, the so-called Single-shot distributed BOTDA sensor for fast measurements [82]. In this analyzer, the distributed fiber can be monitored with only one-shot measurement. For that purpose, this method uses a dual-polarization probe with orthogonal frequency-division multiplexing modulation. In this way, in this scheme neither frequency scanning, nor polarization scrambling, nor averaging are required.

1.5.7 Techniques to simplify the configuration of BOTDA sensors

As it has been discussed in previous subsections, a significant number of research groups have focused their work on extending and improving the performance of BOTDA sensors. Nevertheless, in many potential applications, the most important limitation for the widespread practical use of BOTDA sensors is their cost rather than their current performance.

In Brillouin distributed sensors, the transducer itself, i.e., the standard SMF, is cheap. However, when compared to other sensing technologies, most BOTDA implementations are usually complex and expensive. This is because in order to generate the two optical waves involved in the technique use expensive components such as lasers, synthesized microwave generators, multiple electro-optic modulators, wide-band detectors, acousto-optic modulators or semiconductor optical amplifier switches. As a consequence, the final cost of the sensor is high, and hence, its real-world applicability is limited, being usually bounded to industrial sectors where the cost of the sensor is not the main concern, such as in the field of oil and gas.

For that reason, a great effort has been recently devoted to simplify the experimental setup of the sensor in order to achieve cost-effective commercial systems that can compete,

for instance, with simpler and less-costly distributed sensing techniques, such as Raman sensors for temperature measurements. Recent examples of simplified BOTDA schemes intended to reduce the cost of the sensor include the use of Brillouin generators or Brillouin fiber lasers to obtain the probe wave from the pump [83], the deployment of injection locking to generate the pump and probe waves using distributed feedback lasers [84] or the use of offset-locking [85], time-division pump-probe generation using direct modulation of a laser source [86, 87], or a BOTDA sensor with a pump-probe source based on Brillouin ring laser technology [88].

In chapter 6, a cost-effective BOTDA solution designed in this thesis will be presented, which is based on obtaining all the optical waves involved in the technique by passive optical filtering of the spectral components generated in a single optical source.

Chapter 2: Non-local effects in Brillouin optical time-domain analysis sensors

Contents

2.1 Introduction

During the last few decades, distributed fiber optic sensors based on the Brillouin scattering non-linear effect have been thoroughly researched, mainly due to their ability to provide high precision distributed temperature and strain measurements over extremely large structures. The most successful Brillouin distributed sensors to date are based on the Brillouin optical time-domain analysis (BOTDA) technique, where a pump pulse and a counter-propagating continuous wave (CW) probe interact in the sensing fiber under test (FUT). BOTDA technique can be highly useful for a number of structural health monitoring applications in several industrial sectors, for instance, ensuring the integrity of oil and gas pipelines, the structural health of bridges, tunnels and dams, the detection of fire in tunnels and industrial facilities, or assessing the temperature of sub-sea and underground electric power cables.

As mentioned in chapter 1, in recent years the research in BOTDA sensors has been focused on developing methods to improve their performance in terms of spatial resolution, sensing range and measurement time, as well as simplifying the deployed setups to reduce the cost of the sensor. However, in order to achieve these objectives, latest research on BOTDA sensors is increasingly focused on analyzing the fundamental factors that determine their ultimate performance.

One of the most fundamental limitations in BOTDA sensors comes from the maximum optical power of the pump and probe waves that can be injected into the sensing fiber, because this defines the signal-to-noise ratio (SNR) of the detected sensor response, which is the quantity that ultimately constrains the performance of the sensor [89]. In this context, as explained in chapter 1, the maximum pump pulse power that can be introduced in the fiber is fundamentally limited by the onset of modulation instability (MI) [37] or self-phase modulation [44]. Whereas the maximum probe power that can be deployed in the sensing fiber link is first limited by the so-called non-local effects [31, 33], and secondly by the Brillouin threshold of the fiber, over which significant noise is added to the detected probe signal due to spontaneous Brillouin scattering [34].

In this chapter, we review the physical origins of non-local effects [31, 33] and their consequences in BOTDA measurements. In addition, the different techniques that have been presented in recent years to mitigate the onset of non-local effects are introduced.

2.2 Fundamentals of first-order non-local effects

As previously introduced in chapter 1, two optical waves are used in a BOTDA sensor: a CW probe and a counter-propagating pump pulse. When these two waves have an optical frequency detuning close to the Brillouin frequency shift (BFS) of the fiber, they interact exchanging energy via stimulated Brillouin scattering (SBS) [35]. In a gain-based BOTDA, a pump pulse of higher optical frequency transfers energy to the probe wave that undergoes amplification at the cost of the pump pulse being depleted. On the contrary, in a loss-based BOTDA, the pump pulse has lower frequency and induces an attenuation of the probe by depleting its energy, whereas the pump pulse is amplified.

The probe wave only interacts with the pump pulse over a small length of the fiber, delimited by the pulse duration, which in turn provides the spatial resolution of the sensor, e.g., a 10-ns pump pulse duration corresponds to approximately 1-m spatial resolution. Therefore, the probe gain/loss, which is used for sensing, is rather small. On the other hand, the pump pulse is subjected to a continuous interaction with the probe wave as it crosses the fiber, losing/gaining a small percentage of energy at every step, so that the total accumulated depletion/amplification can be significant [35]. And, since the exchange of energy in the case of the pump pulse is cumulative all along the fiber, the effect reaches its highest level at the far end of the fiber. In this way, the longer the fiber, the higher the pulse depletion.

In the following, the theoretical fundamentals of non-local effects will be derived assuming a gain configuration of the sensor, which can be extrapolated to a loss configuration BOTDA by simply changing the signs of the SBS interaction equations. It must be mentioned that both configurations (gain and loss) show an equal performance regarding non-local effects, which leads to identical measurement errors [31].

In order to estimate the amount of depletion of the pump pulse resulting from the Brillouin interaction with the probe wave, it is mandatory to calculate the pump pulse optical power at the far end of the fiber. As explained above, the probe wave only interacts with the pump pulse over a restricted length of the fiber determined by the pulse duration, therefore, in a first approximation we can assume that the probe signal is only attenuated by the propagation through the optical fiber. Thus, to calculate the pump power, we neglect the probe amplification due to the interaction with the pulse. Consequently, the effect of the Brillouin interaction over the pulsed signal can be calculated directly solving Eq. (1.48a), which gives the pump field, induced by the Brillouin interaction, at the output of a fiber of length L:

$$E_P(L) = E_{Pi} \exp\left(-\frac{\alpha}{2}L\right) \exp\left[-\frac{g_0}{2}\frac{(\Delta\nu_B/2)^2 - i\,(\Delta\nu\Delta\nu_B/2)}{(\Delta\nu_B/2)^2 + \Delta\nu^2}|E_{Si}|^2 L_{eff}\right] \qquad 2.1$$

where E_{Pi} is the injected pump optical field at the input of the fiber ($z = 0$), α is the attenuation of the fiber, g_0 is the peak value of the Brillouin gain coefficient, $\Delta\nu_B$ is is the full-width at half-maximum (FWHM) Brillouin linewidth, $\Delta\nu$ is the frequency detuning between pump and probe waves, E_{Si} is the injected pump optical field at the input of the fiber ($z = L$) and $L_{eff} = (1 - exp(-\alpha L))/\alpha$. From this expression it can be deduced that, despite the fact that the pump pulse depletion increases with the length of the fiber, the amount of depletion stabilizes for fibers longer than the asymptotic non-linear effective length of the fiber, $Leff \approx 22$km (assuming an attenuation of the fiber of 0.2 dB/km).

The pump power at the output of the fiber can be calculated from Eq. (2.1) as follows:

$$P_P(L, \Delta\nu) = P_{Pi} \exp(-\alpha L) exp\left(-\frac{g_B(\Delta\nu)}{A_{eff}} P_{Si} L_{eff}\right) \tag{2.2}$$

where P_{Pi} is the optical power of the pump pulse at the beginning of the fiber, A_{eff} is the effective area of the fiber, g_B is the Brillouin gain coefficient defined in Eq. (1.24), which depends on $\Delta\nu$, and P_{Si} is the probe wave power at the input of the fiber. Note that, from this equation, it can be concluded that the depletion of the pump pulse shows a frequency dependence given by the natural Lorentzian response of the Brillouin interaction. In particular, the depletion of the pulse reaches its peak level when the frequency detuning between pump and probe waves is equal to the BFS of the fiber.

In a fiber with a constant BFS, the depletion of the pump pulse at the far end of the fiber for a particular frequency detuning can be characterized by a dimensionless depletion factor, which is given by [31]:

$$d(L, \Delta\nu) = \frac{P_{P_0}(L, \Delta\nu) - P_P(L, \Delta\nu)}{P_{P_0}(L, \Delta\nu)} \tag{2.3}$$

where, P_{P_0} is the pump pulse power in absence of Brillouin interaction, so that it is only depleted by the fiber attenuation ($P_{P_0} = P_{Pi} exp(-\alpha L)$). Replacing Eq. (2.2) into Eq. (2.3), the following expression is obtained:

$$d(L, \Delta\nu) = 1 - exp\left(-\frac{g_B(\Delta\nu)}{A_{eff}} P_{Si} L_{eff}\right) \tag{2.4}$$

This expression conveys the fact that the pulse depletion depends on the probe power injected into the fiber: the larger the probe power, the higher the energy transferred to it to attain a given amplification and, hence, the larger the pump pulse depletion. On the other hand, the depletion is shown not to depend neither on the power nor on the duration of the pump pulse itself. The maximum tolerable probe wave power for a particular depletion factor can be calculated following:

$$P_{Si} = -ln(1 - d(L, \Delta\nu)) \frac{A_{eff}}{g_B(\Delta\nu) L_{eff}} \tag{2.5}$$

Figure 2.1 schematically depicts the impairment brought by the pump pulse depletion to the measurement. A worst-case scenario is assumed in which a uniform BFS fiber is followed by a small section with a slightly different BFS, $\delta\nu$, where the gain spectrum is measured [31]. The depletion factor of the pump wave depends on the frequency detuning

between pump and probe optical waves along the fiber. This frequency dependence, in turn, induces an additional transfer function that is superimposed on the measured gain spectrum. This is due to the fact that, as presented in section 1.4, the Brillouin gain experienced by the probe wave due to its interaction with the pulse follows a profile given by:

$$G_i(\Delta\nu) = exp\left[\int_{z_i}^{z_i+u} \frac{g_B(\Delta\nu)}{A_{eff}} P_{Pi}\, exp(-\alpha z_i)\, dz\right] \tag{2.6}$$

where u is the interaction length of the probe wave with the pump pulse, which corresponds to the spatial resolution of the sensor (half the temporal distance of the pump pulse).

This frequency dependence distorts the measured spectrum and introduces a bias in the measured BFS that entails a systematic error in the measurement performed [31]. Note that, as highlighted in Fig. 2.1, in a gain configuration BOTDA the peak of the Brillouin spectrum is shifted to higher frequencies, while in a loss configuration it would be displaced to lower frequency values [31]. It is worth mentioning that, this measurement impairment is a non-local effect in the sense that the BFS measurement at a particular location in the fiber is affected by the Brillouin interaction between pump and probe at other locations. In fact, the shape of the transfer function associated with pump pulse depletion at a particular location in the fiber depends on the BFS distribution along all previous locations, as can be seen in Eq. (2.2).

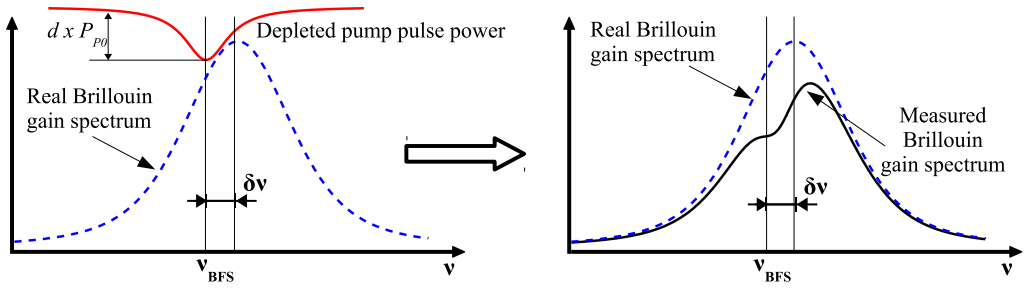

Figure 2.1: *Effect of pump pulse depletion frequency dependence on a Brillouin gain spectrum, when scanning a fiber section displaced $\delta\nu$ MHz from the Brillouin frequency shift (BFS) of the fiber.*

Therefore, it has been found that the measurement error (ν_e) due to the depletion of the pump pulse depends on both, $\delta\nu$ and the depletion factor d. Assuming a small depletion factor, $d < 0.2$, and an error much smaller than the FWHM of the gain spectrum, the measurement error for a given depletion factor of the pulse can be calculated following the expression [31]:

$$\nu_e \cong \frac{d\delta\nu}{\left(1+4\left(\frac{\delta\nu}{\Delta\nu_b}\right)^2\right)^2 - 2d\left(1+2\left(\frac{\delta\nu}{\Delta\nu_b}\right)^2\right)} \tag{2.7}$$

For a fixed d, the frequency shift at which the error is maximum is calculated [31]:

$$\delta\nu = \sqrt{\frac{2-d}{28}}\Delta\nu_B \approx 0.26\Delta\nu_B \tag{2.8}$$

From this equation, it follows that the measurement error is maximum when the BFS difference between the long uniform BFS section and the short final section is around a quarter of the FWHM of the gain spectrum, $\delta\nu \approx \Delta\nu_B/4$ [31]. Moreover, the measurement error raises as the depletion factor increases, as shown in Fig. 2.2, where the relationship between the depletion factor of the pump pulse and the error on the determination of the BFS is depicted. As can be observed, in a long-length sensing fiber considering the worst-case scenario, i.e, with a constant BFS and a final section shifted in frequency $\delta\nu = \Delta\nu_B/4$, for a maximum 1-MHz error in the BFS measurement, the maximum tolerable depletion factor is $d \approx 0.2$ [31]. This, for typical standard single-mode fiber (SMF) parameters ($g_B = 2 \times 10^{-11} m/W$, $Aeff = 80 \times 10^{-12} m^2$, $\alpha = 0.2 dB/km$), translates to an upper limit on the maximum probe power that can be injected into a long-range BOTDA sensing link of around -11 dBm. This result has been obtained using Eq. (2.5). In addition, in order to obtain this result, the relative polarization changes between the probe and the pump waves as the latter travels through the fiber have been considered, so that the Brillouin gain is reduced by a factor of 1/2 [90].

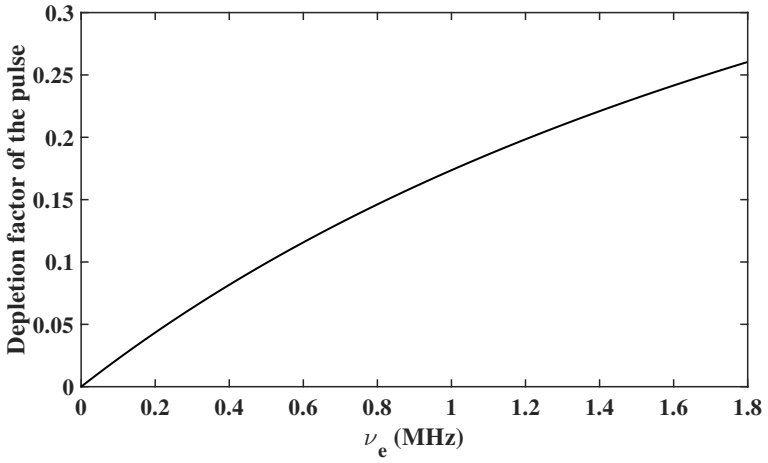

Figure 2.2: *Relation between the depletion factor of the pump pulse and the error that entails on the determination of the BFS for the worst-case scenario.*

2.3 Techniques to mitigate the impairments due to pump pulse depletion

As already explained, the depletion of the pump pulse is one of the main constraints in BOTDA sensors. Since its onset limits the power level of the probe wave that can be injected into the sensing fiber. As a result of this power limitation, the SNR is worsen, which constrains the measurements in both sensing distance and measurement time. For this reason, in the last years many research works have been carried out focused on solving this effect. The main proposals that have been presented to mitigate the impairment of the pump pulse depletion are described below.

One early proposal was the use of a numerical technique for temperature/strain profile reconstruction [91]. This technique was based on searching the BFS distribution that matched a given measurement data by using a multidimensional minimization algorithm to determine the coefficients of the parametrized unknown profile. The method was demonstrated with experimental measurements over a 7 km fiber, proving the capability of the sensor to compensate non-local effects. However, in order to implement the method, it is mandatory to have previous knowledge of some characteristic of the sensing fiber. In addition, the post-processing time of the technique was of the order of 10 minutes for a number of harmonics below 20. So that the applicability of this method to realistic measurement scenarios is rather limited.

Another alternative is the simultaneous use of two probe waves of equal optical power symmetrically separated in optical frequency from the pump [92]. This solution takes advantage of the presence of two sidebands in the probe wave so as to generate a complementary gain and loss Brillouin interaction upon the pump pulse; hence the onset of pulse depletion is mitigated. Figure 2.3 shows the fundamentals of the technique by depicting the spectra of the various optical waves involved in the method. As explained in section 2.2, the lower-frequency probe sideband generates a loss spectrum upon the pulse due to the continuous interaction between both waves along the fiber. Nevertheless, as seen in the figure, a complementary Brillouin gain spectrum is also induced by the upper-frequency probe sideband. Therefore, both spectra compensate each other, so that the depletion of the pulse is completely or at least greatly diminished. Note that, with this method, one probe wave experiences Brillouin gain process while the other probe wave experiences the loss process. And, as both processes occur at the same time, in order to retrieve the information, it is mandatory to filter out one of the probe waves in the receiver.

Another proposal is the use of a time-multiplexing method, which is based on pulsing the probe wave so as to limit the interaction length with the pump pulse [93, 94]. Hence, both waves just interact at a certain section of the fiber and, according to Eq. (2.4), as the pump pulse depletion is cumulative along the interaction section, the total pump pulse depletion is reduced by reducing the interaction segment. The drawback of this method is that the measurement time is greatly increased as the length of the interaction lengths is reduced, because, to retrieve the BFS of the whole sensing fiber, an individual measurement for each section is required. In other words, if the fiber is divided in three sections, you

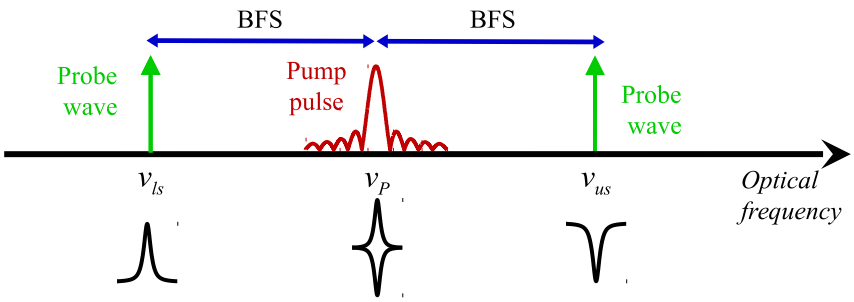

Figure 2.3: *Operation principle of a dual-probe BOTDA by portraying the generated Brillouin spectrum upon the probes signals and the complementary gain-loss Brillouin interaction upon the pump pulse.*

need to perform three separate measurements, one for each section of the fiber. Therefore, in this particular example the total measurement time would be multiplied by three.

A technique tolerant to non-local effects that is based on a phase-modulated probe wave and radio-frequency (RF) demodulation was also presented by our research group [95]. The tolerance to pulse depletion-induced impairments of this method is based on the characteristics of the detection process, which generates a RF phase-shift signal that has been shown to be largely independent of the Brillouin gain magnitude.

Finally, one of the latest techniques to compensate non-local effects involves the use of a modulation or "dithering" of the optical frequency of the probe waves in a conventional dual-probe BOTDA sensor [48, 49]. This technique was devised by our research group, and as it is a subject of study and enhancement during this thesis dissertation, the fundamentals will be explained in detail in chapter 4.

2.4 Pump pulse depletion in a dual-probe BOTDA

Probably the simplest and the most successful alternative to mitigate non-local effects due to pump pulse depletion is the use of the dual-probe setup [92]. As has already been mentioned, the dual-probe BOTDA configuration uses two probe waves of equal power that are symmetrically separated in optical frequency from the pump wave [92]. This leads to two simultaneous Brillouin interactions (gain and loss) upon the pulse that compensate each other; hence, the pulsed wave theoretically is not affected by the Brillouin interaction, so that pulse depletion is suppressed.

However, this is only true for first order approximation if the amplification and depletion experienced by the lower and higher frequency probes, respectively, during their interaction with the pump pulse are neglected. When the detailed interaction is taken into account, it is found that in a dual-probe BOTDA there is still pump pulse depletion, although it is greatly diminished. This is due to the fact that the pulse is interacting with two probe waves with a power slightly unbalanced by the interaction itself [31]. Taken into account this appreciation, and considering two probe waves of equal optical power ($P_{SL} = P_{SU}$), the pump power at the output of the fiber in Eq. (2.2) can be found as follows [31]:

$$P_P(L,\Delta\nu) = \frac{P_{Pi}\exp(-\alpha L)}{1+\frac{g_B(\Delta\nu)^2}{A_{eff}^2}P_{P_i}\left[P_{SL_i}+P_{SU_i}\right]exp(-\alpha L)uL} \tag{2.9}$$

where P_{SL_i} and P_{SU_i} are the respective input powers of the two probe waves at position $z = L$. As before, in a fiber with a constant BFS, the depletion factor of the pulse for a particular frequency detuning can be characterized by [31]:

$$d(L,\Delta\nu) = 1 - \frac{1}{1+\frac{g_B(\Delta\nu)^2}{A_{eff}^2}P_{P_i}\left[P_{SL_i}+P_{SU_i}\right]exp(-\alpha L)uL} \tag{2.10}$$

It is worth mentioning that, from this expression it follows that in a dual-probe BOTDA, unlike for a single-probe BOTDA, the depletion factor d reaches its maximum when the fiber length is equal to $L = 1/\alpha$. Another important conclusion to be drawn from these

equations is that in a conventional dual-probe wave BOTDA configuration the pulse depletion is dependent on the pulse parameters themselves. Specifically, it is found that the pump pulse depletion is no longer independent neither of the pulse peak power nor of its temporal duration. In this way, the greater the power and/or the longer the duration, the higher the depletion factor of the pulse. From Eq. (2.10), the maximum tolerable probe wave power for a particular depletion factor can be obtained [31]:

$$P_{SL_i} + P_{SU_i} = \frac{d(L,\Delta\nu)A_{eff}^2}{g_B(\Delta\nu)^2 P_{P_i}\left(1 - d(L,\Delta\nu)\right) exp(-\alpha L) uL} \tag{2.11}$$

Using Eq. (2.11), it is found that in a long-range dual-probe BOTDA sensor ($L = 1/\alpha$) using a conventional SMF characteristics, and deploying a 10-ns pump pulse with a peak power set just below the typical MI threshold of 20 dBm [37], pump pulse depletion imposes a theoretical upper limit for the probe wave power injected in the fiber of approx. 10 dBm per sideband in order to have a BFS systematic measurement error of less than 1 MHz. Note that for a longer pulse duration, the limit of probe power is more stringent. For instance, for a pulse of 50-ns and a power of 20-dBm the maximum power is set at 3 dBm per sideband.

Therefore, the dual-probe BOTDA sensor configuration could be seen as greatly ameliorating non-local effects due to pump pulse depletion. However, later work showed that the probe power limitation in this setup was actually more restrictive due to the onset of the so-called second-order non-local effects [33] and also due to another non-local effects that have been found in this thesis, which are explained in detail in section 2.5 and in chapter 3 respectively.

2.5 Second-order non-local effects in dual-probe BOTDA sensors

As mentioned, the use of two probe waves to mitigate non-local effects makes this technique a BOTDA configuration that would only be largely limited in probe wave power by the Brillouin threshold limit of the fiber [34]. However, later work showed that the power constraint was actually more restrictive. This is due to the onset of other non-local effects. These second-order non-local effects are associated to the onset of linear distortion of the pump pulse spectrum due to its interaction with the two probe waves [33].

The physical origin of this effect is highlighted in Fig. 2.4. Where the Brillouin interaction on the pump pulse of both probe waves is depicted. As shown in Fig. 2.4(a), when the frequency detuning between pump and probe waves equals the BFS of the fiber, the loss and gain spectra generated upon the pulse perfectly compensate each other and non-local effects are largely avoided. However, in order to retrieve the full Brillouin gain spectrum (BGS), it is mandatory to scan the frequency detuning between pump and probe. In this way, as portrayed in Fig. 2.4(b) and 2.4(c), when the frequency difference does not match the BFS of the fiber, the Brillouin gain and loss spectra generated by both probe waves over the pump pulse do not longer overlap perfectly, leading to linear distortion of the

pump pulse spectrum.

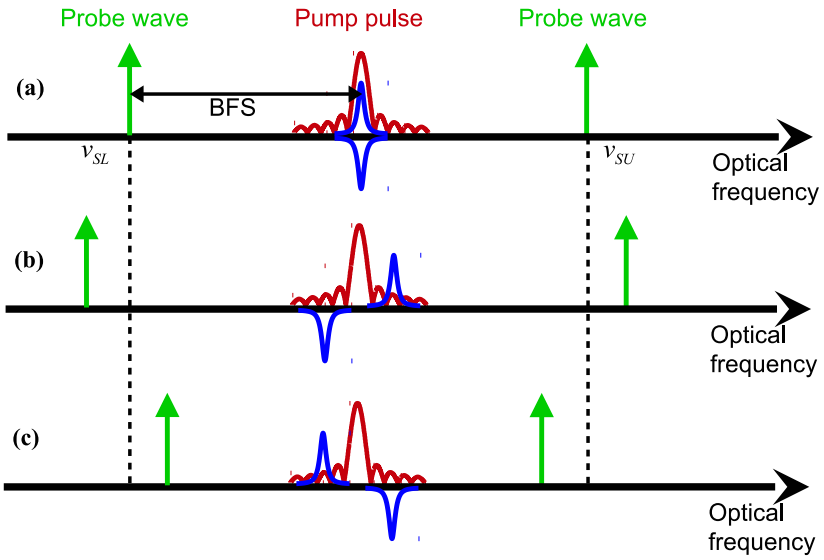

Figure 2.4: *Stimulated Brillouin scattering (SBS) interaction process over the pump pulse in dual-probe wave Brillouin optical time-domain analysis (BOTDA) configurations and its consequences on the pulsed wave for different frequency spacing of the conventional scan process (**a**) when the frequency detuning equals the BFS of the fiber (**b**) when it is higher than the BFS and (**c**) for a smaller frequency shift.*

Specifically, as shown in Fig. 2.4(b), when the frequency detuning is higher than the BFS of the fiber, the amplification process of the pump pulse generated by the upper-frequency probe wave occurs at a higher frequency than the pump pulse frequency, whereas the attenuation generated by the other probe wave happens at a lower frequency. This, leads to a distorted pump pulse spectrum with an up-shifted frequency. On the contrary, as highlighted in Fig. 2.4(c), when the frequency difference between both probe waves and the pump pulse is lower than the BFS, the distortion process occurs in the opposite direction. Hence, the resultant pump pulse spectrum presents a distortion with a down-shifted frequency.

As depicted in Fig. 2.5, the distortion of the pulse spectrum leads to a distortion of the measured gain spectra, which leads to BFS measurement errors [49]. Note that, for a low probe wave power, the pulses at the output of the FUT are not affected by non-local effects, as shown in Fig. 2.5(a), whereas for a high probe power (5 dBm), Fig. 2.5(c), non-local effects can be clearly observed. Thus, the shape of the pulses is clearly affected, except for the pulse that is centered on the BFS of the fiber, around 10.8 MHz, where the gain and loss processes induced by both probe waves upon the pulse compensate each other, as explained in Fig. 2.4(a). The distortion of these pulses, as expected, has a strong impact on the retrieved BGS, as shown in Fig. 2.5(d). Specifically, the BGS at the far end of the fiber presents two lobes around the mean BFS of the fiber, that correspond to the frequency detuning between pump and probe at which the pulse is shown to be highly amplified.

It was found that in order not to exceed an error threshold of 1 MHz, this effect limits the maximum probe wave power to around -3 dBm per sideband for typical standard

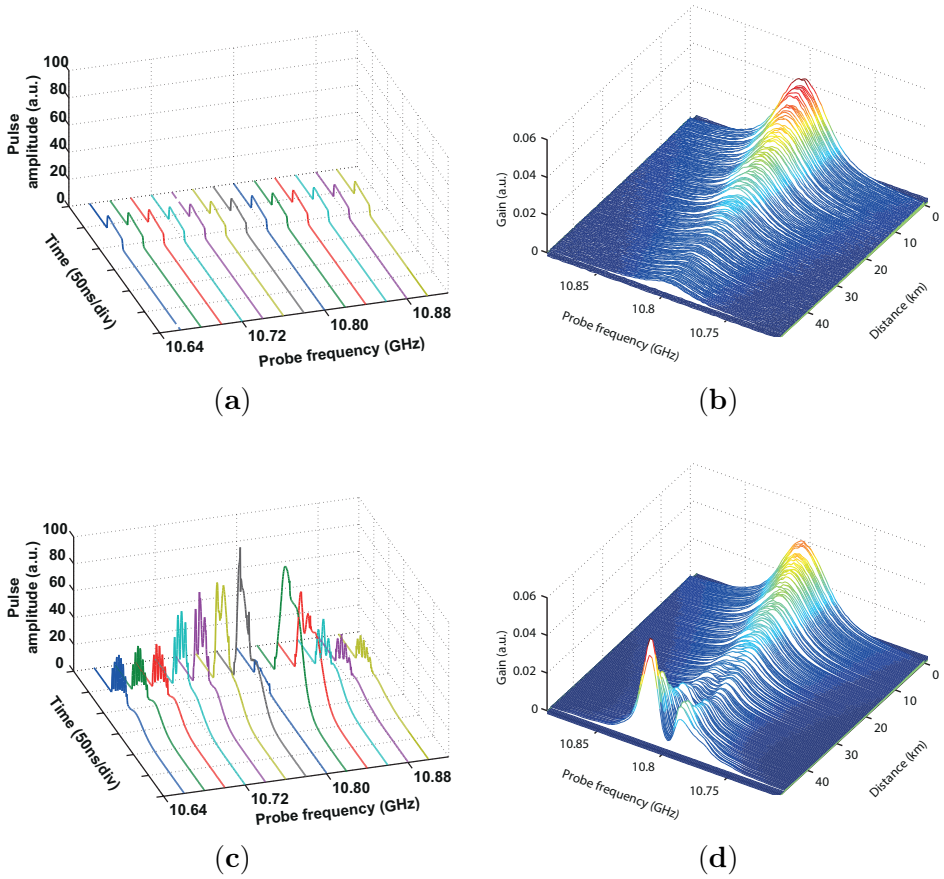

Figure 2.5: *Pulses at the output of the fiber and measured Brillouin spectra for a conventional dual-probe BOTDA in two cases for probe wave powers of −6 dBm (**a**,**b**) and 5 dBm (**c**,**d**). (From R. Ruiz-Lombera, J. Urricelqui, M. Sagues, J. Mirapeix, J. M. López-Higuera and A. Loayssa, "Overcoming Nonlocal Effects and Brillouin Threshold Limitations in Brillouin Optical Time-Domain Sensors," in* IEEE Photonics J. ***2015**, 7, 1–9. With permission. Copyright 2015 IEEE.)*

SMF parameters [33]. This is well below the theoretical limit imposed by the Brillouin threshold of the fiber, which is around 7 dBm for typical SMF [34]. Therefore, at least 10 dB of SNR is being wasted in long-range dual-probe BOTDA sensors. Consequently, the development of techniques to overcome this limit is of paramount importance to enhance the performance of the sensor.

One approach to overcome the distortion of the pump pulse spectrum is the use of an alternative scanning method in the dual-probe BOTDA configuration [96]. The method is based on changing the conventional scanning method to retrieve the Brillouin spectra in order to ensure the continuous overlapping of the gain and loss spectra induced by both probe waves on the pump pulse. This is achieved by maintaining fixed the frequency difference between both probe waves; equal to twice the BFS of the fiber. In this way, the gain and loss spectra generated upon the pump pulse perfectly compensate each other, and hence, second-order non-local effects are prevented. Recently, a more elaborate solution making use of this technique but with four probe waves was also presented [97]. These methods enable an increase of the probe power over the second-order non-local effects limit, at the cost of a somewhat increased complexity of the setup. Nevertheless, the maximum probe wave power injected into the fiber is still limited by the Brillouin threshold of the

fiber.

Another alternative to compensate second-order non-local effects that also enables dual-probe BOTDA setups to overcome the Brillouin threshold of the fiber [48, 49], was devised by our research group. The basis of this technique is to introduce a modulation or "dithering" to the optical frequency of the probe waves. This technique is a subject of study and enhancement during this thesis dissertation, so that the fundamentals of the technique are explained in detail in chapter 4.

2.6 Conclusions

In this chapter, the physical origins of the various non-local effects that constrain the performance of the BOTDA sensor have been introduced. These non-local effects impair the pump pulse wave in such a way that the measurement performed introduce errors. In addition, the most prominent solutions to overcome these effects have been presented.

Non-local effects are amongst the main constraints on the performance of BOTDA sensors since their onset entails limits to the maximum probe wave power that can be injected into the fiber. Consequently, the SNR of the detected probe wave is worsen. As has been addressed in section 1.5, the accuracy of the sensor depends on the SNR, therefore, the lower the probe wave power, the worse the precision of the sensor. Conventional single-probe BOTDA sensors have their probe power severely contained by first-order non-local effects. The maximum probe power that can be introduced in a long-range single-probe BOTDA system is approximately -11 dBm. Dual-probe setups significantly alleviate the issue, enabling the use of higher probe power. However, they are still prone to second-order non-local effects that distort the pulse spectrum and constrain the probe power to around -3 dBm. This level is well below the theoretical limit set by the Brillouin threshold of the fiber.

In summary, non-local effects have been shown to seriously impact BOTDA sensors performance. Therefore, in order to improve the efficiency of long-range BOTDA sensors, it is of paramount importance to overcome the impairments imposed by non-local effects. Chapters 3, 4 and 5 contain extensive studies concerning non-local effects in BOTDA sensors that were performed during this thesis. Furthermore, chapters 4 and 5 introduce some new BOTDA configurations to overcome or mitigate these effects.

Chapter 3: Non-local effects due to the limited extinction ratio of the pump pulses

Contents

3.1 Introduction

In the previous chapter, first-order and second-order non-local effects have been presented. It has been explained that the constraints imposed by the onset of these effects are one of the main constraints of Brillouin optical time-domain analysis (BOTDA) sensors. The reason is the fact that non-local effects limit the maximum probe wave power that can be injected into the fiber, and consequently, the signal-to-noise ratio (SNR) of the sensor performance is worsen. The description of non-local effects in the previous chapter assumes a perfect pump pulse wave, i.e., a signal with optical power only during the pulse duration. However, in real applications every device used to generate the pulse has a limited extinction ratio (ER), so that the pulse is on top of a continuous wave (CW), called the pedestal of the pump wave.

This chapter presents the studies carried out during the work of this thesis focused on analyzing the impairments caused by the limited ER of the pump pulse. First of all, the increase of the pulse depletion originated by the pedestal of the pump wave is analyzed. In addition, as a result of this study, two previously unknown detrimental effects imposed by low ER pump pulses on BOTDA systems are presented. The first one arises from the increased depletion of the pedestal that follows the pump pulse when interacting with a probe wave that has been previously amplified by the pulse. It was found that this pedestal depletion introduces a non-local effect which has analogous impact on the measurement results to that of the well-known non-local effects originated by the depletion of the pulse. The other closely-related effect that was found is due to the transient response of the erbium-doped fiber amplifiers (EDFA) that are usually deployed to amplify the pump pulse

prior to injecting it into the sensing fiber. The EDFA distorts the pedestal that follows the pulse and this, again, induces a non-local effect that impairs the measurements.

The constraints imposed by the ER of the pump pulses are studied with the help of a theoretical model that was devised in this thesis work, which is used for numerical calculations of the interactions between the various waves involved in the BOTDA sensor. Furthermore, the theoretical analysis of non-local effects is verified by experimental results.

3.2 Theoretical model for pump and probe waves interaction

We are concern here with a scenario in which the pump pulse that is launched into the fiber has a limited ER and, hence, it is on top of a CW pedestal. In this way, as highlighted in Fig. 3.1, there are various interactions between the pump pulse wave with limited ER and the probe wave that take place in the sensing fiber. On the one hand, there is the interaction between the pump pedestal and the probe wave, and, on the other hand, the previously studied interaction between the pulse and the probe wave.

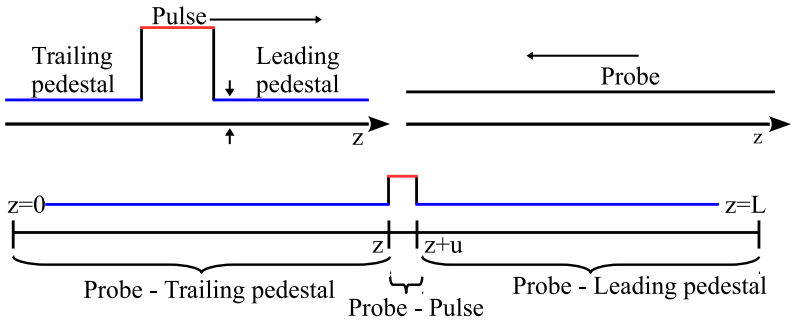

Figure 3.1: *Schematic depiction of probe and pump pulse wave interaction along the fiber.*

The interaction between pump and probe waves can always be solved by using the full time-depend coupled equations for the amplitudes of the pump and probe optical fields and the acoustic wave that were introduced in chapter 1 (Eq. (1.39)). However, this would be computationally intensive, particularly for long-range BOTDA sensors. Therefore, a new simplified model that has been devised during the conduct of this thesis is introduced here. This model will be validated by the experiments in section 3.4.

The model assumes that the pulses are longer than the acoustic phonon lifetime, so that a perturbation method can be used to solve the steady-state coupled power equations for the Brillouin interaction between pump and probe waves along the fiber. These equations were introduced in chapter 1, see Eq. (1.40), and are repeated here for clarity:

$$\frac{d}{dz}P_S(z) = -\frac{g_B(\Delta\nu, z)}{A_{eff}}P_S(z)P_P(z) + \alpha P_S(z) \tag{3.1a}$$

$$\frac{d}{dz}P_P(z) = -\frac{g_B(\Delta\nu, z)}{A_{eff}}P_S(z)P_P(z) - \alpha P_P(z) \tag{3.1b}$$

where P_S and P_P are the optical powers of probe and pump waves respectively, at

each position z of the fiber, g_B is the Brillouin gain coefficient of the fiber introduced in Eq. (1.24), which depends on the frequency shift between pump and probe waves, $\Delta\nu$, at each position z of the fiber, α is the attenuation coefficient of the fiber and A_{eff} is the effective area of the fiber.

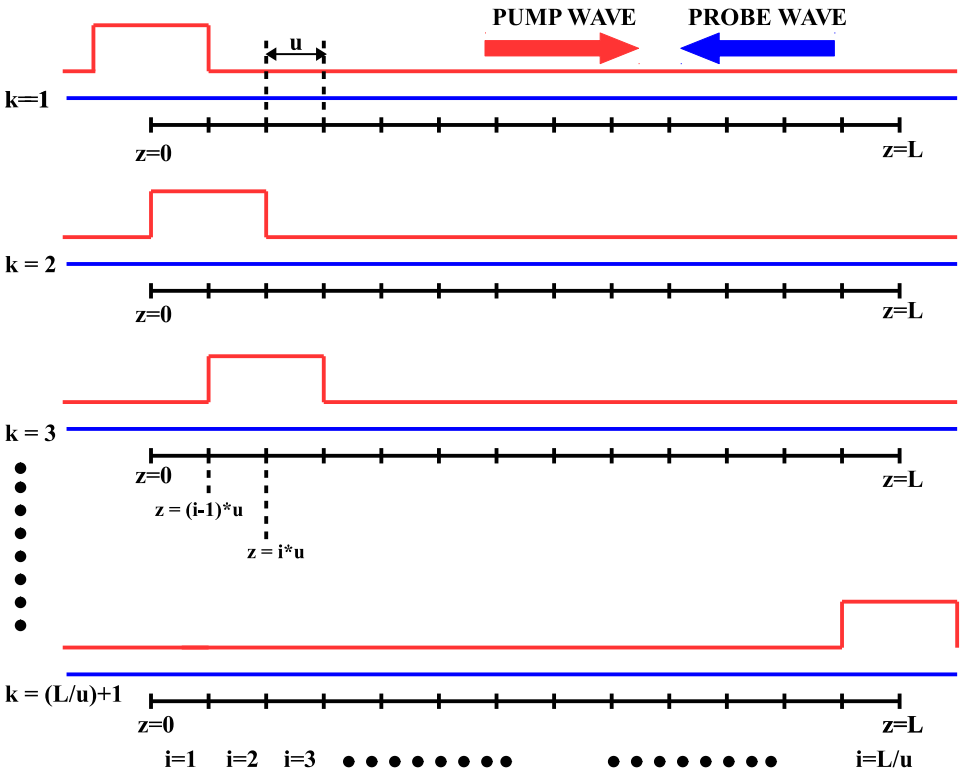

Figure 3.2: *Fundamentals of the theoretical model. The fiber is divided into segments equal to the spatial resolution and the interaction between pump and probe waves is solved for each segment i. The waves are then counter-propagated in successive iterations.*

As it is highlighted in Fig. 3.2, the fiber is first divided into segments of length u equal to the spatial resolution of the sensor, i.e., half the spatial width of the pump pulse in the fiber. Then, in order to calculate the evolving powers of the counter-propagation of pump and probe signals, successive iterations are carried out. At each iteration k, the interaction between pump and probe waves is calculated in all the $N = L/u$ segments in which the fiber has been divided, with L the total fiber length. This is done by solving Eq. (3.1) for each segment, i, from $i = 1$ to $i = N$, using the boundary values of the pump and probe wave powers, which leads to the following expression:

$$P_S\left((i-1)u\right) = P_S\left(iu\right) exp\left(\frac{g_B\left(\Delta\nu, z\right)}{A_{eff}} P_P\left((i-1)u\right) u\right) exp(-\alpha u) \tag{3.2a}$$

$$P_P\left(iu\right) = P_P\left((i-1)u\right) exp\left(-\frac{g_B\left(\Delta\nu, z\right)}{A_{eff}} P_S\left((i-1)u\right) u\right) exp\left(-\alpha u\right) \tag{3.2b}$$

where Eq. (3.2a) gives the amplified probe wave by approximating the pump power as constant along the i-th segment, from $z = (i-1)u$ to $z = iu$, and equal to the power at the

input of the segment, $P_P((i-1)u)$; in other words, neglecting the pulse depletion induced by the probe wave for this calculation. This also assumes that the interaction segment is so small that the attenuation of the fiber can be neglected. Similarly, Eq. (3.2b) is solved by approximating the probe wave to be constant in the segment. Note that the pump and probe interaction is calculated identically in every segment, regardless of whether it is a pulse-probe or a pedestal-probe interaction.

Then, for the next iteration, $k+1$, all the probe and pump waves segments calculated in the previous iteration are advanced one step of length u in opposite directions, and again, the interactions are recalculated in all $i = 1$ to $i = N$ segments. The process continues until the pulse has left the fiber and the probe wave from the farthest location of the fiber has had time to traverse the fiber and leave. Note that the iterations can continue even longer in order to see effects that are due to the propagation of the pedestal that follows the pulse, the trailing pedestal, which will be studied in section 3.4. It is worth mentioning that, before beginning the interaction between pump and probe waves, all the segments of the fiber are filled with the corresponding pump and probe waves values taking only into consideration the attenuation of the fiber. Moreover, it is necessary to start the iterations before the arrival of the pulse to the input of the fiber, so that the initial interaction between the probe wave and the pedestal of the pump that precedes the pulse, the leading pedestal, has time to converge. For this reason, the total number of iterations is typically an order of magnitude larger than $l = 2L/u$, which are the minimum iterations to fully propagate the pump pulse and the amplified probe waves.

This model can be regarded as an enhancement of previous perturbation methods for solving the waves interaction in BOTDA sensors [98, 99]. Note that the model can be applied to BOTDA sensors in either gain or loss configuration. Furthermore, it can also be applied to dual-probe setups simply by adding in Eq. (3.1) the terms corresponding to the additional probe wave component [92].

3.3 Pump pulse depletion increase induced by the pedestal of the pump wave

As explained above, and highlighted in Fig. 3.1, there are three regions of interaction with the pump wave that a probe wavefront finds as it travels along the fiber. The first region extends from the probe wavefront entrance in the fiber at $z = L$ to the location of the pulse at a particular $z = z_0 + u$. In this region, just the leading pedestal of the pump pulse and the probe wave interact, leading to Brillouin amplification of the probe wave. Then, the probe wavefront meets the pulse and is amplified over a length u of fiber equal to half the spatial width of the pulse in the fiber (spatial resolution). Finally, after leaving the pulse location, there is another interaction region, from $z = z_0$ to $z = 0$, where the probe wave is again amplified by the pump wave trailing pedestal.

Therefore, the net effect of the presence of the pump wave pedestal is that the probe wave experiences more gain than just that due to the pulse itself [45]. Indeed, a gain that is useless for sensing [100]. In particular, as shown in Fig. 3.3, the result of the interaction

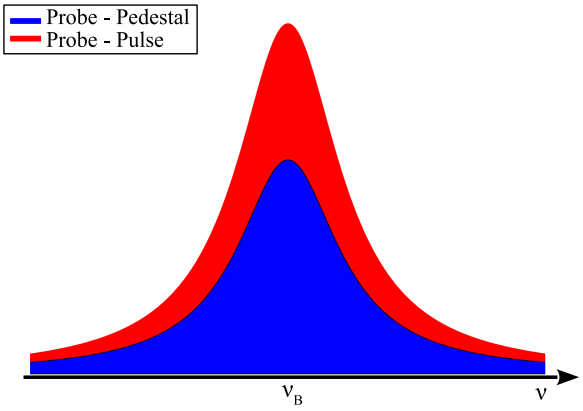

Figure 3.3: *Brillouin gain spectrum due to the interaction between pump and probe waves.*

between the probe and the pedestal of the pump manifests as a Lorentzian gain spectrum, in addition to the gain spectrum induced by the pulse itself. In principle, the latter can be recovered by normalizing the measurements by the spectrum measured with no pulse in the fiber, i.e., subtracting the gain experienced by the probe due to interaction with just the pedestal before the pulse enters the fiber from the total measured gain. However, the additional gain in the probe wave has been shown to degrade the precision of the BFS measurement [45]. Moreover, the presence of this additional gain, apart from the useful signal, can lead to an effective reduction of the SNR because the full-scale dynamic range of the analog-to-digital converter within the signal acquisition device is largely wasted with a detected signal larger than the signal of interest; hence, increasing the quantization noise. In addition, the extra power amplification of the probe wave by the pedestal of the pulse aggravates the onset of the depletion of the pump pulse. This is because the pump pulse meets a higher power probe wave along the entire sensing fiber, and, as explained in section 2.2, the higher the probe wave power, the larger the depletion of the pulse. Therefore, the presence of the pulse pedestal leads to a worsening of first-oder non-local effects in a single-probe gain configuration BOTDA sensor [45].

Furthermore, as has been concluded from the research work made during this thesis, the worsening of the pump pulse depletion takes place even in BOTDA setups deploying two probe waves. In section 2.4, we have assumed that in a dual-probe BOTDA configuration the pump wave interacts with two probe waves of equal optical power. However, this is not the case in BOTDA sensors with a limited ER. In this case, the power of the probe waves becomes unbalanced owing to their interaction with the leading pedestal of the pulse from $z = L$ to $z = z_0 + u$: the upper optical frequency probe is attenuated and the lower frequency probe is amplified. In order to examine the impact that this power difference has on non-local effects, we focus on the pump wave power. Adding the term corresponding to the higher frequency probe wave to the system of equations in (3.1), the variation in the pump wave power in a small length of the fiber, Δz, due to Brillouin interaction (without considering the attenuation of the fiber in Δz) can be calculated as follows:

$$\Delta P_P(\Delta\nu) = P_P(z_0) exp\left(\int_{z_0}^{z_0+\Delta z} \frac{g_B(\Delta\nu)}{A_{eff}}[P_{SU}(z_0) - P_{SL}(z_0)]dz\right) - P_P(z_0) \qquad 3.3$$

where P_{SL} and P_{SU} are the probe wave power of the lower and higher frequency probe waves, respectively.

From Eq. (3.3) it follows that the pump pulse power variation is larger as the power difference between both probe waves increases. It has been explained that the optical power of both probe waves becomes unbalanced due to the interaction with the pedestal of the pump wave. Moreover, the higher the power of the pump pedestal, the larger the amplification/attenuation of the probe waves, and hence, the optical power difference between the two probe waves becomes greater. Therefore, the pump pulse depletion increases with decreasing the ER of the pump pulses. In addition, Eq. (3.3) shows that the amount of depletion depends on the frequency detuning between pump and probe waves. In summary, the pump pedestal unbalances the optical power of both probe waves, and this, in turn, makes the gain and loss Brillouin spectra that both waves induce upon the pulse to be unequal: the gain induced by the higher frequency probe is reduced and the loss induced by the lower frequency probe is increased. Hence, they no longer compensate each other, leading to pulse depletion, which, in turn, introduces a more stringent limitation of the total probe wave power that can be deployed in the sensor. Note that this depletion is, at equal probe power levels, smaller than in a conventional single-probe BOTDA configuration.

In order to assess the influence of the ER of the pump pulse on the depletion factor d, which has been introduced in chapter 2, the Brillouin interaction model presented in section 3.2 is used. In this manner, the amount of pump pulse depletion in a dual-probe BOTDA configuration for different ER of the pulse is numerically calculated. Figure 3.4 shows the calculated depletion spectrum experienced by the pump pulse in an uniform BFS fiber link for different ER values, by depicting the depletion factor as a function of the frequency detuning of the pump and probe waves. The probe wave power was set to -3 dBm per sideband, which, as explained in section 2.5, is the maximum power that can be deployed in a long-range dual-probe sideband BOTDA sensor before the onset of second-order non-local effects [33]. A 10-ns pump pulse was assumed with a peak power of 20 dBm, which is typically the largest pulse power that can be injected in a long-range fiber link before the onset of modulation instability (MI) [37]. Finally, a 25-km length of fiber was chosen as a representative long-range link close to the fiber length for which the pulse depletion in dual-probe BOTDA configurations reaches its maximum value, $L = 1/\alpha \approx 22$ km in a standard single-mode fiber (SMF) [31].

Figure 3.4 highlights the fact that the depletion factor increases considerably for decreasing ER of the pump pulse. Therefore, the tolerable maximum depletion factor for a given error is reached at lower probe wave power. For instance, the approx. 20%-depletion that can be tolerated for around 1-MHz BFS measurement error [31]. It can be observed that the use of a 25 to 30 dB ER of the pump pulses, which is typical of pulses shaped using electro-optic modulators, seriously increases the depletion factor and, hence, the error in the measurement of the BFS. Thus, the maximum probe power that can be injected into the sensing fiber decreases with the pump wave ER, which leads to a worse SNR and, consequently, to a reduction of the accuracy of the sensor.

Note that the presented calculations assume typical standard SMF parameters for the

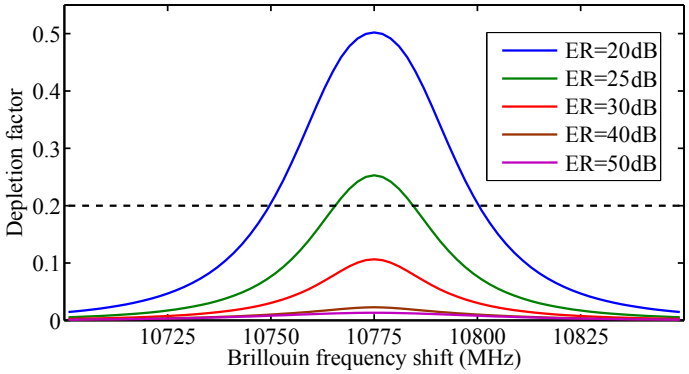

Figure 3.4: *Resultant depletion factor, d, of the pump pulses as a function of their ER in a long-range BOTDA sensor.*

Brillouin interaction: $g_B = 2 \times 10^{-11}$ m/W, $A_{eff} = 80 \times 10^{-12}\text{m}^2$, $\alpha = 0.2$ dB/km and Brillouin linewidth of 30 MHz. Besides, the relative polarization changes between pump and probe waves while the first one crosses the fiber have been considered, so that the Brillouin gain is reduced by a factor of 1/2 [90].

The worsening of the pulse depletion with decreasing ER is not going to be further analyzed since this effect does not take place in isolation. As will be extensively analyzed in section 3.4, it is accompanied by another non-local effect that has been found during the conduct of this thesis, which is due to the depletion of the pulse pedestal.

3.4 Non-local effects due to the pump wave pedestal depletion

In this section, additional non-local effects originated by the limited ER of the pump pulse are introduced, as well as the impairments that these effects entail for BOTDA measurements, which have been discovered during the course of this thesis. First, the measurement distortion caused by the extra depletion of the trailing pedestal is studied, and afterward, the constraints caused by the deformation of the trailing pedestal due to the transient response of EDFAs are analyzed.

In order to carry out the study, the theoretical model presented in section 3.2 is deployed in this section to perform an analysis of the impairments brought by the limited ER of the pump wave in BOTDA sensors. A study that will be supported by experiments performed in the laboratory. Note that all the calculations of this section were performed assuming typical standard SMF parameters for the Brillouin interaction, i.e., same parameters than for the calculations in Fig. 3.4.

3.4.1 Theoretical fundamentals of the impairments induced by the pump wave pedestal depletion

In the previous section, we have described the influence of the limited ER of the pump pulses in the onset of first-order non-local effects. However, apart from the increased pump pulse depletion, there is another effect, which has been found during the course

of this thesis, that also distorts the measurements in BOTDA sensors with limited ER of the pump pulses. In this section, the study of these new effects will be conducted by calculations performed with the model presented in section 3.2. A calculations that will be endorsed by the experiments of sections 3.4.4 and 3.4.5.

Figure 3.5(a) depicts several calculated BOTDA traces, i.e., the gain provided by the pulse to the probe wave as a function of position along the fiber, for different ER of the pump pulse. This BOTDA traces are calculated in the same conditions than the system considered in section 3.3 (Fig. 3.4), that is, the probe wave power was set to -3 dBm per sideband, the 10-ns pump pulse peak power was set to 20 dBm and a 25-km fiber length was defined. In addition, these traces are for a frequency detuning between pump and probe waves equal to the BFS of the fiber, i.e., peak Brillouin interaction. As can be observed, there is a distortion of the shape of the calculated Brillouin gain of the probe wave signal for decreasing the ER of the pump pulse.

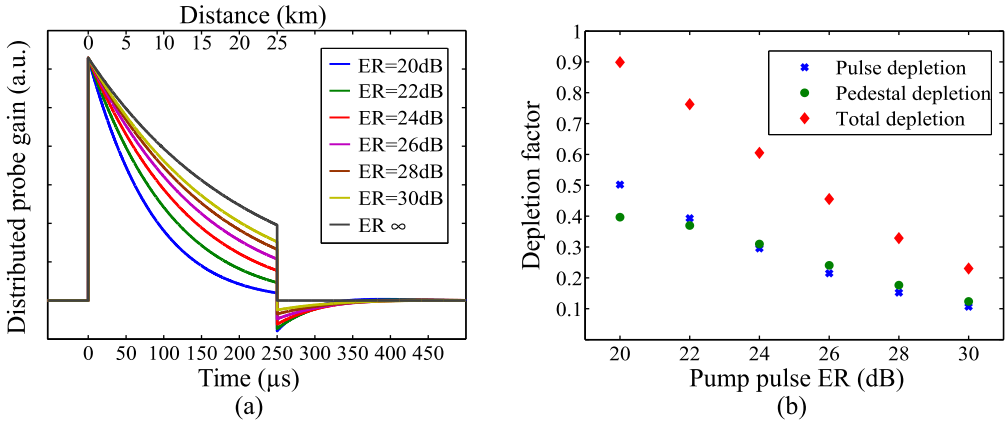

Figure 3.5: *(a) Brillouin gain of the probe wave. The traces are depicted in terms of time-of-flight of the pump pulse with an added axis (top) with the translation to location along the fiber. (b) Values of pulse depletion factor, d, pedestal depletion factor, d_P and total depletion factor, d_T.*

In order to explain the origin of the distortion observed in Fig. 3.5(a), it is mandatory to complete the explanation of the scenario discussed in section 3.2, and outlined in Fig. 3.1. Let's consider first the conventional single-probe BOTDA gain configuration. As has been described above, the pump pulse meets a probe wavefront at a particular $z = z_0 + u$ that had been amplified by interaction with the leading pedestal of the pump pulse in the $z = L$ to $z = z_0 + u$ region, and how it makes the pump pulse to experience an increased depletion. Now, the study will focus on the trailing pedestal of the pulse, which interacts with a probe wavefront that has been amplified by the pulse. Therefore, the trailing pedestal interacts with a higher power probe wave than the one met by the leading pedestal. Hence, in the interaction region from $z = z_0$ to $z = L$, the trailing pedestal experiences an increased depletion compared to the depletion of the leading pedestal, because more energy is transfered from the pedestal of the pump wave to the higher power probe. Moreover, the increased depletion of the trailing pedestal leads to a reduced amplification of the probe wave in its final journey to the exit of the fiber. In other words, the probe wave power is less amplified by the trailing pedestal than by the leading pedestal.

With the purpose of understanding the consequences of this reduced amplification of the probe wavefront by the trailing pedestal, it is necessary to remember that, as explained in section 3.3, the normalized BOTDA trace is obtained by subtracting the gain measured when there is no pulse in the fiber, i.e., before the input of the pulse, from the total measured gain. Note that the total Brillouin gain of the probe wave, as it has been explained, includes contributions from the pump pulse and its pedestal. If there were not increased depletion of the trailing pedestal of the pulse, the gain measured without pulse would be just the part of the measured gain due to the pedestal, and, hence, this normalization operation would give the correct probe gain due to just the interaction with the pulse. However, that is not the case: due to the reduced amplification of the probe in its interaction with the trailing pedestal, the gain measured without pulse is actually larger than the portion of probe gain due to the pedestal. Furthermore, the difference becomes larger as we consider locations $z = z_0$ in the fiber that are closer to the entrance of the probe at $z = L$, since the interaction region between the probe wavefront and the trailing pedestal of the pulse is larger.

In the case of a dual-probe BOTDA sensor the explanation of the effect is similar. As explained before, the optical power of both probe waves gets unbalanced as they interact with the leading pedestal of the pulse from $z = L$ to $z = z_0 + u$. The interaction with the pulse further unbalances the powers of the two-probe wavefronts; hence, the trailing pedestal of the pulse is further depleted (in comparison with the leading pedestal) and the gain of the lower-frequency probe in its journey to the exit of the fiber is reduced. As for pump pulse depletion, this effect of reduced amplification of the probe, at equal power levels, is smaller in a dual-probe BOTDA than in a single-probe setup. If instead of the lower-frequency probe, we keep the loss of the upper-frequency probe for sensing, the effect is identical, but this time it translates into a reduced loss of the upper-frequency probe in its interaction with the trailing pedestal of the pulse.

The explanations above justify the shape of the BOTDA traces in Fig. 3.5(a). Note that, for locations close to the pulse entrance at $z = 0$, the measured gain is largely independent of the ER of the pulse. For these locations, the length of the interaction region between the probe wavefront and the trailing pedestal of the pump pulse is nonexistent or at least very small; hence, the gain without pulse in the fiber is similar to the gain provided by the pedestal, and consequently the normalization process works well. However, as the pulse advances along the sensing fiber, the interaction region between probe and trailing pedestal becomes larger, and hence, the use of the gain without pulse for normalization of the trace overestimates the pedestal contribution, which leads to a progressive reduction of the trace amplitude. As depicts Fig. 3.5(a), the effect is more pronounced for decreasing the ER of the pump pulse.

Furthermore, it can be seen that even after the pulse has left the fiber (at $L = 25$ km), there is still a signal feature which depicts an abrupt fall to negative normalized gains followed by a slow recovery. The existence of this feature is due to the fact that the probe wavefronts that enter the fiber after the pulse has exited still interact with a depleted trailing pedestal. Note that the trailing pedestal of the pulse has been depleted by all the previous probe wavefronts with which it has met during its journey through the fiber.

Therefore, the probe gain is still smaller than the one due to the leading pedestal. Furthermore, as there is no longer a pulse in the fiber, the extra depletion of the trailing pedestal slowly decreases, until the power of the trailing pedestal stabilized.

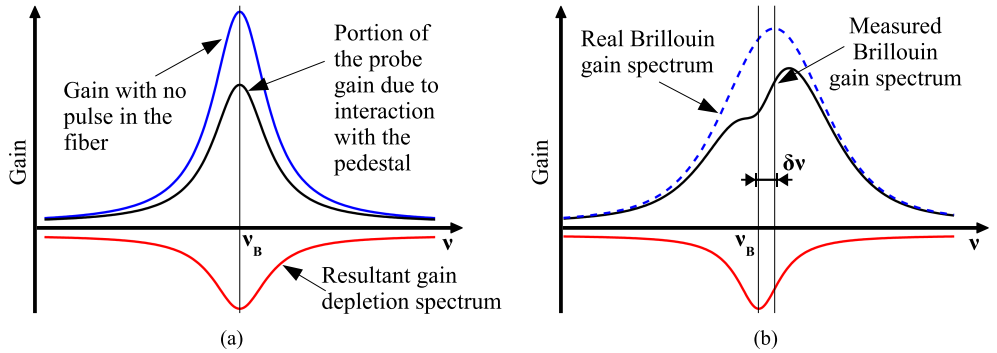

Figure 3.6: *(a) BOTDA gain depletion spectrum induced by the different spectra used in the measurement normalization process. (b) Distortion of the measured spectrum due to gain depletion.*

The distortion due to non-local effects induced by the pump pedestal depletion leads to errors of the measured BFS. In chapter 1, it has has been discussed that the Brillouin interaction defined by Eq. (3.1) depends on the frequency detuning between probe and pump waves. Figure 3.6(a) schematically depicts the frequency dependence of the distortion induced by the depletion of the trailing pedestal of the pulse, assuming a fiber with uniform BFS. On the one hand, the spectrum of the probe gain measured with no pulse in the fiber is displayed. On the other hand, it is also highlighted the calculated spectrum for the portion of the probe gain that comes from interaction with the pedestal at a particular position in the fiber. As can be appreciated, the gain with no pulse in the fiber is higher than the one induced by the trailing pedestal. This effect is due to the extra depletion suffered by the trailing pedestal, as explained above. In addition, it can be seen that the net effect of the trailing pedestal depletion is the introduction of an additional Lorentzian loss transfer function when the resultant spectrum of the probe gain without pulse in the fiber is used for normalization, instead of the smaller real spectrum of the gain due to interaction of the probe with the pedestal.

The additional Lorentzian loss transfer function introduced in the normalization of the measurements leads to errors. As shown in Fig. 3.6(b), if we assume a worst-case scenario in which a length of uniform BFS fiber is followed at the far end of the fiber by a small section with a different BFS, e.g., a hotspot, a distortion is introduced in the measured gain spectrum. This effect is completely analogous to the effect of pump pulse depletion that gives rise to non-local effects, which was outlined in Fig. 2.1. In fact, this is a new form of non-local effect but originated in the pedestal depletion when low ER pulses are deployed. Therefore, this effect can also be characterized by a dimensionless factor d_P, which we call pedestal gain depletion factor, that depends on the frequency difference between pump and probe waves, $\Delta\nu$, and on the position z of the fiber, following the expression:

$$d_P = \frac{G_P - G'_P}{G_P} \tag{3.4}$$

where G'_P is the portion of the probe gain that comes from the pedestal and G_P is the probe gain with no pulse in the fiber. This coefficient can be used in an identical manner to the pulse depletion coefficient to derive the BFS measurement error induced by this non-local effect [31]. Therefore, similar to the pump pulse depletion case explained in section 2.2, the BFS error induced by the pedestal depletion effect reaches its maximum in a worst-case scenario in which a constant BFS fiber has a small segment at its end with a BFS that is separated by that of the rest of the fiber by approximately 1/4 of the Brillouin spectral width [31].

Note that the pedestal-induced non-local effects take place simultaneously to those induced by the depletion of the pump pulse. Altogether, the BFS measurement errors in a BOTDA sensor are given by the total amount of depletion of the BOTDA trace, d_T, which comes from the addition of d and d_P factors.

$$d_T(\nu, z) = d(\nu, z) + d_P(\nu, z) \tag{3.5}$$

In fact, in Fig. 3.5(a) there is some trace amplitude reduction that is due to the increased pump pulse depletion for limited ER pulses that was described in section 3.3. Note that the depletion factor d at a given position in the fiber implies an analogous reduction of the Brillouin gain of the probe wave measured at that location. Therefore, the shape distortion of the Brillouin gain trace observed in the figure is due to both depletion effects, pulse depletion and pedestal depletion. Nevertheless, the effects that the pedestal depletion induces in BOTDA sensors can be clearly appreciated once the pulse has left the fiber (after 25 km), considering that the shape distortion of the trace at this position is exclusively introduced by the depletion of the trailing pedestal.

Figure 3.5(b) depicts the different components of the total depletion factor calculated at the end of the fiber as a function of the ER of the pulse. It can be seen that the depletion factor due to the pedestal depletion has a similar influence than the depletion factor of the pulse. In any case, note that this is for a certain condition of optical power of pump and

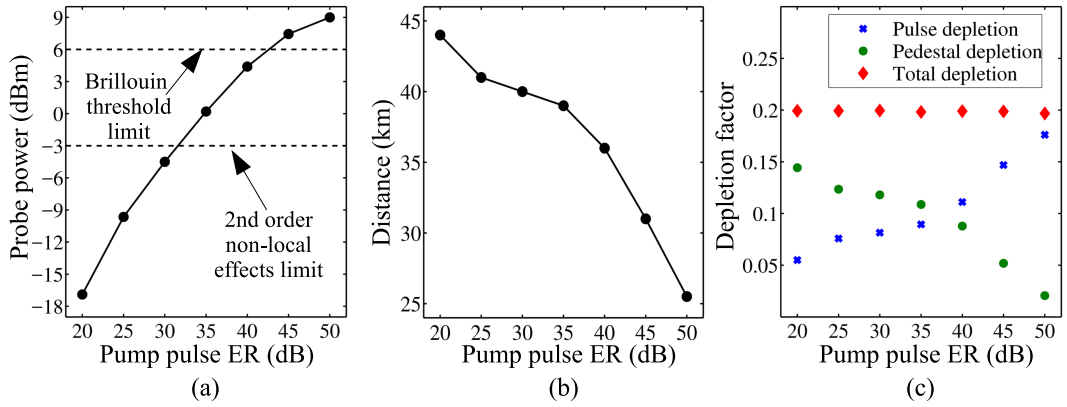

Figure 3.7: *For a maximum tolerable 1-MHz error in a dual-probe BOTDA measurement with a pump pulse of 20 dBm peak power and 10 ns duration: (a) maximum probe wave power per-sideband that can be deployed, (b) length of the sensing fiber where the total depletion factor reaches its maximum value and (c) depletion factor d, d_P and d_T in these conditions.*

probe waves and fiber distance.

The theoretical model presented in section 3.2 can be used to derive guidelines for the design of BOTDA sensors. Figure (3.7)(a) depicts the calculated values for the maximum probe wave power that can be used in a long-range dual-probe BOTDA sensor to obtain a maximum tolerable error of 1-MHz in the determination of the BFS. The results are given as a function of the ER of the deployed pump pulses. This figure has been calculated by finding the maximum probe wave power that lets to $d_T \approx 0.2$ [31]. It can be observed that decreasing the ER of the pump pulse wave translates to a more restrictive power limit for the probe wave. In addition, it can be seen that in order to be able to inject in the fiber a probe power of -3 dBm per sideband, which is the limit for the onset of significant second-order non-local effects [33], an ER higher than 32 dB would be necessary. Note that this is above the ER that conventional electro-optic modulators provide, which typically lies between 25 and 30 dB. Furthermore, if a technique for mitigation of second order non-local effects is deployed [96], then the probe power would be constrained to around 6 dBm due to the Brillouin threshold of the fiber [34]. According to Fig. (3.7)(a), this would require an ER greater than 43 dB. Curiously, in this case, the calculated ER limit coincide with the somewhat arbitrary $ER > L_{eff}/u$ condition stated in previous studies [31]. However, for lower probe powers, that condition is rather conservative.

The maximum probe wave in Fig. (3.7)(a) was calculated for the worst-case length of the fiber link that leads to maximum d_T. Figure 3.7(b) depicts which was that worst-case length as a function of the ER of the pump pulse. It can be observed that for large ER the worst-case length tends to $L = 1/\alpha$, which is consistent with previous studies of non-local effects that consider the ER to be infinite [31]. However, for lower ER the worst-case length of the fiber link becomes larger. Finally, Fig. 3.7(c) depicts, for each ER in Fig. (3.7)(a) and (3.7)(b), which was the relative contribution of d and d_P. As can be seen, the contribution to the total depletion given by pedestal depletion is greater for ER$\leq$ 35 dB. Whereas for larger ER the contribution of pulse depletion is higher. In addition, it can be observed that

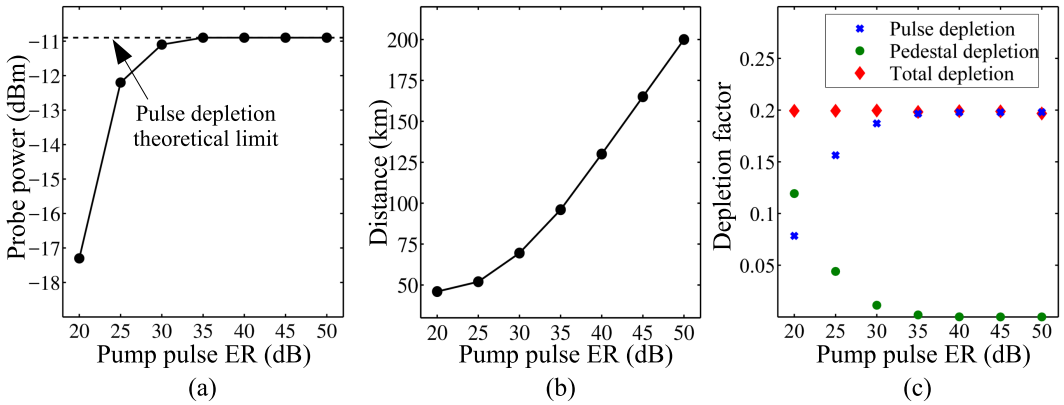

Figure 3.8: *For a maximum tolerable 1-MHz error in a gain configuration single-probe BOTDA measurement with a pump pulse of 20 dBm peak power and 10 ns duration: (a) maximum probe wave power that can be deployed, (b) length of the sensing fiber where the total depletion factor reaches its maximum value and (c) depletion factor d, d_P and d_T in these conditions.*

for pump pulses of an ER up to 40 dB both depletion effects have a significant contribution.

Figure (3.8) highlights the same calculated parameters than in Fig. 3.7 for a long-range gain configuration single-probe BOTDA sensor. As in the dual-probe configuration, it can be observed in Fig. (3.7)(a) that decreasing the ER of the pump pulse wave translates to a more restrictive power limit for the probe wave. Therefore, an important constraint for ER pump pulses below 30 dB is imposed. It is further observed that ER values between 20 and 25 dB severely limit the maximum probe wave power that can be used, and consequently to a significant worsening of the SNR. In addition, note that for an ER higher than 35 dB the maximum probe wave power that can be injected in the sensing fiber stabilizes around the theoretical -11 dBm limit when the ER is infinite.

Figure 3.8(b) highlights the worst-case length of the fiber link that leads to $d_T \approx 0.2$ as a function of the ER of the pulses. It can be observed that as the ER increases the worst-case length tends to infinity, which makes sense considering that the pump pulse depletion is cumulative all along the sensing fiber. However, for smaller ER values, the worst-case fiber length is reduced. This is due to the fact that by reducing the interaction length between pump and probe waves, the interaction takes place with higher optical power of both waves. As a consequence of this higher power, the amplification of the probe wave that the pedestal induces is greater, and hence, the total depletion d_T is larger than even with longer interaction lengths. Besides, as portrayed in Fig. 3.8(c), for small ER values of the pump pulse, both the pump pulse and pump pedestal depletion factors play an important role on the contribution to the total depletion, been more significant d_P as decreasing the ER. However, by increasing the ER of the pulse the total depletion factor can be attributed to the onset of pump pulse depletion. In any case, note that for high ER values, as highlighted in Fig. 3.8(a), the ER of the pump pulses do not introduces a significant penalty to single-probe BOTDA gain configuration schemes.

Finally, it should be pointed out that the theoretical model presented in section 3.2 can also be used to study the dependencies of non-local effects induced by the pedestal depletion on system parameters. It has been found that, as well as in the case of first-order non-local

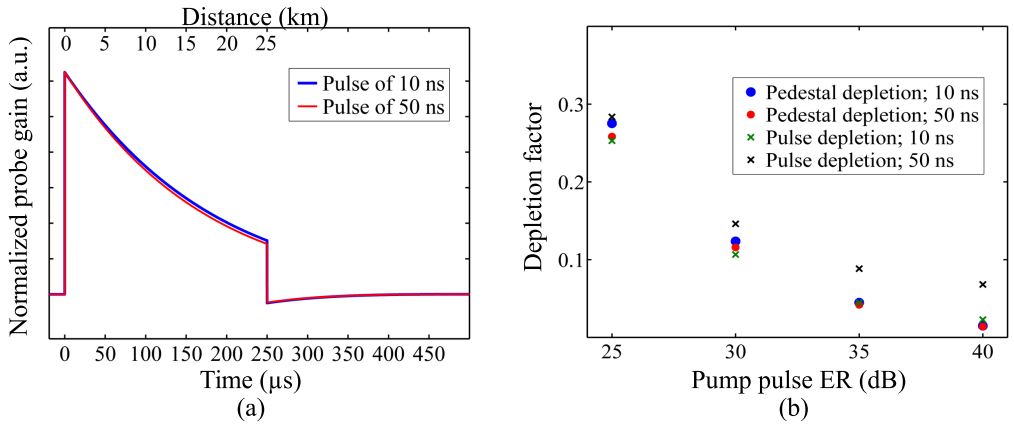

Figure 3.9: *(a) Normalized Brillouin gain of the probe wave as a function of pulse duration. The traces are depicted in terms of time-of-flight of the pump pulse with an added axis (top) with the translation to location along the fiber. (b) Values of pulse depletion factor, d and pedestal depletion factor, d_P.*

effects, the pedestal depletion increases with increasing the optical power of either probe or pump waves. Therefore, the calculations in this section, which have been performed for the highest practical powers of these two waves, constitute a realistic scenario.

The theoretical model was also used to analyze the dependence of the pedestal depletion with the pulse duration. Figure 3.9(a) depicts the normalized Brillouin gain of the probe wave for two different pump pulse duration, 10 ns and 50 ns, of 20 dBm power and a fixed 30 dB ER counter-propagated to a −3 dBm dual-probe wave. As it can be observed, both calculated BOTDA traces have a very similar shape. Figure 3.9(b) highlights the different components of the total depletion factor at the end of the fiber as a function of the ER of the pulses of 10 ns and 50 ns. As it is observed, the depletion factor due to the pedestal depletion has a similar influence for the studied two pump pulse durations. Specifically, the differences in d_P between both pulse duration in the case of small ER values are not very relevant and practically are non-existent when increasing the ER. On the contrary, pump pulse depletion presents a higher influence on the pulse duration, being greater as the duration of the pulse increases, which is consistent with previous studies of pump pulse depletion in which the ER is considered to be infinite [31]. Besides, note that the higher the ER the greater the influence of the pulse duration. Therefore, it can be concluded that the pedestal depletion has a very small dependence with the pulse duration.

3.4.2 Effects of the transient response of EDFAs in BOTDA sensors

In this section, another new measurement distortion effect in BOTDA sensors is explained, which is induced by the interaction between the transient behavior of the EDFA and the pedestal of low-ER pulses. It is well known that EDFAs present a transient behavior when amplifying pulsed signals. This is due to the long recovery time of the population inversion of the erbium ions after amplifying an optical pulse [101, 102]. In BOTDA sensors with low ER pulses, this effect distorts the pump wave shape because the EDFA has a different instantaneous gain before the arrival of the pulse, i.e., for the leading pedestal, than for the trailing pedestal. Specifically, as the pulse arrival depletes the population inversion in the EDFA, the trailing pedestal initially undergoes less amplification than the one that is experienced by the leading pedestal. This amplification slowly recovers but a permanent distortion of the trailing pedestal is induced.

Figure 3.10 schematically describes the influence of EDFA amplification on the pump wave shape, and how the distorted pump wave and the probe wave interact along the

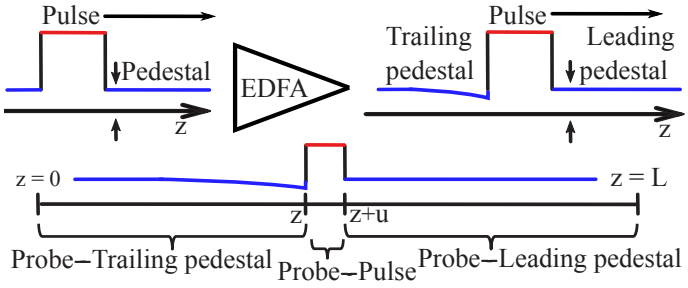

Figure 3.10: *Schematic description of probe and pulse wave interaction along the fiber for the case of a distorted trailing pedestal due to EDFA transient response.*

fiber. The effects of the distortion of the pump pulse pedestal induced by the transient response of the EDFA are similar to those originated by the trailing pedestal depletion that were described in the previous section. The contribution to the measured gain of the probe wave is smaller for the interaction with the distorted trailing pedestal than with the leading pedestal. Hence, again, the use of the probe gain without pulse in the fiber to normalize the measurements induces an error, because the portion of the gain due to interaction with the pedestal becomes overestimated. This leads to an independent and additional depletion factor, which is induced by the EDFA transient response.

Due to the fact that the transient gain response of an EDFA for the pulse amplification depends on the EDFA design itself, the development of a theoretical analysis of this effect is complicated. Moreover, this transient response displays a complex dependence on the pulse power, duration, etc. [102]. Therefore, as the behavior of EDFAs cannot be generalized, the details of this effect are presented and analyzed after its experimental demonstration in section 3.4.5.

3.4.3 Experimental setup

Figure 3.11 depicts the dual-probe BOTDA setup that was deployed to experimentally demonstrate the effects of the limited ER of the pump pulses on BOTDA sensors. In addition, the measurements are also used to validate the theoretical model presented in section 3.2. The optical source was a 1560-nm distributed feedback laser, whose output was divided by a coupler into two branches. In the upper branch, the pump pulse wave with tunable ER was generated by using either a Mach-Zehnder electro-optic modulator (MZ-EOM) or a semiconductor optical amplifier (SOA) switch. The SOA was deployed to provide pulses with a high ER of around 45 dB, and the MZ-EOM was used to generate pulses with ER from 20 to 26 dB by adjusting its bias point and the amplitude of the electrical pulsed signal that was used to drive the device. The pulsed pump signal was then amplified with an EDFA and filtered to reduce the amplified spontaneous emission. Before injecting the pump wave into the fiber under test (FUT) via a circulator, so as to reduce polarization-mismatching-induced fluctuations on the signal, its state of polarization was randomized with a polarization scrambler (PS). The pump peak power was limited to

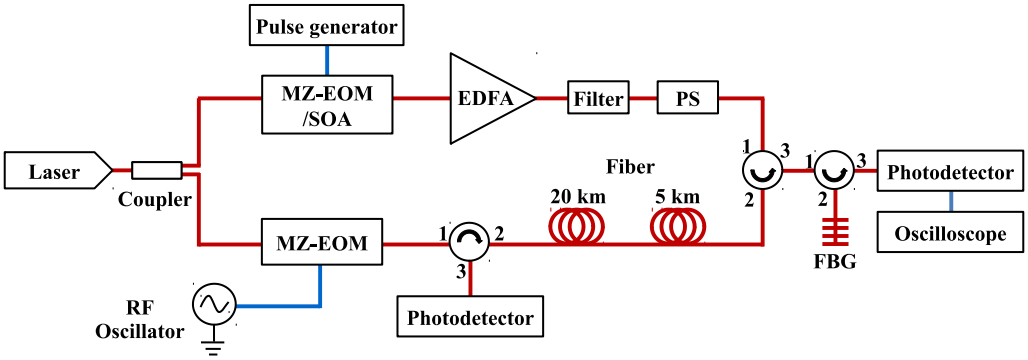

Figure 3.11: *Experimental setup deployed to demonstrate the effects of the pump pulse ER on BOTDA sensors.*

20-dBm in order to avoid MI effects in the fiber [37]. Moreover, in most of the measurements the pump pulse duration was set to 60-ns in order to have a good SNR, particularly in measurements that used very small probe power.

In the lower branch of the setup, a dual-probe wave was generated using another MZ-EOM driven by a radio-frequency (RF) generator tuned to the BFS of the fiber and biased for minimum transmission. Finally, a tunable narrow-band fiber Bragg grating (FBG) was used to filter out the upper frequency probe wave before using a receiver to detect the signal with an oscilloscope. At the other end of the FUT, the depletion of the pump pulses was monitored using a circulator and another detector.

The FUT was comprised of two different fiber spools with 5-km and 20-km length with the same BFS but slightly different Brillouin gain coefficient. In addition, two hotspots were prepared along the FUT using a climatic chamber: one after the first spool and the other at the end of the link.

3.4.4 Demonstration of non-local effects due to pump pulse limited ER

Experiments were conducted to experimentally demonstrate the non-local effects originated by the limited ER pump pulses in BOTDA sensors. As explained in section 2.2, the dual-probe configuration presents essential advantages compared to the single-probe BOTDA setup. This makes the study of a dual-probe setup far more interesting, therefore, the experiments were carried out with a dual-probe BOTDA configuration. In order to avoid or at least mitigate the effects due to the EDFA transient response, an EDFA (Amonics Ltd. Pulsed EDFA) specially designed for amplification of isolated pulses with almost no distortion was deployed in these experiments.

Figure 3.12(a) shows the detected BOTDA traces measured at BFS of the fiber when pump pulses with different ER were counter-propagated to a -3-dBm dual-probe wave. Note that the detected BOTDA trace when the SOA is used to shape the pulses is the only one that undergoes no significant distortion, while the traces obtained using the electro-optic modulator (EOM) are distorted by the interaction between the probe waves and the pump wave pedestal. An interaction that, as explained above, leads to two non-local effects: pump pulse depletion and pump pedestal depletion. As it can be observed, the BOTDA trace distortion increases when the ER of the pump pulse is worsened. The figure also shows the traces calculated using the theoretical model introduced in section 3.2, which agree well with the experimental results. The small deviation between theory and experiments is attributed to the residual effects of the EDFA transient response that will be analyzed in section 3.4.5.

Figure 3.12(b) also depicts BOTDA traces, but this time measured for a fixed ER of the pump pulses of 23 dB and with different probe wave optical power levels. Note that for comparison the black line shows an ER of 45 dB, which was obtained with the SOA switch and a low probe wave power. As it was expected, the distortion of the traces increases for increasing probe power. Whereas, for low probe power, the measured signal matches that obtained with the large-ER SOA switch. However, as the probe power is risen, the trailing pedestal of the pulse starts to deplete due to the interaction with the amplified

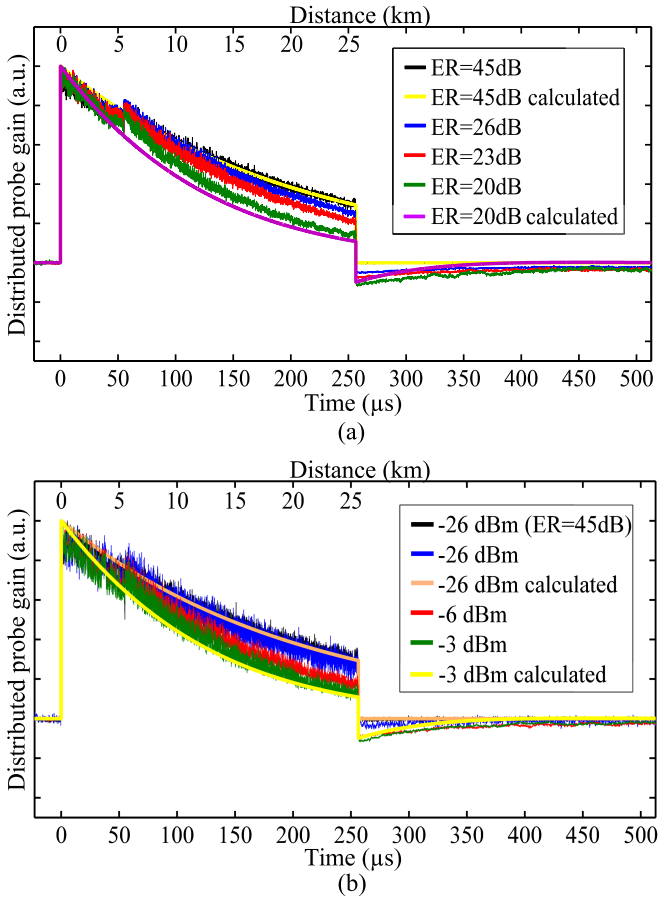

Figure 3.12: *BOTDA trace distortion due to the ER of the pump pulse. (a) Dependence on the ER level; (b) Dependence on the probe wave power for a fixed ER of 23 dB. The black line shows the same for an ER of 45 dB, for comparison.*

probe wave. Therefore, the BOTDA trace is distorted by the normalization performed, as explained in section 3.4.1, leading to the onset of non-local effects. Again, in this figure, the calculated theoretical values are also shown, which show a good agreement with the experiments performed.

In order to examine the contribution of both the depletion of the pedestal and the depletion of the pulse to the distortion of the BOTDA trace, the depletion factor of both effects, d and d_P, were measured. Figure 3.13 depicts the measured depletion factors at the end of the fiber link as a function of the probe power, where pulse depletion, pedestal depletion and total depletion factors are represented. The obtained results are plotted together with the calculations performed using the theoretical model. Note that the theoretical calculation of the pedestal gain depletion is presented with and without taking into account the EDFA transient effects that will be studied in the next section. These effects, as explained in section 3.4.2, are shown to introduce an additional depletion factor, even though the deployed EDFA in these experiments had a very small transient response. Notwithstanding, there was a good general agreement between the experimental results and the model calculations. This figure demonstrates that the non-local effects due to the pedestal depletion in limited ER BOTDA sensors are very significant, contributing

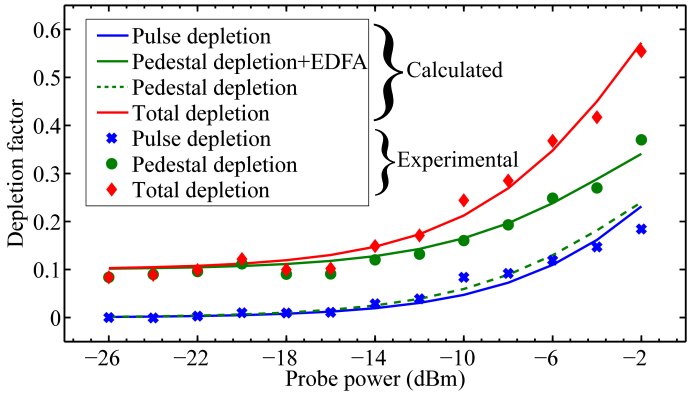

Figure 3.13: *Depletion factor d_p and d dependence on the probe wave power when deploying pump pulses with 23-dB ER.*

in the same order of magnitude than the effects due to the pump pulse depletion.

Finally, the error made by determining the BFS of the fiber due to the effects of the ER of the pump pulses was characterized. For this purpose, the Brillouin gain spectrum (BGS) was measured along the fiber while the temperature of the hotspots was fixed by a climatic chamber at 9° C of difference from the rest of the fiber, which was also controlled by another climatic chamber. The resultant BFS distribution along the 2 hotspot are depicted in Fig. 3.14. As it is observed, the error with respect to the reference measurement performed with the SOA is worsened with increasing the fiber distance, as it was expected. So there is negligible error in the first hotspot, whereas, for the second hotspot at the far end of the FUT, the BFS error becomes significant. In addition, the effect increases when the ER is worsened, so that at the hotspot at the end of the fiber the BFS error raises to 3, 4.5 and 7.5 MHz for 25, 23 and 21 dB ER pulses, respectively. Note that as the temperature was heated the BFS is overestimated, while if the fiber had cooled the BFS would be underestimated, as for other non-local effects.

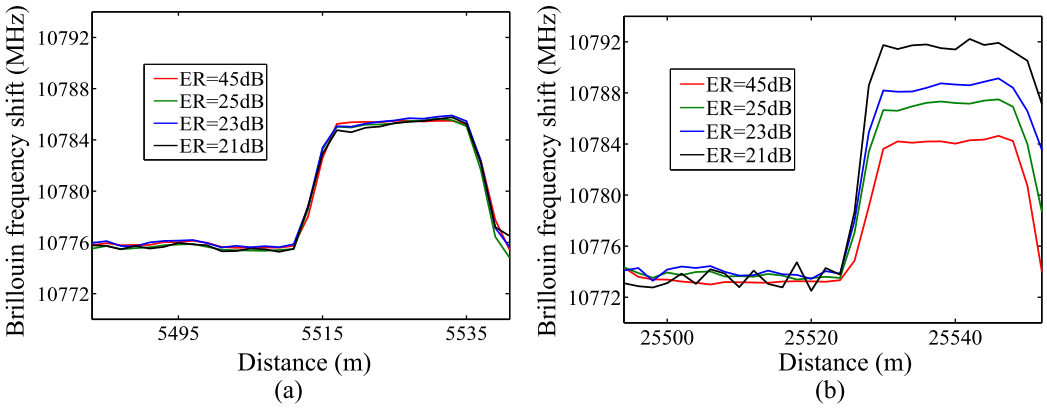

Figure 3.14: *Measurement error induced by 25-dB, 23-dB and 21-dB ER pump wave in different positions of the fiber for a -3 dBm per sideband probe wave power: (a) at a distance of 5 km and (b) at the end of the fiber.*

3.4.5 EDFA transient response characterization and influence on BOTDA sensors

The other measurement distortion effect that was experimentally investigated is due to the interplay between the transient response of EDFAs and the limited ER of the pump pulses in BOTDA sensors. First, a detailed characterization of the transient response of several EDFAs was performed, and then, their distortion effects on BOTDA measurements were assessed.

The transient response of an EDFA while amplifying a pulse cannot be simply characterized by monitoring its time-domain output power. This is because the dynamic range required to be able to observe simultaneously the pulse and the small effects on the pulse pedestal is too large. Therefore, to correctly measure the transient response of the EDFAs available in our laboratory, we devised the experimental setup depicted in Fig. 3.15. The setup is based on adding an extra CW signal, which was generated by another laser, to the pump pulse signal that is subjected to analysis. In this way, when amplifying the signal by an EDFA, the transient variations of the EDFA gain could be monitored on this added CW. The extra laser signal was separated by approximately 0.5 nm from the pump pulse wavelength and its power was set to be 10-dB lower than the average power of the pump wave, so that its addition had a negligible effect on the EDFA transient response. This fact was experimentally checked by measuring the pump pulse and the resultant BOTDA trace with and without the presence of the extra laser signal, verifying that the resultant measured signal in both cases was equal. Finally, at the output of the EDFA the monitored wavelength was separated with a FBG and detected in a photo-receiver followed by an oscilloscope, where the precise variations of the gain of the EDFA while amplifying the pump pulse wave could be measured.

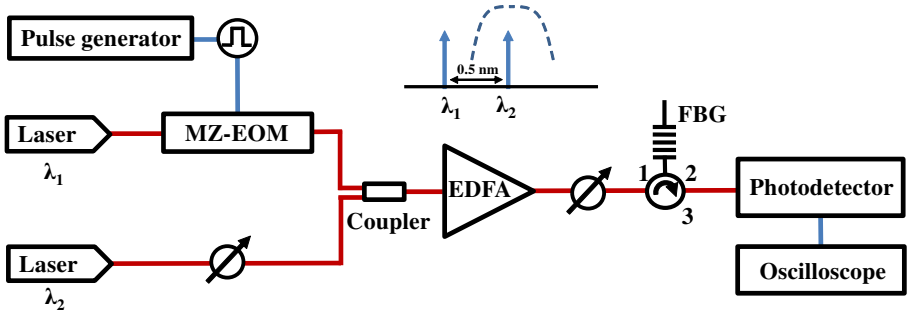

Figure 3.15: *Experimental setup deployed for the characterization of the EDFA transient responses to pulsed signal amplification.*

Three commercial EDFAs set for a nominal 20-dB gain were tested to compare their performances: EDFA I (MPB Communications Inc.), has 3 amplifying stages and 21-dBm saturation power, EDFA II (Manlight S.A.S) provides 23-dBm output saturation power using 2 pump stages and EDFA III (Amonics Ltd. Pulsed EDFA) corresponds to the special amplifier design for pulse amplification deployed in section 3.4.4.

Figure 3.16 shows the temporal variation of the gain of the three EDFAs when amplifying the pulsed pump signals with different ER levels, 20, 23 and 26 dB. Note that the

arrival of the pulse perturbs the gain of EDFA I and II, which clearly display a transient response after the pulse amplification. In particular, EDFA I has a larger variation of the gain than EDFA II, however, the recovery time is longer for the latter. The magnitude of the transient variation of the gain depends on the ER of the pulses. For the two EDFAs, the greater the ER, the larger the gain change. In contrast to EDFAs I and II, EDFA III displays a smaller variation as expected. Although enough to increase significantly the pedestal depletion factor, as has been discussed in section 3.4.4 by observing Fig. 3.13.

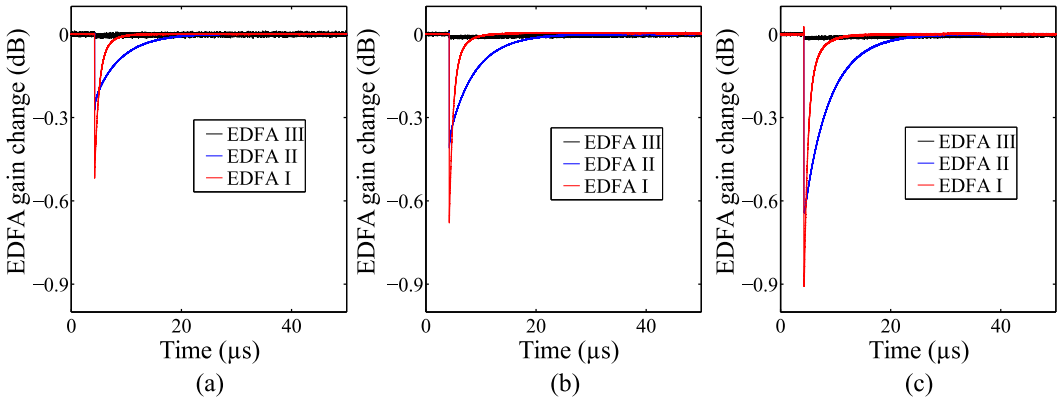

Figure 3.16: *Variation of the EDFA gain after the amplification of pump pulses with ER of (a) 20 dB, (b) 23 dB and (c) 26 dB. Three different commercial EDFA are measured.*

To analyze the constraints that the transient of the EDFA entails in BOTDA sensors, this effect must be isolated from both the pump pulse and the pump pedestal depletion effects. To that end, the probe wave sidebands were set to -18.5-dBm power to ensure that non-local effects, either due to pump pulse or pedestal depletion, were negligible. Figure 3.17(a) and 3.17(b) respectively show the BOTDA trace distortion when EDFA I and EDFA II were deployed to amplify the pump pulse wave with different ER levels, 20 dB, 23 dB, 26 dB and 45 dB. When a 45-dB ER SOA is deployed to shape the pump pulses, the BOTDA traces remain undistorted for the two amplifiers, with just the characteristic 0.2 dB/km roll-off of the fiber loss coefficient. In this case, the transient response of the EDFA has no significant effect since the pedestal of the pulse is negligible. On the contrary, the use of a limited ER MZ-EOM leads to a severe distortion of the measurements. The smaller the ER, the larger the distortion. Moreover, it was found that the distortion does not depend on the probe power, provided the probe wave power is small enough to avoid the onset of non-local effects. Calculations using the model introduced in section 3.2 are also plotted in the figure, showing again excellent agreement with the experimental results. These calculations were made using a pump wave signal incorporating the trailing pedestal distortion shown in Fig. 3.16.

The origin of this BOTDA measurement distortion lies in the variation of the EDFA gain after amplifying the pulse that was depicted in Fig. 3.16. This variation affects the shape of the trailing pedestal of the pump pulse: initially its amplitude is reduced in comparison with the amplitude of the leading pedestal and then slowly recovers until the amplitude equals the one of the leading pedestal. The temporal reduction of the amplitude of the trailing pedestal has a similar effect on the measurements than the previously

discussed depletion of the trailing pedestal by the amplified probe wave. Once again, the amplification of the probe wave due to its interaction with the trailing pedestal is smaller than the obtained when there is no pulse in the fiber. This in turn introduces a depletion of the actual probe gain measurement after the measurement is normalized using the probe gain without pulse in the fiber as reference, because the latter overestimates the contribution of the pedestal to the total gain experienced by the probe. Therefore, in much the same way as before, a specific depletion factor linked to this effect can be defined and used to calculate the BFS error induced in the measurements. Note that the measurement distortion for EDFA II is larger than for EDFA I. This is due to the fact that the energy lost by the trailing pedestal due to its power reduction by the transient response of the EDFA is larger in EDFA II than in EDFA I, because the recovery time of the gain is larger, as it can be seen in Fig. 3.16.

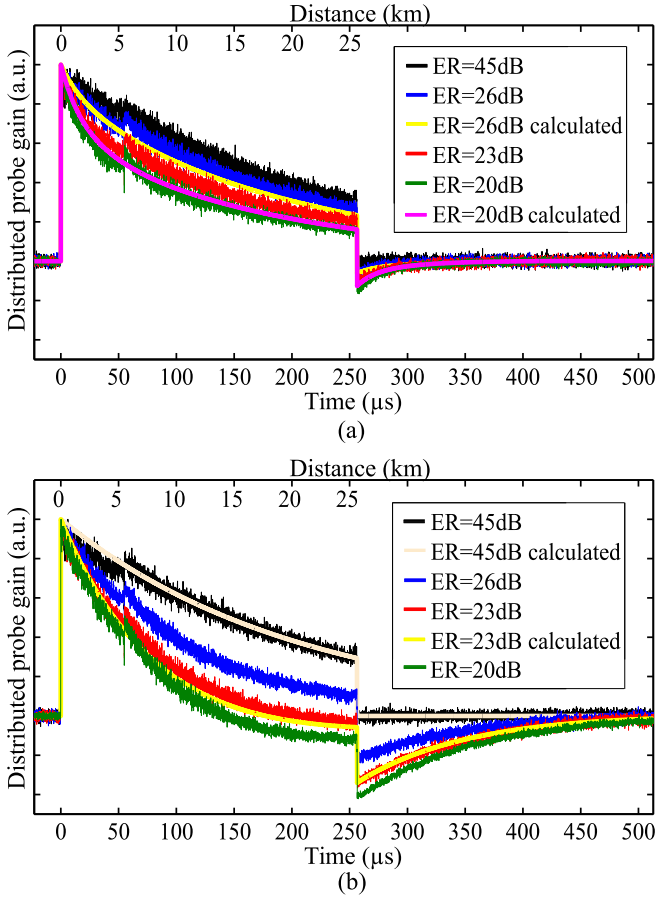

Figure 3.17: *Experimental and theoretical BOTDA trace distortion due to EDFA transient response for different pump pulse ER values and different EDFA, (a) for EDFA I and (b) EDFA II.*

In order to estimate how these distortions affect on the sensor performance, the BFS along the fiber was measured for several ER levels of the pump pulses in the system using EDFA I. For this purpose, the BGS was measured along the fiber while the temperature of the hotspots was fixed by a climatic chamber at 9° C of difference from the rest of the fiber, which was also controlled by another climatic chamber. Figure 3.18(a) and 3.18(b)

show the resultant BFS distribution at the two hotspots along the link. Again, the probe power was kept low at -18.5 dBm in order to suppress the influence of pulse and pedestal depletion on the measurements. Note that a very significant BFS error is introduced by this effect, not only at the end of the FUT but even at the 5th kilometer, where the induced error is of a similar order to that at the end of the fiber. This response is caused by the distorted shape of the trailing pedestal due to the transient behavior of the EDFA explained in Fig. 3.16. It is important to underline that the measurement in Fig. 3.18(b) displays some BFS variations before the hotspot start (indicated with a vertical dashed line), which was due to an unintended strain introduced between measurements.

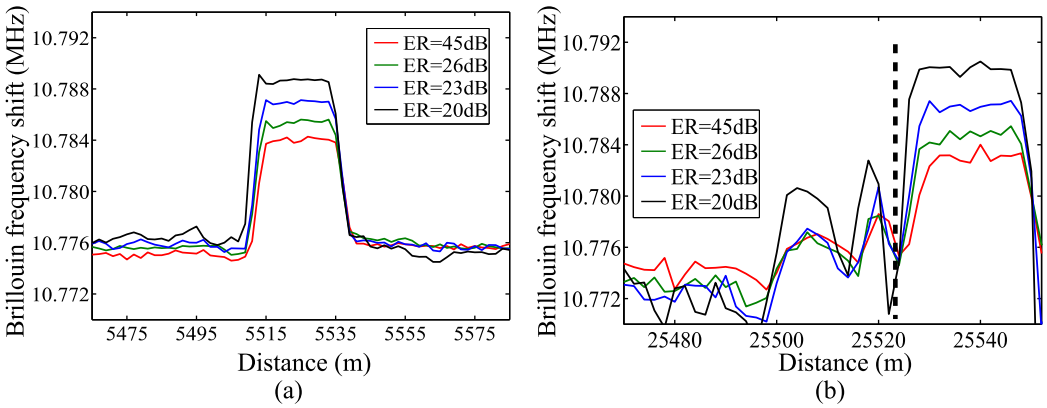

Figure 3.18: *Resultant Brillouin frequency shift along the hotspots deployed using the EDFA I: (a) hotspot I (b) hotspot II.*

3.5 Conclusions

In this chapter, the impairments caused by the limited ER of the pump pulses have been introduced, which have been shown to severely constrain the performance of BOTDA sensors. This is because the effects induced by the low-ER pump pulse constrain the SNR of the detected probe wave. In this way, we have analyzed how the pulse depletion grows when the ER of the pulses decreases. So, even the dual-probe BOTDA sensor performance is still seriously compromised when pump pulses with limited ER are deployed because, first of all, the pump pulse depletion is increased. In addition, two unknown non-local effects in BOTDA sensors induced by the limited ER of the pump pulses have been presented, with theoretical and experimental analysis. These effects are due to the depletion of the pump pedestal and the EDFA transient-induced pedestal distortion. Therefore, conventional BOTDA sensors have their probe power severely contained by these non-local effects that distort the pump wave: pump pulse depletion, pump pedestal depletion and pump trailing pedestal distortion due to the EDFA transient response.

The onset of pulse depletion in a dual-probe setup results from the power unbalance between both probe waves due to their Brillouin interaction with the pump pedestal. Furthermore, it has been found that together with first-order non-local effects, the limited ER of the pump wave generates other non-local effects, which are due to the pump pedestal depletion. This effect originates in the extra depletion of the trailing pulse pedestal due

to the interaction with a probe wave that has been previously amplified by the pulse. The depletion of the trailing pedestal can be characterized by a dimensionless depletion factor that we called pedestal gain depletion factor. We have seen that this depletion factor has a magnitude that is of the same order than the one coming from the depletion of the pulse, and hence, it introduces an impairment of identical nature to the measurement accuracy of the BOTDA sensor. The addition of these two non-local effects constrains the performance of the sensor. In this way, it is found that, for instance, in a conventional dual-probe BOTDA setup, an ER>32 dB is needed to have less than 1-MHz BFS measurement error. Moreover, another deleterious effect has been found. This effect arises when amplifying the limited ER pulses with an EDFA, because the EDFA transient response distorts the trailing pedestal. The impairments brought by this effect can be even more important than the constraints induced by previous non-local effects, depending on the particular EDFA device used to amplify the pulse. The constraint that the EDFA transient response imposes is independent of the probe wave power deployed; hence, they set an upper bound to the BOTDA sensor performance. In addition, due to the pedestal depletion, if a technique for mitigation of second order non-local effects is deployed, an ER greater than 43 dB would be required.

Such a large ER is typically just within the reach of SOA switches or acousto-optic modulators (AOMs). However, these pulse shaping devices have rise and fall times that are typically of the order of 1 ns for SOAs and longer for AOMs, which compromise the capability to perform high-spatial-resolution measurements using, for instance, the differential pulse-width pair (DPP) technique [70]. Furthermore, pulses with less steep leading and trailing edges are prone to the deleterious effects of self-phase modulation, which has been shown to degrade the BOTDA sensor performance [44]. Therefore, in order to generate the sharp pulses that are needed for high-spatial-resolution measurements using the DPP technique, a MZ-EOM is required. However, MZ-EOMs usually have low ER, typically of the order of 20 to 30 dB, which would not comply with the rigid condition for the ER stated above. Note that two cascaded MZ-EOMs could be used in order to keep the fast response with an improved ER, but at the expense of an added setup complexity and an increased cost of the sensor.

In summary, the effects of the ER of the pump pulse have been shown to seriously impact the BOTDA sensor performance, particularly those that deploy EOMs to shape the pulses. Therefore, it is of paramount importance the research work focused to overcome these effects, so that to improve the performance of long-range BOTDA sensors. In this way, in the following chapters solutions to these non-local effects are presented. Moreover, in chapter 5, a study of the errors induced by the depletion of the pulse in a coded-pump wave BOTDA system is reported. Further research will be focused on investigating the significance of the pump pedestal induced effects in BOTDA systems deploying pump pulse coding. It is expected that the degradations imposed by both the pulse depletion and pedestal depletion will have a more pronounced impact in such systems because of the use of large sequences of pulses. This may impose even stronger constraints on the ER of the pulses deployed.

Chapter 4: Frequency modulation of the probe wave wavelength in BOTDA sensors

Contents

4.1 Introduction

The ultimate performance of long-range Brillouin optical time-domain analysis (BOTDA) sensors is determined by the signal-to-noise ratio (SNR) at the receiver. In this sense, due to the attenuation of the optical fiber, which makes the optical power of the probe and pump waves to be significantly reduced, the sensing length of BOTDA sensors is limited. In addition, as explained in chapters 2 and 3, non-local effects (NLE) are among the main obstacles in BOTDA sensors, considering that their onset limits the maximum probe wave power that can be deployed into the sensing fiber. As a consequence of this power constraint, NLE worsen the SNR and, therefore, limit the sensing range of the analyzer. Furthermore, even though NLE were completely overcome, another limit for the probe power would remain: the Brillouin threshold of the fiber [34]. That is why the research efforts to overcome NLE and the Brillouin threshold of the fiber are of paramount importance. A significant contribution in this research field, which was devised by our research group, lies in adding an optical frequency modulation or dithering to the probe wave [48, 49]. This technique has been employed to mitigate or even overcome the various

NLE presented in chapter 2: first-order NLE [31] and second-order NLE [33]. In addition, the noise induced by spontaneous Brillouin scattering (SpBS) on the detected probe wave can also be overcome [48, 49].

In this chapter, the benefits of using the probe dithering method in BOTDA sensors are presented. Section 4.2 introduces the theoretical fundamentals of the technique, together with the explanation of the improvement of the impairments induced by first-order and second-order NLE brought by the method [48, 49]. After outlining this procedure, inasmuch as we have continued studying the advantages of the method, the next sections present the outcomes obtained during the conduct of this thesis dissertation.

First, an extra constraint of the techniques presented so far in the literature to compensate second-order NLE (see section 2.5), including the probe dithering, is reported. This constraint is due to the fact that all the methods designed to overcome second-order NLE are only fully effective in case the Brillouin frequency shift (BFS) of the sensing fiber is uniform. This will be shown by a theoretical and experimental demonstration. Additionally, a new method to completely compensate second-order NLE that works with any distribution of BFS along the fiber, and also may be applied to all the methods introduced in section 2.5, is presented. This BOTDA sensor is based on dynamically modifying the wavelength of the probe wave to adapt to the changes in average BFS of each section of the fiber sensing link. We demonstrate this technique by adding it to the probe dithering method.

Second, as stated in chapter 3, a limited extinction ratio (ER) pump pulse severely constrains the performance of BOTDA sensors. In this chapter, we describe how the probe dithering technique is not only able to overcome first-order and second-order NLE, but also greatly diminishes the impairments caused by the low ER pump pulse. By using this method, the gain induced by the pedestal of the pump wave is reduced, and consequently, the depletion of both pump pulse and pump pedestal are overcome. Furthermore, the errors induced by the distortion of the trailing pedestal when an erbium-doped fiber amplifier (EDFA) is used to amplify the pump pulse are also diminished.

4.2 Theoretical fundamentals of the probe-dithering BOTDA sensor

The theoretical foundations of the proposed technique are schematically depicted in Fig. 4.1, where the optical waves involved in the method, as well as the Brillouin interaction on the pump and probe waves are highlighted. As can be observed in the figure, the idea is to introduce a modulation or "dithering" to the optical frequency of the probe waves.

In the example shown in Fig. 4.1, the optical frequency of the probe waves is modulated in the time domain following a saw-tooth shape [55]. However, note that other modulation shapes are possible, for instance, a sinusoidal or a triangular shape could be deployed, which have been shown to have a similar performance response [48, 49]. In addition, this frequency modulation (FM) is synchronized to the pump pulses, so that a series of pulses experience the same optical frequency of the probe waves at any given location of the

fiber. Altogether, this makes the effective optical frequency of the probe wave vary along the optical fiber following the applied FM shape. Therefore, the pump pulse, as it travels along the fiber, experiences stimulated Brillouin scattering (SBS) interaction with probe wavefronts that have a different frequency detuning. In this way, the resulting Brillouin interaction between pump and probe waves is given by the frequency detuning from the center of the Brillouin spectrum at each position of the fiber:

$$\Delta\nu_L(z) = \nu_{SL}(z) - \nu_P + BFS(z) \tag{4.1a}$$

$$\Delta\nu_G(z) = \nu_P - \nu_{SU}(z) + BFS(z) \tag{4.1b}$$

where $\Delta\nu_L$ and $\Delta\nu_G$ are the detuning of the Brillouin loss and gain spectra respectively, ν_P is the pump pulse frequency and ν_{SL} and ν_{SU} are the optical frequencies of the lower-frequency probe sideband and the upper-frequency probe sideband at a particular position z of the fiber, respectively. From this expression it follows that having a real variation in BFS due to the fiber characteristics is equivalent to having the same variation in the probe wave frequency. Therefore, the net effect is completely analogous to having a virtual BFS distribution in the fiber, in the sense of having a fiber whose BFS profile has the same shape as the FM provided to the probe wave [48].

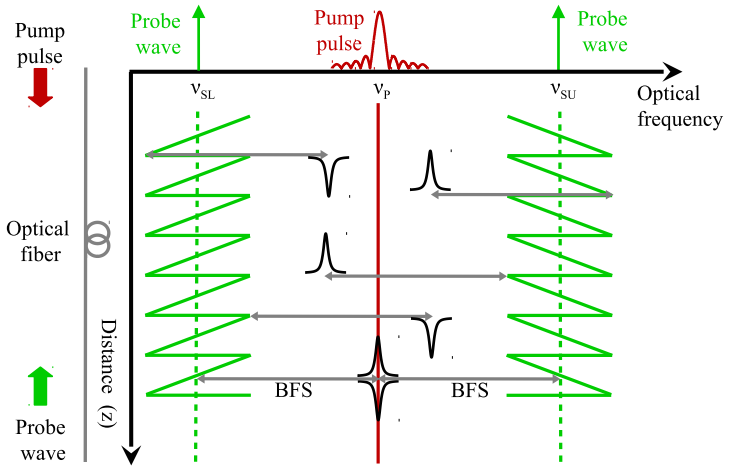

Figure 4.1: *Fundamentals of the technique for mitigation of non-local effects.*

This virtual BFS profile can be used, as it will be presented in the following subsections, to compensate NLE and also to increase the Brillouin threshold of the fiber, which reduces the noise at the detected probe wave. The presented technique is based on the same idea as the methods that, in order to mitigate NLE, use an optical fiber compounded of various fiber segments with different BFS characteristics [50]. With the main advantage that it is not necessary to modify the fiber along the sensing structure, which is a tiresome process. On the contrary, the technique can use any optical fiber that is already installed and create a virtual BFS profile along the sensing fiber by using a wavelength modulation of the probe wave.

This method has been proved by direct modulation of the optical source used to generate both waves, the pump and the probe, and also by modulation of the optical device used to generate the probe wave. Both methods are presented in the following subsections.

4.2.1 BOTDA sensor based on the modulation of the optical source wavelength

Figure 4.2 depicts the fundamentals of the BOTDA sensor based on the direct modulation of the optical source wavelength used to generate the two optical waves that are involved in BOTDA sensors: the pump and the probe waves [48]. As shown in the figure, the injection current of the laser is directly modulated using a sinusoidal wave signal generator, which is synchronized to the pump pulse generator. This induces a modulation of the output optical signal wavelength via the chirp of the laser, which follows the shape of the modulation signal [103]. Note that, in the figure, a sinusoidal wave is portrayed as an example, however, as explained before, other modulation shapes are possible [48].

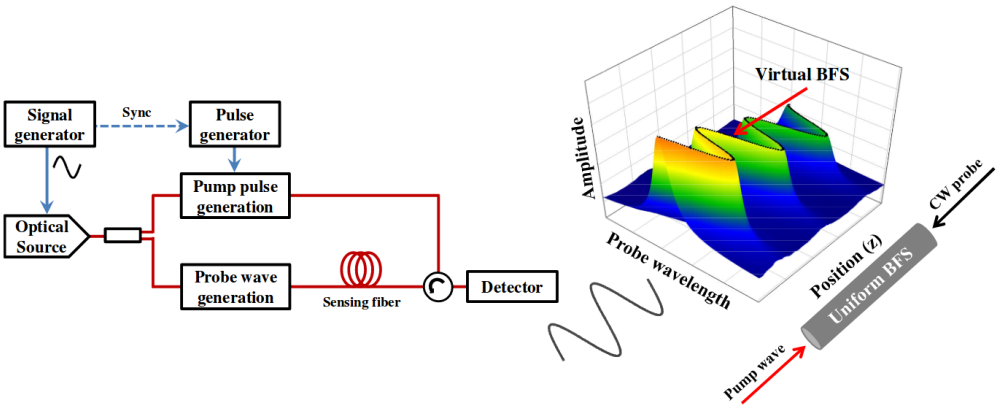

Figure 4.2: *Fundamentals of the laser wavelength dithering technique.*

The laser source is split into two branches. The upper branch is used to generate the pump pulse wave, whereas the lower branch is used to generate the probe wave. Therefore, the optical signal that is used to generate the two waves that interact in the BOTDA sensor has a wavelength modulation. Depending on the particular BOTDA configuration (gain, loss or dual-probe) to be implemented, the procedure to generate both optical waves, as well as the frequency sweep used to scan the Brillouin spectrum, vary. Either way, the pump pulse generation must be synchronized with the FM of the optical waves, inasmuch as the particular frequency shift between the pulse and the probe wave at each location of the fiber needs to be known and controlled.

It is worth mentioning that the only difference of the sensor setup with respect to a conventional BOTDA setup lies in the addition of a FM of the optical source, which is performed using a low frequency periodic wave synchronized to the pulse generator. However, in contrast to conventional BOTDA sensors, the frequency of the probe wave varies along the optical fiber according to the FM applied to the optical source. As a consequence, the pump pulse meets a probe wave of different frequency at each location of the fiber, as explained before. Therefore, a virtual BFS profile is synthesized by the FM of the probe wave. In addition, note that the pump wave pedestal and the probe wave have their wavelengths modulated following the same shape.

4.2.2 BOTDA sensor based on the optical FM of the probe wave

This variation of the technique is based on introducing a modulation or "dithering" just to the optical frequency of the probe wave. To that end, in contrast to the method introduced in the previous subsection, the FM of the probe wave is directly generated during the generation process of the probe itself. Hence, the pump pulse wave does not have its optical frequency modulated, and consequently, the pump pedestal consists of a single wavelength. The fundamentals of the technique are schematically depicted in Fig. 4.3, where the optical waves involved in the method as well as the Brillouin interaction on the pump and probe waves are depicted. As shown in the figure, in this particular example the optical frequency of the probe waves is modulated in the time domain following a saw-tooth shape [55]. Nevertheless, as explained before, other modulation shape can be used.

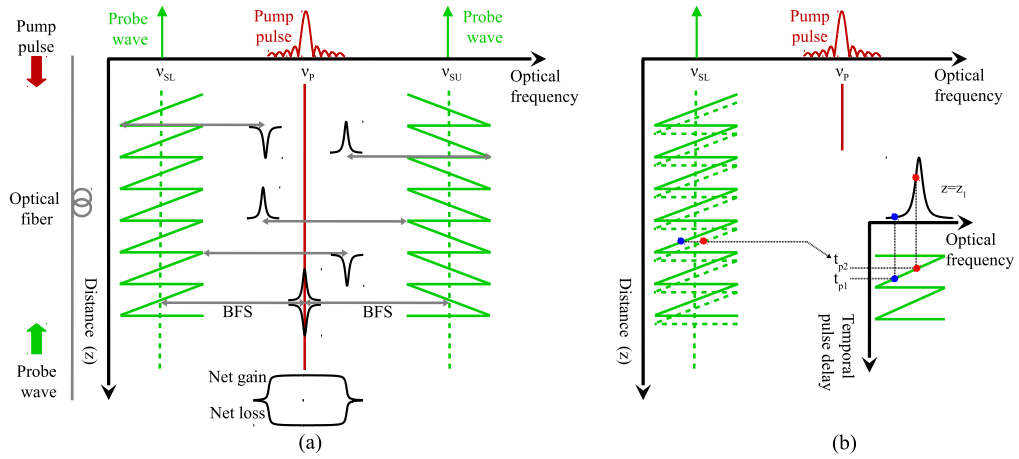

Figure 4.3: *Fundamentals of the probe dithering technique: (a) Brillouin interaction on the pump pulse and (b) frequency scanning method based on the temporal delay change (t_{p1} and t_{p2}) between probe and pump waves.*

The dual-sideband probe wave can be generated, for instance, using a Mach-Zehnder electro-optic modulator (MZ-EOM) driven by an arbitrary waveform generator (AWG) and biased at the minimum transmission point of its transfer curve [49]. The AWG provides a FM microwave signal whose instantaneous frequency varies around the average BFS of the fiber following a specific periodic shape. Additionally, this FM is synchronized to the pump pulses so that a series of pulses experience the same optical frequency of the probe waves at any given location. Altogether, this makes the effective optical frequency of the probe wave vary along the optical fiber following the applied FM modulation shape. As with the optical source wavelength modulation technique, which has been described in the previous subsection, the pump pulse interacts via SBS with a probe wave of different frequency at each location of the fiber. Therefore, a virtual BFS profile is synthesized by the FM of the probe.

It is important to point out that, as schematically depicted in Fig. 4.3(b), the FM of the probe wave is also used to perform the frequency scan of the Brillouin spectra, instead of doing it by a conventional frequency sweep. For that purpose, at each location of the fiber, the pump pulse is made to interact with different probe wave frequencies simply by

changing the relative delay between the probe wave FM and the pump pulse [49]. Note that the number of relative delay steps is given by the relation between the peak-to-peak frequency deviation of the FM, which defines the range of frequencies to scan, and the desired frequency step; hence, the number of measurements to scan all the frequencies is exactly the same as in a conventional BOTDA scheme. Therefore, there is no penalty at all regarding measurement time in comparison with a conventional frequency sweep. This is the main advantage of this variation of the method in comparison to the one presented in the previous section, inasmuch as in the latter, as the frequency scan is performed by making a frequency sweep, in order to measure the total Brillouin spectrum the measurement time is increased. In addition, due to the frequency sweeping, the compensation of NLE is not as efficient.

The final Brillouin spectra is obtained after a post-processing of the measurement to compensate the frequency shift introduced to the probe wave at each location due to the FM. This post-processing needs to know the probe frequency along the fiber for a given delay between pump and probe waves. This is accomplished by measuring the length of the fiber and the optical path difference between the pump and the probe branches. These parameters allow to compensate the frequency shift that the FM of the probe wave involves. To do this, all measured data are introduced in a matrix, in a way that the trace measured for each pulse delay is stored in a different row of the matrix. The method is simply to apply a shift to the elements of the columns of the matrix containing the probe wave samples (rows) for each relative delay between the FM and the pump pulses [49]. So, by making a sequential shift of each column, in each row of the matrix the measured data corresponding to a certain frequency detuning is recovered.

4.2.3 Mitigation of the impairments induced by first-order NLE

As explained in section 2.2, when a fiber with a uniform BFS is used, the pump pulse depletion manifests as a frequency dependent variation of the peak pulse power that follows a Lorentzian profile [31]. This is a consequence of the continuous Brillouin interaction between the pump and probe waves along the fiber. Thus, as introduced in section 2.2, and is repeated here for clarity, the pump power under Brillouin interaction in a single-probe BOTDA gain configuration can be simply calculated from the basic model that governs the Brillouin interaction assuming small gain condition [98]:

$$P_P(z) = P_{Pi}exp(-\alpha z)exp\left[-\frac{P_{Si}exp(-\alpha L)}{A_{eff}}\int_0^z \frac{g_0}{1+\left[2\Delta\nu(z)/\Delta\nu_B\right]^2}exp(\alpha z)dz\right] \quad 4.2$$

where z is a particular location of the fiber, P_{Pi} and P_{Si} are the input pump and probe powers, respectively, L is the fiber length, A_{eff}, α and g_0 are the effective area, the attenuation and the local Brillouin peak gain of the fiber, $\Delta\nu_B$ is the Brillouin linewidth and $\Delta\nu$ is the frequency shift between pump and probe waves. This expression shows that, indeed, the pump pulse depletion depends on $\Delta\nu$ and, as explained in section 2.2, follows a Lorentzian shape. In addition, remember that, as explained in section 2.2, the depletion

of the pump pulse can be characterized by a dimensionless depletion factor, d [31].

However, using the dithering of the probe wave technique, this impairment is ameliorated, because, even in the worst-case scenario, the frequency difference of pump and probe waves varies along the sensing fiber. Therefore, as the pump pulse crosses the fiber, it experiences SBS interaction with probe wavefronts that have a different frequency detuning. That is to say, for each position of the fiber, the Brillouin interaction between both optical waves varies due to the different frequency detuning. As a consequence of this position dependency, the maximum energy transfer occurs at those positions of the fiber where the frequency difference between probe and pump waves matches the natural BFS of the fiber. Whereas in all other positions of the fiber, the energy exchange due to SBS interaction is smaller, and hence, as the pulse depletion is cumulative along the fiber, interacting with different frequencies within the Brillouin spectrum leads to a decreased depletion factor of the pulse. Therefore, there is less frequency dependence of the pulse power and hence, less NLE and measurement error.

In short, the FM of the probe wave greatly reduces the amount of the pump pulse depletion, so that the tolerable maximum depletion factor for a given measurement error is reached at higher probe wave power. For instance, the approx. 20% depletion that can be tolerated for around 1-MHz BFS measurement error [31]. This means that a higher probe wave power can be injected into the fiber, and hence, the SNR at the receiver is improved.

4.2.4 Brillouin threshold increase using FM of the probe

As explained in section 1.5.1, the so-called Brillouin threshold of the fiber arises from the injection of high power components into the optical fiber, which can lead to SBS amplification of thermally-induced SpBS waves. This threshold establishes the maximum optical power that can be injected into a fiber before significant power begins to be reflected back so that the launched signal is depleted, and also noise is added to the signal. Another advantage of using a virtual BFS profile is the reduction of the Brillouin induced noise in the detected signal [49]. Once again, the basic idea is to imitate the approaches that increase the Brillouin threshold by using fiber links composed of segments with different BFS along their length [104], but synthesizing a virtual BFS profile instead of implementing a real one. In this sense, as the Brillouin threshold is overcome, a higher probe wave power can be launched into the fiber, so that, again, the SNR at the receiver is improved.

4.2.5 Mitigation of the impairments induced by second-order NLE

Another significant contribution of the probe dithering technique is that it allows to overcome the so-called second-order NLE. As explained in section 2.5, second-order NLE are due to the spectral deformation of the pump pulse, which is caused by the continuous Brillouin interaction of the pump pulse with the two probe waves deployed in a dual-probe BOTDA sensor [33]. The onset of this spectral distortion effectively limits the maximum probe wave power to approximately -3 dBm for typical long-range BOTDA systems [33].

However, in a dithered dual-probe BOTDA sensor, as explained above, the wavelength of the probe waves is modulated following a particular FM shape. Therefore, as the pulse

crosses the fiber, the SBS interaction of the pulse with the probe wavefronts occurs at a different frequency detuning between pump and probe waves for each location of the fiber. In this way, as highlighted in Fig. 4.3(a), the Brillouin interaction induced by both probe waves upon the optical pulse spreads over a large frequency range. As a result of the spreading of the interaction region, the Brillouin gain interaction integrated along the fiber generates a flat gain spectrum that does not distort the pump pulse spectrum, provided that a suitable FM shape is chosen. Simultaneously, the integrated Brillouin loss interaction along the fiber provides a complementary flat spectrum. Making use of Eq. (4.2), and adding the interaction effect produced by the other probe wave, the optical frequency response due to the interaction with both probe waves at the end of the fiber is given by:

$$H_{B-SBS} = exp\left[-\frac{P_{Si}e^{-\alpha L}}{A_{eff}}\int_0^L\left(\frac{g_0}{1+\left[\frac{2\Delta\nu_G(z)}{\Delta\nu_B}\right]^2}-\frac{g_0}{1+\left[\frac{2\Delta\nu_L(z)}{\Delta\nu_B}\right]^2}\right)e^{\alpha z}dz\right] \quad 4.3$$

Note that as a result of the spreading of the interaction region, the net gain and loss spectra induced by both probe waves broadens. In addition, these spectra mutually compensate to avoid any distortion of the pulse spectrum, so that no distortion is introduced in the pump pulse spectrum and, hence, second-order NLE are suppressed [49].

4.3 Tracking of the BFS in probe-dithering BOTDA for full non-local effects compensation

During the work of this thesis, we found that second-order NLE depends also on the BFS distribution of the fiber link. Specifically, we found that all the methods designed to overcome second-order NLE are only effective in case the BFS of the sensing fiber is uniform. In this section, the impairments brought by this side-effect are theoretically and experimentally introduced. In addition, a novel BOTDA sensor to completely overcome second-order NLE is also described and experimentally demonstrated.

4.3.1 Second-order non-local effects in non-uniform BFS fiber links

In section 2.5, two different methods to solve second-order NLE have been introduced [96, 49]. The first one relies on the idea of maintaining a constant frequency difference between both probe waves during the scanning process, which should be fixed to twice the BFS of the fiber, as shown in Fig. 4.4(a) [96]. Nevertheless, if the BFS varies along the fiber, the Brillouin gain and loss spectra generated by both probe waves do not longer completely overlap, giving rise to a non-flat transfer function over the pump pulse signal, as it can be seen in Fig. 4.4(b) and (c). Furthermore, as discussed below, this issue cannot be solved by adjusting the probe spacing using the average BFS of a particular section of the fiber, for instance, to the BFS of the so-called effective length of the fiber from the probe input. In this case, the injected probe wave power is so high that even when the

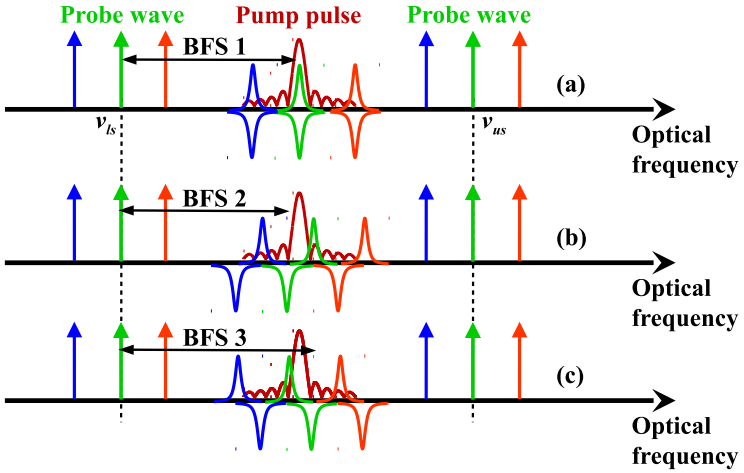

Figure 4.4: *Brillouin interaction on the pump pulse in BOTDA sensors with two probe waves that maintain constant frequency spacing during the scanning process when the frequency spacing of the pump between the probes (a) equals, (b) is larger, or (c) is smaller than twice the BFS of the sensing fiber. Different colors (red, blue, green) are shown for different frequencies of the probes waves during the spectral scanning process.*

probe wave has been greatly attenuated due to the propagation in the fiber, the interaction between pump and probe waves can still introduce significant spectral deformation on the pump pulse spectrum [97].

The second solution proposed to overcome second-order NLE, as explained in the previous section, is based on the FM of the optical probe waves [49]. In this method, by adjusting the average frequency of both probe waves to the BFS of the fiber, both spectra cancel out leading to no distortion of the pulse. However, as in the previous case, if there is a portion of the fiber with a different BFS, both interactions shift and, hence, the pulse is affected by a non-flat transfer function, as shown in Fig. 4.5. This leads to a distortion

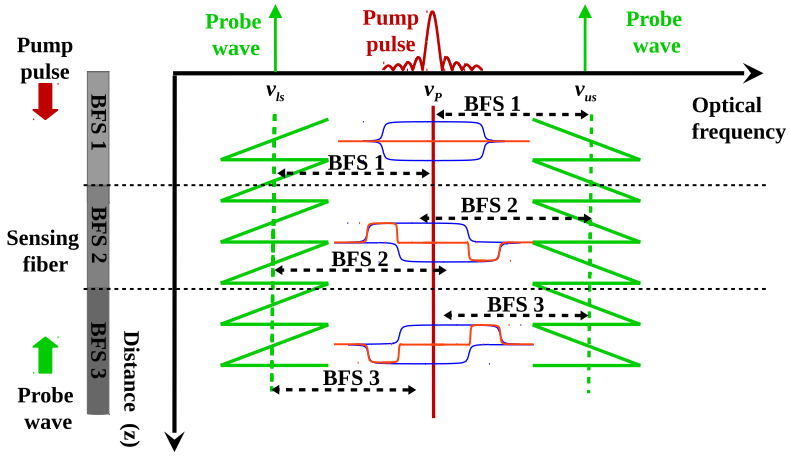

Figure 4.5: *Brillouin interaction on the pump pulse in BOTDA sensors with frequency modulation of the probe waves when the mean frequency spacing of the probes from the pump (BFS 1) equals, (BFS 2) is smaller, or is larger than the BFS of the sensing fiber (BFS 3).*

of the pump pulse frequency, i.e., if the BFS is not uniform, second-order NLE are not completely overcome.

It is worth mentioning that the influence of the Brillouin interaction over the pump pulse is going to be less significant with the method based on the frequency-modulated probe waves than in the one using a constant frequency separation between the probe waves. This is due to the fact that the FM spreads the energy of the interaction into a larger frequency region, and hence, the amplitude of the transfer function is reduced. Nevertheless, there is still some distortion of the high frequency components of the pulse that, as it is explained below, limits the maximum probe wave power that can be injected in fiber links with BFS variations along the fiber.

In summary, to be effective, all the techniques presented in section 2.5 to compensate second-order NLE require a fiber link with a fairly uniform BFS. In contrast, the use of a fiber with variations in the BFS leads to residual second-order NLE, which in turn may affect the pulsed signal. In order to quantify this effect, we add the terms corresponding to the additional probe wave component to Eq. (4.2). In addition, assuming that the optical power at the input of the fiber of the upper and lower frequency probe waves is equal, $P_{SLi} = P_{SUi} = P_{Si}$, this gives the following expression of the pump pulse propagating along the fiber:

$$P_P(z) = P_{Pi}e^{-\alpha z}exp\left[-\frac{P_{Si}}{A_{eff}}\int_0^z\left(\frac{g_0}{1+\left(\frac{2\Delta\nu_G(z)}{\Delta\nu_B}\right)}-\frac{g_0}{1+\left(\frac{2\Delta\nu_L(z)}{\Delta\nu_B}\right)}\right)e^{\alpha z}dz\right] \quad 4.4$$

Note that this expression assumes pulses longer than the acoustic phonon lifetime ($\sim$ 10 ns).

As an example of the distortion caused by second-order NLE in non-uniform BFS fiber links, Eq. (4.4) is used to calculate the spectral distortion of the pump pulse in a link with the BFS distribution shown in Fig. 4.6. In this particular example, the fiber link is comprised of two consecutive 50-km fiber sections with a BFS of 10.8 and 10.79 GHz, respectively, followed by another fiber section of 20 km with a BFS value, again, of 10.8 GHz. This can be a fairly realistic scenario in which two types of fibers with slightly different

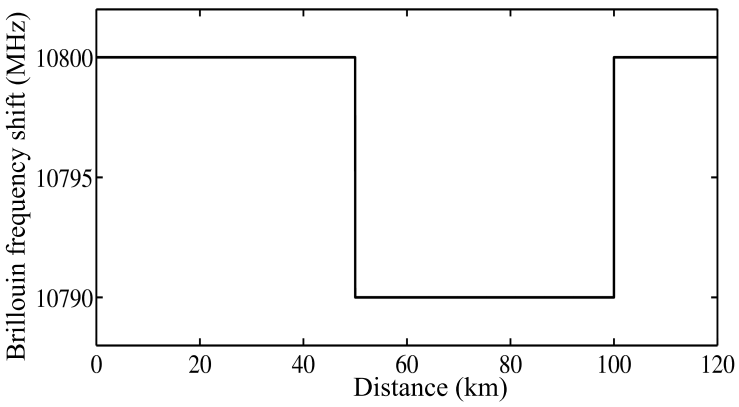

Figure 4.6: *BFS profile used for simulation.*

BFS due to manufacturing are used in a link.

Figure 4.7 depicts the transfer function experienced by the pulse due to Brillouin interaction with different probe wave power levels injected into the fiber when the two techniques for compensation of second-order NLE are used [49, 96]. That is to say, the transfer function is calculated on the one hand deploying two probe waves with constant frequency spacing during the spectral scanning, see Fig. 4.7(a), and also with the method of the FM of the probe waves, see Fig. 4.7(b). Note that the horizontal axis represents the frequency deviation from the central frequency of the pulse spectrum. In both cases, the peak-to-peak frequency deviation of the probe waves was set to 300 MHz. And the frequency detuning between the probe and pump waves for a perfect compensation of second-order NLE was set assuming a BFS value of 10.8 GHz, which is the predominant BFS in the fiber. Moreover, this value matches the BFS of the fiber in the first 20-km section from the input end of the probe wave.

First of all, from the calculations in Fig. 4.7 it follows that adjusting the probe wave frequencies taking into account just the BFS of a particular section of the fiber, which is approximately equal to the effective length, is not enough to get rid of second-order NLE. Indeed, the calculations show significant spectral distortion of the pump pulse spectra even

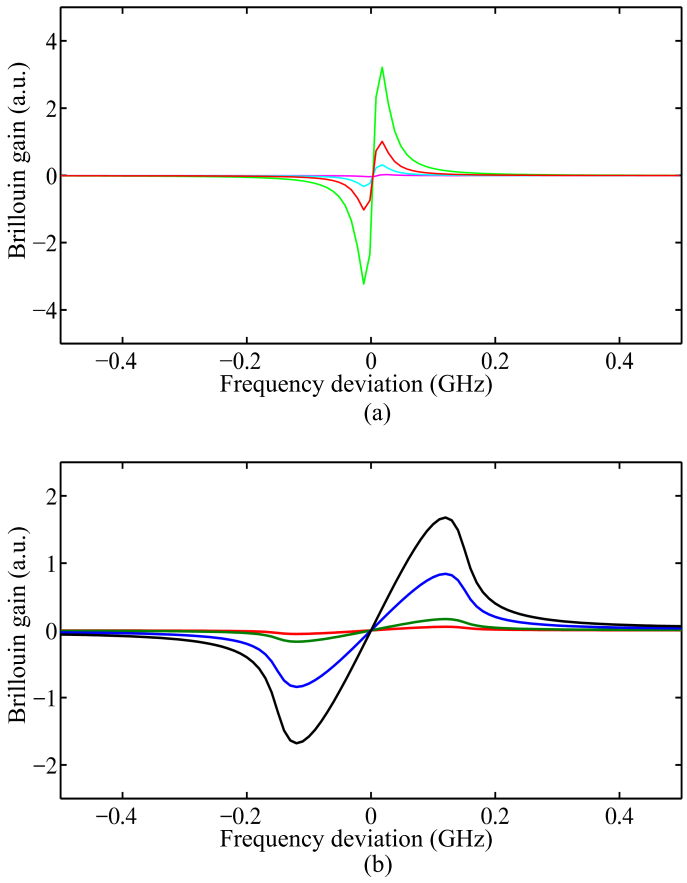

Figure 4.7: *Brillouin interaction frequency response (a) for the system presented in [95] using a probe power of -15 dBm (magenta), -5 dBm (cyan), 0 dBm (red) and 5 dBm (green) and (b) using the FM technique presented in [48] when the probe levels are 0 dBm (red), 5 dBm (green), 12 dBm (blue) and 15 dBm (black).*

at moderate probe powers. Secondly, the calculations in Fig. 4.7 also highlight that the technique that introduces a FM of the probe waves is more tolerant to BFS variations of the fiber than the method using probe waves with constant frequency spacing: at equal probe waves power level the amplitude of the spectral distortion is much smaller. In this way, for a distortion of the same order of magnitude, probe power levels up to 10 dB larger can be used with the FM method. As explained before, this advantage is due to the spreading of the interaction upon the pump pulse into a larger frequency region, which in turn reduces the distortion experienced by the pulse.

4.3.2 Second-order non-local effects mitigation by tracking the BFS of the fiber

In this section a novel method to solve the constraint on probe wave power imposed by the non-uniformity of the BFS along the fiber link in BOTDA sensors that compensate second-order NLE is introduced. This research work is an important part of the thesis of a colleague, Juanjo, work in which I cooperated. The fundamentals of the BFS tracking technique are schematically depicted in Fig. 4.8. The method is based on dynamically tuning the optical frequency of the probe wave, so that the BFS changes along the sensing fiber can be tracked. This is achieved by introducing an additional optical FM to the probe waves, as depicted in the figure. In this example the tracking of the BFS is combined with the FM method. However, note that this method can be used in all the previously presented techniques to mitigate second-order NLE [49, 96]. As explained before, these BOTDA sensors use the Brillouin interaction not only for monitoring purposes but also to compensate second-order NLE. Consequently, both systems should track the BFS profile

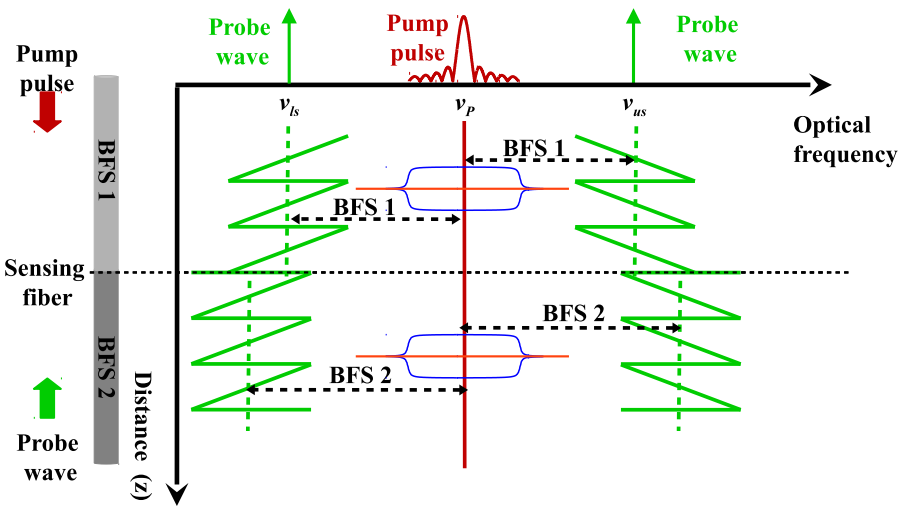

Figure 4.8: *Schematic of the fundamentals of the technique for compensation of BFS changes along the fiber in a BOTDA setups that uses frequency modulation of the probe wave optical frequency to mitigate second-order NLE. An example scenario in a fiber with two sections having different BFS is depicted. A frequency offset is added to the optical frequency modulation of the probe wave so as to make the central frequency of the probe wave match the BFS at each location.*

to properly correct these changes in the BFS, and hence, obtain a negligible response given by the Brillouin interaction over the pump pulse spectrum.

As it can be observed in Fig. 4.8, a frequency shift is added to the probe wave optical FM. In order to be effective, this added frequency shift must be set so that the average frequency of the probe waves matches the average BFS of each section of the fiber. Therefore, the gain and loss spectra induced by both probe waves on the pump pulse frequencies cancel out at each section of the fiber, and hence, the spectral distortion of the pump pulse due to second-order NLE that was analyzed above is avoided.

It is worth mentioning that the BFS tracking of the fiber just described does not need to be very precise or very fast. It is sufficient to adapt to changes in the average BFS profile of the different sections of the fiber. This is because minor deviations of the local BFS in small sections of fiber are not very significant, considering that their contribution to the total integrated gain and loss affecting the pulse as crosses the fiber is going to be small. In other words, it is enough to have an approximate BFS profile of the sensing fiber. A profile that can be extracted from the measurements that the BOTDA sensor is continuously performing, or even from a previous characterization of the BFS along the fiber using low spatial resolution, as it will be shown in experimental results. Moreover, the technique can work both in the case of sudden changes in the BFS profile due to the use of different types of concatenated fibers, as well as with slow variations of the average BFS of the fiber link due to environmental or cabling effects.

The experimental work performed to demonstrate the capabilities of the presented technique is introduced below.

4.3.3 Experimental setup

In order to evaluate the potential of the technique, the experimental setup depicted in Fig. 4.9 was assembled. The output of a distributed feedback (DFB) laser was divided by a coupler into two branches to generate the pump and probe waves. In the upper branch, so as to generate the pump pulse wave, the output of the coupler was pulsed by a semiconductor optical amplifier (SOA) driven by an AWG. Then, the pump pulse was boosted to a peak of 19 dBm using an EDFA, and its state of polarization was randomized with a polarization scrambler (PS) before being launched into the sensing fiber via a circulator.

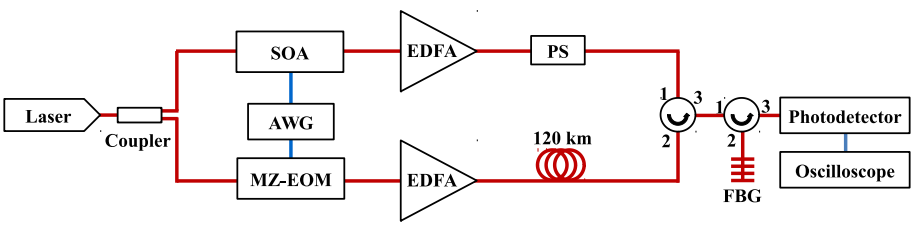

Figure 4.9: *Experimental setup for the BOTDA sensor based on tracking the BFS with frequency modulation of the probe wave.*

In the lower branch, a dual-probe wave was generated using a MZ-EOM that was biased at minimum transmission to generate a double sideband suppressed-carrier signal. The MZ-EOM was driven by the AWG, which provides a microwave signal with a saw-tooth

FM centered at 10.8 GHz and with a peak-to-peak deviation of 300 MHz. In addition, the AWG provides a synchronization between the electrical pulse used to generate the pump pulse wave and the FM of the microwave signal, so that the pump pulses always interact with the same instantaneous frequency at the same location of the fiber [49]. The power of the probe waves was amplified by another EDFA before being injected into the sensing fiber in a counter-propagate direction to the pump pulse. Finally, after the Brillouin interaction of these probe waves with the pump pulse, they were directed to a fiber Bragg grating (FBG) via a circulator in order to filter out the upper-frequency probe, and the remaining lower-frequency probe was detected by a photo-detector, which was connected to an oscilloscope.

4.3.4 Experimental validation of the technique

In order to analyze the detrimental effect that a non-uniform BFS profile of the sensing fiber has on the compensation of second-order NLE, a 120-km standard single-mode fiber (ITU G.652) composed of segments with different BFS was deployed in the setup of Fig. 4.9. In addition, the setup was also used to demonstrate the capabilities of the proposed tracking technique to overcome second-order NLE in fibers with non-uniform BFS profiles. Figure 4.10 depicts the measured BFS profile of the fiber, where three different fiber spools with a slightly different BFS are clearly distinguishable. The BFS difference between the first two reels (50-km length each one) was around 17 MHz, while the deviation between the second and third one (this one with 20-km length) was a bit larger, approximately 46 MHz. This measurement was performed using the setup in Fig. 4.9 without adding the BFS tracking. The probe power was 12 dBm (9 dBm per sideband) and long duration pulses of 200 ns were used, because, as explained before, it is sufficient to measure the evolution of the average BFS along the fiber. During the measurement, the last 20 km of the fiber were kept in a climatic chamber at constant temperature.

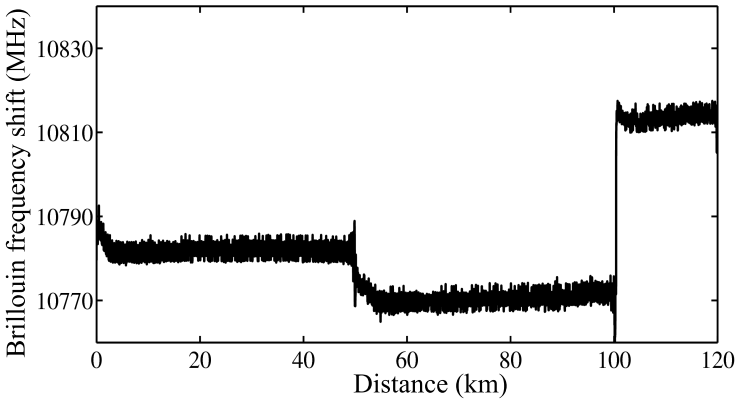

Figure 4.10: *Measured BFS distribution along the fiber.*

Once the BFS of the different fiber sections were measured, the optical frequency response experienced by the pump wave as a result of its interaction with the probe waves was characterized. In order to perform this measurement we devised the experimental setup in Fig. 4.11, which is a modification of that in Fig. 4.9. The idea is to deploy the technique for

optical transfer function measurement based on the use of optical single-sideband (OSSB) modulation [105]. For that purpose, the upper branch of the setup in Fig. 4.9 was modified to generate a OSSB signal whose sideband could be tuned in the range of frequencies of the pump pulse. Then, this OSSB signal was counter-propagated with the probe waves so as to make the sideband experienced the same transfer function that the pump pulse would experience. Finally, the OSSB signal was extracted at the far end of the fiber using a circulator and detected in a microwave bandwidth photodetector, which translated the optical transfer function from the optical to the electrical domain [105]. In addition, a 20-GHz electrical vector network analyzer (VNA) was used to scan the frequency of the OSSB sideband and measure the optical transfer function.

The method to derive the OSSB from the laser in Fig. 4.11 used first a MZ-EOM biased at minimum transmission and driven by a radio-frequency (RF) generator at 10 GHz to generate a double-sideband suppressed-carrier signal. The lower-frequency sideband was later removed using and optical filter (OF), which left a single spectral component that became the optical carrier of the OSSB and was spaced 10-GHz from the pump central frequency. Then this optical carrier was fed to an optical single-sideband modulator (OSSB-EOM), which was based on a MZ-EOM with two RF electrodes driven using a 90° hybrid coupler [106]. The OSSB-EOM was driven by the VNA that scans the sideband frequency, by generating a microwave frequency sweep between 9.5 GHz and 10.5 GHz, and measures the optical transfer function experienced by the pump along the fiber and up to the microwave photodetector.

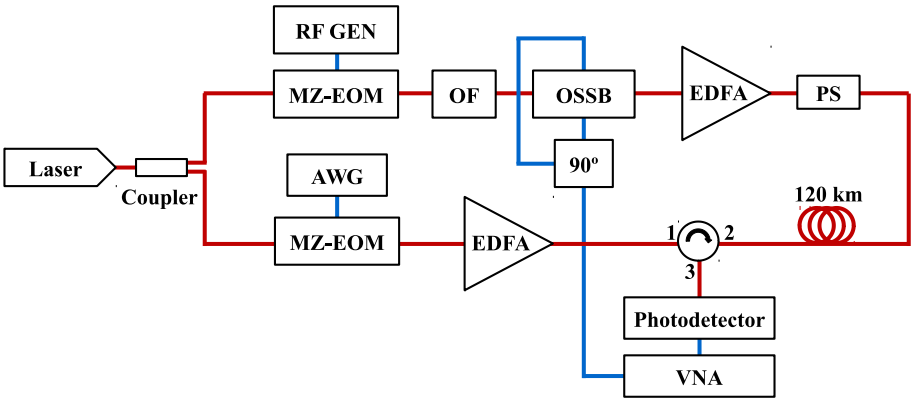

Figure 4.11: *Experimental setup used in order to characterize the optical frequency response of the Brillouin interaction that the pump wave spectrum experiences.*

Figure 4.12 depicts the distortion of the frequency transfer function that the pump pulse experienced due to its interaction with the probe waves, measured using the OSSB method, for increasing probe power levels. It can be clearly observed that as the probe power raises, the distortion of the pump wave increases. Indeed, for probe wave powers of 0 dBm and 5 dBm the pump wave spectral distortion is negligible. However, when the probe power is increased to 15 dBm, the pump wave spectrum experiences a large distortion: the low and high frequencies of the spectrum experience a 4-dB peak loss and gain, respectively. Besides, this last measurement is compared in the figure with the calculations using the model in Eq. (4.4), showing good agreement in shape, despite some

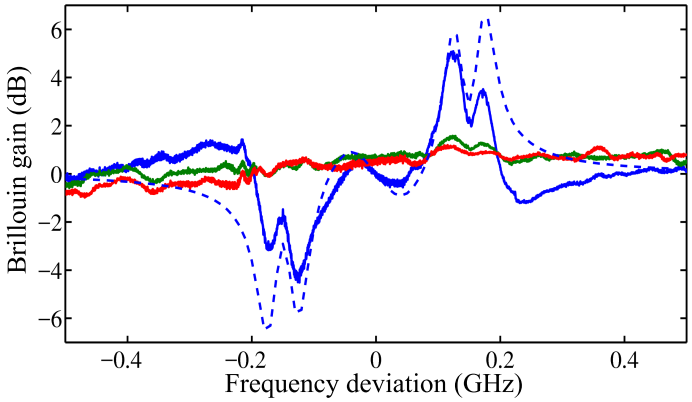

Figure 4.12: *Measured Brillouin interaction frequency response over the pump pulse when the probe wave is 0 dbm (red), 5 dBm (green) and 15 dBm measurement (solid blue). Also shown (dashed blue) are calculations using Eq. 4.4 and 15-dBm probe wave.*

small differences attributable to the SpBS generated over the OSSB signal frequencies by the counter-propagating continuous probe waves. It is important to point out that the frequency separation of the gain and loss peaks in Fig. 4.12 equals the peak-to-peak frequency deviation of the FM introduced to the probe wave. In addition, the frequencies of the two lobes of each peak can be directly related to the difference between the central frequency of the frequency modulated probe waves and the BFS of the different sections of the fiber.

The distortion of the optical transfer function experienced by the pump pulse due to its interaction with the probe waves results in a distortion of the temporal shape of the pulses. This is highlighted in Fig. 4.13, where the temporal shape of 20-ns pulses is displayed. These pulses were measured at the output of the fiber in the setup of Fig. 4.9, when different probe wave power levels were employed. It can be observed that for a probe wave power lower than 12 dBm the pulse shape does not experience nearly any distortion. Whereas for a larger probe power level, the shape of the pulses starts to experience some distortion. For instance, for a 12-dBm probe wave power a ripple of around 11% of the

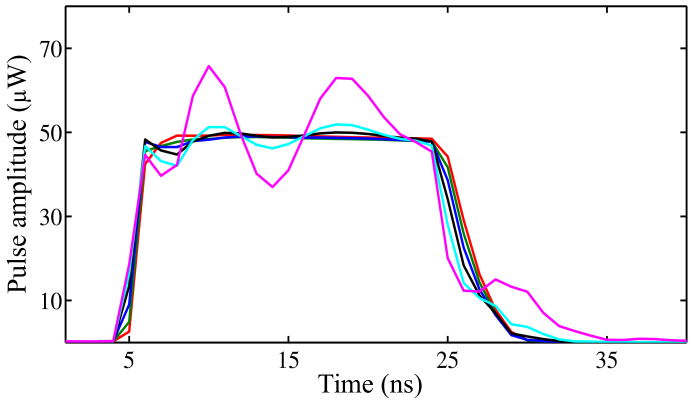

Figure 4.13: *20 ns pump pulses at the output of the fiber when the probe wave power is 0 dBm (red), 3 dBm (green), 6 dBm (blue), 9 dBm (black), 12 dBm (cyan) and 15 dBm (magenta).*

pulse amplitude appears on the top of the pulse. Moreover, as can be seen, when the probe power is raised to 15 dBm this ripple is increased to a variation of 53% of the amplitude of the pulse and, in addition, the fall edge of the pulse loses its original shape.

Once the detrimental effect on the pump pulse wave that the BFS difference along the sensing fiber was studied, to analyze the performance of the BFS tracking technique, distributed temperature measurements were performed. For that purpose, the first step was to measure the average BFS profile of the sensing fiber, which has been already displayed in Fig. 4.10. Afterward, the measured BFS profile was used to compensate the average BFS variation of the fiber, by adding an offset frequency to the probe wave modulation, as it was schematically explained in Fig. 4.8. Finally, distributed measurements of the BFS of the fiber were performed using 30-ns pump pulses, which corresponds to approximately 3-m spatial resolution, and a probe power of 15 dBm. Note that this probe wave power was found to be the maximum tolerable value imposed by the Brillouin threshold of the fiber.

Figure 4.14 shows the measured BFS along the fiber when the BFS tracking technique was applied. Note that this is a "virtual" BFS, since to obtain the real BFS it is mandatory to subtract the frequency offset added to the probe wave modulation at each position of the fiber (for the different fiber sections). In addition, as it can be observed, the BFS is not completely flat in Fig. 4.14, this is because only the last 20 km of the sensing fiber were kept inside a climate chamber during measurements. Therefore, the first 100 km were exposed to laboratory temperature variations between the initial measurement of the average BFS in Fig. 4.10 and the measurements with tracking in Fig. 4.14. This fact explains that the BFS of the first 100 km is slightly offset from the expected 10.8 GHz value. Nevertheless, in a real application of the system, the BFS tracking would be continuously in operation using previous measurement results, so that the BFS variation would be perfectly compensated.

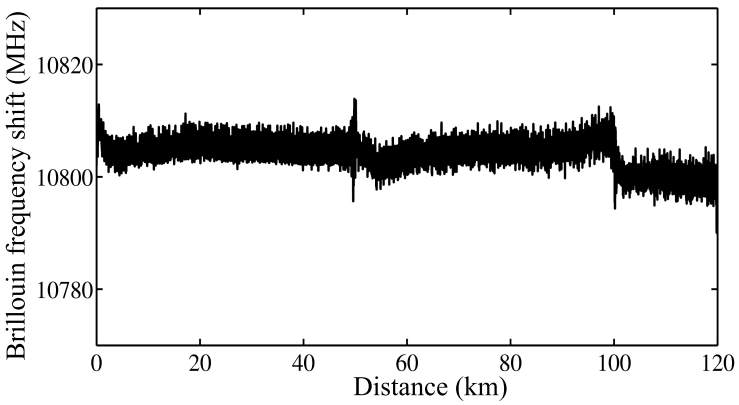

Figure 4.14: *Measured "virtual" BFS profile along the fiber when the BFS tracking method is deployed.*

Figure 4.15 depicts the obtained temporal shape of the pump pulses of 20 ns duration after counter-propagate along the whole fiber with different probe wave power levels, when the BFS tracking technique is applied. It can be observed that for a lower probe power than 15 dBm there is negligible pulse distortion, while for a probe power of 15 dBm a small ripple of around 11% appears. This small distortion, which does not impair the measurements,

is due to the residual variation of the BFS that can be observed in Fig. 4.14. Nevertheless, as explained before, it would be completely suppressed in a system with a continuous BFS tracking. In addition, it can be appreciated that unlike the measurements without tracking the BFS of the fiber, in this case the fall edge of the pulse preserves its original shape. Therefore, the improvement obtained with the proposed technique can be seen in the reduction of the pulse distortion by a factor of 4.8 times in relation to the distortion obtained when the tracking technique is not applied.

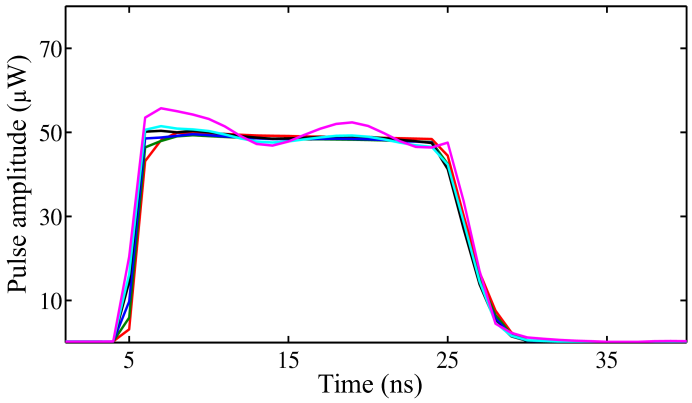

Figure 4.15: *20 ns pulses at the output of the fiber when probe wave is 0 dBm (red), 3 dBm (green), 6 dBm (blue), 9 dBm (black), 12 dBm (cyan) and 15 dBm (magenta).*

Finally, in order to evaluate the precision of the system, a series of 18 consecutive measurements for stable temperature conditions of the last 20 km of the sensing fiber were performed. Figure 4.16 highlights the precision along the sensing fiber calculated from the standard deviation of those measurements at each location. From these measurements, an approx. 2-MHz (1σ) precision was obtained at the worst-contrast position. All these measurements were performed with 1024 averages of the BOTDA traces.

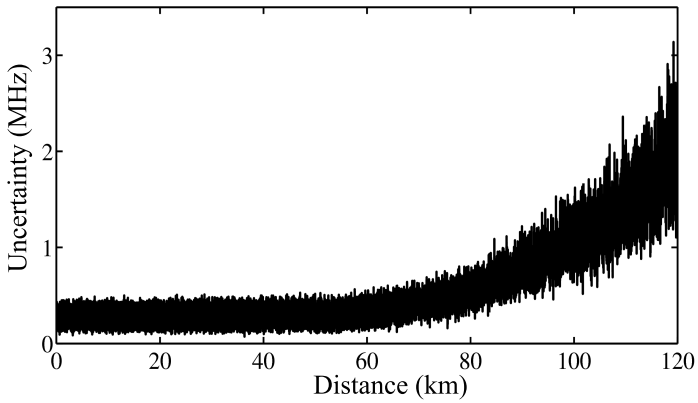

Figure 4.16: *Precision of the BFS measurement obtained along the fiber.*

4.4 Mitigation of non-local effects due to pump pulse extinction ratio by dithering of the optical source

As explained in chapter 3, an important factor limiting the performance of long-range BOTDA sensors is the pedestal or leakage of the pump pulses. To better understand the work that will be presented below, we will briefly summarize the concept of the origin of the constraints that were discussed in chapter 3. As it was explained, any device used to shape the pump pulses has a limited ER, and hence, in addition to the pulse, there is a continuous wave (CW) pump power that leaks and counter-propagates with the probe wave. That is to say, the pump pulse is on top of a CW, the pedestal of the pump wave.

As explained in chapter 3, the origin of the constraints imposed by the limited ER pump pulses is the extra amplification experienced by the probe wave due to its Brillouin interaction with the pedestal of the pump wave. First of all, as noted in section 3.3, this additional gain limits the amplitude of the probe wave that can be detected and processed in detection. This leads to an effective reduction of the SNR, because the full-scale dynamic range of the analog-to-digital converter within the signal acquisition device is largely wasted with a detected signal larger than the signal of interest; hence increasing the quantization noise. In addition, this is a gain that is not useful for sensing, because the measured gain spectrum due to the interaction of the pulse and probe for a particular location in the fiber is the Brillouin gain spectrum for that location on top of another spectrum that is due to the pedestal with probe interaction integrated along the fiber. And despite the fact that in principle the Brillouin gain spectrum can be obtained by normalizing the measurements by the spectrum measured with no pulse in the fiber, it has been shown that the additional gain in the probe wave degrades the precision of the BFS measurement [45].

Besides these constraints, the pedestal of the pump wave increases the onset of the depletion of the pump pulse. This is due to the fact that the pump pulse meets a higher power probe wave along the fiber, and hence, the energy transfer from the pump pulse to the probe is larger, increasing the depletion of the pulse. Moreover, as explained in detail in section 3.4, the presence of the pump pulse pedestal causes the onset of two additional NLE. The first one originates in the extra depletion of the trailing pedestal of the pump pulse. This effect is due to the fact that the trailing pedestal interacts with a probe wavefront that has been previously amplified by the pulse. Therefore, the trailing pedestal experiences an increased depletion, because more energy is transfered from the pedestal of the pump wave to the higher power probe. This consequently implies a reduced amplification of the probe wave, and hence, the normalization process by the gain measured without pulse in the fiber cannot be properly performed, leading to measurement errors. The second effect is due to the transient response of the EDFAs that are normally deployed to amplify the pump wave. The EDFA modifies the pedestal that follows the pulse in such a way that it also leads to a distortion of the measured gain spectra after normalization. As explained in chapter 3, in order to prevent the onset of these effects, a large ER pump pulse (greater than 43 dB if a technique for mitigation of second-order NLE is deployed) is required.

Therefore, there is a clear need to relax the requirements on ER of the devices used for

generating the pump pulses. In this section, we introduce the benefits of the dithering of the optical source technique used to generate the pump and probe waves to alleviate the impairments brought by the limited ER of the pulses. As explained in section 4.2.1, by direct modulation of the injection current of a laser, a modulation of the output optical signal wavelength via chirp of the laser is induced. This modulation can be generated for instance using a sinusoidal wave signal generator, which is synchronized to the pump pulse generator. It has been previously shown that with this method it is possible to generate a sort of virtual BFS profile along the fiber, which, increases the tolerance of the sensor to NLE. Moreover, when this technique is applied to a BOTDA sensor with limited ER pulses, the effect is to reduce the Brillouin gain provided by the pedestal of the pump pulse to the probe wave.

Figure 4.17 shows the theoretical fundamentals of the technique, whose operation is similar, in principle, to the interaction between pump and probe waves in Brillouin optical correlation-domain analysis sensors [15]. As it can be observed, the pedestal of the pump pulse and the probe wave have their wavelengths modulated with the same sinusoidal shape. When these two waves counter-propagate in the fiber, their wavelength difference is correlated just at certain locations in the fiber (correlation peaks). In other words, each of the probe wavefronts have a maximum Brillouin interaction with the pedestal of the pump wave just at certain locations of the fiber, specifically in those in which the frequency detuning between the probe wavefront and the pump pedestal equals the BFS. These correlation peaks are spaced by a distance equal to:

$$C_{peaks} = \frac{\nu_g}{2f_m} \tag{4.5}$$

where ν_g is the group velocity of light in the fiber and f_m is the wavelength modulation frequency. At all other locations in the fiber the pedestal and the probe wavefronts become uncorrelated, thus reducing the energy transfer between both waves via Brillouin interaction.

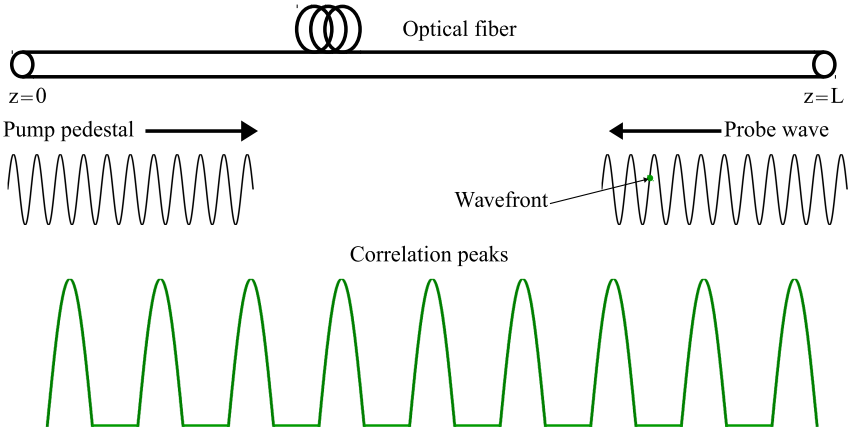

Figure 4.17: *Theoretical explanation of the probe-pump uncorrelated interaction in an optical source dithering technique.*

In this way, the parasitic gain provided to the probe wave by the pump wave pedestal is greatly reduced. Therefore, the full-scale dynamic range of the analog-to-digital converter is

reduced, improving the SNR of the sensor. In addition, as the probe wave is less amplified, the pulse depletion is also reduced. First, because, as previously explained in section 4.2.3, the depletion of the pulse power spreads into several scanning frequencies, and second, because the probe wave power with which the pulse interacts is lower. Not only the pulse depletion is diminished, but also the impairments induced by the depletion of the pedestal are overcome. This is due to the fact that the depletion of the trailing pedestal is decreased, and additionally, because the gain induced by the pedestal is smaller, and hence, its consequences are reduced. Even more, considering that the total Brillouin gain contribution of the pedestal is diminished, the deleterious effects of the EDFA transients are also ameliorated. In summary, the detrimental effects caused by the limited ER pump pulses described above are considerably lessened, as it will be highlighted with experimental results in next sections.

4.4.1 Experimental setup

Figure 4.18 depicts the dual-probe BOTDA setup that was assembled to experimentally demonstrate the compensation of the impairments caused by the limited ER of the pump pulses.

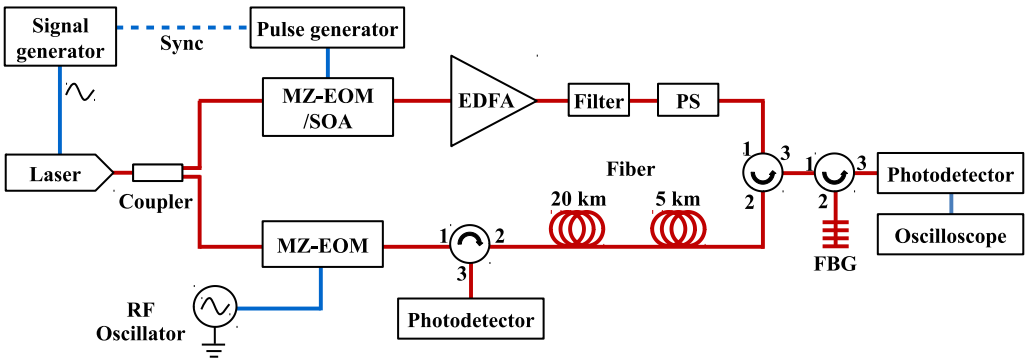

Figure 4.18: *Experimental setup deployed to demonstrate the capabilities of the presented technique.*

The optical source was a DFB laser at 1560-nm whose injection current was modulated by a 80-kHz sinusoid from a signal generator that was synchronized to the pulse generator. Once the optical signal was modulated, it was divided by a coupler into two branches. In the upper branch, the pulses were generated in an electrical pulse generator that drove by either a MZ-EOM or a SOA switch. The SOA was deployed to provide pulses with a high ER of around 45 dB. The MZ-EOM was used to generate pulses with 26-dB ER by adjusting its bias point and the amplitude of the electrical pulsed signal driving the device. These pulses where then amplified in an EDFA, filtered to reduce the amplified spontaneous emission, and directed to a PS before launching them into the sensing fiber. The pump peak power was limited to 20-dBm in order to avoid MI effects in the fiber [37], and the pulse duration was set to 20-ns, corresponding to approximately 2-m spatial resolution.

In the lower branch of the setup, the probe wave was generated using another MZ-EOM driven by a RF generator that provided frequencies close to the BFS of the fiber. This modulator was biased for minimum transmission so as to generate a double-sideband

suppressed-carrier modulation. In this way a dual-probe wave power of -3 dBm per side-band, which is the limit for the onset of significant second-order NLE [33], was injected into the fiber. Note that this is a conventional dual-probe BOTDA setup with the only addition of the chirp modulation of the optical source. Before the detector, a tunable narrow-band FBG was used to retain just the highest wavelength probe wave. Finally, in these proof-of-concept experiments, two different standard single-mode (ITU G.652) fiber spools of 5-km and 20-km length with a fairly uniform BFS distribution but slightly different Brillouin gain coefficient were deployed as sensing fiber. In addition, two hotspots were prepared along the fiber under test (FUT) using a climatic chamber: one after the first spool and the other at the end of the link.

4.4.2 Experimental validation of the technique

Experimental measurements were performed to demonstrate the capabilities of the optical source modulation technique to overcome the impairments caused by the limited ER of the pump pulses in BOTDA sensors. In order to demonstrate the compensation of the distortion caused by the pedestal depletion and the constraints induced by the transient response of the EDFAs, two different EDFAs were deployed for the amplification of the pump pulses. The used EDFAs are two of the EDFAs presented in section 3.4.5. Specifically, the used EDFA to demonstrate the solution to the pedestal depletion induced impairments, EDFA I, was the special amplifier designed for pulse amplification with almost no distortion (EDFA III in section 3.4.5), and the second one, EDFA II (MPB Communications Inc., EDFA I in section 3.4.5), was used to demonstrate how the technique overcomes the constraints induced by the transient response of EDFAs.

Figure 4.19 depicts the enhancement in deleterious effects induced by the limited ER pulses brought by the presented technique. The figure compares measured BOTDA traces with a 26-dB ER pump pulses, i.e., probe wave signal as a function of time or distance, with and without optical source dithering. The detected probe wave without pump wave in the fiber is also shown for comparison purposes. As it can be seen, the trace for the

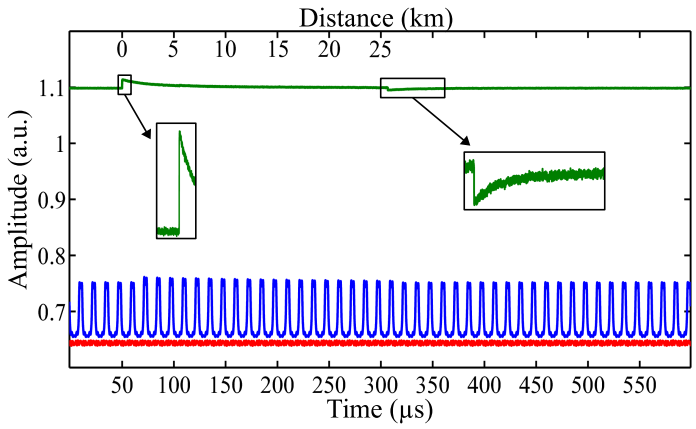

Figure 4.19: *BOTDA signal measured for the BFS in a conventional setup (green), for the setup with dithering of the optical source (blue) and, finally, received probe wave without pump wave in the fiber (red).*

conventional BOTDA is flat before the pulse enters the fiber, then the probe gain can be observed at every position due to the interaction with the pump pulse and finally, there is a non-flat response due to the pedestal depletion. In the flat area, before the pulse is in the fiber, the increased amplitude of the probe wave, compared with the response with no pulse in the fiber, is just due to the gain of the probe caused by the Brillouin interaction with the pulse pedestal. Note that this gain is much larger than the gain due to the pulse interaction, which, as it was explained before, leads to errors in the measurement. Finally, the trace once the optical source dithering is turned on is also highlighted. It can be observed that the Brillouin gain in the area without pulse in the fiber is greatly reduced.

It is worth mentioning that the BOTDA trace before arriving the pulse is no longer flat for the optical source dithering technique, but displays an oscillatory behavior. The reason is that we are seeing the gain experienced by the probe wavefronts when meets the pump pedestal wave with a variable wavelength difference. In addition, note that the MZ-EOM presents a non-flat frequency response, so that for different frequencies the optical power output of the modulator is slightly different. As a consequence, the Brillouin spectra are revealed once the gain due to the pulse pedestal and the power response of the modulator power response are subtracted from the traces.

The relaxation of ER requirements brought by the application of the presented technique can be quantified by the reduction in probe gain, g_{probe}, due to the Brillouin interaction with the pedestal, which is given by:

$$g_{probe} = \exp\left(\frac{g_B}{A_{eff}} P_{ped} L_{eff}\right) \tag{4.6}$$

where g_B is the Brillouin gain coefficient, P_{ped} is the pump pulse pedestal optical power and $L_{eff} = (1 - exp(-\alpha L))/\alpha$, with α the attenuation of the fiber and L the length of the FUT. Using Eq. (4.6), we can find the equivalent enhancement in ER that would be associated to the reduction in probe gain that the optical source dithering technique implies. In this particular experiment, the probe gain was reduced by a factor equivalent to at least 6.2-dB enhancement in the ER of the MZ-EOM.

As can be seen in Fig. 4.19, the necessary full-range scale of the analog-to-digital converter signal acquisition device is reduced; hence decreasing the quantization noise. Furthermore, in the research work performed by a colleague, Jon, work in which I cooperated, we studied another benefits of the technique regarding the impairments brought by the limited ER pump pulses. First, the negative effects due to the depletion of the pump pulse were investigated. Figure 4.20(a) shows the received pump pulses at the far end of the FUT when no modulation was applied to the light source. From these measurements, the pump pulse depletion factor when EDFA I and EDFA II were deployed to amplify the pump pulses was measured to be around 10%. The pulse with no probe in the fiber was used as a reference to calculate the depletion factor of the pulses. On the contrary, Fig. 4.20(b) also depicts the pulses at the far end of the fiber, but in this case when the optical FM of the laser is turned on. The measured depletion factor of the pulses was reduced to approximately 1%, demonstrating the capabilities of the technique to overcome first-order NLE induced by the limited ER of the pulse. In this way, as shown in Fig. 4.20,

since the probe amplification due to the pedestal is reduced, the depletion of the pump pulse is mitigated.

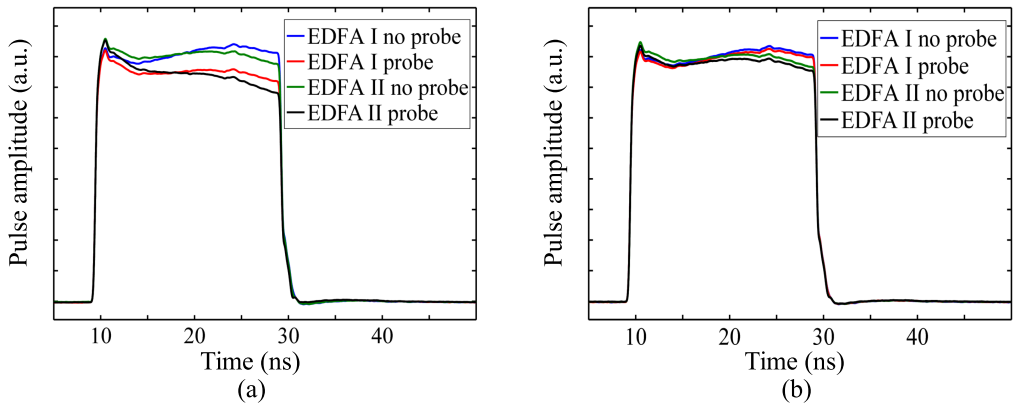

Figure 4.20: *Obtained optical pump pulses at the far end of the fiber deployed, when there is no probe in the fiber, and with probe wave using EDFA I and EDFA II to amplify the pump wave: (a) when the dithering of the optical source is off and (b) with the dithering turn on.*

Figure 4.21 highlights the potential of the technique to overcome the detrimental effects caused by the pedestal depletion (in these measurements we used EDFA I to amplify the pump wave). Figure 4.21(a) depicts the distortion of the probe gain profile due to its interaction with the depleted pump pedestal, by comparing the Brillouin gain profile measured using the MZ-EOM to shape the pulses with the one obtained using the SOA. Note that the latter has a high ER and consequently the measured BOTDA trace does not present any significant distortion, so that will be used as a reference measurement. However, the BOTDA traces obtained using a MZ-EOM that generates 26-dB ER pump pulses are distorted. In this way, when using EDFA I to amplify the pump wave, the BOTDA trace shape is slightly deformed due to the pump pulse pedestal depletion effect studied in section 3.4.

Figure 4.21(b) highlights the compensation of the distortion suffered on the Brillouin probe gain profile when the optical source dithering technique is applied. First of all, note that the measured Brillouin probe gain when using the dithering technique presents an oscillatory response. This is due to the the fact that, as explained before, the probe wave is composed of several different frequencies following the FM shape introduced to the laser source. Therefore, each wavefront has a different frequency detuning regarding the pump pulse, and hence, the probe gain is also different. As explained before, once all the measurements are detected, in order to recover the Brillouin gain profile, this effect must be compensated by reordering the acquired data.

As seen in the figure, the detected probe gain profile shows a similar shape when low and high ER pump pulses are deployed. In addition, note that the Brillouin gain level obtained with high ER pump pulses (with the SOA) when the dithering of the optical source is turned off is of the order of the gain measured when the dithering source is turned on. Besides, it can be seen that the fall to negative normalized gain after the pulse has left the fiber (at L = 25 km) that can be observed in Fig. 4.21(a) has been normalized to a

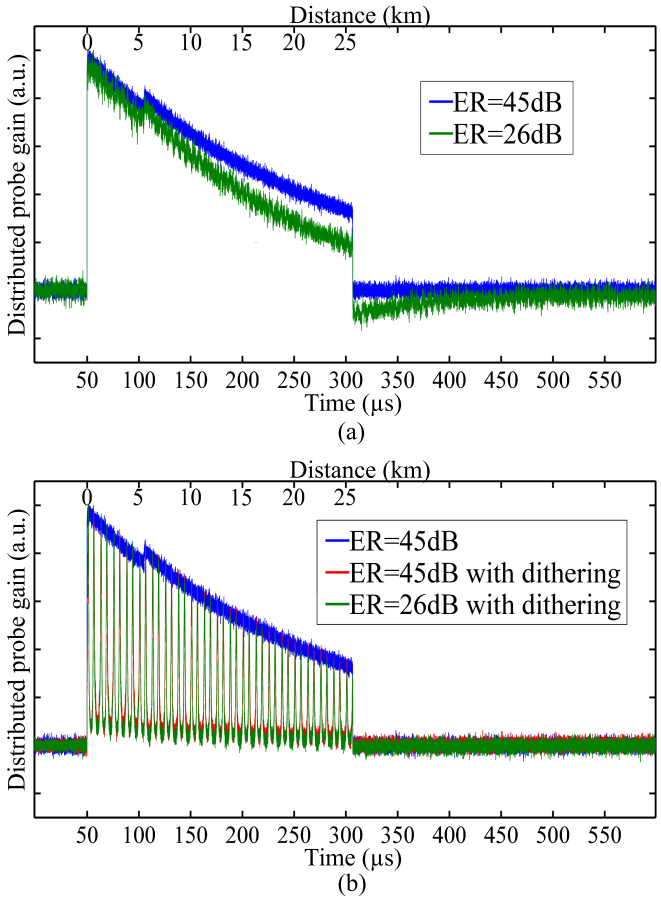

Figure 4.21: *BOTDA trace for different ER values of the pump pulse wave when EDFA I is deployed, (a) when the dithering of the optical source is turned off and (b) for a high ER without FM of the optical source and high and low ER with the dithering turned on.*

flat response in the measurements shown in Fig. 4.21(b). This proves that the dithering technique is capable of overcoming the pedestal depletion induced distortions.

Besides that, Fig. 4.22 shows the potential of the technique to greatly ameliorate the detrimental effects caused by either the pedestal depletion and the EDFA transient response induced pedestal deformation (for these measurements we used EDFA II to amplify the pulsed pump wave). Figure 4.22(a) depicts the distortion of the probe gain profile due to both effects, the one due to its interaction with the depleted pump pedestal and the effect caused by the EDFA transient response when amplifies low ER pulsed signals. Again, the Brillouin gain profile measured using the SOA to shape the pulses is also shown for comparison purposes. As can be observed, the BOTDA traces obtained using a MZ-EOM that generates 26-dB ER pump pulses are severely distorted. In this way, when EDFA II is deployed for amplification, a large distortion of the probe gain is introduced, which is due to the pump pedestal depletion and the EDFA transient response effects (see section 3.4).

Figure 4.22(b) highlights the compensation of the distortion suffered on the Brillouin probe gain profile along the fiber when the optical source dithering technique is applied. As seen, the detected probe gain profile shows a similar level when low and high ER pump pulses are deployed. Besides, it can be seen that the abrupt fall to negative normalized

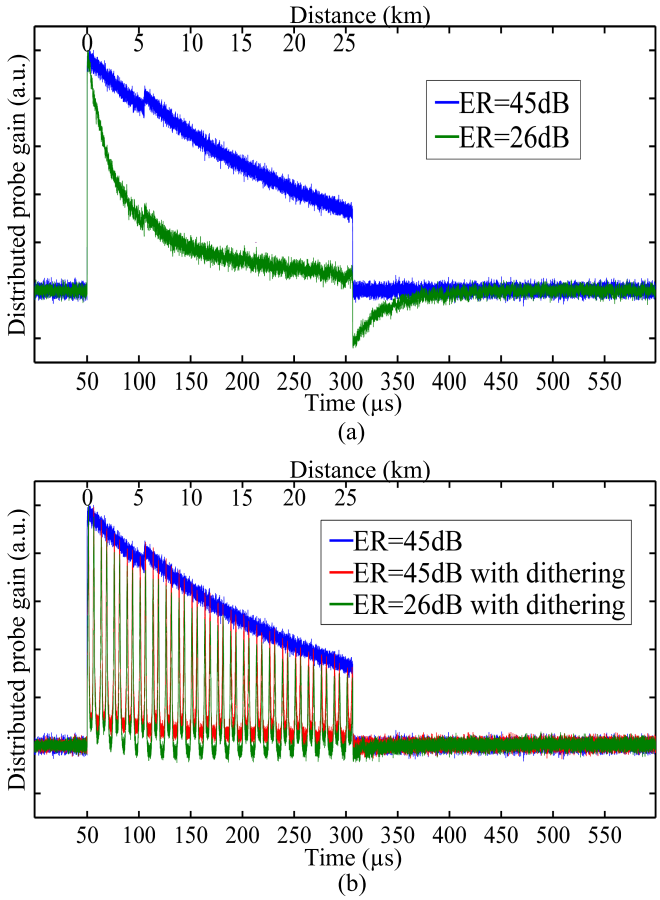

Figure 4.22: *BOTDA trace shape due to pump pedestal depletion and due to EDFA transient response for different pump pulse ER values, (a) when the dithering of the optical source is turned off and (b) for a high ER without FM of the optical source and high and low ER with the dithering turned on.*

gains after the pulse has left the fiber (at L = 25 km) that are portrayed in Fig. 4.22(a) has been improved and presents a nearly flat response in these measurements. This proves the capability of the dithering technique to overcome the pedestal depletion and also the EDFA transient response induced impairments. Therefore, confirming the compensation of all NLE even for a limited ER pump pulse.

Finally, in order to quantify the BFS measurement error compensation in BOTDA sensors brought by this technique, distributed temperature measurements were performed. For that purpose two hotspots were prepared with a fixed temperature by a climatic chamber at 10° C of difference from the rest of the fiber, which was also controlled by another climatic chamber. Figure 4.23 shows the resultant BFS distribution along the two hotspots when EDFA I was deployed to amplify the pump pulses. As it is observed, the error with respect to the reference measurement performed with the SOA is negligible in the first hotspot, whereas for the second hotspot at the far end of the FUT the BFS error becomes significant. Reaching up to 4 MHz error for a conventional dual-probe BOTDA with a limited pump pulse ER of 26 dB. However, as expected, this error is compensated when the FM of the optical source is turned on.

In order to demonstrate the improvement of the impairments brought by the EDFA

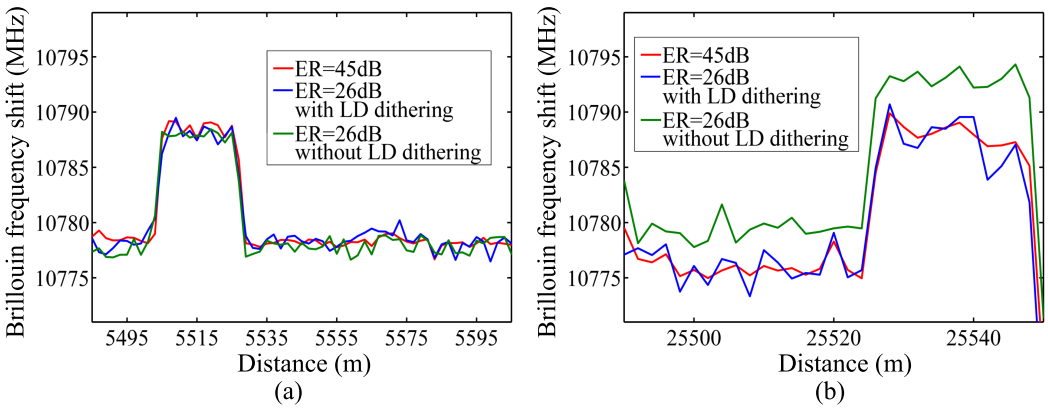

Figure 4.23: *Calculated BFS as a function of distance for an ER of 45 dB, and for a low ER of 26 dB with and without the dithering of the laser turned on: (a) at a distance of 5 km and (b) at the end of the fiber.*

transient response effects, we performed the same distributed measurements but, in this case, using EDFA II to amplify the pulsed wave. Figure 4.24(a) and 4.24(b) depict the measured BFS distribution at the two hotspots along the link. As can be seen, in this case a very significant BFS error is introduced even at the first kilometers of the fiber. Particularly, the measurement error in the first hotspot when using a conventional dual-probe BOTDA with a limited pump pulse ER of 26 dB raises up to 5.5 MHz, and to 11 MHz at the end of the FUT. Nevertheless, as it is depicted with blue color line, the measurement errors are compensated to a great extent when the optical source modulation is applied, demonstrating the validity of this technique to ameliorate the constraints induced by both detrimental effects.

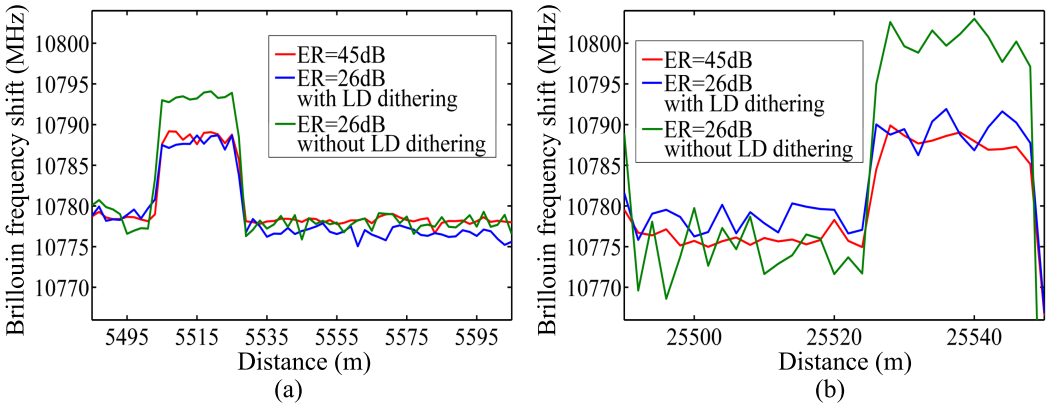

Figure 4.24: *Resultant BFS along the hotspots deployed using the EDFA II: (a) hotspot I (b) hotspot II.*

4.5 Conclusions

In this chapter, the capabilities of the BOTDA sensor based on the synthesis of a virtual BFS profile along the sensing fiber to overcome the various NLE have been introduced. To achieve this virtual BFS, the technique is based on introducing a modulation or "dither-

ing" to the optical frequency of the probe waves. This technique has been theoretically studied and proof-of-concept experiments have been performed to demonstrate its benefits to solve one of the main constraints on the performance of BOTDA sensors, i.e., the NLE. We have demonstrated that this technique is able to overcome the pump pulse depletion, second-order NLE and reaching a significant reduction of ER-related impairments. Therefore, the method for probe optical FM or dithering provides a comprehensive solution to most of these issues. In addition, its use allows BOTDA configurations to deploy a probe wave power above the Brillouin threshold of the fiber. All this with very little complexity added to the conventional dual-probe BOTDA setup.

It is worth mentioning that in order to overcome all the impairments brought by the limited ER of the pump pulses, it is mandatory not only to modulate in frequency the probe wave but also the pump wave. Otherwise, the pulse pedestal would be composed of a single frequency. And, as a result, the Brillouin gain received by each probe wavefront with a frequency detuning equal to the BFS of the fiber, would be exactly the same than in a conventional BOTDA sensor. Which, in turn, would increase the quantization noise, and reproduce the same impairments due to the EDFA transient response than in a conventional BOTDA setup. However, the constraints generated by both the depletion of the pulse and the pedestal depletion would be clearly improved.

In addition, we identified the factor that constrains the performance of all currently available second-order NLE compensation methods: the inability of those methods to cope with variations of the BFS profile along the fiber. This is a limitation that restricts real world applications of long-range BOTDA sensors. Considering that in real-world field-application scenarios a variety of fibers with different BFS and subjected to different environmental conditions are typically deployed. We have demonstrated that indeed, this was the limiting factor by developing a theoretical model for the pump pulse distortion due to the interaction with the probe waves. A model that has been verified experimentally.

Additionally, we have presented a new technique that makes BOTDA sensors to completely compensate second-order NLE by adding an optical FM to the probe to track the variations in average BFS found along the fiber. Therefore, the new limit to probe wave power is the effective Brillouin threshold of the sensing fiber. Nevertheless, the probe FM technique pushes this limit to higher powers than in standard BOTDA setups. Using this BOTDA setup, we have proved that it is possible to deploy a probe wave up to 15 dBm, which, to the best of our knowledge, is the largest probe power ever injected in a long-range BOTDA setup.

Therefore, to our knowledge, the FM technique is the only one capable to overcome all known NLE in BOTDA sensors, and also overtake the Brillouin threshold limit of the fiber. This, in turn, allows to use a higher probe wave power level, and hence, obtain an improvement in the SNR. The enhancement in the detected SNR brought by the use of such power leads to an excellent sensor performance without resorting to additional means such as the use of pump pulse coding or Raman gain. Moreover, the FM technique can provide side benefits such as the amplification of the pump pulses [55], SNR improvement by the addition of gain and loss processes in a dual-probe BOTDA [107] and enhancement of SNR in pulse coding BOTDA.

In summary, the FM has been shown to be an important contribution to long-range BOTDA sensors and a simple solution to BOTDA sensors that deploy EOMs to shape the pulses. The MZ-EOM facilitates the high-spatial-resolution measurements using the differential pulse-width pair technique [108]. It is of paramount importance the research work focused to overcome NLE, specially in those sensors that make use of coding techniques. Therefore, in the next chapter, the research will be focused on investigating the significance of the dithering technique in BOTDA systems deploying pump pulse coding.

Chapter 5: Mono-color cyclic coding in Brillouin optical time-domain analysis sensors

Contents

5.1 Introduction

The scope of Brillouin optical time-domain analysis (BOTDA) sensors, covers a wide range of structural health monitoring applications, such as the monitoring of oil and gas pipelines, assessment of high voltage cables and railway inspection. Several of these applications require a large sensing range, even reaching up to hundreds of kilometers. However, as noted before, the sensing range of BOTDA sensors is limited by the signal-to-noise ratio (SNR) at the receiver, which is ultimately limited by the maximum pump and probe waves power that can be deployed in the fiber. As explained in the previous chapters, this maximum optical power, in turn, is constrained by the onset of several non-local and non-linear effects that distort the measurements. Thus, the sensing range of BOTDA sensors is fundamentally limited by the attenuation suffered by the pump and probe waves along the optical fiber, which eventually makes the measured signal to be too small to be properly detected with the required SNR.

In chapter 1, more specifically in section 1.5.4, we introduced several techniques to enhance the SNR of the sensor. Among them, we could highlight the use of the different coding methods. In this chapter, a significant contribution to the study and improvement of coded pump wave BOTDA sensors is presented. The chapter begins with an explanation of the theoretical fundamentals of coding techniques. Then, we demonstrate a BOTDA sensor that combines two different techniques to enhance the SNR of the analyzer: the use of probe-dithering, which has been introduced in detail in chapter 4, and mono-color cyclic

coding. As noted in chapter 4, the use of a probe-dithered BOTDA sensor allows to inject a larger probe wave power in the fiber, increasing the SNR of the sensor. In addition, the use of mono-color cycling coding, with its associated coding gain, further increases the performance of the sensor in terms of SNR. However, as higher power levels are used, several limitations related to pump pulse coding become significant. These constraints of coding techniques applied to BOTDA sensors are also theoretically and experimentally analyzed in this chapter. Specifically, we study the distortion in the decoding process, and the errors in the measurement that this distortion introduces, due to three factors: the power difference of the successive pulses of a sequence, the onset of pump pulse depletion due to first-order non-local effects and the non-linear amplification of the probe wave that results when using mono-color cyclic coding. Finally, the results of this analysis is deployed to demonstrate an improved long-range BOTDA setup.

5.2 Optical pulse coding techniques in BOTDA sensors

As mentioned in chapter 1, in a BOTDA sensor there is a trade-off between SNR and spatial resolution, as well as between SNR and measurement time (consider that increasing the number of averages, and in consequence the measurement time, enhances the SNR). Any increase in the SNR at the receiver entails an improvement of the performance of the BOTDA sensor, which in turn can be used to extend the measurement range, to enhance the spatial resolution and/or to reduce the measurement time.

One of the most widely used approaches to enhance the SNR of the BOTDA sensor is the use of optical pulse coding [109]. This improvement is due to the increased pump energy in the fiber, without raising the peak power, and it does not compromise the spatial resolution of the sensor. This is accomplished by injecting into the fiber a pump wave made up by sequences of pulses with some particular properties instead of a single pulse. In a way that allows to retrieve the Brillouin frequency shift (BFS) of the sensing fiber by using a particular decoding process.

In recent years, different pulse coding techniques applied to BOTDA sensors have been studied. These coding methods, which include complementary-correlation Golay codes [110] and simplex coding [109, 58], cyclic coding [59], bipolar coding [89, 60] and color coding [47, 111], have been proved to be useful for long sensing range BOTDA systems. All of these coding techniques are characterized by different features and advantages in terms of coding gain. In the following, the fundamentals of these methods are introduced.

Golay and Simplex pulse coding are based on the use of pulse sequences that follow a specific criteria. In this way, the measured BOTDA traces match the linear combination of the single pulse traces, each of which is delayed in time as a function of the used code sequence itself. In order to retrieve the BFS of the fiber, a linear decoding process is performed, following the specific code sequence used in the system. The BOTDA trace obtained after decoding presents a significantly improved SNR compared to the single-pulse measurement. This SNR increment given by the coding gain depends on the number of bits of the used pulse sequence.

Cyclic coding is based on quasi-periodic Simplex bit sequences, and its main difference

with simplex pulse coding is the required measurement time. Cyclic codes allow the use of coding techniques in fast distributed measurements over several kilometers of fiber [59]. In this thesis, we have used mono-color cyclic coding, thus, in the following subsection a detailed description of this technique is provided.

Bipolar codes use sequences comprised of bits of 1's and -1's, whereas the other coding methods use unipolar codes, which are comprised of sequences of 1's and 0's (where 1 represents the presence of a pulse and 0 no pulse, that is, on/off intensity modulation of the pump pulses). In bipolar coding, the 1's elements of the code are pump pulses at frequencies higher than the probe wave, inducing Brillouin gain on the probe wave, while the -1's are pump pulses at lower frequencies than the probe wave, inducing Brillouin loss on the probe wave. Due to the double intensity contrast provided by bipolar codes, the influence of the noise during the decoding process is reduced, and hence, there is an enhancement of the coding gain of 3 dB in comparison with unipolar codes [89]. Nevertheless, this technique has been shown to be negatively affected by pump pulse depletion [60], so that to reduce this issue a complex BOTDA setup is necessary [60].

Color coding is based on the use of different frequencies in the generation of the pump wave. Therefore, while in conventional coding techniques all the pulses of the code have the same frequency, so that they could be denominated as mono-color coding, in color coding each of the bits of the code represents a different frequency. In color coding, the code length (L_C) is equal to the number of discrete frequencies scanning the Brillouin gain/loss spectrum (BGS/BLS). The different coding techniques presented (simplex, cyclic and bipolar coding) can deploy a single frequency, which makes them mono-color coding, or different frequencies, as for instance simplex color coding [111] or cyclic color coding [47]. It is worth mentioning that the coding gain is the same for the color coding method than in its equivalent mono-color coding implementation. However, as the frequency detuning between the probe and the successive pulses of a sequence is only close to the BFS for certain pulses, the total gain provided by all the pulses is greatly reduced. This is the main advantage of color coding.

5.2.1 Mono-color cyclic coding technique

Cyclic coding, as well as Simplex coding, uses optical codes derived from the Hadamard matrix [109, 112]. A Hadamard matrix is a bipolar square matrix (whose entries are either 1 or -1) that fulfills the property of having mutually orthogonal rows. Due to its bipolar elements, it is not possible to use directly the Hadamard matrix in Simplex and cyclic coding BOTDA systems, since both require unipolar codes. Therefore, to obtain useful pulse sequences, Simplex and cyclic codes require a transformation of the Hadamard matrix [112]. Note that as explained before, cyclic codes remain on quasi-periodic Simplex bit codes, so that both coding implementations require the same transformation method: a transformation that generates a matrix containing unipolar elements (1's and 0's) and orthogonal rows, called S-matrix (Simplex-matrix). Each row of the S-matrix defines a particular sequence of the codeword [109].

The S-matrix can be obtained from the Hadamard matrix by simply removing the first

row and the first column of the Hadamard matrix, and then, replacing the 1's by 0's and the -1's by 1's [112]. In this way, simplex and cyclic coding can be easily implemented in BOTDA systems by simply turning on and off the optical device used to shape the pulses, following the sequences of 1's and 0's defined in the S-matrix [59]. Eq. (5.1) represents an example of a Simplex code matrix of order 3.

$$S_3 = \begin{pmatrix} 1 & 0 & 1 \\ 0 & 1 & 1 \\ 1 & 1 & 0 \end{pmatrix} \tag{5.1}$$

The matrix in Eq. (5.1) can be used in a Simplex coding BOTDA as well as a in a cyclic coding owing to the cyclic characteristics of the matrix. A matrix has cyclic properties, when it is possible to generate all the rows of the matrix from a single one. In this way, as shown in Fig. 5.1, each row of the matrix can be generated from the preceding row by a circular shift of the first bit of the latter. In Simplex coding, we must generate as many pulse sequences as rows have the matrix. Nevertheless, in cyclic coding, due to the cyclic properties of the matrix, as highlighted in Fig. 5.1, we can generate all the sequences, one for each row of the matrix, using a single sequence of bits of length $2L_C - 1$, that in the particular example of the matrix represented in S_3 is the following bit sequence: $\{1\ 0\ 1\ 1\ 0\}$. Therefore, the measurement time is reduced in cyclic coding compared to Simplex coding.

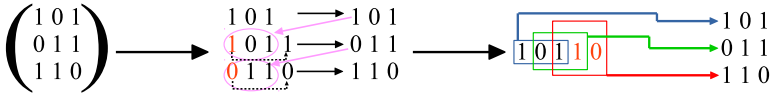

Figure 5.1: *Generation process of a cyclic matrix from a particular bit sequence of length* $2L_C - 1$.

A BOTDA sensor with cyclic coding uses a pump wave shaped by multiple pulses following the sequence of bits from which the entire Code matrix is generated. This sequence must fulfill that all the pulses of a particular row of the matrix fill the entire fiber length. In other words, when crossing the fiber, each of the wavefronts of the probe must interact with the pulses referred to a certain row of the matrix, but never with any other additional pulse. The probe interact with several pulses, so that the obtained BOTDA trace is the result of the Brillouin gain of all the interactions. An illustration of the obtained BOTDA trace at the receiver for a particular cyclic code of length $L_C = 7$ (using the bit sequence $\{1\ 1\ 0\ 1\ 0\ 0\ 1\ 1\ 1\ 0\ 1\ 0\ 0\}$) is depicted in Fig. 5.2.

As shown in the figure, the obtained coded BOTDA trace (black solid line) is the combination of the Brillouin gain induced by the successive pulses of the sequence. The dashed lines of different colors represents the gain of each of the pulses of the sequence in an individual manner [113]. First of all, let's consider each row of the code matrix as an M bit pattern $P = \{P_0, ..., P_{M-1}\}$ with $P_j = 0$ or 1 for $j = 0, 1, ..., M-1$, and that each row is the right-shifted copy of the previous one. Now, if we define H as the number of acquired samples between two adjacent bits of the pattern (either 1's or 0's), the total

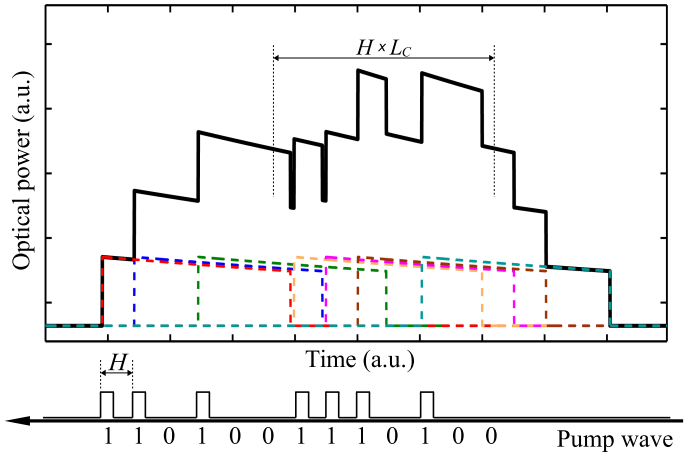

Figure 5.2: *Obtained BOTDA trace as a function of time when using a particular cyclic code sequence of bits of length* $L_C = 7$.

samples, T_S, of the received information needed to recover the BOTDA trace is determined as $T_S = HxL_C$.

By using a further index $i = 0, ..., (H-1)$, we can define, on the one hand, $y[i+jH]$ as the array of the coded BOTDA acquired samples, and on the other, $x[i+jH]$ as the array of the single pulse BOTDA response samples to be decoded. In this way, j scans the intervals of the successive bits of the pattern and i scans the whole samples within each interval. From Fig. 5.2 it follows that each sample of the acquired data, $y[i+jH]$, is due to the Brillouin contribution induced by the pulses launched in the j-th interval and in the $M-1$ previous ones. Therefore, the following relationship for x and y samples is fulfilled [113]:

$$y[i+jH] = \sum_{k=0}^{M-1} P_{|j-k|_M} x[i+kH] \tag{5.2}$$

For a particular i, Eq. (5.2) can be considered as a linear system of M equations (one for each j value) with a cyclic coefficient matrix. Therefore, once the coded BOTDA traces are obtained, in order to recover the conventional single pulse BOTDA traces, we have to apply the inverse Hadamard transform to the measured coded traces just like in the conventional Simplex coding technique [114].

From the perspective of the noise of the system, x and y samples can be considered as an uncorrelated random variables [113]. Therefore, the noise affecting the decoded x samples is established by the system of the linear equations itself, i.e., by the inverse of the cyclic code matrix. This gives rise to a coding gain equal to that obtained in the case of a Simplex coding matrix [113]. The improvement of the SNR granted by both the Simplex coding and cyclic coding techniques, i.e., its related coding gain, can be expressed as [114]:

$$C_{gain} = \frac{L_C + 1}{2\sqrt{L_C}} \tag{5.3}$$

Figure 5.3 depicts the expected SNR enhancement in a Simplex and cyclic coding

BOTDA sensor compared to a conventional single pulse BOTDA scheme, as a function of the used L_C.

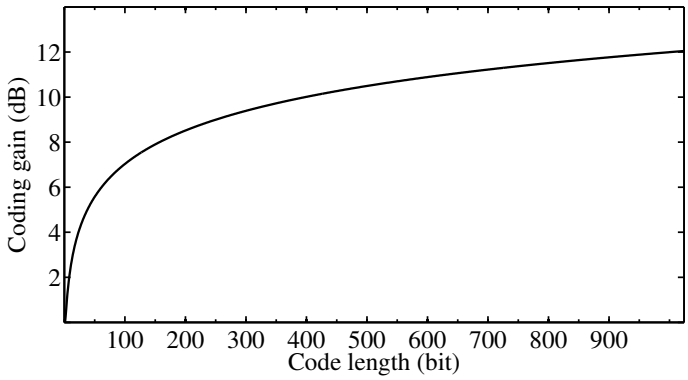

Figure 5.3: *SNR enhancement in the BOTDA measurement as a function of the code length.*

5.3 Fundamentals of the BOTDA sensor based on combining mono-color cyclic coding and probe-dithering

After outlining the theoretical foundations of the coding techniques, the contribution of this thesis in the form of a BOTDA sensor that combines probe-dithering (explained in detail in chapter 4) and mono-color cyclic coding is presented. The fundamentals of the BOTDA sensor are schematically described in Fig. 5.4, where the optical waves involved in the technique are depicted. As it is highlighted in the figure, the optical frequency of the probe waves is modulated following a saw-tooth shape [55]. Additionally, this frequency modulation (FM) is synchronized to the pump pulses so that a pulse sequence experiences the same wavelength of the probe waves at any given location. In this setup, as explained in chapter 4, first-order and and second-order non-local effects [33] are prevented because

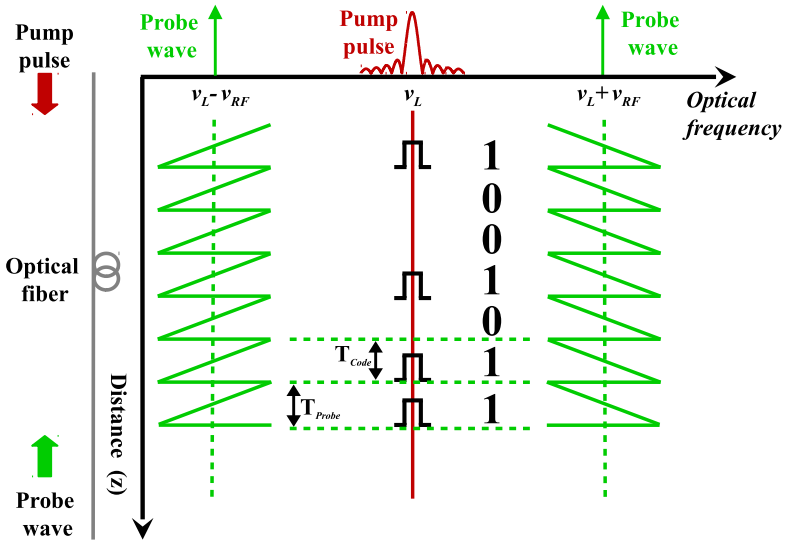

Figure 5.4: *Fundamentals of the technique*

the FM of the probe waves makes the Brillouin interaction upon the optical pulse to spread over a large frequency range. Moreover, the FM increases the Brillouin threshold limit of the fiber. Therefore, a very large probe power can be deployed in the sensing fiber in order to enhance the SNR in detection.

In order to further increase the SNR, we combine the probe-dithering technique with mono-color cyclic coding. For this purpose, we introduce a code based on a circulant matrix of dimension L_c, with L_c a prime number [47]. The code is generated following the recurrence equation for an integer n:

$$\begin{cases} u_1 = 0 \\ u_{n+1} = (u_n + n)\ mod\ L_c \end{cases} \tag{5.4}$$

where mod is the modulo function and $n \in [1, \frac{L_c+1}{2}]$. The position p_n of the consecutive "1" bits for the first line of the code matrix is simply given by the relation: $p_n = u_n + 1$. As an example, the code matrix for a code length of seven is represented in Eq. (5.5), note that the first line of the matrix is also portrayed in Fig. 5.4(a).

$$S_7 = \begin{pmatrix} 1 & 1 & 0 & 1 & 0 & 0 & 1 \\ 1 & 0 & 1 & 0 & 0 & 1 & 1 \\ 0 & 1 & 0 & 0 & 1 & 1 & 1 \\ 1 & 0 & 0 & 1 & 1 & 1 & 0 \\ 0 & 0 & 1 & 1 & 1 & 0 & 1 \\ 0 & 1 & 1 & 1 & 0 & 1 & 0 \\ 1 & 1 & 1 & 0 & 1 & 0 & 0 \end{pmatrix} \tag{5.5}$$

The improvement of the SNR given by the coding gain, as explained in section 5.2, is the same as for simplex coding and is defined by Eq. (5.3). Note that, as explained, cyclic coding presents the important advantage of a reduced measurement time in comparison to the Simplex coding: as the code scheme is cyclic, there is no need to repeat each sequence that corresponds to a line of the coding matrix. In this way, the first sequence is simply repeated in a continuous loop, providing fast averaging. Moreover, the number of possible code lengths using this recurrence equation can be chosen between any prime number, in contrast to conventional code generation methods, where the code length has to be a number given by $2n - 1$, n being an integer [47]. Therefore, a significantly higher number of code lengths can be chosen.

Note that the presented BOTDA sensor combines a frequency modulated probe wave, which, as explained in chapter 4, requires a reordering of the acquired data, with multiple pulses. This fact must be taken into account in order to decode the signal properly. In this way, the easier way we found to correctly decode the signal is that the period of the FM of the probe waves has to be equal to the code period ($T_{probe} = T_{code}$), i.e., the temporal distance between two of the contiguous bits of the generated cyclic code. In addition, as explained above, in a cyclic code all codewords of a sequence must fit simultaneously inside the fiber. Therefore, for a given fiber length, the code period, together with the FM period, needs to be modified depending on the code length. Finally, to properly decode the

signal and retrieve the BGS of the fiber, the frequency shift of the probe waves must be compensated by reordering the decode matrix, following the method explained in chapter 4.

5.4 Optical power limitation in a BOTDA sensor with a coded pump wave

An important consideration when deploying a BOTDA sensor with coding is related to the constraints faced regarding the maximum pump and probe power that can be injected in a given fiber sensing link. As explained before, due to the dithering technique the optical power of the probe wave can be increased considerably. This, in turn, has allowed us to analyze some limitations of the coding techniques applied to BOTDA sensors that until now had not been described in detail. In the following, these limitations are presented. Note that, some of the considerations are equally valid for all the coded pump wave BOTDA configurations (Simplex, cyclic, bipolar and color coding), although some others present a different relative severity of the various impairments that constrain the use of coding.

5.4.1 Coded pump wave optical power fluctuations

The first limitation comes from the fact that, in order to decode the signal properly, it is mandatory that all the coded pump pulses have the same optical power. This indirectly constrains the pump power due to the transient behavior of the erbium-doped fiber amplifiers (EDFA) that are typically deployed to amplify the pulses before injecting them into the fiber [102]. This transient behavior worsens for large input powers making the pump pulses in a sequence to experience different gain, and consequently, the coded pump wave is composed of pulses with different optical power.

In order to overcome this limitation, a simple solution is to replace each "1" of the original coding matrix by the weighted pulse power of the used pump pulse wave. However, this requires monitoring the pump wave during the measurement process. Therefore, in order to correct the effects of the power fluctuations on the pump wave, and in consequence, retrieve an undistorted BGS, another detector is needed [111].

5.4.2 Non-local effects in a coded pump wave BOTDA sensor

Another important limitation regarding the maximum pump and probe waves power that can be injected in the fiber in a BOTDA sensor that deploys a coding technique comes from the onset of non-local effects. In a conventional BOTDA setup without coding, as introduced in chapter 2, the pump pulse depletion is directly linked to the probe power injected into the fiber [31]. As explained in section 2.2 and repeated here for clarity, the pump pulse power at the output of the fiber is given by the following expression (assuming a BOTDA in a gain configuration):

$$P_P(L) = P_{Pi}\, exp(-\alpha L)\, exp\left(\frac{-g_B(\Delta\nu)}{A_{eff}} P_{Si}\, L_{eff}\right) \tag{5.6}$$

where $L_{eff} \equiv (1 - exp(-\alpha L))/\alpha$ is the effective length, α, L and A_{eff} are the attenuation, length and effective area of the sensing fiber, respectively, P_{Pi} is the pulse power at the input of the fiber, P_{Si} is the input probe power at the far end of the fiber link and g_B is the Brillouin gain introduced in Eq. (1.24), which depends on the frequency shift between pump and probe waves, $\Delta\nu$.

However, Eq. (5.6) is no longer valid for a coded pump wave, because, the successive pulses interact with a probe wavefront that has been already amplified by previous pulses. Therefore, the amount of the pump pulse depletion suffered by single pulses, instead of being just related to the power of the probe wave injected into the fiber, as given by Eq. (5.6), also depends on the amplification of the probe wavefronts by previous pulses in the coded sequence. Hence, non-local effects will appear earlier in BOTDA setups using pump pulse coding than in conventional single-pulse BOTDA sensors.

Furthermore, even for a dual-probe wave BOTDA configuration, which mitigates the onset of non-local effects [92], the presence of multiple pulses in the fiber when implementing a coding method makes the pump pulse depletion to become significant at lower input probe wave power than for single-pulse dual-probe systems. This is due to the fact that, while one probe wave is amplified by the pump pulses, the other probe wave is attenuated, and hence, the optical power of both waves is unbalanced, so that the compensation of the Brillouin gain and loss upon the pulse granted by the dual-probe technique is no longer effective. In fact, all BOTDA setups deploying pulse coding are affected by the depletion of the pump pulses, but the amount of the depletion will be different for each configuration. In this way, the probe-dithered BOTDA makes the sensor more robust to pump pulse depletion in comparison to other BOTDA configurations, due to the FM of the probe wave. In addition, the amount of the depletion of the pulse will be different for the various coding techniques, being higher the impairment for mono-color coding than for color coding and bipolar coding. This is due to the fact that, the total Brillouin gain and/or loss experienced by the probe is larger for mono-color coding than for the other two methods, and hence, the depletion of the pulse will also be higher.

Finally, another assumption regarding non-local effects that becomes invalid for BOTDA systems with coding is the independence of the pump pulse depletion on the pump pulse power that is conveyed by Eq. (5.6). In a BOTDA sensor with coding, the higher the pump pulse power, the larger the amplification of the probe wave by previous pulses in a sequence, and hence, the larger the depletion of a particular pump pulse. Therefore, non-local effects in BOTDA sensors with coding may lead to the need to reduce the probe power as well as the pump pulse power compared to the sensor without coding, which is counterproductive for the sensor performance.

5.4.3 Non-linear amplification of the probe wave

Finally, another limitation for pump and probe powers in BOTDA sensors with coding comes from the fact that, as explained previously, coding techniques can only be applied to linear interactions. However, as explained in chapter 1, in BOTDA sensors, the Brillouin gain experienced by the probe wave does not depend linearly on the pump pulse power,

but exponentially. Indeed, using the equations of the Brillouin interaction upon the probe wave presented in section 1.4, we can conclude that the variation in the continuous wave (CW) probe signal power, ΔP_S, detected in the receiver at a given instant, t, due to the stimulated Brillouin scattering gain interaction at a location z_j along the fiber with a pump pulse is given by:

$$\Delta P_S(t, \Delta\nu) = P_{Si}\, exp(-\alpha L)\, [G_j(t, \Delta\nu) - 1] \tag{5.7}$$

where $G_j(t, \Delta\nu)$ is the Brillouin gain defined as follows:

$$G_j(t, \Delta\nu) = exp\left[\int_{z_j}^{z_j+\Delta z} \frac{g_B(\Delta\nu)}{A_{eff}} P_{Pi}\, exp(-\alpha z_j)\, dz\right] \equiv exp(g_j) \tag{5.8}$$

where Δz is the spatial resolution given by the pulse duration. Only assuming that the Brillouin gain is very small ($g_j \ll 1$), can Eq. (5.7) be simplified considering that the BOTDA sensor operates in a small signal regime:

$$G_j(t, \Delta\nu) \approx 1 + \int_{z_j}^{z_j+\Delta z} \frac{g_B(\Delta\nu)}{A_{eff}} P_{Pi}\, exp(-\alpha z_j)\, dz = 1 + g_j \tag{5.9}$$

Hence, the Brillouin gain in a single-pulse BOTDA configuration can be approximately considered to depend linearly on the gain provided by single pulses, so that in principle linear optical pulse coding techniques could be applied. However, the total amount of gain that the probe wave experiences in a BOTDA deploying coding is provided by the interaction with all the pulses in the sequence for the whole codeword, so that ΔP_{CW} is obtained as follows:

$$\Delta P_S(t, \Delta\nu) = P_{Si}\, exp(-\alpha L)\, [G_T(t, \Delta\nu) - 1] \tag{5.10}$$

where $G_T(t, \Delta\nu)$ is the total Brillouin gain provided by the successive pulses, which is given by:

$$G_T(t, \Delta\nu) = G_1 G_2 G_3 ... G_{L_c} = exp\left(\sum_{j=1}^{L_c} g_j\right) \approx 1 + \sum_{j=1}^{L_c} g_j \tag{5.11}$$

where $G_j = exp(g_j)$ is the gain provided by each pulse with position j in the coded sequence. In order for coding to be applicable, the approximation in the last equality term of Eq. (5.11) needs to be valid, so that the total gain experienced by the probe wave is the linear superposition of the gains provided by each pulse. However, this requires the total Brillouin gain induced by the pump pulses sequence on the probe to be relatively small ($\sum_{j=1}^{L_c} gj \ll 1$), which is much more difficult because, despite the fact that the individual gains provided by each pulse may be small, the accumulated gain provided by the many pulses in a long pulse sequence becomes much larger. Therefore, in order to avoid distortion, it becomes necessary to reduce the gain induced by each individual pulse by further limiting the pump power below the thresholds imposed by the onset of non-linear effects such as modulation instability (MI).

5.5 Experimental setup and measurements

In order to evaluate the power constraints of cyclic coding and to demonstrate the capabilities of the proposed technique, a BOTDA setup following the scheme in Fig. 5.5 was assembled. The optical source was a 1550-nm DFB laser, whose output was divided by a coupler into two branches. In the lower branch of the setup, a dual-probe wave was generated using a Mach-Zehnder electro-optic modulator (MZ-EOM). This modulator was driven by an arbitrary waveform generator (AWG), and biased for minimum transmission so as to generate a frequency modulated double-sideband suppressed-carrier signal. For this purpose, the AWG provides a microwave signal with an instantaneous frequency varying around the BFS of the fiber following a saw-tooth shape. Then, an EDFA was used to amplify the probe wave power level. Finally, before the receiver, a tunable narrow-band fiber Bragg grating (FBG) was used to filter out one of the probe sidebands and the Rayleigh backscattering originating from the pump wave.

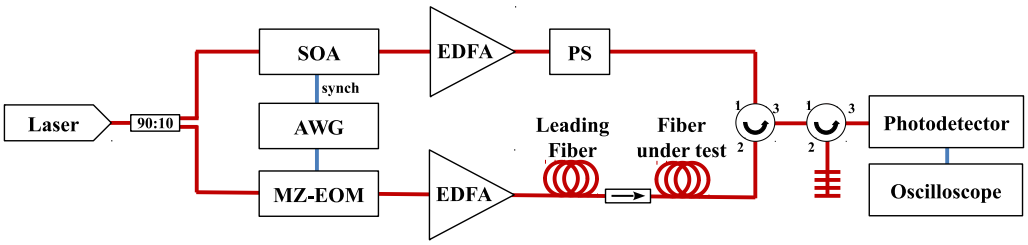

Figure 5.5: *Experimental setup for the BOTDA sensor.*

In the upper branch, so as to generate a pump pulse with a high extinction ratio (ER), the pump signal was pulsed by a semiconductor optical amplifier (SOA), with an ER up to 50 dB. The AWG was used to generate the coding pulse sequences, and also to synchronize them with the FM of the probe waves. Then, the pump pulse power was amplified in another EDFA, and the polarization state of the pulsed pump was randomized with a polarization scrambler (PS), to smooth polarization effects in the Brillouin interaction along the fiber, before being launched into the sensing fiber.

5.5.1 Experimental validation of the limits imposed by mono-color cyclic coding

In order to evaluate the limitations explained in section 5.4, we deployed in the setup of Fig. 5.1 a mono-color cyclic coding technique. As explained in chapter 4, the use of a dithered probe wave makes the system less affected by non-local effects than a conventional dual-probe BOTDA scheme. We chose a dithered-probe BOTDA configuration to analyze more effectively the different constraints, considering that as the pump pulse depletion is less significant, some other impairments can be analyzed in more detail, as for instance the non-linearity of the Brillouin gain.

A 25 km length of standard single-mode fiber (ITU G.652) was used initially to evaluate the limits on the probe and pump power that can be injected in the fiber when using mono-color cyclic coding before the onset of distortions and measurement errors in the

decoded signal. In order to satisfy the condition explained in section 5.3, according to which the period of the FM must be the same that the temporal distance between two bits of the code, the FM of the saw-tooth of the probe waves was changed for each of the used code lengths. The same slope of the saw-tooth shape was maintained for all the measurements, so that the peak-to-peak frequency deviation of the FM was changed for different code lengths. The probe power was fixed to -7 dBm per sideband at the input of the fiber, so as to simulate the maximum probe power that could be obtained at the fiber under test (FUT) in a 200 km loop configuration. That probe power was obtained by subtracting the attenuation of the 100 km leading fiber (approximately 20 dB) from the maximum power that can be injected in the fiber due to the Brillouin threshold with probe-dithering (approximately 13 dBm per sideband). Finally, the pump wave was modified in terms of pulse duration, pulse power and code length.

First, the effect of the power variations of the different pulses of the coded sequences was investigated. To that end, a sequence of 20-ns pulses with a code length of $L_c = 263$ was used. In order to make sure that there was no pulse depletion, the pump pulses were first amplified to 19 dBm by an EDFA and then reduced by an attenuator to a maximum peak power of 13 dBm. To ensure that there was no pump pulse depletion, the pump wave was detected at the output of the fiber by another detector. Figure 5.6 depicts the power of each pulse in the used cyclic sequence that clearly shows a non-flat response due to the transient behavior of the EDFA [102].

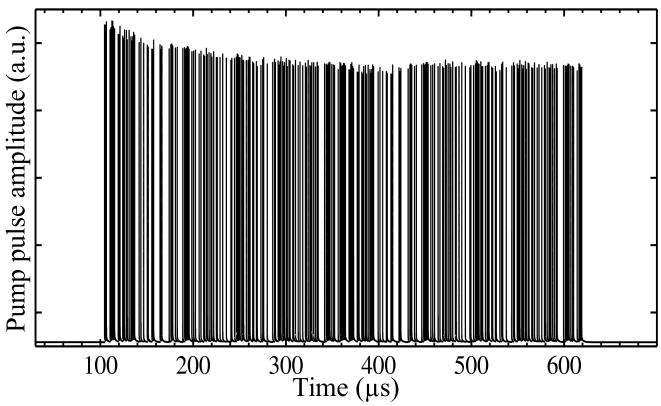

Figure 5.6: *Power measurement of the cyclic pulse train of the first sequence for* $L_c = 263$.

As explained in section 5.4.1, if this optical power difference of the pulses of the sequence is not taken into account during the decoding process, the obtained measurement will be distorted. This distortion is highlighted in Fig. 5.7(a), where rapid variations of the amplitude of the decoded BOTDA trace can be seen. This, in turn, will lead to significant errors in the measurement of the BFS of the fiber. In order to retrieve an undistorted smooth signal, as in Fig. 5.7(b), the pulse power fluctuations have to be corrected, and therefore, each "1" of the original coding matrix has to be actually replaced by the weighted pulse power, which needs to be monitored by another detector [111].

Note that this effect is reduced, if not completely suppressed, by repeating the coded sequence in a continuous way, so that the EDFA has a more linear behavior. Another

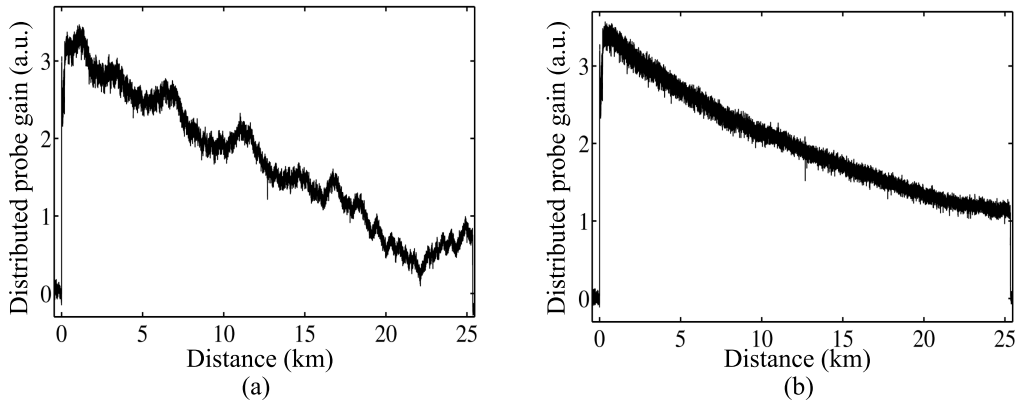

Figure 5.7: *Decoded BOTDA trace at BFS of the fiber for a pulse of 13 dBm power and 20 ns; (a) without taking into account the pulse power variations and (b) taking into account the pulse power variations.*

alternative could be the use of an alternative technique to suppress the transients of the EDFA [115]. However, the several options to overcome this constraint increase the complexity and the price of the sensor.

After analyzing the behavior of the decoding process when pulses of different optical power are deployed, we analyzed the distortion in the decoded signal produced by the pump pulse depletion due to non-local effects. For this purpose, the peak power level of the pulse was raised to 19 dBm, while the pulse duration was maintained at 20 ns. Figure 5.8(a) shows the pump pulse depletion factor that the successive pulses of a cyclic sequence suffer for different code lengths. It can be observed that even with the FM of the probe waves, which makes the system less affected by non-local effects than a conventional dual-probe BOTDA system, and for a relatively short code length of $L_c = 71$, there is already a small depletion in the pulses (smaller than 0.01).

In addition, note that the depletion suffered by each pulse of a sequence is not the same, increasing accordingly with the amplification of the probe wave by previous pulses. Indeed, it can be observed that the depletion of the pulses follows a cascade effect, since the

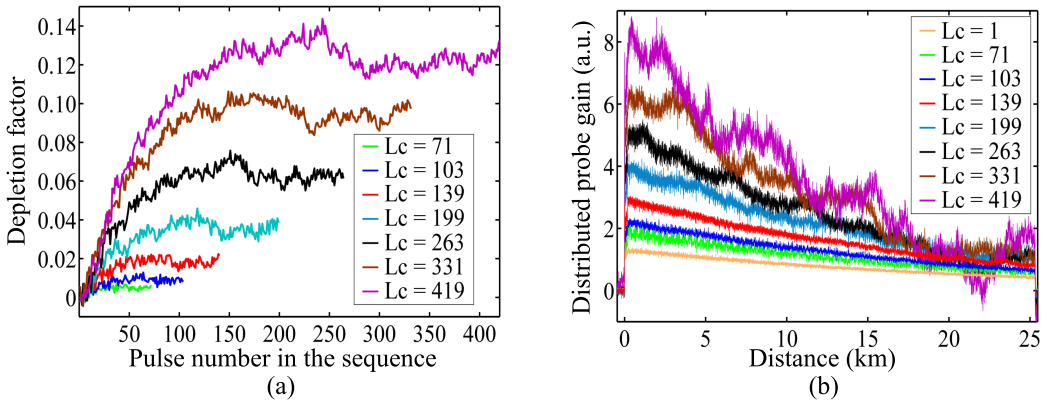

Figure 5.8: *For a pulse of 19 dBm power and 20 ns; (a) Depletion of the pulses of the sequence for different code lengths (b) distortion in BOTDA trace due to pulse depletion for different code lengths.*

depletion factor of the nth pulse would be affected by the amplification suffered by the probe wave for all the coding units before (1st to n-1th). However, notice that in Fig. 5.8(a) a given code unit experiences a different depletion factor depending on the total code length. This is due to the fact that, as explained before, the code period needs to be modified as a function of the code length. For larger code lengths, the code period is reduced so that the i^{th} pulse of the sequence interacts with a probe waves with a slightly higher unbalanced optical power, and hence, this leads to stronger overall pump pulse depletion.

Figure 5.8(b) depicts the decoded BOTDA traces at the BFS of the sensing fiber for different code lengths (same code lengths than in Fig. 5.8(a)). Note that the difference in the depletion factor for the successive pulses of a code sequence has an analogous distortion effect on the decoded traces to those due to amplitude variations of the pulses induced by the transient effects in the EDFA highlighted in Fig. 5.7(a). This is reasonable, considering that the difference in depletion induces a difference in pulse amplitude, and hence, the effect in the decode process is similar to the one investigated and depicted in Fig. 5.7(a). The figure also shows that the larger the pulse depletion of the pulses of the sequence, the higher the distortion. Furthermore, even for a small pulse depletion, e.g., for a code length of $L_c = 139$, in which a maximum depletion factor of approximately 0.02 is reached, there is a small distortion in the decoding process that is more visible at the end of the BOTDA trace. Note that some traces of Fig. 5.8(b) are noisier than they should, for instance, for $L_c = 71$. This anomaly is attributed to the PS deployed, which was found to change

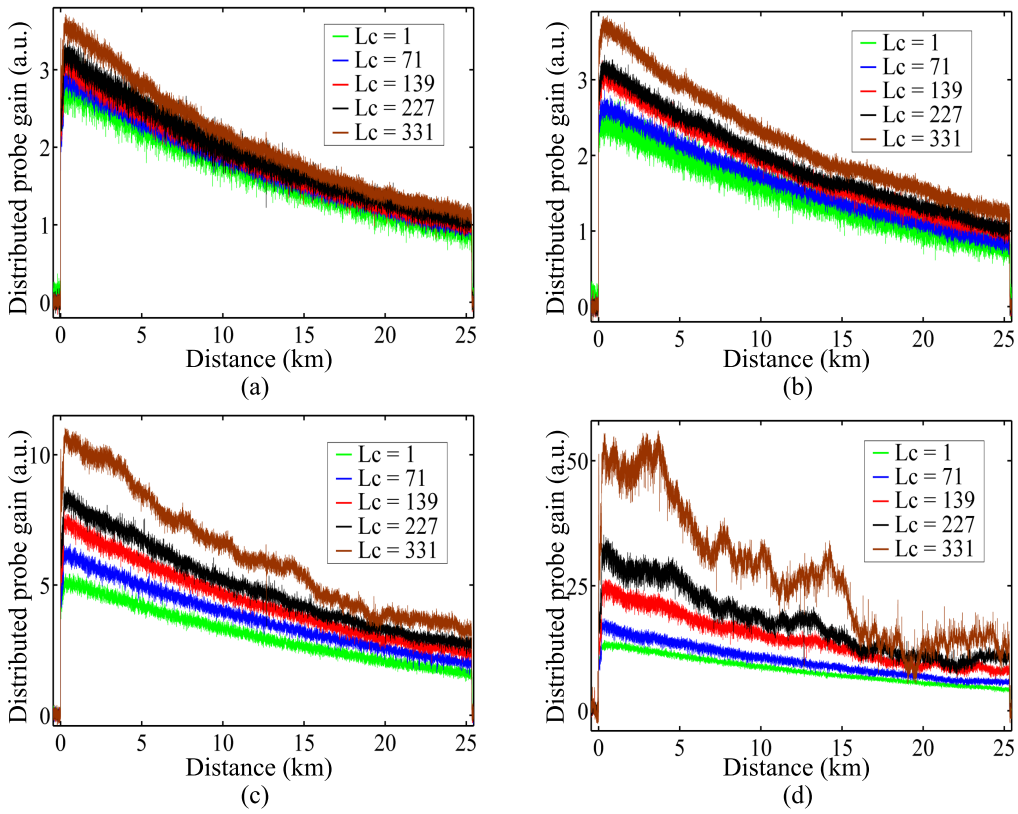

Figure 5.9: *Obtained BOTDA trace at BFS of the fiber for a pulse of (a) 13 dBm and 20 ns, (b) 16 dBm and 10 ns, (c) 16 dBm and 20 ns and (d) 16 dBm and 40 ns.*

slightly the time-averaged degree of polarization that it generated over time, probably due to heating.

Additionally, we studied the non-linear amplification of the signal due to the code length. In a purely linear interaction, the amplitude of the decoded BOTDA trace should be the same for all code lengths. However, Fig. 5.9 highlights the different amplitudes of the decoded BOTDA trace due to the non-linear amplification measured close to the peak of the BGS. The non-linear amplification was studied as a function of the code length, pulse duration and pulse power. As it can be seen, the amplitude of the decoded BOTDA traces increases with the code length, resulting in a measurement distortion. Furthermore, this distortion is also frequency-depend because for frequencies further away from the peak of the BGS (BFS of the fiber), the gain provided by the pump pulses to the probe wave will be so small that the linear interaction condition will be fulfilled.

Notice also that as expected, the non-linear amplification effects increase with increasing pulse duration (more gain to the probe due to increased interaction length) and power. The additional distortion in the form of rapid variations of the signal in the decoded traces in Fig. 5.9 can be attributed to the onset of the pulse depletion due to non-local effects already visualized in Fig. 5.8(b). In any case, it is important to clarify that, as non-local effects and non-linear amplification occur both at same time, the distortion in the form of rapid variations of the trace could be a consequence of both, considering that they can both reinforce each other.

Figure 5.10 summarizes the non-linear amplification effect by depicting the normalized amplitude in percentage value of the beginning of the decoded BOTDA trace (entry point of the pump pulses) for different code lengths. To normalize the amplitude, for each of the different pulse duration and power, the amplitude value of a single pulse is used as a reference. It can be seen that for low pulse optical power, the non-linearity of the gain interaction cannot be clearly discerned for small code lengths, but in the case where code length, pulse power or duration is higher, the non-linear regime becomes noticeable. Therefore, it is clear that the non-linear amplification has a direct link to the pump power, the code length and also to the pump duration.

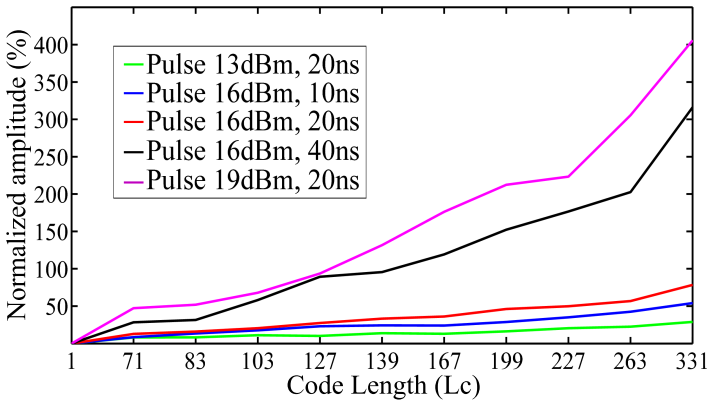

Figure 5.10: *Non-linear amplification for different code lengths, and different pulse power and duration.*

As noted above, the non-linear amplification and the depletion of the pulses occur both

simultaneously, and both effects cannot be separated experimentally. Therefore, with the aim of analyzing the contribution of each one to the distortion of the decoded BOTDA trace, the model presented in chapter 3 was used. As in experimental measurements, a fiber length of 25 km was used, with a pump pulse peak power of 19 dBm and -7 dBm probe wave power per-sideband. The pulse duration was set to 20 ns and the code length was $L_C = 331$. However, in this case, instead of using a dithered probe BOTDA, a conventional dual-probe BOTDA sensor was used, and hence, non-local effects become more significant.

Figure 5.11 compares the calculated BOTDA trace at BFS of the sensing fiber when using a single pump pulse wave with two decoded BOTDA traces of $L_C = 331$. Note that one of the decoded BOTDA traces was calculated avoiding completely the effect of the pump pulse depletion, for which the model presented in chapter 3 was slightly modified. As can be seen, both decoded traces have a higher amplitude than the trace obtained in the case of a single pulse. However, the trace that avoids the depletion of the pump pulses presents a slightly larger amplitude, which is attributed to the fact that as the pulses have a slightly higher optical power, the Brillouin gain provided by each pulse is greater and hence the non-linear amplification is larger. In addition, it can be observed that the BOTDA trace distortion in form of rapid variations is higher in the case that pump pulse depletion affects the measurement than in the one without pulse depletion. Therefore, it might be argued that the distortion in the form of rapid variations in the amplitude of the decoded BOTDA trace is mostly due to the pump pulse depletion.

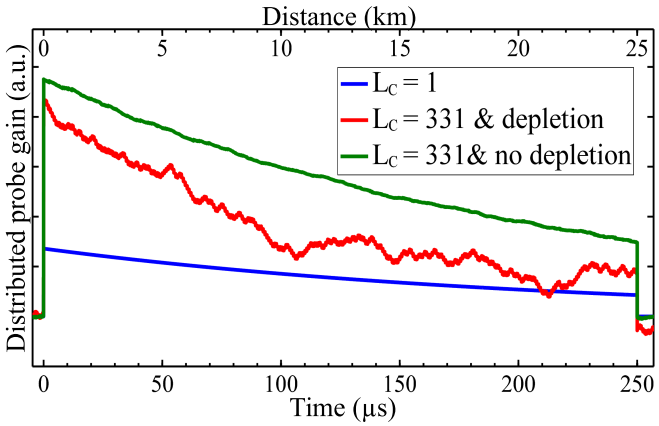

Figure 5.11: *Calculated BOTDA trace at BFS of the fiber for a single pump pulse BOTDA configuration and for a 331-bit mono-color cyclic coded pump pulse BOTDA with and without pump pulse depletion.*

Finally, in order to analyze the error in the experimental measurements that all these distortions introduce, distributed temperature measurements were performed. The pulse power was set to 19 dBm and the duration was set to 20 ns, corresponding to approximately 2 m spatial resolution. The traces were averaged 1000 times. The final meters of the fiber were placed loose in a climatic chamber with a fixed temperature, while the rest of the fiber was held at room temperature in a spool. The BFS along the fiber was calculated by performing a quadratic fit on the measured BGS.

Figure 5.12 depicts the evolution of the measured BFS at the end of the fiber for

different code lengths and for a single-pulse measurement. The heated section is clearly visible at the end of the fiber, and as expected, the measured BFS of the single-pulse measurement agrees with the smaller code length measurements, while for the others the error increases. Specifically, it can be observed that for $L_c = 1$ to $L_c = 103$ there is no significant error while for $L_c = 139$ and $L_c = 199$ the error in the measured hot spot are 2.2 MHz and 4 MHz respectively. Which makes sense, since the greater the distortion the larger the error. Therefore, the error increases for a longer code length.

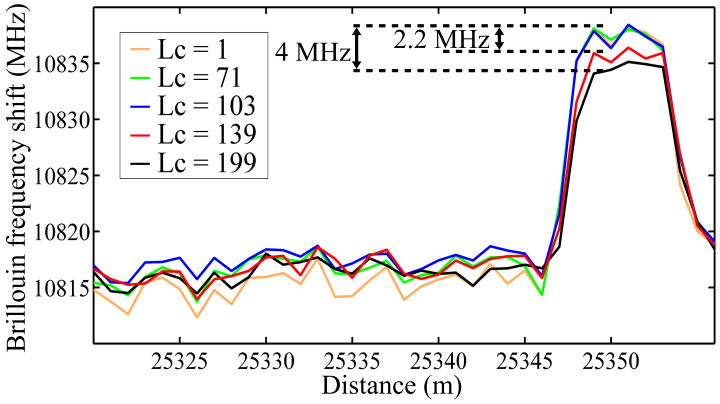

Figure 5.12: *Calculated BFS as a function of distance at the final locations of the fiber, with a fix temperature for different code lengths.*

For all of these reasons, in order to avoid distortions in the decoded signal, that leads to an error in the precision of the analyzer, it is mandatory to reduce the pump power, the probe power, the code length or the pump duration, which can lead, in several cases, to a non-existing improvement of the SNR of the analyzer.

5.5.2 SNR enhancement for a long-range BOTDA sensor

Once the constraints of mono-color cyclic coding were studied, and in order to analyze the ultimate performance of our BOTDA sensor combining cyclic coding and probe dithering, distributed temperature measurements were performed over a loop of 164 km length of standard single-mode (ITU G.652) fiber. The final meters of the fiber were placed loose in a climatic chamber at controlled temperature, while the rest was held at room temperature in a spool. The pulse duration was set to 10 ns, corresponding to approximately 1-m spatial resolution, and the code length was set to $L_c = 79$, which was found to be the largest code length that could be used without the onset of the previously analyzed impairments in mono-color cyclic coding, without decreasing the power of the optical waves, which would lead to a decrease SNR. In this case, the code period was set to 10.7 μs. Therefore, in order to satisfy the requirement explained in section 5.3, the FM of the probe waves was set also to a period of 10.7 μs and a peak-to-peak frequency deviation of 250 MHz.

The probe wave was boosted to 15 dBm, so that there was 12 dBm per sideband, by a conventional EDFA before being injected into the 82-km leading fiber, so that at the input of the sensing fiber the probe power was -1.8 dBm. This value was measured to be the maximum tolerable value before the onset of noise induced by spontaneous

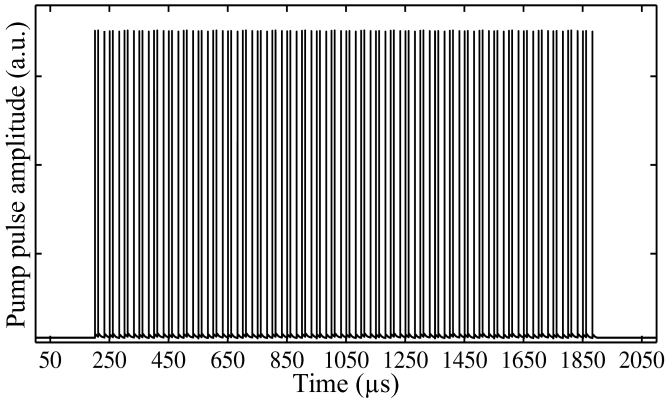

Figure 5.13: *Power measurement of the cyclic pulse train of the first sequence for* $L_c = 79$.

Brillouin scattering. Note that in a conventional BOTDA, the Brillouin threshold limits the maximum probe power that can be injected into the fiber to approximately 6 dBm. Hence, the use of the probe-dithering method entails an intrinsic enhancement in SNR.

The pulse power was amplified to 20 dBm, a level close to the limit before MI becomes significant [37], by a specific EDFA (Nano-second Pulsed EDFA, Amonics) for generating pulses, so as to generate a flat power pulse train of the codeword, as highlighted in Fig. 5.13. In this case, the decoding process is simplified, with no need for an additional detector to measure the power of the sequence of pulses injected in the fiber. In case that this special EDFA is not available, the supplementary detector would be deployed to monitor the pump pulses, or, as explained before, other alternative technique to suppress the transients of the EDFA could be used [115].

The setup in Fig. 5.5 was completed by adding an EDFA preamplifier before the receiver. This EDFA was placed between two tunable narrow-band FBGs that were used to filter out one of the probe sidebands and the Rayleigh backscattering originating from the pump wave. In addition, the final FBG served to limit the amplified spontaneous emission noise being detected.

In order to analyze the measurement precision of the sensor, a series of 10 consecutive measurements in stable temperature conditions were performed. For that purpose, the

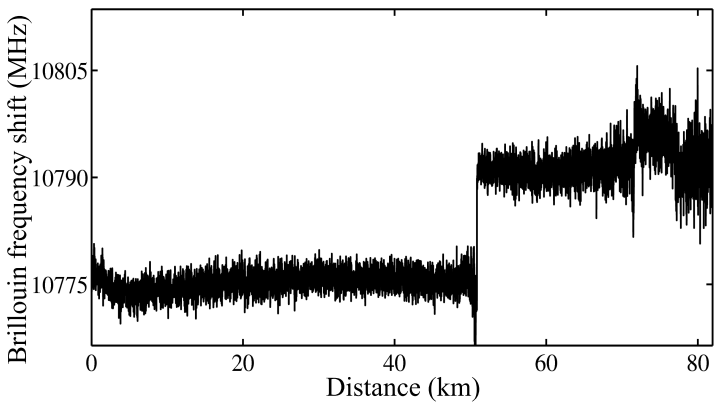

Figure 5.14: *Distribution of the BFS profile of the sensing fiber.*

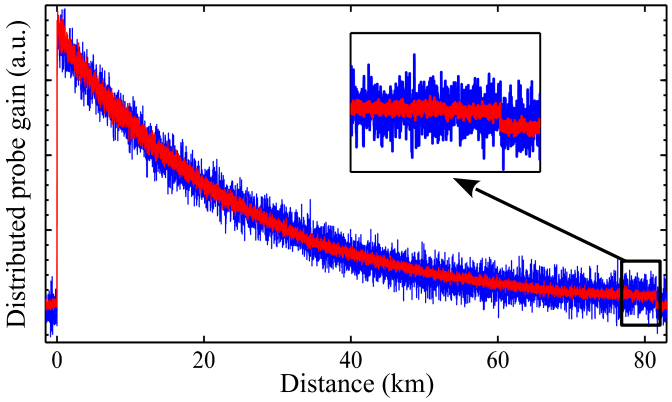

Figure 5.15: *BOTDA traces at BFS obtained for the analyzer with a 79-bit cyclic coding (red) and without aplying coding (blue).*

final 5 km of the fiber was placed in a climatic chamber at constant temperature. From these measurements, the uncertainty of the BFS measurement was found to be 3 MHz (1-σ) at the end of the FUT. Figure 5.14 depicts the BFS along the whole sensing fiber, where four fiber spools are clearly distinguishable, with a fairly uniform BFS in all of them. Note that the BFS along the fiber was calculated by performing a simple quadratic fit on the BGS. The frequency step of the spectral scan was 2.3 MHz and 16000 averages were used to obtain the final traces.

The noise reduction effect provided by the coding technique can be clearly appreciated in Fig. 5.15, which compares a conventional BOTDA trace (blue trace) obtained with a single pulse BOTDA configuration with the one obtained after decoding. The measured SNR enhancement was 6.2 dB, in good agreement with the theoretical expected value (6.5 dB) for a 79-bit code length. It is worth mentioning that as explained before, the code length was limited to $L_C = 79$ by the onset of the distortions studied in section 5.4 for longer lengths.

Finally, we introduced in a climatic chamber the last 3 m of the sensing fiber, while the rest of the fiber was placed at room temperature in spools. The difference between

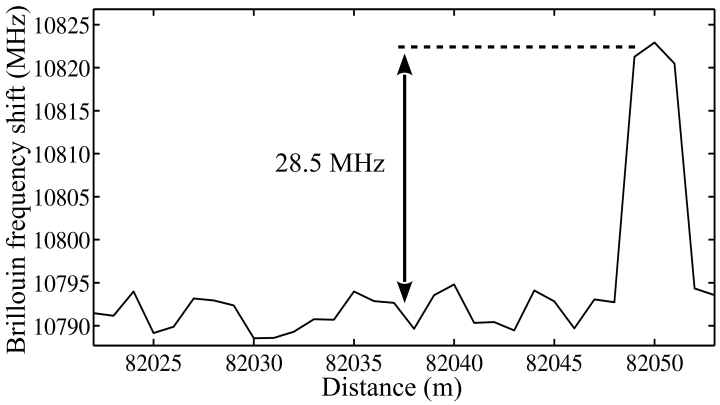

Figure 5.16: *Calculated BFS as a function of distance at the final locations of the fiber, with the last 3 meters in a climatic chamber.*

the room temperature and the climatic chamber was set to 27°C. Figure 5.16 depicts the obtained BFS at the far end of the FUT, where the hot spot can clearly be observed, with a BFS difference of 28.5 MHz between the hot spot and the ambient temperature, which matches with the expected value.

5.6 Conclusions

In this chapter, we have presented a study on the practical constraints on probe and pump power in a BOTDA sensors that uses a coding technique. To carry out this study we implemented an analyzer with mono-color cyclic coding. In particular, we have studied and experimentally demonstrated the distortion of the decoded BOTDA trace and the error that corrupts the measurement because of three factors: the power fluctuations of the pulse sequence, the onset of pump pulse depletion and the non-linear amplification of the probe wave.

We reach to the conclusion that, in order to avoid errors in the decoded signal, there is a trade-off between the maximum pump and probe powers that can be injected in the fiber, the code length, the pump pulse duration and the fiber length. The use of coding is limited to cases in which the obtained coding gain has a real benefit in the measurement in comparison with a single-pulse configuration In other words, if, in order to deploy a coding technique it is mandatory to reduce the pump and/or the probe optical power, which in turn entails a reduction of the effective SNR, the use of coding ceases to be useful. In fact, there may be configurations of the BOTDA setup in which the SNR decrement due to the limited pump and/or probe power could completely counteract the enhancement brought by the coding gain.

Based on these considerations, it can be argued that mono-color cyclic coding is really more useful in long-range loop configurations, where only half of the fiber is used for the sensing while the other half is used as a leading fiber to take the probe wave to the remote end of the sensing link. In this configuration, the probe power injected into the long-length leading fiber is constrained to the Brillouin threshold of that fiber; hence, the power finally reaching the end of the leading fiber and being injected into the sensing fiber is reduced. Fortunately, the loop configuration is the one deployed in most long-range sensing systems on the field, such as BOTDA sensors used to monitor gas or oil pipelines.

It is important to point out that the different coding techniques presented so far in the literature will be affected differently by the presented impairments. For instance, color coding [47, 111] could alleviate the limitations regarding non-linear amplification, while three-tone bipolar coding [60] could get rid of non-linear amplification and reduce the impact of the pump pulse depletion, but at the cost of a great increase in setup complexity. In any case, all the coding methods should consider the presented constraints in order to reach the most suitable sensor performance.

In addition, we have introduced an enhanced BOTDA sensor that combines a frequency modulated dual-probe wave configuration and mono-color cyclic coding. The probe dithering method serves to increase the effective Brillouin threshold of the leading fiber, and hence, the probe power that can reach the sensing fiber can still be sizable, leading to

an improvement of the SNR. Moreover, as explained before, the use of a dithered-probe waves makes the sensor more robust to the pump pulse depletion, so that higher pump and probe powers can be injected in the fiber. Therefore, the use of a dithered-probe wave alleviates the limitation caused by the cascade effect of the pump pulse depletion due to the interaction between the probe wave with multiple pulses. Thus, leading again to an enhancement of the SNR.

The capabilities of the technique have been analyzed by performing distributed temperature measurements over a 164 km loop length of fiber with high precision (3 MHz) and spatial resolution (1 m). After a correct adjustment of the sensor parameters, the effective code gain corresponding to the used code length (Lc = 79) is in good agreement with the theoretical value, thus proving the usefulness of the combined methods. To the best of our knowledge, this is the longest sensing distance achieved with a BOTDA sensor using mono-color cyclic coding.

Finally, with regard to the future, is of paramount importance to finish the study of the constraints of the coded pump wave BOTDA sensors. For that purpose, first, a study of the limitations that the pedestal depletion introduced in chapter 3 entails to coding methods should be made. In addition, in order to assess how each of the coding techniques is affected by these constraints, and hence, consider the advantages and disadvantages of the use of each of them, it would be highly interesting to conduct an exhaustive study of the performance of the different coding techniques presented to date. Second, it will be necessary to continue analyzing and studying different solutions to overcome these limitations and thus attain all the benefits of coding applied to BOTDA sensors. But, of course, trying not to increase the complexity and the final price of the sensor.

Chapter 6: Cost-effective Brillouin optical time-domain analysis sensor based in the use of a single optical source and passive optical filtering

Contents

6.1 Introduction

Brillouin optical time-domain analysis (BOTDA) sensors have proved their capability to perform distributed measurements of temperature and strain over large structures with high accuracy. That is why BOTDA sensors are particularly interesting for a large set of industrial sectors, including oil and gas pipeline monitoring, assessment of high voltage cables, railway inspection and many other structural health monitoring applications. In this context, as explained in previous chapters, significant number of research groups have focused their work on extending and improving the performance of BOTDA sensors, for instance, extending their sensing range to hundreds of kilometers [47, 116], improving their spatial resolution to centimeters [117, 118] or reducing the measurement time to perform dynamic measurements [119, 120].

In addition, as presented in chapters 2, 3 and 4, in order to improve the capabilities of the sensor, significant research work is focused on finding the physical origin of the several impairments that constrain the performance of BOTDA sensors. Among them, the several non-local effects studied in this thesis stand out. Another important limiting factor comes from the different non-linear effects, such as the onset of modulation instability (MI) [40] or self-phase modulation (SPM) [44]. As discussed in chapter 3, the extinction ratio (ER) of the pump pulses also results in an important limitation of the performance for the BOTDA sensor. All these has brought with it a great research effort focused on overcoming these constraints: to mitigate the effects of MI [42] to overcome the detrimental outcomes caused by non-local effects [92, 49, 96], or as introduced in chapter 3, to reduce the impairments caused by the limited ER pump pulse, among other important contributions.

Nevertheless, in many potential applications, the most important limitation for the widespread practical use of BOTDA sensors is their cost rather than their performance. This is because most BOTDA implementations, in order to generate the two optical waves involved in the technique, use expensive components such as lasers, multiple electro-optic modulators (EOMs), acousto-optic modulators or semiconductor optical amplifier (SOA)

switches. As a consequence, the final cost of the sensor is high, and hence, its real-world applicability is constrained, being usually bounded to industrial sectors where the cost of the sensor is not the main concern, such as in the field of oil and gas. Therefore, in recent years a new line of research in BOTDA sensors has emerged with the aim of simplifying the setups in order to achieve cost-efficient commercial systems that can compete with other less costly technologies such as, for instance, Raman sensors for temperature monitoring [121].

In this chapter, firstly, the main contributions aimed at finding cost-effective BOTDA solutions are presented and, then, in the next sections, we introduce an alternative configuration of the BOTDA sensor focused on reducing the potential cost of the sensor. This configuration seeks a simplification of the sensor by obtaining all the optical waves involved in the technique by passive optical filtering of the spectral components generated in a single optical source that is driven by a pulsed radio-frequency (RF) signal. This way the sensor obtains a further reduction of the used optical components, avoiding the need of any EOM or SOA in the setup, and hence, reaching a significant simplification of the setup, and consequently a reduction of the final cost of the analyzer.

6.2 A general overview of simplified and cost-efficient BOTDA sensors

As pointed out above, in the last years several contributions have been presented intended to simplify the different BOTDA configurations, and in this way obtain a reduction of the cost of the sensor. In the following some of the most noteworthy techniques are presented.

One early proposal is the use of a distributed Brillouin sensor system with offset locking technique [85]. In this method, in order to generate the probe and pump waves needed in BOTDA sensors, two distributed feedback (DFB) lasers are phase locked at the Brillouin frequency using a hardware proportional-integral-derivative controller. Specifically, in order to achieve the offset locking, this method uses the frequency stabilization technique by making use of a laser heterodyne source and an optical delay line. Therefore, using this offset locking with optical delay line method, fast and large tuning range measurements can be performed.

Another proposal is a simplified BOTDA sensor based on direct current modulation of a laser diode [86, 87]. The operation of the sensor is based on time-division pump-probe generation using direct modulation of a laser source, which reduces the number of components removing one SOA or one EOM from the conventional sensor scheme. Note that for this purpose, the sensor needs a delay fiber to generate a lag which controls the propagation of pump and probe waves. In addition, this method is free of expensive microwave generators, considering that the conventional frequency sweep between pump and probe waves is performed by a cost-effective arbitrary function generator. Thus, this simplified sensor reduces the optical and electrical devices and, hence, obtains a reduction of the cost of the sensor.

Another simplified alternative is a cost-effective method for fast-BOTDA sensors [122]. The aim of this technique is to retrieve the full Brillouin gain spectrum (BGS) at high speed, which in turn leads to fast BOTDA measurements. To that end, the method employs a frequency swept microwave source for the generation of the probe wave, so that the entire BOTDA measurement is taken within the duration of the frequency sweep itself. Therefore, by properly setting the duration of the sweep, the repetition rate of the pump pulses and the number of averages, this technique allows truly distributed and dynamic measurements of the BGS using a set-up at a fraction of the cost and complexity of the previously reported fast-BOTDA methods.

Finally, one of the latest techniques to simplify the setup is the BOTDA sensor with a pump-probe source based on Brillouin ring laser (BRL) technology [88]. In a BRL scheme, the probe wave is generated through stimulated Brillouin scattering of the pump signal implemented through a recirculation loop employing a modified BRL. With this technology, the analyzer is capable of a tuning range of 200 MHz without using phase-locked loop or optical sideband generation techniques. Therefore, this method is an efficient alternative to the commonly employed techniques based on phase-locked loop or optical sideband generation methods in BOTDA sensors.

6.3 Fundamentals of the technique

In this section the theoretical foundations of a novel cost-effective BOTDA sensor that was devised in this thesis are presented. The basic principle of the proposed sensor setup is schematically described in Fig. 6.1. The first step is to drive an optical source with a pulsed RF signal in order to generate an optical signal comprising a carrier and two pulsed-modulated sidebands. Both the continuous wave (CW) probe and the pulsed pump wave required in the BOTDA sensor, are derived from this modulated optical signal: the optical carrier of the modulation will act as the CW probe, whereas one of the pulsed sidebands of the modulated signal will act as the pump wave. For that purpose, a simple passive filtering is used to separate this signal into both waves, as it is described below. In this way, the two optical waves required in the BOTDA sensor are generated by a single optical source, while in a conventional scheme three optical devices are commonly deployed.

Once the modulated signal is generated, the output of the optical source is directed to the upper branch of the setup using a circulator. Here, the signal encounters an optical filter, which is tuned in such a way that one of the two pulsed sidebands of the modulation goes through it, whereas the optical carrier is reflected backwards, returning to the circulator, where it is redirected into the fiber under test (FUT). As will be explained below, the filtering process is critical in this sensor.

Simultaneously, the pulsed sideband in the upper branch is injected from the other end of the fiber using a second circulator. In this way, both signals counterpropagate in the fiber, where Brillouin interaction between both waves takes place. The frequency of the microwave oscillator used to generate the pulsed RF signal is selected to be close to the Brillouin frequency shift (BFS) of the fiber. As a result, the interaction between the pump pulse and the probe wave induces Brillouin gain/loss on the optical carrier. Afterward, the

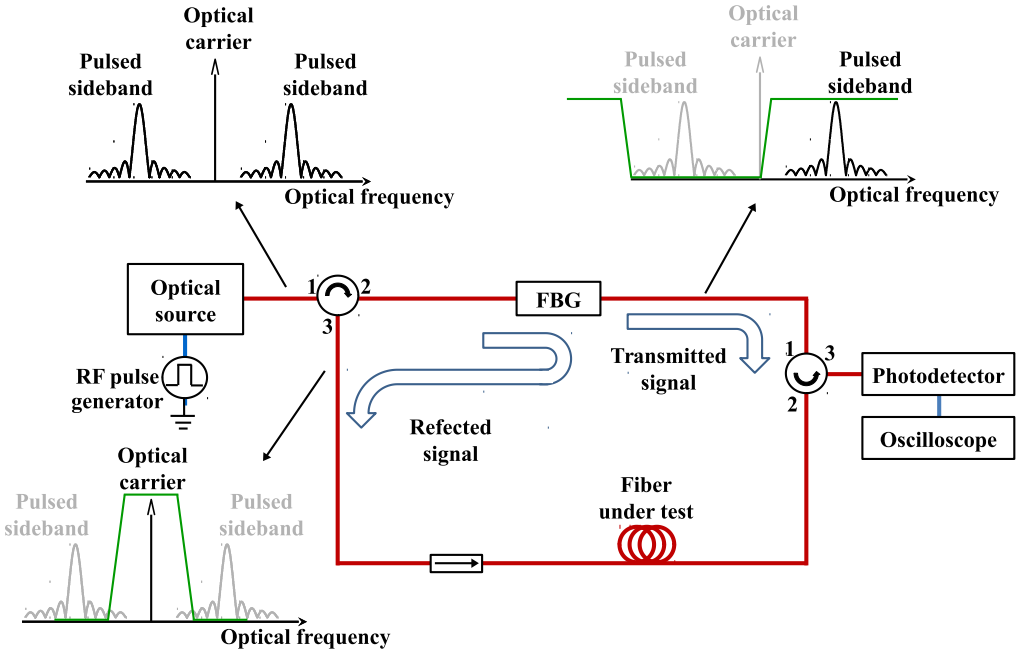

Figure 6.1: *Schematic representation of the fundamentals of the technique. The spectra of the signals involved in the setup (black and grey) and the filter response (green) are sketched in the figure. Note that the pulsed nature of the sidebands of the modulation is graphically represented by a sync spectrum.*

resultant probe wave is directed to a baseband photo-receiver and the detected electrical signal is captured in a digital oscilloscope. Finally, the measurement is repeated as the modulation frequency is swept, so that the Brillouin gain/loss spectrum (BGS/BLS) of the fiber can be reconstructed.

For the optical source, the best option is to deploy a DFB laser monolithically integrated with an electro-absorption modulator (EAM). The use of such externally-modulated laser (EML) compact device, typically in the form of a transmitter optical sub-assembly (TOSA), has become a standard in optical communications. There are Multi-source Agreement within the industry that have dramatically brought down the cost of these devices in the market. Therefore, we can use in the technique an EML TOSA designed for 10Gb/s operation and generate all the necessary optical waves at a cost comparable to that of a single DFB laser source. This implies a significant reduction in the cost of the BOTDA sensor.

6.4 Experimental setup and measurements

In order to analyze the capabilities of the proposed technique, the experimental setup depicted in Fig. 6.2 was assembled. The optical source was a 1551.7 nm DFB laser source followed by an integrated EAM. The modulator was driven by high ER RF pulses obtained using a microwave oscillator followed by a microwave switch, which was driven by a pulse generator. In this way, the RF pulse shape is directly translated to the optical domain by the modulator [45]. Low cost commercial microwave switches are available with extremely

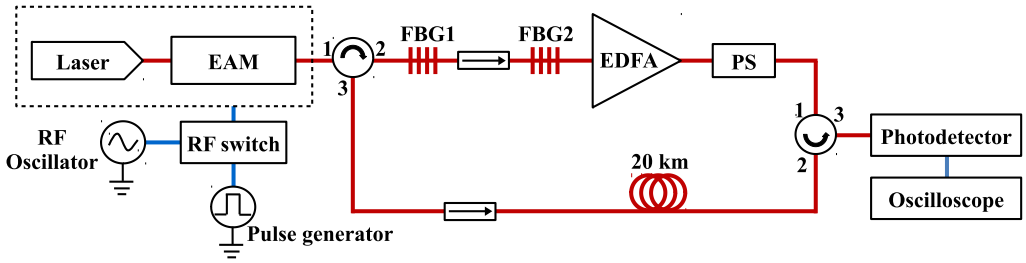

Figure 6.2: *Experimental setup for the cost-efficient BOTDA sensor based on RF-pulsed optical double-sideband modulation and passive optical filtering.*

high isolation and very fast responses. As a result, in this BOTDA setup it is possible to obtain inexpensive and fast optical pulses (below 1 ns rise-time) with an extremely high ER ($> 60dB$) [45]. In chapter 3, we have discussed the importance of having such a large ER pump pulse to avoid several detrimental effects. Figure 6.3 shows the temporal shape of the obtained optical pulse, where the fast response of the pulse is observed. Note that pulses with less steep leading and trailing edges are prone to the deleterious effects of SPM, which has been shown to degrade the BOTDA sensor performance [44].

It is worth mentioning that the amplitude of the pulses changes slightly at different frequencies due to the small power differences in the frequency response of the microwave generator and the microwave switch. However, this effect can be easily characterized and compensated in the measurements results, or even in the process of generating the pulsed optical signal.

Once the modulated optical wave was generated, the output of the optical source was directed using a circulator to the upper branch of the setup, where it was filtered employing two narrow-band fiber Bragg gratings (FBG). Figure 6.4(a) shows the optical spectrum obtained at the output of the optical EML source and the transfer function of both filters. The first FBG was tuned so that the CW optical carrier is reflected, while the pulsed sidebands of the modulation are transmitted. Then, the reflected optical carrier, which acts as the probe wave, was injected into the sensing fiber through an optical isolator, where the probe power was set to -10 dBm. This probe power was found to be the largest optical power for which non-local effects were negligible. The second FBG was tuned

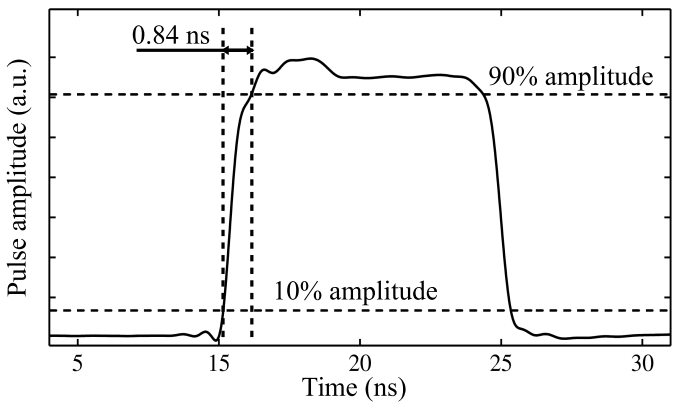

Figure 6.3: *Obtained optical pump pulse at the beginning of the fiber at* $f = 10830$ *MHz.*

so that the pulsed upper sideband of the modulation was transmitted, while the other sideband and the remains of the CW optical carrier were reflected, so that a gain-based BOTDA sensor was arranged. Nevertheless, the technique can also be applied to loss-based BOTDA sensors, by simply selecting the lower pulsed sideband of the modulation instead of the upper one.

In the upper branch of the setup, the pulsed pump wave at the output of the second FBG was amplified with an erbium-doped fiber amplifier (EDFA) to a peak power of 20 dBm. A level close to the limit before MI becomes significant [37]. Before being launched into the sensing fiber, the polarization of the pulsed pump wave was randomized with a polarization scrambler (PS), so as to reduce the polarization-mismatching-induced fluctuations on the signal. Note that instead of using a polarization scrambler, a polarization switch or a passive polarization scrambler [123] could be deployed to further reduce the final cost of the sensor setup. Finally, after interaction with the pump pulse along the fiber, the probe wave was detected in a 125-MHz photo-receiver and captured in a digitizer.

It should be pointed out that the optical filtering deployed in the setup is not ideal; hence, there will always be some degree of crosstalk between the generated optical waves in both branches of the setup. This is highlighted in Fig. 6.4(b), where the optical spectrum

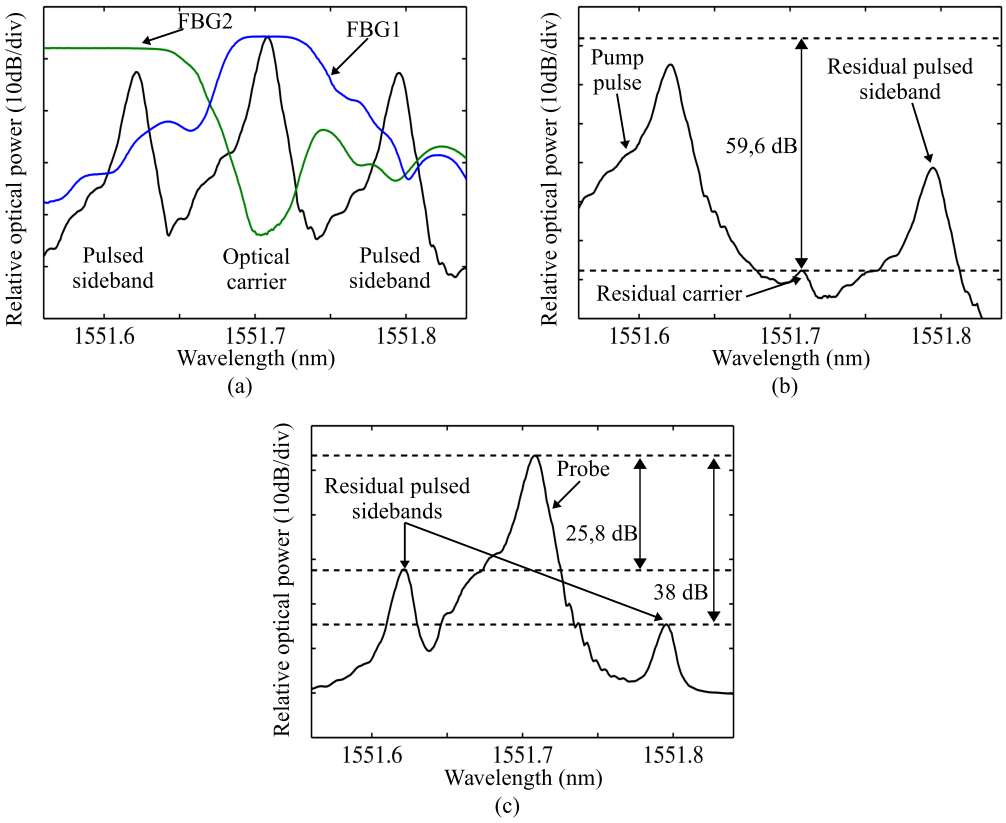

Figure 6.4: *Optical spectrum of the optical signal at $f = 10830$ MHz (measured BFS of the fiber) in different positions of the setup (black) (a) at the output of the DFB-EAM module, alongside the transfer function of the FBG1 (blue) and FBG2 (green), (b) at the input of the EDFA in the upper branch of the setup, and (c) at the beginning of the fiber in the lower branch of the setup.*

of the pump pulse in the upper branch of the setup after being filtered and amplified is shown. Note that it is possible to see residuals of the optical carrier and also of the other pulsed sideband alongside the desired optical component. Although at a significantly lower optical power level. Moreover, Fig. 6.4(c) shows the optical spectrum of the probe wave at the lower branch of the setup at the beginning of the FUT, where not only appears the probe wave, but also residuals of the pulsed spectral components. As will be discussed later, these residual signals impair the performance of the sensor.

6.4.1 Experimental results of the technique

In order to analyze the performance of the presented BOTDA sensor, distributed temperature measurements were performed over a roughly 20-km length of standard single-mode (ITU G.652) fiber. The final 30-m of the fiber were placed loose in a climatic chamber at constant controlled temperature, while the rest was held at room temperature in a spool. The pulse duration was set to 10 ns, corresponding to approximately 1-m resolution. The modulation frequency was swept at 2 MHz steps and 4096 averages were used to obtain the final BOTDA traces.

Figure 6.5(a) depicts the calculated BGS at the heated section of the fiber, i.e., at the far end of the fiber, together with the corresponding fitting curve. The BFS along the sensing fiber was calculated by performing a mathematical fit to a Voigt profile on the measured Brillouin gain spectra. In this measurement, the section of the fiber placed inside the climatic chamber was also maintained at room temperature, with a BFS close to 10830 MHz. In addition, the measured Brillouin full-width at half maximum linewidth was measured to be $\sim$ 100 MHz, which is close to the expected value for a pulse duration of 10 ns [32].

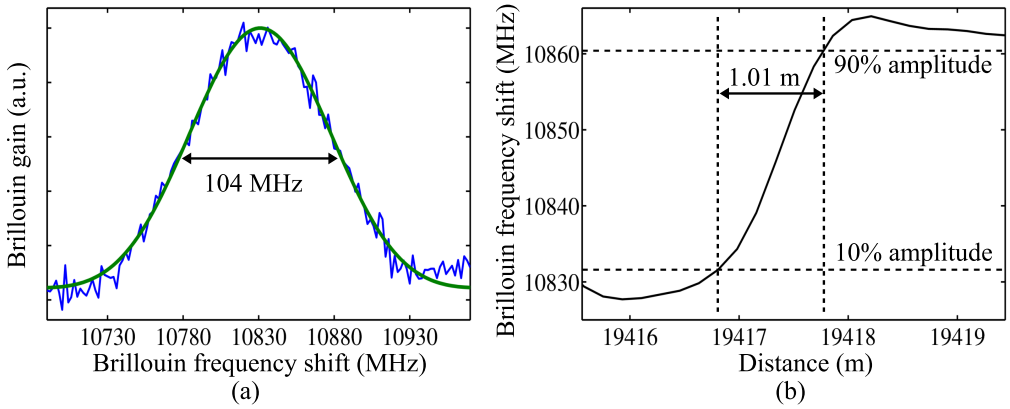

Figure 6.5: *(a) Measured BGS at the far end of the sensing fiber (blue) and its Voigt fitting curve (green). (b) Normalized amplitude of the detected signal at the transition between the heated and the room temperature sections of the fiber.*

The spatial resolution of the sensor was confirmed to be 1 m by measuring the rise time between two adjacent sections of the fiber at different temperatures. For that purpose, the fiber at the hotspot was heated to a temperature of 60°C, while the rest of the fiber was kept at room temperature. This is shown in Fig. 6.5(b), where the rise time equivalent

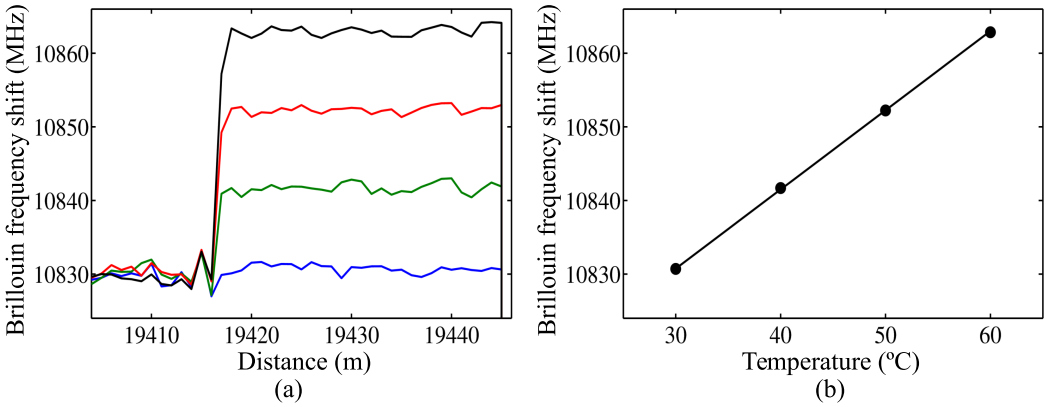

Figure 6.6: *(a) Calculated BFS as a function of distance at the final locations of the fiber, as the temperature is raised in the climatic chamber in 10 °C steps. (b) Calculated BFS as a function of temperature in the climatic chamber (symbols) and linear regression (solid line).*

length, in meters, for the transition between the heated and the room temperature sections of the fiber was calculated.

Also, the temperature of the climatic chamber (hotspot) was modified in order to evaluate the performance of the sensor. Figure 6.6(a) depicts the evolution of the measured BFS at the end of the fiber for different temperatures. The 30-m section corresponding to the hot spot is clearly visible and a fast transition between the heated section and the rest of the fiber is also observed. As it was expected, the measured BFS of the heated section increases in frequency as the temperature is risen. The relation between temperature and BFS in the fiber is depicted in Fig. 6.6(b), where a linear regression is performed to obtain a temperature coefficient of 1.0756 MHz/°C.

Finally, in order to evaluate the measurement precision of the analyzer, a series of 10 consecutive measurements for stable temperature conditions were performed. For that purpose, the final 2.5 km of fiber were placed in the climatic chamber. Figure 6.7 highlights the precision along the last kilometers of the sensing fiber, which was calculated from the standard deviation of those measurements at each location. From these measurements,

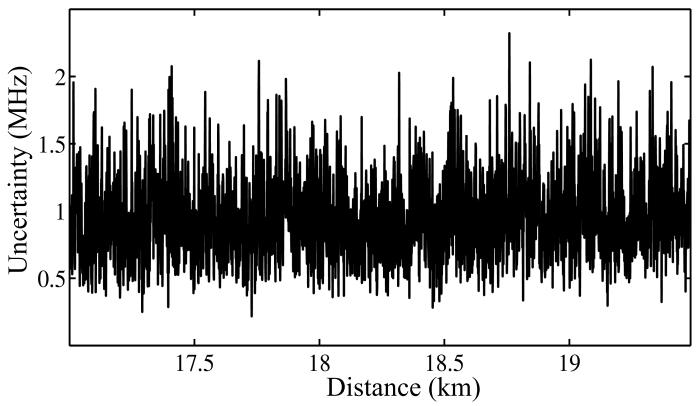

Figure 6.7: *BFS uncertainty (2σ) obtained by the technique in the last 2.5-km.*

the 2-sigma BFS measurement precision at the worst-contrast position was found to be 0.95-MHz. Furthermore, based on the obtained results, the figure-of-merit (FoM) of this BOTDA setup was calculated [32], obtaining a value of 1.1. This FoM turns out to be of the same order of more complex BOTDA setups that deploy several EOMs or SOAs to generate the required optical waves [32].

6.5 Limitations of the simplified-BOTDA technique

In this section the main factors that limit the performance of this simplified-BOTDA setup are discussed. Particularly those associated to the crosstalk between the optical signals in both sensor branches that were introduced in section 6.4.

Figure 6.8 highlights the detrimental effect caused by the residuals of the pulsed sidebands present in the probe wave (Fig. 6.4(c)) upon the measured BOTDA trace. Note that there is an abrupt loss of signal in the middle of the fiber. This effect was found to be originated by the residuals of the pulsed sidebands traveling along the fiber in the direction of the probe wave. As it was previously mentioned, the remains of the pulses that are not completely suppressed by the FBG were transmitted alongside the probe wave in the fiber. Therefore, the arrival of this pulse at the output of the fiber saturates the photo-receiver amplifier invalidating the measurement until it returns to a stable condition after the pulse passes. The inset of Fig. 6.8 expands the signal-loss area and, as it can be seen, for a time duration equivalent to an approximately 60-m the measurement is corrupted.

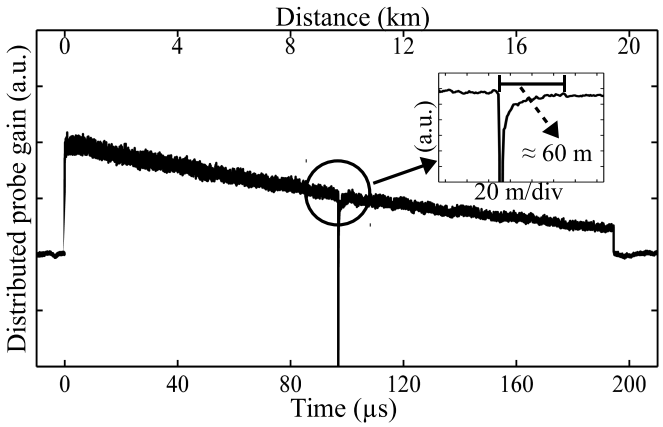

Figure 6.8: *BOTDA trace at BFS of the fiber (f = 10830 MHz) for the 20-km fiber with the corrupted middle section of the fiber in a zoomed area.*

In any case, this constraint is not really serious because it can be overcome in a number of ways, depending on the measurement configuration that is deployed. An obvious solution would be to enhance the optical filtering process to increase the unwanted components suppression in the probe wave. However, there are practical limits for this approach. On the other hand, BOTDA sensors typically use a loop configurations, e.g., when monitoring a pipeline, in which there is a leading fiber, used to bring the probe wave to the middle of the loop where the sensing fiber starts. Therefore, in this case the problem is solved altogether, because the corrupted measurement span would be outside the sensing fiber.

Nevertheless, if we are interested in measuring along the full fiber length, this fact could be taken into account when the fiber is installed in the structure that is going to be monitored by simply installing an extra length of fiber (60 meters) in the middle section. So the measurement impairment is completely overcome.

The other significant limitation that was studied comes from the residuals of the optical carrier on the pump pulse wave (see Fig. 6.4(b)). This residual carrier propagates along the fiber with the pump pulse, generating a Rayleigh backscattered (RB) signal that reaches the receiver together with the probe wave, which has identical wavelength; thus leading to interference and noise. This is an extra-noise that is added to the conventional noise sources in BOTDA sensors: the thermal, shot noise sources and the relative intensity noise coming from the laser source [9]. This extra-noise can be quantified by considering the total optical field that reaches the photo-receiver, which can be approximated by:

$$E(t) = E_S e^{(2\pi\jmath\nu_S t+\phi_S)} + E_{RB} e^{(2\pi\jmath\nu_{RB} t+\phi_{RB})} \tag{6.1}$$

where E_S and E_{RB} are the amplitude of the probe wave and RB components, respectively, ν_S and ν_{RB} are the optical frequency of probe and RB waves and ϕ_S and ϕ_{RB} are the phases of the probe wave and the RB.

The total intensity (optical power) detected at the photo-receiver includes a noise term generated by the RB beating with the probe wave, which can be written as:

$$I(t)\Big|_{RB-S} = 2E_S E_{RB}\cos(2\pi\Delta\nu t + \Delta\Phi) \tag{6.2}$$

where $\Delta\nu = \Delta\nu_{RB} - \Delta\nu_{Pr}$ is the frequency detuning between probe and RB waves and $\Delta\Phi$ is the phase difference between probe and RB, which can be assumed to be a random variable with uniform distribution between -π and π. This is a stationary random process, whose autocorrelation function is [124]:

$$R(\tau) = 2P_S P_{RB}\cos(2\pi\Delta\nu\tau) \tag{6.3}$$

where P_S and P_{RB} are the probe power and RB power at the receiver respectively. As Eq. (6.2) is a random process with zero mean, the standard deviation of the RB-probe beating noise can be calculated as:

$$\sigma_{RB-S} = \sqrt{R(0)} = \sqrt{2P_S P_{RB}} \tag{6.4}$$

Therefore, the total noise power at the photo-receiver output can be expressed as follow:

$$\sigma_T^2 = \sigma_{th}^2 + \sigma_{sh}^2 + \sigma_{RB-S}^2 \tag{6.5}$$

where σ_{th}^2 and σ_{sh}^2 are the variance of the thermal and shot noise at the photo-receiver, respectively, and σ_{RB}^2 is the noise variance calculated using Eq. (6.4), induced by the Rayleigh backscattering beating with the probe wave. Note that other noises have been neglected in this expression because they tend to be much less significant.

In order to estimate the impact of the RB-probe beating noise in the sensor, the optical

powers of the probe wave and RB arriving at the photo-receiver were measured, giving values of -14 dBm and -70 dBm, respectively. Applying Eq. (6.4) to these experimentally obtained results, and using the value of the responsivity of the photo-receiver, a value of 3.6-mV for the standard deviation of the RB-probe beating noise was obtained.

This value was double-checked using Eq. (6.5). To this end, first of all, the total noise at the receiver was measured with the EDFA in the upper branch turned off (without pump wave in the fiber), giving a standard deviation of noise (thermal and shot) of 2.6 mV. Afterward, the EDFA was turned on and the total standard deviation of noise was measured again, with a value in this case of 4.9 mV. By using Eq. (6.5), these results translate to an added noise with standard deviation of 4.1 mV. This agrees well with the calculated value using the model in Eqs. (6.1) to (6.4). Therefore, it is confirmed that the main constraint regarding the noise of the system is originated by the residual of the optical carrier in the pump pulse wave, which introduces a 5.5-dB penalty in the signal-to-noise ratio (SNR) of the detected sensor response.

From Eq. (6.4) it follows that the total noise added by RB is directly proportional to the optical carrier suppression. Therefore, in order to enhance the detected SNR, one option would be to apply more filtering, for instance, adding other FBG in the upper branch of the setup to improve the optical carrier suppression. As an example, adding 10-dB additional suppression to the carrier, which is relatively simple to achieve, would reduce the SNR penalty to less than a decibel.

6.6 Conclusions

In this chapter we have presented another line of research in BOTDA sensors, which is focused on reducing the cost of the sensor by simplifying the configuration and/or reducing the cost of the used devices. In addition, a novel simplified-BOTDA sensor based on passive optical filtering of the spectral components generated in a single RF-pulsed optical source have been introduced and demonstrated. The aim of the proposed scheme is to simplify the setup by reducing the number of the optical components required to implement the sensor. Specifically, as the pump and probe waves are implemented by a single optical source, the sensor does not need any EOM or SOA, so that the optical components are significantly reduced. Note that in a conventional BOTDA system two EOM or one EOM and a SOA are commonly used to generate both optical waves, therefore, this simplified-BOTDA sensor removes two optical devices from the configuration. In this way, the cost of the sensor is reduced and, therefore, it becomes a cost-effective alternative to conventional BOTDA configurations.

The capabilities of the presented technique have been analyzed performing distributed temperature measurements over a 20 km length of fiber. These measurements have shown high precision and resolution, so that it has been proved that this BOTDA sensor presents a performance comparable to more complex setups. Therefore, for scenarios in which the price of the sensor is a major limitation, it is an interesting alternative to other analyzers usually cheaper than BOTDA sensors. This is of great importance when it comes to creating real practical applications of BOTDA sensors, since most of the structures that

require a structural health monitoring are not as large as for instance gas pipelines. This is the case of many applications to measure the deformation of the structure in geotechnical and civil engineering, as for instance the deformation of bridges, tunnels or PVC pipes [125]. So, in these scenarios, the most important feature of the sensor is not the possibility of measuring hundreds of kilometers. On the contrary, what they need is a robust and a cost-effective solution.

In addition, the factors that limit the performance of the presented BOTDA sensor have been studied and the way to overcome them outlined. We have shown that the most important constraint of the technique is due to the optical residuals presented in both the probe and the pump waves. These optical residuals are generated in the filtering process of the output signal of the optical source. Therefore, an easy way to overcome or at least mitigate the influence of these optical residuals on the performance of the sensor is to enhance the selectivity of the filters. However, it is worth mentioning that this technique cannot be applied in a dual-probe BOTDA sensor, which is a configuration that has been shown to alleviate the onset of the pulse depletion [92], and hence, allows to increase the optical probe power and in consequence improves the SNR in detection.

Finally, given the importance of getting cost-efficient BOTDA sensors, future research work will focus on improving the performance of the presented BOTDA sensor, as well as in further simplifying its implementation. In addition, a research work focused on finding other simplified configurations of the sensor will be carried out, so that BOTDA sensors can reach applications and industries from which they are now excluded because of cost concerns.

Chapter 7: Conclusions and future research

Contents

7.1 Conclusions

This section summarizes the conclusions derived from the work performed during this thesis dissertation. The conclusions are grouped according to the specific research topic.

Non-local effects

In this thesis work we have carried out an exhaustive analysis of non-local effects (NLE) in Brillouin optical time-domain analysis (BOTDA) sensors. To begin with, we have introduced the theoretical explanation of the pump pulse depletion and the frequency-dependant spectral deformation of the pulses, the so-called first-order and second-order NLE, respectively [31, 33]. These effects have been shown to degrade the precision of the sensor response. Indeed, the different BOTDA sensor schemes are severely affected by the pump pulse depletion, so that the probe wave optical power that can be deployed is constrained. In this way, due to the onset of first-order NLE, the use of a single-probe configuration in long-range BOTDA sensors is restricted as a function of the maximum tolerable error. Dual-probe BOTDA setups significantly alleviate this issue, enabling the use of a higher probe power. However, they are still prone to second-order NLE that distort the pulse spectrum and constrain the probe power to well below the theoretical limit set by the Brillouin threshold of the fiber. Therefore, NLE limit the optical power that can be deployed in the sensing fiber, and hence, the signal-to-noise ratio (SNR) in detection is worsen.

Then, we have contributed in this thesis with a series of findings related to NLE. First, the impairments related to the limited extinction ratio (ER) of the pump wave have been analyzed. We have shown that even the dual-probe BOTDA sensor performance is still seriously compromised when pump pulses with limited ER are deployed because, the pump pulse depletion is increased. Furthermore, the limited ER of the pump wave in BOTDA sensors leads to a previously unknown non-local effect, which is due to the pump pedestal depletion. This effect, originated in the extra depletion of the trailing pedestal of the pump wave, introduces a similar measurement error to that introduced by the depletion of the pulse. For instance, it is found that, in a conventional dual-probe BOTDA setup with 1-m spatial resolution, an ER$>$32 dB is needed to have less than 1-MHz Brillouin frequency shift (BFS) measurement error. Furthermore, if a technique for mitigation of second-order NLE is deployed, an ER greater than 43 dB would be required.

Such a large ER is typically just within the reach of semiconductor optical amplifier (SOA) switches or acousto-optic modulators (AOM). However, both devices have rise and

fall times that are typically of the order of 1 ns for SOAs and longer for AOMs, which compromise the capability to perform high-spatial-resolution measurements using, for instance, the differential pulse-width pair technique. Furthermore, pulses with less steep leading and trailing edges are prone to self-phase modulation, which has been shown to severely constrain the performance of the BOTDA sensor. Therefore, in order to generate the sharp pulses that are needed for high-spatial-resolution measurements using the differential pulse-width pair technique, a Mach-Zehnder electro-optic modulator (MZ-EOM) is required. However, MZ-EOMs usually have low ER, typically between 20 to 30 dB, which would not comply with the rigid condition for the ER stated above. Note that two cascaded MZ-EOMs could be used in order to keep the fast response with an improved ER, but at the expense of an added setup complexity and an increased cost of the sensor.

In addition, another impairment caused by the limited ER of the pulses has been found. This limitation comes from the pedestal distortion induced by the transient response of the erbium-doped fiber amplifiers (EDFA), which are typically deployed to amplify the pump wave. This detrimental effect has similar characteristics to those induced by the pedestal depletion. Depending on the particular EDFA device used to amplify the pump pulse wave, the distortion due to the EDFA transient can be even more important than the one introduced by the depletion of the pedestal. Note that the limitation that this effect impose is independent of the probe wave power deployed; hence, they set an upper bound to the BOTDA sensor performance.

We also found that all the currently available second-order NLE compensation methods are only valid in case the BFS of the sensing fiber is fairly uniform. This is an important limitation that restricts real world applications of long-range BOTDA sensors, considering that in real-world field-application scenarios a variety of fibers with different BFS and subjected to different environmental conditions are typically deployed. We have demonstrated that, indeed, this is an important limiting factor of the sensor by developing a theoretical model for the pump pulse distortion due to the interaction with the probe waves, which was verified by experimental measurements.

Finally, another important consideration concerning NLE is the limitation that the depletion of the pulse entails to coding techniques. In this thesis, we have demonstrated that the use of mono-color cyclic coding is clearly limited in BOTDA sensors due to the depletion of the pulse. This is due to the fact that the successive pulses of a sequence interact with a probe wave that has been amplified by the previous pulses of the sequence, and therefore, the depletion of the pulse is greater. In addition, we have shown that even a dual-probe BOTDA sensor is still limited by this impairment.

In summary, we have presented two previously unknown NLE, as well as some extra limitations of first-order and second-order NLE. These effects are amongst the main constraints on the performance of BOTDA sensors, considering that their onset limits the optical probe power, and hence, worsens the SNR of the detected probe wave. Therefore, it is of paramount importance to find solutions to these constraints.

Probe-dithering to overcome non-local effects

In this thesis we have demonstrated the capabilities of the probe-dithering technique to overcome the various NLE. This technique was devised by our research group. Previous works have demonstrated that this technique is able to overcome first-order and second-order NLE. In addition, its use allows BOTDA configurations to deploy a probe wave power above the Brillouin threshold of the fiber. Therefore, the technique allows to introduce a higher probe wave power, and hence, the SNR at the receiver is enhanced.

In this thesis work, we have demonstrated that this technique also alleviates all the impairments brought by the limited ER pump pulses. The experimental results show how this technique gets rid of the pedestal depletion and also greatly ameliorate the impairments of the EDFA transient response. It is worth mentioning that in order to do that, it is mandatory not only to modulate in frequency the probe wave but also the pump wave. Otherwise, the pulse pedestal would be composed of a single frequency, and hence, the Brillouin interaction with each probe wavefront of a frequency detuning equal to the BFS of the fiber would be exactly the same than in a conventional BOTDA sensor. This, in turn, would increase the quantization noise, and reproduce the same impairments due to the EDFA transient response than in a conventional BOTDA setup. However, the constraints generated by both the depletion of the pulse and the pedestal depletion would be clearly improved.

Additionally, we have presented a new technique that makes BOTDA sensors to completely compensate second-order NLE: the BFS tracking technique. This is based on adding an optical frequency modulation to the probe wave so as to track the variations in average BFS found along the fiber. In this way, the probe wave power limitation is the effective Brillouin threshold of the sensing fiber. However, the probe-dithering technique pushes this limit to higher powers than in standard BOTDA setups. Therefore, by combining the tracking technique with the probe-dithering, we have proved that it is possible to deploy a probe wave up to 15 dBm, which, to the best of our knowledge, is the largest probe power injected in a long-range BOTDA setup.

Finally, to the best of our knowledge, the probe-dithering technique is the only approach that can mitigate all known NLE in BOTDA sensors. In addition, this technique also overtakes the Brillouin threshold limit of the fiber. This, in turn, allows the use of a higher probe wave power levels, and hence, the SNR at the receiver is enhanced. The improvement in the detected SNR brought by the use of such power leads to an excellent sensor performance without resorting to additional means such as the use of pump pulse coding or Raman gain. In summary, the probe-dithering technique has been shown to be an important contribution to long-range BOTDA sensors and a simple solution to the impairments brought by BOTDA sensors that deploy MZ-EOMs to shape the pulses.

Coding techniques in BOTDA sensors

In this thesis, we have made two substantial contributions to the development of coded pump wave BOTDA sensors. On the one hand, we have presented a study on the practical limitations on the probe and pump power in BOTDA sensors that uses a coding technique.

To carry out the experimental study of these limitations we have used a mono-color cyclic coding technique. On the other hand, we have introduced an enhanced BOTDA sensor that combines the mono-color cyclic coding and the probe-dithering techniques.

We have theoretically and experimentally demonstrated that the optical power of the probe and pump waves is limited by three factors: the power fluctuations of the pulse sequences, the onset of pump pulse depletion and the non-linear amplification of the probe wave. Due to these impairments, in order to avoid errors in the decoded signal when using a coding technique in BOTDA sensors, there is a trade-off between the maximum pump and probe powers that can be injected in the fiber, the code length, the pump pulse duration and the fiber length. Note that the use of coding techniques to enhance the SNR is limited to cases in which the obtained coding gain has a real benefit in the measurement in comparison with a single-pulse configuration. That is to say, if to properly decode the signal it is mandatory to reduce the pump and/or the probe optical power, which in turn entails a reduction of the effective SNR, the use of the coding technique ceases to be useful. Based on these considerations, we can argue that mono-color cyclic coding is really more useful in long-range loop configurations, considering that the probe wave power at the input of the sensing fiber is reduced in this configuration, and hence, the studied limitations are less significant.

It is important to point out that the different coding techniques presented so far in the literature are affected differently by the presented limitations. For instance, color coding could alleviate the limitations regarding non-linear amplification, while the three-tone bipolar coding technique could get rid of non-linear amplification and reduce the impact of the pump pulse depletion, but at the cost of a great increase in setup complexity. In any case, all the coding techniques must consider the presented limitations in order to improve the sensor performance.

In addition, we have introduced an enhanced BOTDA sensor that combines mono-color cyclic coding and a frequency modulated dual-probe wave configuration. Both techniques, probe-dithering and mono-color cyclic coding, improve the SNR. Therefore, by combining both methods it is possible to measure long distances. Note that, the dithering of the probe waves alleviates the onset of the pulse depletion, and hence, a larger code length can be deployed. The capabilities of the technique have been analyzed by performing distributed temperature measurements over a 164 km loop length of fiber with high precision (3 MHz) and spatial resolution (1 m). To the best of our knowledge, this is the longest sensing distance demonstrated with a BOTDA sensor using mono-color cyclic coding.

Simplification of the BOTDA sensor

Another line of research in BOTDA sensors is focused on reducing the cost of the sensor by simplifying its configuration. In this thesis we have presented a novel simplified-BOTDA sensor based on passive optical filtering of the spectral components generated in a single optical source. In this way, the number of the optical components required to implement the sensor are reduced. Specifically, the sensor removes one or two optical devices compared to other BOTDA setups. Therefore, the cost of the sensor can be reduced and, consequently,

it becomes a cost-effective alternative to conventional BOTDA configurations.

The capabilities of the sensor were analyzed performing distributed temperature measurements over a 20 km length of fiber, showing a performance comparable to more complex setups. In addition, the factors that limit the performance of the simplified BOTDA sensor was studied and the way to overcome them outlined. The most important limitation of the technique is due to the optical residuals presented in both the probe and the pump waves, which are generated in the filtering process of the output signal of the optical source. The way to overcome them has also been outlined.

Finally, it is worth mentioning that this technique cannot be applied in a dual-probe BOTDA sensor, which is the main disadvantage of the method. In any case, the great advantage of the sensor is the possibility to employ it in industrial sectors where the cost of the analyzer could be a problem.

7.2 Future research

The following lines present the resultant open research fields coming from the work performed during this thesis:

Non-local effects

As noted, NLE are amongst the most significant limitations in BOTDA sensors. In addition, the effects of the limited ER of the pump pulses have been shown to seriously impact the BOTDA sensor performance. Therefore, it is of paramount importance that future research work focuses on overcoming these effects, so that to improve the performance of the BOTDA sensor.

Apart from that, further research should be focused on investigating the significance of these effects in BOTDA systems deploying pump pulse coding. It is expected that the degradations imposed by the pedestal depletion will have a more pronounced impact in such systems than in a single-pulse configuration because of the use of large sequences of pulses. This may impose even stringer constraints on the ER of the pulses deployed. In addition, it should be checked whether the probe-dithering technique also improves the limitations of coding techniques with respect to the ER of the pump pulses. Thus, as with the pump pulse depletion, the pedestal depletion will also be ameliorated.

Coding techniques in BOTDA sensors

Future work in this line of research can be focused on three different branches. First, the study of the limitations of the coding techniques applied to BOTDA sensors should be completed. In addition, in order to assess how each of the coding techniques is affected by these limitations, and hence, consider the advantages and disadvantages of the use of each of them, it would be highly interesting to conduct an exhaustive study of the performance of the different coding techniques presented to date.

Second, it is necessary to continue analyzing and studying different solutions to overcome the limitations related to the use of coding techniques. Specifically those related to

the pump pulse depletion and to the non-linear amplification of the probe wave, which have been shown to severely degrade the sensor performance. In this way, longer code lengths could be used, so that the SNR of the sensor will be improve.

Finally, we should study the possibility of combining the probe-dithering technique with bipolar and color coding techniques. It is expected that the combination of these techniques could improve the sensor performance, and hence, longer distances could be monitored. This is due to the fact that both bipolar and color coding are less affected by the pump pulse depletion and the non-linear amplification of the probe, so that combined with the probe-dithering technique, which enables the use of a higher probe wave power, the SNR of the sensor could be enhanced.

Simplification of BOTDA setup

An important limitation in real applications of BOTDA sensors is the cost of the analyzer. Therefore, future work should focus on improving the performance of the sensor and further simplifying its implementation, so that BOTDA sensors can reach applications and industries from which they are now excluded because of cost concerns. In addition, due to the advantages of dual-probe BOTDA configurations, it is important to find simplified dual-probe BOTDA configurations.

Bibliography

[1] "Distributed fiber optic sensor/sensing (DFOS) market analysis by application (temperature sensing, acoustic/vibration sensing), by technology, by vertical, by region, and segment forecasts, 2018 - 2025," *Grand View Research, Inc*, no. GVR-1-68038-462-8, 2017.

[2] A. Barrias, J. Casas, and S. Villalba, "A review of distributed optical fiber sensors for civil engineering applications," *Sensors (Switzerland)*, vol. 16, no. 5, 2016.

[3] L. Schenato, "A review of distributed fibre optic sensors for geo-hydrological applications," *Applied Sciences (Switzerland)*, vol. 7, no. 9, 2017.

[4] L. Brillouin, "Diffusion de la Lumiere et des Rayonnes X par un Corps Transparent Homogene; Influence del'Agitation Thermique," *Annales des Physique*, vol. 9, no. 17, pp. 88–122, 1922.

[5] R. Boyd, *Nonlinear Optics*, 3rd ed. Academic Press, 2007.

[6] G. P. Agrawal, *Lightwave Technology: Components and Devices*. Wiley, 2004, vol. 1.

[7] L. Thévenaz, *Advanced Fiber Optics*. EPFL Press, 2011.

[8] T. Horiguchi, T. Kurashima, and M. Tateda, "Tensile strain dependence of Brillouin frequency shift in silica optical fibers," *IEEE Photonics Technology Letters*, vol. 1, no. 5, pp. 107–108, 1989.

[9] G. P. Agrawal, *Nonlinear Fiber Optics*, 5th ed. Academic Press, 2013.

[10] M. J. Damzen, V. I. Vlad, V. Babin, and A. Mocofanescu, *Stimulated Brillouin Scattering, Fundamentals and Applications*. Bristol and Philadelphia: Institute of Physics Publishing, 2003.

[11] T. P. Gill, *The Doppler effect: an introduction to the theory of the effect*. Logos Press, 1965.

[12] T. Kurashima, T. Horiguchi, and M. Tateda, "Thermal effects of Brillouin gain spectra in single-mode fibers," *IEEE Photonics Technology Letters*, vol. 2, no. 10, pp. 718–720, 1990.

[13] W. Zou, Z. He, and K. Hotate, "Investigation of Strain- and Temperature-Dependences of Brillouin Frequency Shifts in GeO_2 -Doped Optical Fibers," *Journal of Lightwave Technology*, vol. 26, no. 13, pp. 1854–1861, 2008.

[14] M. Nikles, L. Thevenaz, and P. A. Robert, "Brillouin gain spectrum characterization in single-mode optical fibers," *Journal of Lightwave Technology*, vol. 15, no. 10, pp. 1842–1851, 1997.

[15] K. Hotate, "Measurement of Brillouin gain spectrum distribution along an optical fiber using a correlation-based technique." *IEICE Transactions on Electronics*, vol. E83-C, no. 3, pp. 405–411, 2000.

[16] ——, "Recent achievements in BOCDA/BOCDR," *IEEE SENSORS 2014 Proceedings*, no. 6984953, pp. 142–145, 2014.

[17] K. Song, Z. He, and K. Hotate, "Distributed strain measurement with millimeterorder spatial resolution based on Brillouin optical correlation domain analysis," *Optics Letters*, vol. 31, no. 17, pp. 2526–2528, 2006.

[18] K. Song, M. Kishi, Z. He, and K. Hotate, "High-repetition-rate distributed Brillouin sensor based on optical correlation-domain analysis with differential frequency modulation," *Optics Letters*, vol. 36, no. 11, pp. 2062–2064, 2011.

[19] D. Garus, K. Krebber, F. Schliep, and T. Gogolla, "Distributed sensing technique based on Brillouin optical-fiber frequency-domain analysis," *Optics Letters*, vol. 21, no. 17, pp. 1402–1404, 1996.

[20] R. Bernini, A. Minardo, and L. Zeni, "Distributed sensing at centimeter-scale spatial resolution by BOFDA: Measurements and signal processing," *IEEE Photonics Journal*, vol. 4, no. 1, pp. 48–56, 2012.

[21] T. Horiguchi, K. Shimizu, T. Kurashima, M. Tateda, and Y. Koyamada, "Development of a Distributed Sensing Technique Using Brillouin Scattering," *Journal of Lightwave Technology*, vol. 13, no. 7, pp. 1296–1302, 1995.

[22] M. Alahbabi, Y. Cho, and T. Newson, "150-km-range distributed temperature sensor based on coherent detection of spontaneous Brillouin backscatter and in-line Raman amplification," *Journal of the Optical Society of America B: Optical Physics*, vol. 22, no. 6, pp. 1321–1324, 2005.

[23] Y. Zhang, X. Wu, Z. Ying, and X. Zhang, "Performance improvement for long-range BOTDR sensing system based on high extinction ratio modulator," *Electronics Letters*, vol. 50, no. 14, pp. 1014–1016, 2014.

[24] F. Wang, W. Zhan, X. Zhang, and Y. Lu, "Improvement of Spatial Resolution for BOTDR by Iterative Subdivision Method," *Journal of Lightwave Technology*, vol. 31, no. 23, pp. 3663–3667, 2013.

[25] Q. Li, J. Gan, Y. Wu, Z. Zhang, J. Li, and Z. Yang, "High Spatial Resolution BOTDR Based on Differential Brillouin Spectrum Technique," *IEEE Photonics Technology Letters*, vol. 28, no. 14, pp. 1493–1496, 2016.

[26] T. Kurashima, T. Horiguchi, and M. Tateda, "Distributed-temperature sensing using stimulated Brillouin scattering in optical silica fibers," *Optics Letters*, vol. 15, no. 18, pp. 1038–1040, 1990.

[27] T. Horiguchi, T. Kurashima, and M. Tateda, "Nondestructive measurement of optical fiber tensile strain distribution based on Brillouin spectroscopy," *Trans. IEICE*, vol. 73, no. 2, pp. 144–152, 1990.

[28] A. Minardo, G. Porcaro, D. Giannetta, R. Bernini, and L. Zeni, "Real-time monitoring of railway traffic using slope-assisted Brillouin distributed sensors," *Applied Optics*, vol. 52, no. 16, pp. 3770–3776, 2013.

[29] F. Ravet, E. Rochat, and M. Niklès, "BOTDA based DTS robustness demonstration for subsea structure monitoring applications," *Proceedings of SPIE*, vol. 9634, p. 96345Z, 2015.

[30] T. Horiguchi and M. Tateda, "BOTDA-nondestructive measurement of single-mode optical fiber attenuation characteristics using Brillouin interaction: theory," *Journal of Lightwave Technology*, vol. 7, no. 8, pp. 1170–1176, 1989.

[31] L. Thévenaz, S. F. Mafang, and J. Lin, "Effect of pulse depletion in a Brillouin optical time-domain analysis system," *Opt. Express*, vol. 21, no. 12, pp. 14 017–14 035, Jun 2013.

[32] M. A. Soto and L. Thévenaz, "Modeling and evaluating the performance of Brillouin distributed optical fiber sensors," *Opt. Express*, vol. 21, no. 25, pp. 31 347–31 366, Dec 2013.

[33] A. Dominguez-Lopez, X. Angulo-Vinuesa, A. Lopez-Gil, S. Martin-Lopez, and M. Gonzalez-Herraez, "Non-local effects in dual-probe-sideband Brillouin optical time domain analysis," *Opt. Express*, vol. 23, no. 8, pp. 10 341–10 352, Apr 2015.

[34] T. Shimizu, K. Nakajima, K. Shiraki, K. Ieda, and I. Sankawa, "Evaluation methods and requirements for the stimulated Brillouin scattering threshold in a single-mode fiber," *Optical Fiber Technology*, vol. 14, no. 1, pp. 10–15, 2008.

[35] T. Horiguchi, K. Shimizu, T. Kurashima, M. Tateda, and Y. Koyamada, "Development of a distributed sensing technique using Brillouin scattering," *J. Lightwave Technol.*, vol. 13, no. 7, pp. 1296–1302, Jul 1995.

[36] D. Asaf and H. Moshe, "Low-frequency transmitted intensity noise induced by stimulated Brillouin scattering in optical fibers," *Opt. Express*, vol. 19, no. 12, pp. 11 792–11 803, 2011.

[37] M. Alem, M. A. Soto, and L. Thévenaz, "Analytical model and experimental verification of the critical power for modulation instability in optical fibers," *Opt. Express*, vol. 23, no. 23, pp. 29 514–29 532, Nov 2015.

[38] D. Alasia, M. Herráez, L. Abrardi, S. López, and L. Thévenaz, "Detrimental effect of modulation instability on distributed optical fibre sensors using stimulated Brillouin scattering," *Proceedings of SPIE*, vol. 5855 PART II, pp. 587–590, 2005.

[39] S. Foaleng and L. Thévenaz, "Impact of Raman scattering and modulation instability on the performances of Brillouin sensors," *Proceedings of SPIE*, vol. 7753, p. 77539V, 2011.

[40] M. Alahbabi, Y. Cho, T. Newson, P. Wait, and A. Hartog, "Influence of modulation instability on distributed optical fiber sensors based on spontaneous Brillouin scattering," *Journal of the Optical Society of America B: Optical Physics*, vol. 21, no. 6, pp. 1156–1160, 2004.

[41] M. Soto, M. Alem, W. Chen, and L. Thévenaz, "Mitigating modulation instability in Brillouin distributed fibre sensors," *Proceedings of SPIE*, vol. 8794, p. 87943J, 2013.

[42] M. Alem, M. Soto, L. Thévenaz, J. Urricelqui, M. Sagues, and A. Loayssa, "Performance limit of two-pump Brillouin fiber sensors obtained by Manakov modulation instability," *2015 Spatiotemporal Complexity in Nonlinear Optics, SCNO 2015*, p. 7324006, 2015.

[43] Y. Dong and X. Bao, "High spatial resolution and long-distance BOTDA using differential Brillouin gain in a dispersion shifted fiber," *Proceedings of SPIE*, vol. 7503, p. 750384, 2009.

[44] S. M. Foaleng, F. Rodríguez-Barrios, S. Martin-Lopez, M. González-Herráez, and L. Thévenaz, "Detrimental effect of self-phase modulation on the performance of Brillouin distributed fiber sensors," *Opt. Lett.*, vol. 36, no. 2, pp. 97–99, Jan 2011.

[45] A. Zornoza, D. Olier, M. Sagues, and A. Loayssa, "Brillouin distributed sensor using RF shaping of pump pulses," *Measurement Science and Technology*, vol. 21, no. 9, 2010.

[46] J. Mompo, H. Iribas, J. Urricelqui, and A. Loayssa, "Second-Order Nonlocal Effects Mitigation in Brillouin Optical Time-Domain Analysis Sensors by Tracking the Brillouin Frequency Shift Profile of the Fiber," *IEEE Photonics Journal*, vol. 9, no. 5, 2017.

[47] S. L. Floch, F. Sauser, M. Llera, and E. Rochat, "Novel Brillouin Optical Time-Domain Analyzer for Extreme Sensing Range Using High-Power Flat Frequency-Coded Pump Pulses," *Journal of Lightwave Technology*, vol. 33, no. 12, pp. 2623–2627, June 2015.

[48] J. Urricelqui, M. Sagues, and A. Loayssa, "Synthesis of Brillouin frequency shift profiles to compensate non-local effects and Brillouin induced noise in BOTDA sensors," *Optics Express*, vol. 22, no. 15, pp. 18 195–18 202, 2014.

[49] R. Ruiz-Lombera, J. Urricelqui, M. Sagues, J. Mirapeix, J. M. López-Higuera, and A. Loayssa, "Overcoming Nonlocal Effects and Brillouin Threshold Limitations in Brillouin Optical Time-Domain Sensors," *IEEE Photonics Journal*, vol. 7, no. 6, pp. 1–9, Dec 2015.

[50] Y. Dong, L. Chen, and X. Bao, "Extending the Sensing Range of Brillouin Optical Time-Domain Analysis Combining Frequency-Division Multiplexing and In-Line EDFAs," *J. Lightwave Technol.*, vol. 30, no. 8, pp. 1161–1167, Apr 2012.

[51] S. Martin-Lopez, M. Alcon-Camas, F. Rodriguez, P. Corredera, J. Ania-Castañon, L. Thévenaz, and M. Gonzalez-Herraez, "Brillouin optical time-domain analysis assisted by second-order Raman amplification," *Optics Express*, vol. 18, no. 18, pp. 18 769–18 778, 2010.

[52] M. Soto, G. Bolognini, and F. Di Pasquale, "Optimization of long-range BOTDA sensors with high resolution using first-order bi-directional Raman amplification," *Optics Express*, vol. 19, no. 5, pp. 4444–4457, 2011.

[53] X. Angulo-Vinuesa, S. Martin-Lopez, J. N. no, P. Corredera, J. D. A.-C. non, L. Thévenaz, and M. González-Herráez, "Raman-Assisted Brillouin Distributed Temperature Sensor Over 100 km Featuring 2 m Resolution and 1.2 C Uncertainty," *J. Lightwave Technol.*, vol. 30, no. 8, pp. 1060–1065, Apr 2012.

[54] J. Urricelqui, M. Sagues, and A. Loayssa, "Brillouin optical time-domain analysis sensor assisted by Brillouin distributed amplification of pump pulses," *Opt. Express*, vol. 23, no. 23, pp. 30 448–30 458, Nov 2015.

[55] J. J. Mompó, J. Urricelqui, and A. Loayssa, "Brillouin optical time-domain analysis sensor with pump pulse amplification," *Opt. Express*, vol. 24, no. 12, pp. 12 672–12 681, Jun 2016.

[56] X.-H. Jia, H.-Q. Chang, L. Ao, X.-L. Ji, C. Xu, and W.-L. Zhang, "BOTDA sensors enhanced using high-efficiency second-order distributed Brillouin amplification," *Optics Express*, vol. 24, no. 13, pp. 14 079–14 085, 2016.

[57] A. Zornoza, M. Sagues, and A. Loayssa, "Self-heterodyne detection for SNR improvement and distributed phase-shift measurements in BOTDA," *Journal of Lightwave Technology*, vol. 30, no. 8, pp. 1066–1072, 2012.

[58] M. A. Soto, G. Bolognini, F. D. Pasquale, and L. Thévenaz, "Long-range Brillouin optical time-domain analysis sensor employing pulse coding techniques," *Measurement Science and Technology*, vol. 21, no. 9, p. 094024, 2010.

[59] M. Taki, Y. Muanenda, C. J. Oton, T. Nannipieri, A. Signorini, and F. D. Pasquale, "Cyclic pulse coding for fast BOTDA fiber sensors," *Opt. Lett.*, vol. 38, no. 15, pp. 2877–2880, Aug 2013.

[60] Z. Yang, M. A. Soto, and L. Thévenaz, "Increasing robustness of bipolar pulse coding in Brillouin distributed fiber sensors," *Opt. Express*, vol. 24, no. 1, pp. 586–597, Jan 2016.

[61] S. Le Floch, F. Sauser, M. Llera, and E. Rochat, "Colour cyclic code for Brillouin distributed sensors," *Proceedings of SPIE*, vol. 9634, pp. 963 431–963 431–4, 2015.

[62] M. Soto, J. Ramírez, and L. Thévenaz, "Intensifying the response of distributed optical fibre sensors using 2D and 3D image restoration," *Nature Communications*, vol. 7, 2016.

[63] M. Soto, J. Ramirez, and L. Thevenaz, "Optimizing Image Denoising for Long-Range Brillouin Distributed Fiber Sensing," *Journal of Lightwave Technology*, 2017.

[64] J. Urricelqui, M. Soto, and L. Thévenaz, "Sources of noise in brillouin optical time-domain analyzers," *Proceedings of SPIE*, vol. 9634, p. 963434, 2015.

[65] M. Soto and L. Thévenaz, "Towards 1'000'000 resolved points in a distributed optical fibre sensor," *Proceedings of SPIE*, vol. 9157, p. 9157C3, 2014.

[66] F. Rodríguez-Barrios, S. Martín-López, A. Carrasco-Sanz, P. Corredera, J. Ania-Castañón, L. Thévenaz, and M. González-Herráez, "Distributed Brillouin fiber sensor assisted by first-order Raman amplification," *Journal of Lightwave Technology*, vol. 28, no. 15, pp. 2162–2172, 2010.

[67] A. Dominguez-Lopez, A. Lopez-Gil, S. Martin-Lopez, and M. Gonzalez-Herraez, "Strong cancellation of RIN transfer in a Raman-assisted BOTDA using balanced detection," *IEEE Photonics Technology Letters*, vol. 26, no. 18, pp. 1817–1820, 2014.

[68] X. Angulo-Vinuesa, D. Bacquet, S. Martin-Lopez, P. Corredera, P. Szriftgiser, and M. Gonzalez-Herraez, "Relative intensity noise transfer reduction in Raman-assisted BOTDA systems," *IEEE Photonics Technology Letters*, vol. 26, no. 3, pp. 271–274, 2014.

[69] D. Cotter, "Stimulated Brillouin Scattering in Monomode Optical Fiber," *Journal of Optical Communications*, vol. 4, no. 1, pp. 10–19, 1983.

[70] W. Li, X. Bao, Y. Li, and L. Chen, "Differential pulse-width pair BOTDA for high spatial resolution sensing," *Optics Express*, vol. 16, no. 26, pp. 21 616–21 625, 2008.

[71] X. Bao, A. Brown, M. DeMerchant, and J. Smith, "Characterization of the Brillouin-loss spectrum of single-mode fibers by use of very short (<10-ns) pulses," *Optics Letters*, vol. 24, no. 8, pp. 510–512, 1999.

[72] K. Kishida and C.-H. Li, "Pulse Pre-Pump-BOTDA technology for new generation of distributed strain measuring system," *Structural Health Monitoring and Intelligent Infrastructure, SHMII 2005*, vol. 1, pp. 471–477, 2006.

[73] A. Brown, B. Colpitts, and K. Brown, "Distributed sensor based on dark-pulse Brillouin scattering," *IEEE Photonics Technology Letters*, vol. 17, no. 7, pp. 1501–1503, 2005.

[74] S. Foaleng, M. Tur, J.-C. Beugnot, and L. Thévenaz, "High spatial and spectral resolution long-range sensing using Brillouin echoes," *Journal of Lightwave Technology*, vol. 28, no. 20, pp. 2993–3003, 2010.

[75] R. Bernini, A. Minardo, and L. Zeni, "Dynamic strain measurement in optical fibers by stimulated Brillouin scattering," *Optics Letters*, vol. 34, no. 17, pp. 2613–2615, 2009.

[76] Y. Peled, A. Motil, L. Yaron, and M. Tur, "Slope-assisted fast distributed sensing in optical fibers with arbitrary Brillouin profile," *Optics Express*, vol. 19, no. 21, pp. 19 845–19 854, 2011.

[77] A. Motil, O. Danon, Y. Peled, and M. Tur, "Pump-power-independent double slope-assisted distributed and fast Brillouin fiber-optic sensor," *IEEE Photonics Technology Letters*, vol. 26, no. 8, pp. 797–800, 2014.

[78] D. Ba, B. Wang, D. Zhou, M. Yin, Y. Dong, H. Li, Z. Lu, and Z. Fan, "Distributed measurement of dynamic strain based on multi-slope assisted fast BOTDA," *Optics Express*, vol. 24, no. 9, pp. 9781–9793, 2016.

[79] A. Voskoboinik, O. Yilmaz, A. Willner, and M. Tur, "Sweep-free distributed Brillouin time-domain analyzer (SF-BOTDA)," *Optics Express*, vol. 19, no. 26, pp. B842–B847, 2011.

[80] A. Voskoboinik, A. Willner, and M. Tur, "Extending the Dynamic Range of Sweep-Free Brillouin Optical Time-Domain Analyzer," *Journal of Lightwave Technology*, vol. 33, no. 14, pp. 2978–2985, 2015.

[81] Y. Peled, A. Motil, and M. Tur, "Fast Brillouin optical time domain analysis for dynamic sensing," *Optics Express*, vol. 20, no. 8, pp. 8584–8591, 2012.

[82] J. Fang, P. Xu, Y. Dong, and W. Shieh, "Single-shot distributed Brillouin optical time domain analyzer," *Optics Express*, vol. 25, no. 13, pp. 15 188–15 198, 2017.

[83] V. Lecœuche, D. Webb, C. Pannell, and D. Jackson, "Brillouin based distributed fibre sensor incorporating a mode-locked Brillouin fibre ring laser," *Optics Communications*, vol. 152, no. 4-6, pp. 263–268, 1998.

[84] L. Thévenaz, S. Le Floch, D. Alasia, and J. Troger, "Novel schemes for optical signal generation using laser injection locking with application to Brillouin sensing," *Measurement Science and Technology*, vol. 15, no. 8, pp. 1519–1524, 2004.

[85] Y. Li, X. Bao, F. Ravet, and E. Ponomarev, "Distributed Brillouin sensor system based on offset locking of two distributed feedback lasers," *Applied Optics*, vol. 47, no. 2, pp. 99–102, 2008.

[86] K. Song and S. Yang, "Simplified brillouin optical time-domain sensor based on direct modulation of a laser diode," *Optics Express*, vol. 18, no. 23, pp. 24 012–24 018, 2010.

[87] J. Hong and K. Song, "Simplified BOTDA System Based on Direct Modulation of a Laser Diode with an Extended Measurement Range," *Journal of Lightwave Technology*, vol. 33, no. 10, pp. 1979–1984, 2015.

[88] D. Marini, M. Iuliano, F. Bastianini, and G. Bolognini, "BOTDA sensing employing a modified Brillouin fiber laser probe source," *Journal of Lightwave Technology*, vol. PP, no. 99, pp. 1–1, 2017.

[89] M. A. Soto, S. L. Floch, and L. Thévenaz, "Bipolar optical pulse coding for performance enhancement in BOTDA sensors," *Opt. Express*, vol. 21, no. 14, pp. 16 390–16 397, Jul 2013.

[90] M. van Deventer and A. Boot, "Polarization Properties of Stimulated Brillouin Scattering in Single-Mode Fibers," *Journal of Lightwave Technology*, vol. 12, no. 4, pp. 585–590, 1994.

[91] A. Minardo, R. Bernini, L. Zeni, L. Thevenaz, and F. Briffod, "A reconstruction technique for long-range stimulated Brillouin scattering distributed fibre-optic sensors: Experimental results," *Measurement Science and Technology*, vol. 16, no. 4, pp. 900–908, 2005.

[92] A. Minardo, R. Bernini, and L. Zeni, "A Simple Technique for Reducing Pump Depletion in Long-Range Distributed Brillouin Fiber Sensors," *IEEE Sensors Journal*, vol. 9, no. 6, pp. 633–634, June 2009.

[93] Y. Dong, L. Chen, and X. Bao, "Time-division multiplexing-based BOTDA over 100 km sensing length," *Optics Letters*, vol. 36, no. 2, pp. 277–279, 2011.

[94] A. Zornoza, A. Minardo, R. Bernini, A. Loayssa, and L. Zeni, "Pulsing the probe wave to reduce nonlocal effects in Brillouin optical time-domain analysis (BOTDA) sensors," *IEEE Sensors Journal*, vol. 11, no. 4, pp. 1067–1068, 2011.

[95] J. Urricelqui, M. Sagues, and A. Loayssa, "BOTDA measurements tolerant to nonlocal effects by using a phase-modulated probe wave and RF demodulation," *Optics Express*, vol. 21, no. 14, pp. 17 186–17 194, 2013.

[96] A. Dominguez-Lopez, Z. Yang, M. A. Soto, X. Angulo-Vinuesa, S. Martin-Lopez, L. Thevenaz, and M. Gonzalez-Herraez, "Novel scanning method for distortion-free BOTDA measurements," *Optics Express*, vol. 24, no. 10, pp. 10 188–10 204, 2016.

[97] X. Hong, W. Lin, Z. Yang, S. Wang, and J. Wu, "Brillouin optical time-domain analyzer based on orthogonally-polarized four-tone probe wave," *Opt. Express*, vol. 24, no. 18, pp. 21 046–21 058, Sep 2016.

[98] X. Bao, J. Dhliwayo, N. Heron, D. Webb, and D. Jackson, "Experimental and Theoretical Studies on a Distributed Temperature Sensor Based on Brillouin Scattering," *Journal of Lightwave Technology*, vol. 13, no. 7, pp. 1340–1348, 1995.

[99] A. Zornoza, R. A. Pérez-Herrera, C. Elosúa, S. Diaz, C. Bariain, A. Loayssa, and M. Lopez-Amo, "Long-range hybrid network with point and distributed Brillouin sensors using Raman amplification," *Opt. Express*, vol. 18, no. 9, pp. 9531–9541, Apr 2010.

[100] S. A. V., G. A. Ferrier, X. Bao, and L. Chen, "Effect of the finite extinction ratio of an electro-optic modulator on the performance of distributed probe-pump Brillouin sensor systems," *Opt. Lett.*, vol. 28, no. 16, pp. 1418–1420, 2003.

[101] Y. Sun, J. Zyskind, and A. Srivastava, "Average inversion level, modeling, and physics of erbium-doped fiber amplifiers," *IEEE Journal on Selected Topics in Quantum Electronics*, vol. 3, no. 4, pp. 991–1007, 1997.

[102] K. Y. Ko, M. S. Demokan, and H. Y. Tam, "Transient analysis of erbium-doped fiber amplifiers," *IEEE Photonics Technology Letters*, vol. 6, no. 12, pp. 1436–1438, Dec 1994.

[103] H. Shalom, A. Zadok, M. Tur, P. Legg, W. Cornwell, and I. Andonovic, "On the various time constants of wavelength changes of a DFB laser under direct modulation," *IEEE Journal of Quantum Electronics*, vol. 34, no. 10, pp. 1816–1822, 1998.

[104] K. Shiraki, M. Ohashi, and M. Tateda, "SBS threshold of a fiber with a Brillouin frequency shift distribution," *Journal of Lightwave Technology*, vol. 14, no. 1, pp. 50–57, 1996.

[105] A. Loayssa, R. Hernández, D. Benito, and S. Galech, "Characterization of stimulated Brillouin scattering spectra by use of optical single-sideband modulation," *Optics Letters*, vol. 29, no. 6, pp. 638–640, 2004.

[106] G. Smith, D. Novak, and Z. Ahmed, "Technique for optical ssb generation to overcome dispersion penalties in fibre-radio systems," *Electronics Letters*, vol. 33, no. 1, pp. 74–75, 1997.

[107] H. Iribas, A. Loayssa, F. Sauser, M. Llera, and S. Le Floch, "Enhancement of signal-to-noise ratio in Brillouin optical time domain analyzers by dual-probe detection," *Proceedings of SPIE*, vol. 10323, p. 103237D, 2017.

[108] A. Minardo, A. Coscetta, L. Zeni, and R. Bernini, "High-spatial resolution DPP-BOTDA by real-time balanced detection," *IEEE Photonics Technology Letters*, vol. 26, no. 12, pp. 1251–1254, 2014.

[109] M. D. Jones, "Using simplex codes to improve OTDR sensitivity," *IEEE Photonics Technology Letters*, vol. 5, no. 7, pp. 822–824, July 1993.

[110] M. Nazarathy, S. A. Newton, R. P. Giffard, D. S. Moberly, F. Sischka, W. R. Trutna, and S. Foster, "Real-time long range complementary correlation optical time domain reflectometer," *Journal of Lightwave Technology*, vol. 7, no. 1, pp. 24–38, Jan 1989.

[111] S. Le Floch, F. Sauser, M. Llera, M. A. Soto, and L. Thévenaz, "Colour simplex coding for Brillouin distributed sensors," *Proceedings of SPIE*, vol. 8794, pp. 879 437–879 437–4, 2013.

[112] M. Harwit and N. J. Sloane, *Hadamard Transform Optics*. Academic Press, 1979.

[113] F. Baronti, A. Lazzeri, R. Roncella, R. Saletti, A. Signorini, M. A. Soto, G. Bolognini, and F. D. Pasquale, "SNR enhancement of Raman-based long-range distributed temperature sensors using cyclic Simplex codes," *Electronics Letters*, vol. 46, no. 17, pp. 1221–1223, August 2010.

[114] D. Lee, H. Yoon, P. Kim, J. Park, and N. Park, "Optimization of SNR Improvement in the Noncoherent OTDR Based on Simplex Codes," *J. Lightwave Technol.*, vol. 24, no. 1, p. 322, Jan 2006.

[115] F. Wang, C. Zhu, C. Cao, and X. Zhang, "Enhancing the performance of BOTDR based on the combination of FFT technique and complementary coding," *Optics Express*, vol. 25, no. 4, pp. 3504–3513, 2017.

[116] M. Soto, X. Angulo-Vinuesa, S. Martin-Lopez, S.-H. Chin, J. Ania-Castañon, P. Corredera, E. Rochat, M. Gonzalez-Herraez, and L. Thévenaz, "Extending the real remoteness of long-range Brillouin optical time-domain fiber analyzers," *Journal of Lightwave Technology*, vol. 32, no. 1, pp. 152–162, 2014.

[117] R. Cohen, Y. London, Y. Antman, and A. Zadok, "Brillouin optical correlation domain analysis with 4 millimeter resolution based on amplified spontaneous emission," *Optics Express*, vol. 22, no. 10, pp. 12 070–12 078, 2014.

[118] S. Diakaridia, Y. Pan, P. Xu, D. Zhou, B. Wang, L. Teng, Z. Lu, D. Ba, and Y. Dong, "Detecting cm-scale hot spot over 24-km-long single-mode fiber by using differential pulse pair BOTDA based on double-peak spectrum," *Optics Express*, vol. 25, no. 15, pp. 17 727–17 736, 2017.

[119] J. Urricelqui, A. Zornoza, M. Sagues, and A. Loayssa, "Dynamic BOTDA measurements based on Brillouin phase-shift and RF demodulation," *Optics Express*, vol. 20, no. 24, pp. 26 942–26 949, 2012.

[120] D. Zhou, Y. Dong, B. Wang, T. Jiang, D. Ba, P. Xu, H. Zhang, Z. Lu, and H. Li, "Slope-assisted botda based on vector sbs and frequency-agile technique for wide-strain-range dynamic measurements," *Optics Express*, vol. 25, no. 3, pp. 1889–1902, 2017.

[121] J. Dakin, D. Pratt, G. Bibby, and J. Ross, "Distributed optical fibre Raman temperature sensor using a semiconductor light source and detector," *Electronics Letters*, vol. 21, no. 13, pp. 569–570, 1985.

[122] A. Minardo, E. Catalano, and L. Zeni, "Cost-effective method for fast Brillouin optical time-domain analysis," *Optics Express*, vol. 24, no. 22, pp. 25 424–25 431, 2016.

[123] S. Diaz, S. Mafang, M. Lopez-Amo, and L. Thévenaz, "A high-performance optical time-domain Brillouin distributed fiber sensor," *IEEE Sensors Journal*, vol. 8, no. 7, pp. 1268–1272, 2008.

[124] A. B. Carlson, P. B. Crilly, and J. Rutledge, *Communication Systems: An Introduction to Signals and Noise in Electrical Communication.* McGraw-Hill Higher Education, 2002.

[125] K. Lim, L. Wong, W. Chiu, and J. Kodikara, "Distributed fiber optic sensors for monitoring pressure and stiffness changes in out-of-round pipes," *Structural Control and Health Monitoring*, vol. 23, no. 2, pp. 303–314, 2016.

International journals

1. **H. Iribas**, J. Urricelqui, J. Mariñelarena, M. Sagues, and A. Loayssa, "Cost-effective Brillouin optical time-domain analysis sensor using a single optical source and passive optical filtering," *J. Sensors*, 2016, Art. no. 8243269, 2016.

2. **H. Iribas**, A. Loayssa, F. Sauser, M. Llera, and S. Le Floch, "Cyclic coding for Brillouin optical time-domain analyzers using probe dithering," *Opt. Express*, vol. 25, no. 8, pp. 8787-8800, 2017.

3. **H. Iribas**, J. Urricelqui, J.J. Mompó, J. Mariñelarena, and A. Loayssa, "Non-local effects in Brillouin optical time-domain analysis sensors," *Applied Sciences (Switzerland)*, vol. 7, no. 8, Art. no. 761, 2017.

4. J.J. Mompó, **H. Iribas**, J. Urricelqui, and A. Loayssa, "Second-Order Nonlocal Effects Mitigation in Brillouin Optical Time-Domain Analysis Sensors by Tracking the Brillouin Frequency Shift Profile of the Fiber," *IEEE Photonics Journal*, vol. 9, no. 5, pp. 1-12, 2017.

5. **H. Iribas**, J. Mariñelarena, C. Feng, J. Urricelqui, T. Schneider, and A. Loayssa, "Effects of pump pulse extinction ratio in Brillouin optical time-domain analysis sensors," *Opt. Express*, vol. 25, no. 22, pp. 27896-27912, 2017.

Conference proceedings

1. **H. Iribas**, M. Sagues, J. Mariñelarena, and A. Loayssa, "Egituren egoeraren monitorizaziorako zuntz optikoan oinarritutako sentsore sinplifikatua," *Ikergazte Nazioarteko ikerketa*, vol. 2015, p. 475, 2015.

2. **H. Iribas**, J. Urricelqui, J. Mariñelarena, M. Sagues, and A. Loayssa, "Simplified Brillouin sensor for structural health monitoring applications based on passive optical filtering," *Proceedings of SPIE*, vol. 9634, n. 96346O, 2015.

3. **H. Iribas**, J. Urricelqui, M. Sagues, and A. Loayssa, "Enhanced tolerance to pulse extinction ratio in Brillouin optical time domain analysis sensors by dithering of the optical source," *Proceedings of SPIE*, vol. 9634, n. 96344Z, 2015.

4. **H. Iribas**, A. Loayssa, F. Sauser, M. Llera, and S. Le Floch, "Brillouin optical time-domain analyzer for extended sensing range using probe dithering and cyclic coding," *Proceedings of SPIE*, vol. 10323, n. 103230Q, 2017.

5. **H. Iribas**, A. Loayssa, F. Sauser, M. Llera, and S. Le Floch, "Enhancement of signal-to-noise ratio in Brillouin optical time domain analyzers by dual-probe detection," *Proceedings of SPIE*, vol. 10323, n. 103237D, 2017.

6. J.J. Mompó, **H. Iribas**, J. Urricelqui, and A. Loayssa, "Second-order non-local effects mitigation in BOTDA sensors by tracking the BFS profile," *Proceedings of SPIE*, vol. 10323, n. 103237E, 2017.

7. **H. Iribas**, J. Mariñelarena, and A. Loayssa, "Zuntz optikoan oinarritutako sentsoreen prestazioen muga-efektu berria, egituren egoera monitorizatzea helburu," *Ikergazte Nazioarteko ikerketa*, vol. 2017, p. 97, 2017.

8. C. Feng, **H. Iribas**, J. Mariñelarena, T. Schneider, and A. Loayssa, "Detrimental effects in brillouin distributed sensors caused by EDFA transient," *CLEO 2017 - Proceedings*, vol. 2017-January, pp. 1-2, 2017.

Book chapters

1. A. Loayssa, J. Urricelqui, **H. Iribas**, J.J. Mompó, and J. Mariñelarena, "Fiber-optic Brillouin distributed sensors: from dynamic to long-range measurements," In: Sensors for Diagnostics and Monitoring, *CRC Press*, K338070, ch. 2, 2018 (to be published).

Symbols

A	Strain coefficient
A'	Normalized strain coefficient
A_{eff}	Effective area
α	Attenuation coefficient of the medium
α_{snd}	Sound absorption coefficient
α_S	Attenuation coefficient at the Stokes wavelength
α_P	Attenuation coefficient at the pump wavelength
B	Temperature coefficient
B'	Normalized temperature coefficient
C	Compressibility of the medium
C_{gain}	Coding gain
C_{peaks}	Correlation peaks
C_s	Constant entropy of the compressibility
c	Speed of light in vacuum
χ	Dielectric susceptibility
d	Depletion factor of the pump pulse
d_P	Depletion factor of the pump pedestal
d_T	Total depletion factor of the pump wave
$\delta\epsilon$	Strain variation
$\Delta\chi$	Fluctuation of the dielectric susceptibility
ΔP_S	Optical power variation of the probe wave
$\Delta\epsilon$	Fluctuation of the dielectric constant
$\Delta\rho$	Density variations
$\Delta\nu$	Frequency detuning of probe wave from the Brillouin peak frequency
$\Delta\nu_L$	Frequency detuning of the lower-frequency probe wave from the Brillouin peak
$\Delta\nu_G$	Frequency detuning of the upper-frequency probe wave from the Brillouin peak
$\delta\nu$	Frequency shift
$\Delta\nu_B$	Brillouin linewidth
$\Delta\Phi$	Phase difference between probe and Rayleigh backscattered signals
Δw	Work per unit volume
Δz	Spatial resolution
δ	Frequency sampling step
$\mathbf{E}$	Electric field
E_1	Young's modulus
E_{RB}	Electric field of the Rayleigh backscattered signal
E_S	Electric field of the probe wave
E_{Si}	Input electric field of the probe wave
E_P	Electric field of the pump wave
E_{Pi}	Input electric field of the pump wave
ϵ	Relative dielectric constant

ϵ_0	Dielectric permittivity of free space
f_m	Wavelength modulation frequency
Γ	Damping rate of acoustic wave
Γ_B	Phonon decay rate
γ_e	Electrostrictive constant
g_0	Brillouin peak coefficient
g_B	Brillouin gain coefficient
g_{probe}	Reduction in probe gain
G_i	Brillouin gain experienced by the probe wave
G_T	Brillouin gain experienced by the probe wave in coding system
G_P	Probe gain with no pulse in the fiber
G'_P	Probe gain due to the pedestal interaction
h	Planck constant
H_{B-SBS}	Pulse optical frequency response due to the interaction of both probe waves
I_P	Intensity of the pump wave
I_S	Intensity of the Stokes wave
K_s	Bulk modulus
$\mathbf{k}$	Wave vector
L	Length of the optical fiber
L_C	Code length
L_{eff}	Effective length
μ_0	Magnetic permittivity in vacuum
n	Refractive index of medium
ν	Optical frequency
ν_B	Brillouin frequency shift
ν_e	Brillouin frequency shift accuracy
ν_g	Group velocity of light
ν_P	Optical frequency of the pump wave
ν_{RB}	Optical frequency of the Rayleigh backscattered signal
ν_S	Optical frequency of the probe wave
ν_{SL}	Optical frequency of the lower-frequency probe wave
ν_{SU}	Optical frequency of the upper-frequency probe wave
ν_{B0}	Brillouin frequency shift measured at reference temperature
Ω	frequency of the acoustic wave
Ω_B	Angular Brillouin frequency shift
ω	Optical frequency of the incident field
ω_P	Optical frequency of the pump wave
ω_S	Optical frequency of the Stokes wave
$\mathbf{P}$	Polarization field
$\mathbf{P^{NL}}$	Non-linear polarization field
P_S	Optical power of Stokes wave
P_{Si}	Input optical power of probe wave

P_{SL_i}	Input optical power of the lower-frequency probe wave
P_{SU_i}	Input optical power of the upper-frequency probe wave
P_P	Optical pump wave power
P_{P_0}	Optical pump pulse power in absence of Brillouin interaction
P_{Pi}	Input optical power of pump wave
P_{ped}	Optical power of the pump pulse pedestal
p_{st}	Strictive pressure
P_{rx}	Optical power at the receiver
P_{th}^{SBS}	Critical pump power defined as the stimulated Brillouin scattering threshold
p_{st}	Strictive pressure
$\mathbf{q}$	Acoustic wave vector
Q	Acoustic wave field
R	Autocorrelation function
ρ	Density of medium
ρ_0	Density of silica fiber
σ_{BFS}	Brillouin frequency shift precision
σ_{RB-S}	Standard deviation of the Rayleigh backscattered-probe beating noise
σ_T^2	Variance of the total noise of the sensor
σ_{th}^2	Variance of the thermal noise
σ_{sh}^2	Variance of the shot noise
τ_p	Phonon lifetime
t	Time
T	Temperature
T_0	Reference temperature
T_P	Temporal pulse duration
Θ	Poisson's ratio
u	Interaction length of the probe wave with the pump pulse
υ_a	Velocity of the acoustic wave
z	Position of the fiber
ζ	Fraction of peak level

Acronyms

AOM	Acousto-optic modulator
ASE	Amplified spontaneous emission
AWG	Arbitrary waveform generator
BFS	Brillouin frequency shift
BGS	Brillouin gain spectrum
BLS	Brillouin loss spectrum
BOCDA	Brillouin optical correlation-domain analysis
BOFDA	Brillouin optical frequency-domain analysis
BOTDA	Brillouin optical time-domain analysis
BOTDR	Brillouin optical time-domain reflectometry
BRL	Brillouin ring laser
c.c.	Complex conjugate
CW	Continuous wave
DFB	Distributed feedback
DFOS	Distributed fiber optic sensors
DPP	Differential pulse-width pair
DSF	Dispersion shifted fiber
EAM	Electro-absorption modulator
EDFA	Erbium-doped fiber amplifier
EML	Externally-modulated laser
EOM	Electro-optic modulator
ER	Extinction ratio
FBG	Fiber Bragg grating
FM	Frequency modulation
FoM	Figure-of-merit
FOS	Fiber optic sensors
FUT	Fiber under test
FWHM	Full-width at half-maximum
MI	Modulation instability
MZ-EOM	Mach-Zehnder electro-optic modulator
NLE	Non-local effects
OF	Optical filter
OSSB	Optical single-sideband
OSSB-EOM	Optical single-sideband modulator
PS	Polarization scrambler
RB	Rayleigh backscattered
RF	Radio-frequency
RIN	Relative intensity noise
SA	Slope-assisted
SBS	Stimulated Brillouin scattering

SMF	Single-mode fiber
SNR	Signal-to-noise ratio
SOA	Semiconductor optical amplifier
SpBS	Spontaneous Brillouin scattering
SPM	Self-phase modulation
TOSA	Transmitter optical sub-assembly
VNA	Vector network analyzer